JOURNAL OF THE AERONAUTICAL SCIENCES

PUBLIC LIBRARY
DEC 17 1955
ST. LOUIS

VOLUME 22 DECEMBER, 1955 NUMBER 12

CONTENTS

The Supersonic Conical Wing of Minimum Drag.....S. H. TSIEN 805

An Investigation of the Bending of Angle Beams in the Plastic Range.....
.....H. NORMAN ABRAMSON, HARRY A. WILLIAMS, AND BRUCE G. WOOLPERT 818

Transient Temperature Distributions and Thermal Stresses in a Skin-Shear Web Configuration at High-Speed Flight for a Wide Range of Parameters...H. SCHUH 829

Computation of Vibration Modes and Frequencies on SEAC.....
.....WILLIAM F. CAHILL AND SAMUEL LEVY 837

The Flat Plate with an Angle of Attack in a Choked Wind Tunnel.....
.....K. GOTTFRIED GUDERLEY 844

Readers' Forum: "The Load Carrying Capacity of Initially Flat Circular Steel Plates Under Reversed Loading," by R. M. Haythornthwaite and E. T. Onat; "On the Decay of a Flow Nonuniformity," by William J. Guman; "An Electrochemical Method of Visualizing the Boundary Layer," by Edward W. Geller; "Comment on 'Calculation of Span Loading for Arbitrary Plan Forms,'" by Johannes Weissinger; "Aerodynamic Derivatives for Both Steady and Nonsteady Motion of Slender Bodies," by R. M. Wood and C. H. Murphy; "Comment on 'Hypersonic Similarity and the Tangent-Cone Approximation for Unyawed Bodies of Revolution,'" by V. Halbmillion; "Variation of Maximum Thermal Stress in Free Plates," by P. J. Schneider; "Rapid Estimation of the Elastic-Plastic Euler Buckling Loads for Simply Supported Tapered Columns Under Varying Axial Loading," by Bertram Klein.....867–874

Index to Volume 22..... 875

Published by
INSTITUTE OF THE AERONAUTICAL SCIENCES, INC.

JOURNAL OF THE AERONAUTICAL SCIENCES

Editor: HUGH L. DRYDEN, *Director, NACA*
Associate Editor: ROBERT R. DEXTER
Managing Editor: RITA J. TURINO
Editorial Assistant: CAROLINE TAYLOR

Editorial Committee

Aerodynamics

Dean R. Chapman
Francis H. Clauser
Antonio Ferri
Alexander Flax
R. Paul Harrington
R. T. Jones
Carl Kaplan
H. W. Liepmann
C. C. Lin
H. F. Ludloff
Harold Luskin
John R. Markham
Clark B. Millikan
Shatswell Ober
W. Bailey Oswald
C. D. Perkins
Elliott G. Reid
H. J. E. Reid
Russell Robinson
George S. Schairer
G. B. Schubauer
W. R. Sears
John Stack
Theodore Theodorsen
Th. von Kármán

Air Transport

Charles Froesch
J. A. Herlihy
R. D. Kelly
Otto E. Kirchner
Jerome Lederer
John C. Leslie
R. Dixon Speas

Flight Testing

R. R. Gilruth
Melvin N. Gough
W. L. Howland
W. F. Milliken, Jr.
E. G. Stout

Structures and Materials

W. B. Bleakney
E. W. Conlon
John E. Duberg
E. C. Hartmann
N. J. Hoff
Samuel Levy
J. F. McBrearty
Alfred S. Niles
W. Ramberg
F. R. Shanley
C. R. Strang
S. Timoshenko

Rotating Wing Aircraft

F. B. Gustafson
K. H. Hohenemser
Bartram Kelley
R. B. Maloy
Ralph McClarren
R. H. Miller
R. H. Prewitt
Igor I. Sikorsky

Vibration and Flutter

Lee Arnold
M. A. Biot
R. L. Bisplinghoff
William Bollay
Chieh-Chien Chang
J. P. Den Hartog
I. E. Garrick
Martin Goland
Theodore Theodorsen

Aircraft Design

W. E. Beall
E. H. Heinemann
Hall L. Hibbard
Richard Hutton
C. L. Johnson
A. A. Kartveli
E. G. Stout
F. K. Teichmann
Robert J. Woods

Electronics in Aviation

Welcome W. Bender
K. C. Black
M. V. Kiebert, Jr.
David S. Little
S. B. Rogers
Paul Rosenberg
L. M. Sherer

Physiologic Problems

H. G. Armstrong
Louis H. Bauer
Robert J. Benford
W. Randolph Lovelace, II
Ross A. MacFarland

Fuels and Oils

D. P. Barnard
J. H. Doolittle
Graham Edgar
R. T. Goodwin
A. M. Rothrock

Flight Propulsion

George W. Brady
Frank W. Caldwell
L. S. Hobbs
E. E. Johnson
Joseph Keenan
R. P. Kroon
Hans Reissner
Abe Silverstein
C. Fayette Taylor
E. S. Taylor
P. B. Taylor
E. S. Thompson

Instruments

Allan G. Binnie
Charles H. Colvin
Frank R. Cook
C. S. Draper
S. G. Eskin
O. E. Esval
C. F. Savage
R. C. Sylvander

Meteorology

C. F. Brooks
D. M. Little
F. W. Reichelderfer
K. C. Spengler

SUBSCRIPTION RATES

JOURNAL OF THE AERONAUTICAL SCIENCES, Published Monthly.—United States and Possessions: 1 Year, $12.00; Single Copies, $1.50. Foreign Countries Including Canada (American Currency Rates): 1 Year, $13.00; Single Copies, $1.50.

AERONAUTICAL ENGINEERING REVIEW, Published Monthly.—United States and Possessions: 1 Year, $3.00; Single Copies, $0.50. Foreign Countries Including Canada (American Currency Rates): 1 Year, $3.50; Single Copies, $0.50.

Notices of change of address should be sent to the Institute at least 30 days prior to actual change of address.

Manuscripts for publication, proofs, and all correspondence should be addressed to the Editorial Office of the JOURNAL.

Correspondence regarding subscriptions may be addressed to Publication Office, 20th and Northampton Sts., Easton, Pa., or to the Editorial Office of the JOURNAL OF THE AERONAUTICAL SCIENCES, 2 East 64th Street, New York 21, N.Y.

Copyright, 1955, by the Institute of the Aeronautical Sciences, Inc.

Entered as Second Class Matter at the Post Office, Easton, Pa., May 1, 1937. Acceptance for mailing at a special rate of Postage provided for in the Act of August 24, 1912. Authorized April 29, 1937.

JOURNAL OF THE AERONAUTICAL SCIENCES

VOLUME 22 DECEMBER, 1955 NUMBER 12

The Supersonic Conical Wing of Minimum Drag*

S. H. TSIEN†

Cornell University

ABSTRACT

A theoretical investigation is made of thin lifting wings of the conical family, with subsonic leading edges, cambered to give minimum pressure drag at supersonic speeds. The method is an approximate one based on the linear small-perturbation theory and an approximation to the lift distribution in series form. Two different assumptions are made concerning leading-edge suction: (1) full theoretical value of this thrust component, and (2) no thrust component, representing an extreme case of flow separation at the leading edge.

The results show that in case (1) the minimum drag coefficient of the conical wing is almost identically the same as that of a flat triangular wing, at the same lift coefficient, except when the leading edge lies close behind the Mach cone of the apex. Thus little improvement over a flat wing can be achieved, within the conical family, if full leading-edge suction is obtained. In case (2), on the other hand, substantial improvement over the flat delta wing can be achieved by suitable camber; in fact, the drag can be reduced to a value that is again approximately the same as that of the flat wing *with* full leading-edge suction.

The camber distributions and lift distributions of these wings are worked out and are presented in charts.

In a brief supplementary investigation, the effect of chordwise camber of parabolic shape is also determined. It is found that for cases with leading-edge suction there is negligible improvement in minimum drag-due-to-lift as compared to the conical family. For cases with suction omitted, this type of camber affords appreciable improvement in drag, at least for wings whose leading edges are swept back well inside the Mach cone.

NOTATION

C = root chord
C_D = coefficient of drag due to lift
C_{D_s} = coefficient of thrust due to leading-edge singularities—i.e., coefficient of total leading-edge suction force—defined by $\dfrac{D_s}{\text{wing area} \times \text{dynamic pressure}}$
C_L = lift coefficient
D = drag due to lift
D_s = thrust due to leading-edge singularities—i.e., total leading-edge suction force
E = elliptical integral of the second kind
$f(\zeta)$ = analytic complex function (of ζ), whose real part is u
$F(t)$ = analytic complex function (of t), whose real part is u
$g(\zeta)$ = analytic complex function (of ζ), whose real part is w
K = complete elliptical integral of the first kind. Also, constant of integration in the evaluation of wing camber
M = free-stream Mach Number
m = leading-edge slope in xy-plane
R = modulus of complex variable t
S_{2k} = the integral $\displaystyle\int_0^{\pi/2} \sin^{2k}\theta \sqrt{1 - m^2 \sin^2\theta}\, d\theta$
s = modulus of complex variable ϵ
t = complex variable
U = free-stream velocity
u, v, w = nondimensional perturbed velocities in x, y, and z directions, respectively (perturbed velocity/free-stream velocity)
β = $\sqrt{M^2 - 1}$
ϵ = complex variable
ζ = y/x, also complex variable
θ = $\sin^{-1}(\zeta/m)$
ρ = $\sqrt{y^2 + z^2}/x$
τ = argument of complex variable ϵ
ψ = argument of complex variable t

Received September 13, 1954.

* Based on a Ph.D. thesis submitted at Cornell University, June, 1953. The author wishes to express appreciation to Professors W. R. Sears and N. Rott of the Graduate School of Aeronautical Engineering, Cornell University, for their guidance and assistance in its preparation. The research was supported by the United States Air Force under Contract No. AF 33 (038)-21406, monitored by the Office of Scientific Research, Air Research and Development Command.

† Formerly, Research Associate, Graduate School of Aeronautical Engineering; Now, Associate Professor of Mechanical Engineering, University of Toledo.

INTRODUCTION

THE DETERMINATION OF THE OPTIMUM configuration for minimum pressure drag of a three-dimensional supersonic wing is in general a complex problem, even within the approximation of linear theory in which thickness drag and lifting drag are independent. Jones[1] has established a general criterion for the optimum wing loading, but a conclusive solution like the subsonic case based on lifting-line theory is still lacking.

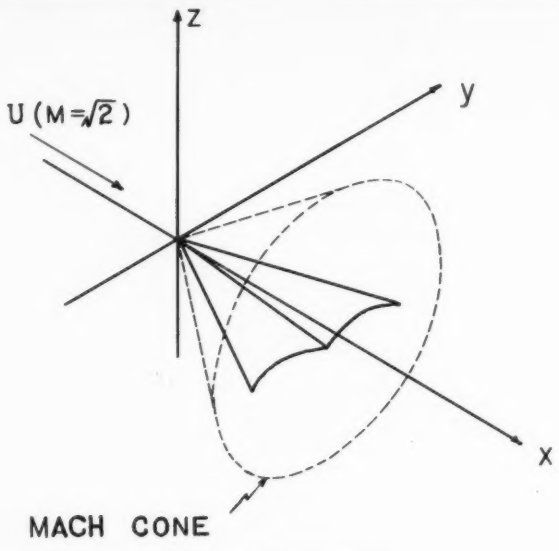

FIG. 1. Coordinate system.

However, the problem has been made accessible in certain investigations by (1) confining attention to slender wings,[2, 3] (2) confining attention to fixed plan forms with one or more parameters held constant,[4–6] and (3) by successive adjustments.[7] Graham's drag-reduction method[7] requires fewer restrictions on the parameters (camber, twist, and thickness) and theoretically leads to the exact solution for a wing with fixed plan form, but unlike the investigations referred to in (1) and (2), it is not one that permits a direct approach. The present paper deals with optimum lifting conical wings of zero thickness symmetric about the streamwise axes. Attempts are made to find the theoretically obtainable minimum values of C_D/C_L^2 and the corresponding shapes of such wings at various aspect ratios, based on linear theory.

The "conical" limitation brings great simplifications so as to make possible a direct approach by available mathematical methods and to dispose of the limitation of slenderness. The accessibility is similar to those in category (2) mentioned above, but instead of varying only one parameter (such as, for the nonlifting case, the position of the ridge line of a delta wing with constant[4] or linearly-varied[5] thickness-chord ratio), here the variables consist of camber and twist combining so as to give conical shapes, but otherwise arbitrary. The restriction of generality involved, therefore, is just the restriction to a function of one independent variable (the conical variable), whereas, for complete generality the shape would be described by a function of two independent variables. A similar restriction was made in reference 6, where the rectangular wing was permitted to have arbitrary camber but no twist. Thus, this investigation also leads to supersonic wings of "restricted minimum" drag and indicates some of the possibilities of drag-reduction compared with the flat plate.

Another restriction has been imposed—i.e., the leading edges are subsonic. The superiority of subsonic over supersonic leading edges for such wings has long been recognized.[8] The effect of leading-edge suction and the accompanying phenomenon of possible flow separation is thus involved, as the total leading-edge thrust is not of negligible order for most aspect ratios.

The method of series representation for the velocity components used in this paper was first applied to conical flow in a paper by Baldwin[9] for evaluating camber shapes and drags corresponding to certain specified lift distributions with no leading-edge singularities.

For the sake of simplicity, the analysis is carried out at Mach Number $\sqrt{2}$. Results are easily converted to other Mach Numbers by simple similarity relations.

CONICAL FLOW THEORY AND DRAG DUE TO LIFT

The wing investigated is sketched in Fig. 1, with the wing surface lying approximately in the xy-plane and the x-axis in the free-stream direction. The conical wing creates inside the Mach cone a conical flow field of which the velocity components can be represented by the two-dimensional Laplace equation after the Chaplygin transformation,

$$\left.\begin{aligned} &\epsilon = se^{i\tau} = [\rho/(1 + \sqrt{1 - \rho^2})]e^{i\tau} \\ \text{with} \quad &\rho = (\sqrt{y^2 + z^2})/x \text{ and } \tau = \tan^{-1} z/y \end{aligned}\right\} \tag{1}$$

After another well-known transformation, viz.,

$$\zeta = 2\epsilon/(1 + \epsilon^2) \tag{2}$$

the region inside the unit circle of the Chaplygin plane (see Fig. 2) is mapped into the entire ζ-plane (see Fig. 3) with the advantage that the wing coordinate is not distorted—i.e., when $z \to 0$, $\zeta \to y/x$. In these complex coordinates the existing conical theory[10, 11] shows that the perturbation velocity components are related

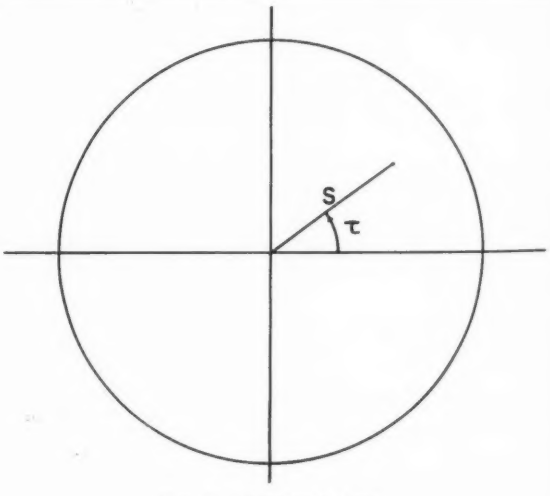

FIG. 2. Chaplygin plane.

by compatibility relations such that when u is given, one can evaluate w by the following integral:

$$g(\zeta) = -i \int^{\zeta} \frac{\sqrt{1-\zeta^2}}{\zeta} df(\zeta) \tag{3}$$

where $f(\zeta)$ = an analytic complex function whose real part is u and $g(\zeta)$ = an analytic complex function whose real part is w.

Also, within the linear theory, one can obtain the following expressions for coefficients of lift and drag (due to this lift) in the same coordinates:

$$C_L = \frac{4}{m} \int_0^m u(\zeta) d\zeta \tag{4}$$

$$C_D = -\frac{4}{m} \int_0^m u(\zeta) w(\zeta) d\zeta - C_{D_s} \tag{5}$$

in which $u(\zeta)$, $w(\zeta)$ are values on the upper surface of the wing ($z = +0$, $\zeta = y/x$) and C_{D_s} is the coefficient of total thrust due to the leading-edge singularities, commonly designated as the leading-edge suction force.

The presence of leading-edge thrust has been recognized in thin-airfoil theory[12] as a result of the square-root type singularity of pressure distribution for subsonic two-dimensional wings. The same concept can be extended to conical wings of subsonic leading edges in view of the fact that the pressure distribution in the neighborhood of the leading edge is identical in the limit with that for a two-dimensional wing in subsonic flow. Under this reasonable assumption, it has been found that for a flat delta wing of subsonic leading edges,[13]

$$C_{D_s} = [C_L^2/(4\pi m)] \sqrt{1-\beta^2 m^2} \tag{6}$$

where $\beta = \sqrt{M^2 - 1}$. As it will be shown later that the lift distribution of a conical wing may be represented by a linear combination of components including one which has the flat-plate distribution, Eq. (6) can be extended to such wings, if the value of C_L is interpreted as the total lift contributed by that particular component. To avoid confusion, one may denote this portion of lift by C_L', to distinguish it from the total lift coefficient C_L, and say, for conical wings

$$C_{D_s} = [C_L'^2/(4\pi m)] \sqrt{1-\beta^2 m^2} \quad (C_L' \leq C_L) \tag{7}$$

Series Representation for Lift Distribution

In the present approach, the minimum-drag problem will be solved by the determination of the optimum lift distribution, which will be represented in a form of a series. The constituent terms are linearly combined with arbitrary coefficients, the values of which will be determined. The necessary conditions that the series should satisfy are: (1) consistency with the boundary conditions (i.e., antisymmetry about the real axis, symmetry about the center line, and vanishing on the Mach cone and on the real axis off the wing), (2) convergence (so that a finite number of terms may be taken for sufficient approximation), (3) correct singularities acceptable from physical considerations, and (4) no loss of generality.

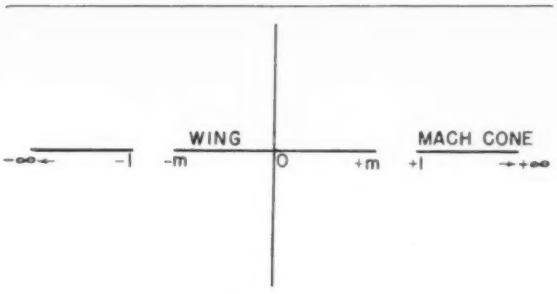

Fig. 3. ζ-plane.

It is found that the following infinite series, which is an extended form of Baldwin's,[9] satisfies all the above requirements:

$$u(\zeta) = \text{R.P.} \left\{ a_0 \left(i \log \frac{\zeta + m}{\zeta - m} \right) + a' \left(\frac{m}{\sqrt{m^2 - \zeta^2}} \right) + \sum_{n=1}^{\infty} b_{2n-1} \left[i \left(\frac{\zeta - \sqrt{\zeta^2 - m^2}}{m} \right)^{2n-1} \right] \right\} \tag{8}$$

in which a_0, a', and b_{2n-1} are the arbitrary coefficients (real). The first and second terms are respectively the "constant lift"[14] and "constant upwash"[15] components, while the remaining part as a whole represents components giving a lift distribution of arbitrary shape but with zero intensity at the leading edge. That the above series satisfies conditions (3) and (4) is obvious. Thus it need only be shown that the infinite series satisfies conditions (1) and (2). This is easily seen after a Joukowski transformation:

$$\zeta = (m/2)\,[t + (1/t)] \tag{9}$$

or

$$t = (\zeta \pm \sqrt{\zeta^2 - m^2})/m = Re^{i\psi} \tag{10}$$

such that the ζ-plane is mapped into the interior of a unit circle in the t-plane with the surface of the wing lying on the circle $|t| = 1$ (upper surface on lower semicircle) and the Mach cone on real axis extending from $(1 - \sqrt{1 - m^2})/m$ to $(-1 + \sqrt{1 - m^2})/m$ (see Fig. 4).

Thus,

$$\text{R.P.} \left\{ \sum_{n=1}^{\infty} b_{2n-1} \left[i \left(\frac{\zeta - \sqrt{\zeta^2 - m^2}}{m} \right)^{2n-1} \right] \right\} = \text{R.P.} \left(i \sum_{n=1}^{\infty} b_{2n-1} t^{2n-1} \right)$$

$$= -\sum_{n=1}^{\infty} b_{2n-1} R^{2n-1} \sin (2n-1)\psi \qquad (R \leq 1) \tag{11}$$

Equation (11) clearly indicates that condition (1) is satisfied. For condition (2), one needs to know the nature of b_{2n-1}. Putting

$$\zeta = y/x = m \sin \theta \tag{12}$$

one can observe from Eq. (8) the lift distribution on the

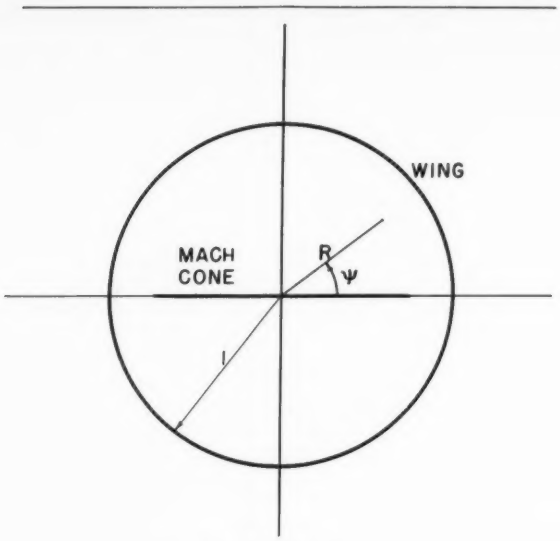

FIG. 4. t-plane.

top surface of the wing is

$$u = a_0\pi + a' \sec\theta + \sum_{n=1}^{\infty} b_{2n-1}(-1)^{n-1}\cos(2n-1) \quad (13)$$

or

$$u - a' \sec\theta = a_0\pi + \sum_{n=1}^{\infty} b_{2n-1}(-1)^{n-1}\cos(2n-1)\theta \quad (14)$$

It is immediately seen that a_0, $b_{2n-1}(-1)^{n-1}$ are coefficients of the Fourier cosine series representing an arbitrary curve $u - a' \sec\theta$, bounded in the interval $0 \leq \theta \leq 2\pi$. Hence, the convergence of the infinite series is proved.

Assume that the curve $u - a' \sec\theta$ represented by Eq. (14) is bounded, continuous and with finite number of maxima and minima. Then the series is uniformly convergent. This permits one to use for approximation a finite number of terms to represent the lift distribution u. In fact, if $u - a' \sec\theta$ has merely a bounded first derivative, b_{2n-1} will decrease with increasing n like $(2n-1)^{-2}$, which indicates a fairly rapid convergence. A four-term approximation for $u - a' \sec\theta$ gives for the lift distribution on the top surface of the wing:

$$u = a_0u_0 + a'u' + b_1u_1 + b_3u_3 + b_5u_5 \quad (15)$$

where

$$u_0 = \pi \quad (16)$$

$$u' = m/\sqrt{m^2 - \zeta^2} = \sec\theta \quad (17)$$

$$u_{2n-1} = \text{R.P.}\left\{i[(\zeta - \sqrt{\zeta^2 - m^2})/m]^{2n-1}\right\} = (-1)^{2n-1}\cos(2n-1)\theta \quad (18)$$

Or, one may split u_1 such that

$$u_1 = \sqrt{m^2 - \zeta^2}/m = [m/(2\sqrt{m^2 - \zeta^2})] + [(m^2 - 2\zeta^2)/(2m\sqrt{m^2 - \zeta^2})] \quad (19)$$

and

$$u = a_0u_0 + b_1'u_1' + b_1''u_1'' + b_3u_3 + b_5u_5 \quad (20)$$

where

$$u_1' = m/(2\sqrt{m^2 - \zeta^2}) \quad (21)$$

$$u_1'' = (m^2 - 2\zeta^2)/(2m\sqrt{m^2 - \zeta^2}) \quad (22)$$

$$b_1' = 2a' + b_1 \quad (23)$$

$$b_1'' = b_1 \quad (24)$$

Substituting Eq. (20) into Eq. (4), one obtains the total lift coefficient,

$$C_L = \pi(4a_0 + b_1') \quad (25)$$

instead of $\pi(4a_0 + 2a' + b_1)$ which would be obtained if Eq. (15) were used. This facilitates the succeeding manipulations a great deal, including the avoidance of certain integration difficulties.

The upwash distribution compatible with the lift can be evaluated from Eq. (3)—viz.,

$$w = a_0w_0 + b_1'w_1' + b_1''w_1'' + b_3w_3 + b_5w_5 \quad (26)$$

where

$$w_0 = \frac{\sqrt{1-m^2}}{m}\left[\cosh^{-1}\left|\frac{1+m\zeta}{m+\zeta}\right| + \cosh^{-1}\left|\frac{1-m\zeta}{m-\zeta}\right|\right] - \frac{2}{m}\cosh^{-1}\left|\frac{1}{\zeta}\right| \quad (27)$$

$$w_1' = -[1/(2m)]\,E(\sqrt{1-m^2}) \quad (28)$$

$$w_1'' = \frac{1}{m}\left[\sqrt{1-\zeta^2} - \cosh^{-1}\left|\frac{1}{\zeta}\right| + K(\sqrt{1-m^2}) - \frac{1}{2}E(\sqrt{1-m^2})\right] \quad (29)$$

$$w_3 = \frac{1}{m^2}\left[-4(\sqrt{1-\zeta^2})^3 - 3m\sqrt{1-\zeta^2} + 3m\cosh^{-1}\left|\frac{1}{\zeta}\right| + \frac{m^2+4}{m} - 5mK(\sqrt{1-m^2})\right] \quad (30)$$

$$w_5 = \frac{5}{m^5}\left\{\frac{16}{5}(\sqrt{1-\zeta^2})^5 + \left(4m^2 - \frac{16}{3}\right)(\sqrt{1-\zeta^2})^3 + m^4\sqrt{1-\zeta^2} - m^4\cosh^{-1}\left|\frac{1}{\zeta}\right| + \frac{1}{15}[(32 - 52m^2 - 3m^4)E(\sqrt{1-m^2}) + (-16m^2 + 39m^4)K(\sqrt{1-m^2})]\right\} \quad (31)$$

The expressions for w_0, w_1', w_1'', and w_3 are obtained, directly or with modifications, from a previous paper.[9]

Equations (20) and (26) suffice for the evaluation of $\int_0^m u(\zeta)w(\zeta)d\zeta$ in Eq. (5) for an arbitrary lift distribution. With Eqs. (7) and (25), it can be shown that

$$C_D = -\frac{4}{m}\left\{\left(\frac{A_{00}}{16} - \frac{B_{01'}}{4} + A_{1'1'} + \frac{\pi}{16}\sqrt{1-m^2}\right)b_1'^2 + \left(B_{1'1''} - \frac{B_{01''}}{4} - \frac{\pi}{8}\sqrt{1-m^2}\right)b_1'b_1'' + \left(B_{1'3} - \frac{B_{03}}{4}\right)b_1'b_3 + \left(B_{1'5} - \frac{B_{05}}{4}\right)b_1'b_5 + \left(A_{1''1''} + \frac{\pi}{16}\sqrt{1-m^2}\right)b_1''^2 + (B_{1''3})\,b_1''b_3 + (B_{1''5})b_1''b_5 + (A_{33})b_3^2 + (B_{35})b_3b_5 + (A_{55})b_5^2 + \left[\left(-\frac{A_{00}}{8} + \frac{B_{01'}}{4}\right)\left(\frac{C_L}{\pi}\right)\right]b_1' + \left[\frac{B_{01''}}{4}\left(\frac{C_L}{\pi}\right)\right]b_1'' + \left[\frac{B_{03}}{4}\left(\frac{C_L}{\pi}\right)\right]b_3 + \left[\frac{B_{05}}{4}\left(\frac{C_L}{\pi}\right)\right]b_5 + \frac{A_{00}}{16}\left(\frac{C_L}{\pi}\right)^2\right\} \quad (32)$$

where A_{ii} and B_{ij} stand for $\int_0^m u_i w_i d\zeta$ and $\left(\int_0^m u_i w_j d\zeta + \int_0^m u_j w_i d\zeta\right)$ and $A_{i'i}$ stands for $\int_0^m u_i' w_i d\zeta$, etc., which are functions of m. In the above expression, C_{D_s} is included. As $a'u'$ is the only component of u which produces leading-edge thrust [see Eq. (15)], it comes naturally that

$$C_L' = 2\pi a' = \pi(b_1' - b_1'') \quad (33)$$

Hence,

$$C_{D_s} = [(\pi\sqrt{1-m^2})/(4m)]\,(b_1' - b_1'')^2 \quad (34)$$

The parameters $\int_0^m u_i w_i d\zeta$ and $\int_0^m u_i w_j d\zeta$ are tabulated as follows:

$$\int_0^m u_0 w_0 d\zeta = 2\pi\left\{(1-\sqrt{1-m^2})\log m - \log(1+\sqrt{1-m^2}) + \frac{1}{m}\left[(1-m^2)\sin^{-1}m + \cos^{-1}m - \frac{\pi}{2}\right]\right\} \quad (35)$$

$$\int_0^m u_1' w_0 d\zeta = \frac{\sqrt{1-m^2}}{2} I_1 - I_2 \quad (36)$$

where

$$I_1 = 2\int_0^{\pi/2} \log(\sqrt{1-m^2} + \sqrt{1-m^2\sin^2\theta})d\theta + \frac{\pi}{2}\log\frac{2}{m} \quad (37)$$

$$I_2 = \int_0^{\pi/2} \log(1+\sqrt{1-m^2\sin^2\theta})d\theta + \frac{\pi}{2}\log\frac{2}{m} \quad (38)$$

(The integrals in I_1 and I_2 may be expanded into series.)

$$\int_0^m u_0 w_1' d\zeta = -\frac{\pi}{2}E(\sqrt{1-m^2}) \quad (39)$$

$$\int_0^m u_1'' w_0 d\zeta = -E(m) \quad (40)$$

$$\int_0^m u_0 w_1'' d\zeta = \frac{\pi}{m}\left[\frac{m}{2}\sqrt{1-m^2} - m\log\left(\frac{1+\sqrt{1-m^2}}{m}\right) + \frac{1}{2}\sin^{-1}m + \cos^{-1}m + mK(\sqrt{1-m^2}) - \frac{m}{2}E(\sqrt{1-m^2}) - \frac{\pi}{2}\right] \quad (41)$$

$$\int_0^m u_3 w_0 d\zeta = 2[E(m) - S_2]^* \quad (42)$$

* $S_{2k} = \int_0^{\pi/2} \sin^{2k}\theta\sqrt{1-m^2\sin^2\theta}\,d\theta$. For evaluation, see Appendix II.

$$\int_0^m u_0 w_3 d\zeta = \pi \left\{ -\frac{1}{2m^3}\left[2m(\sqrt{1-m^2})^3 + 3m\sqrt{1-m^2} + 3\sin^{-1} m\right] + \frac{3}{2m}\left[-m\sqrt{1-m^2} + 2m\log\left(\frac{1+\sqrt{1-m^2}}{m}\right) - \sin^{-1} m - 2\cos^{-1} m + \pi\right] + \frac{m^2+4}{m^2}E(\sqrt{1-m^2}) - 5K(\sqrt{1-m^2})\right\} \quad (43)$$

$$\int_0^m u_5 w_1 d\zeta = -2E(m) + \frac{22}{3}S_2 - \frac{16}{3}S_4 \quad (44)$$

$$\int_0^m u_0 w_5 d\zeta = \frac{5\pi}{m^5}\left\{\frac{1}{15}\left[8m(\sqrt{1-m^2})^5 + 10m(\sqrt{1-m^2})^3 + 15m\sqrt{1-m^2} + 15\sin^{-1} m\right] + \left(\frac{m^2}{2} - \frac{2}{3}\right)\left[2m(\sqrt{1-m^2})^3 + 3m\sqrt{1-m^2} + 3\sin^{-1} m\right] + \frac{m^4}{2}\left[m\sqrt{1-m^2} - 2m\log\left(\frac{1+\sqrt{1-m^2}}{m}\right) + \sin^{-1} m + 2\cos^{-1} m - \pi\right] + \frac{m}{15}\left[(32-52m^2-3m^4)E(\sqrt{1-m^2}) + (-16m^2+39m^4)K(\sqrt{1-m^2})\right]\right\} \quad (45)$$

$$\int_0^m u_1' w_1' d\zeta = -\frac{\pi}{8}E(\sqrt{1-m^2}) \quad (46)$$

$$\int_0^m u_1'' w_1' d\zeta = 0 \quad (47)$$

$$\int_0^m u_1' w_1'' d\zeta = \frac{1}{2}\left\{E(m) + \frac{\pi}{2}\left[K(\sqrt{1-m^2}) - \frac{1}{2}E(\sqrt{1-m^2})\right] - I_2\right\} \quad (48)$$

$$\int_0^m u_3 w_1' d\zeta = 0 \quad (49)$$

$$\int_0^m u_1' w_3 d\zeta = \frac{1}{2}\left\{-\left(\frac{4}{m^3} + 3\right)E(m) + \frac{\pi}{2}\left[\left(\frac{m^2+4}{m^2}\right)E(\sqrt{1-m^2}) - 5K(\sqrt{1-m^2})\right] + 4S_2 + 3I_2\right\} \quad (50)$$

$$\int_0^m u_5 w_1' d\zeta = 0 \quad (51)$$

$$\int_0^m u_1' w_5 d\zeta = \frac{5}{2m^4}\left\{\frac{16}{5}\left[E(m) - 2m^2 S_2 + m^4 S_4\right] + \left(4m^2 - \frac{16}{3}\right)\left[E(m) - m^2 S_2\right] + m^4\left[E(m) - I_2\right] + \frac{\pi}{30}\left[(32-52m^2-3m^4)E(\sqrt{1-m^2}) + (-16m^2+39m^4)K(\sqrt{1-m^2})\right]\right\} \quad (52)$$

$$\int_0^m u_1'' w_1'' d\zeta = \frac{1}{2}\left[-E(m) + S_2\right] \quad (53)$$

$$\int_0^m u_3 w_1'' d\zeta = E(m) - 2S_2 + S_4 \quad (54)$$

$$\int_0^m u_1'' w_3 d\zeta = \frac{3}{2}\left[E(m) - 5S_2 + 4S_4\right] \quad (55)$$

$$\int_0^m u_5 w_1'' d\zeta = -\frac{1}{3}\left[3E(m) - 14S_2 + 19S_4 - 8S_6\right] \quad (56)$$

$$\int_0^m u_1'' w_5 d\zeta = -\frac{5}{2}\left[E(m) - 13S_2 + 28S_4 - 16S_6\right] \quad (57)$$

$$\int_0^m u_3 w_3 d\zeta = -3\left[E(m) - 6S_2 + 9S_4 - 4S_6\right] \quad (58)$$

$$\int_0^m u_3 w_5 d\zeta = 5\left[E(m) - 14S_2 + 41S_4 - 44S_6 + 16S^8\right] \quad (59)$$

$$\int_0^m u_5 w_3 d\zeta = 3E(m) - 26S_2 + 75S_4 - 84S_6 + 32S_8 \tag{60}$$

$$\int_0^m u_5 w_5 d\zeta = -\frac{5}{3}\left[3E(m) - 50S_2 + 235S_4 - 460S_6 + 400S_8 - 128S_{10}\right] \tag{61}$$

Most of the integrations are lengthy, but about half of them can be obtained from a general formula which is derived in Appendix I.

Determination of Minimum Drag at Constant Lift

Equation (32) shows that C_D is a quadratic function of the coefficients b_1', b_1'', b_3, and b_5. Differentiation with respect to each of these coefficients leads to four linear simultaneous equations that determine the appropriate set of the coefficients giving minimum C_D. All these coefficients are multiples of C_L. Thus, numerical values of minimum C_D/C_L^2 and the corresponding lift distributions (u) in terms of C_L can be obtained for any particular m.

In the determination of minimum C_D/C_L^2, it appears that the role of leading-edge suction force is of importance. This is expected, since it has been illustrated in the case of a flat delta wing that the magnitude of this thrust may amount to as much as one-half of the total drag for very small aspect ratios.[2] Some consideration is thus given to the question of leading-edge flow separation that may greatly reduce the contributions of leading-edge force, and hence, the values of C_D/C_L^2. In fact, the theoretical effect of suction forces can hardly be taken into account for a wing with sharp leading edges moving in a real fluid. This has been verified by experiments[16, 17] that indicate that the pressure peak at the leading edge is smoothed due to the presence of local flow separation. This phenomenon occurs for sharp leading edges and is explained[16] as the result of the "thin-airfoil stall," occurring at small angles of attack, in which the flow separates and reattaches to the surface near the leading edge.

Attention to the effects of flow separation will therefore lead one to different answers for minimum C_D/C_L^2, based on various assumptions concerning leading-edge suction. In the present analysis, the following cases are investigated.

(a) *Suction Force Included*

Full theoretical effect of the leading-edge suction is assumed to be present. Thus, Eq. (32) may be directly used for the evaluation of minimum C_D/C_L^2 and the corresponding lift distribution.

(b) *Suction Force Omitted*

The suction force is assumed to be totally ineffective. Results are obtained by omitting C_{D_s} and carrying out the same calculations as in (a). This, however, implies an assumption that the actual lift distribution can be approximated by the theoretical one (as if there were no separation) without introducing appreciable error in the results. This approximation is motivated by the following observations: (1) experiment[16] indicates that at sufficiently small angles of attack, the lift distribution agrees well with the theoretical curve except for a small region very near to the leading edge and (2) for this case, the appropriate value of $a'[= 1/2(b_1' - b_1'')]$, the only component of u which shows a pressure peak at leading edge, happens to be very small in comparison with the same in case (a).

(c) *No Suction Force*

The lift distribution is so restricted that its intensity at the leading edge is finite. Thus, theoretically, there will be no suction force developed. Results can be obtained by putting $b_1' = b_1'' = b_1$ and going through the same calculations. Values of minimum C_D/C_L^2 obtained for this case, if compared with those of (a), will give an idea to what extent the suction force actually contributes to drag reduction, as compared to the best available distributions without such forces.

Determination of Optimum Conical Wing Shapes

For any arbitrary $w(\zeta)$, one may obtain the wing shape $z/x = h(\zeta)$ from the boundary condition $\partial z/\partial x = w(\zeta)$* which is equivalent to

$$h(\zeta) - \zeta h'(\zeta) = w(\zeta) \tag{62}$$

with $\zeta = y/x$. Thus, the optimum shape that produces minimum C_D/C_L^2 is readily known:

$$\left(\frac{z}{x}\right)_{\text{opt.}} = -\zeta\left\{\int^{\zeta}\frac{[w(\zeta)]_{\text{opt.}}}{\zeta^2}d\zeta + K\right\} \tag{63}$$

where $[w(\zeta)]_{\text{opt.}}$ is obtained by substituting the appropriate coefficients determined in the last section into Eq. (26), and K is an arbitrary constant. The presence of K in the equation indicates that a unique solution cannot be obtained by the linear theory. This, in fact, is true, since, according to linear theory, a flat-plate delta wing with dihedral at zero angle of attack creates no disturbance velocities. Nevertheless, K should be such that the assumption of small z everywhere on the wing is not violated, since it is one upon which Eq. (63) is based. Using similar notations as those for u and w, one may write, for convenience,

$$(z/x)_{\text{opt.}} = a_0(z_0/x) + b_1'(z_1'/x) + b_1''(z_1''/x) + b_3(z_3/x) + b_5(z_5/x) - K\zeta \tag{64}$$

where a_0, b_1', b_1'', b_3, and b_5 are the appropriate set of coefficients and

* The method of deriving wing shapes from $w(\zeta)$ has appeared in reference 9, with slightly different approach.

$$\frac{z_0}{x} = -\zeta \int^{\zeta} \frac{w_0(\zeta)}{\zeta^2}\, d\zeta$$

$$= \frac{\sqrt{1-m^2}}{m}\left(\frac{m+\zeta}{m}\cosh^{-1}\left|\frac{1+m\zeta}{m+\zeta}\right| + \frac{m-\zeta}{m}\cosh^{-1}\left|\frac{1-m\zeta}{m-\zeta}\right|\right) + \frac{2}{m}\sqrt{1-\zeta^2} - \frac{2}{m}\cosh^{-1}\left|\frac{1}{\zeta}\right| \tag{65}$$

$$\frac{z_1'}{x} = -\zeta \int^{\zeta} \frac{w_1'(\zeta)}{\zeta^2}\, d\zeta$$

$$= -[1/(2m)]E(\sqrt{1-m^2}) \tag{66}$$

$$\frac{z_1''}{x} = -\zeta \int^{\zeta} \frac{w_1''(\zeta)}{\zeta^2}\, d\zeta$$

$$= (2/m)\sqrt{1-\zeta^2} + (\zeta/m)\sin^{-1}\zeta + (1/m)K(\sqrt{1-m^2}) - [1/(2m)]\,(\sqrt{1-m^2}) - (1/m)\cosh^{-1}|1/\zeta| \tag{67}$$

$$\frac{z_3}{x} = -\zeta \int^{\zeta} \frac{w_3(\zeta)}{\zeta^2}\, d\zeta$$

$$= -\frac{6}{m^3}\zeta^2\sqrt{1-\zeta^2} - \frac{4}{m^2}(\sqrt{1-\zeta^2})^3 - \frac{3}{m}\left(1+\frac{2}{m^2}\right)\zeta\sin^{-1}\zeta - \frac{6}{m}\sqrt{1-m^2} + \frac{m^2+4}{m^3}E(\sqrt{1-m^2}) - \frac{5}{m}K(\sqrt{1-m^2}) + \frac{3}{m}\cosh^{-1}\left|\frac{1}{\zeta}\right| \tag{68}$$

$$\frac{z_5}{x} = -\zeta \int^{\zeta} \frac{w_5(\zeta)}{\zeta^2}\, d\zeta$$

$$= \frac{5}{m^5}\left\{\frac{16}{5}(\sqrt{1-\zeta^2})^5 + 4\zeta^2(\sqrt{1-\zeta^2})^3 + \left(4m^2 - \frac{16}{3}\right)(\sqrt{1-\zeta^2})^3 - 2(1-3m^2)\zeta^2\sqrt{1-\zeta^2} + 2m^4\sqrt{1-\zeta^2} - (2-6m^2-m^4)\zeta\sin^{-1}\zeta + \frac{1}{15}\left[(32-52m^2-3m^4)E(\sqrt{1-m^2}) + (-16m^2+39m^4)K(\sqrt{1-m^2})\right]\right\} - \frac{5}{m}\cosh^{-1}\left|\frac{1}{\zeta}\right| \tag{69}$$

Equations (65), (67), (68), and (69) all contain a singular term, $\cosh^{-1}|1/\zeta|$. It is expected that $(z/x)_{\text{opt.}}$ will have an infinite value at the centerline of the wing due to the use of finite number of terms for approximation. This undesirable feature, however, can be avoided by adjusting one of the appropriate coefficients, say b_5, so that the terms containing $\cosh^{-1}|1/\zeta|$ will add up to zero. Calculation shows that the error introduced in the value of minimum C_D/C_L^2 by such an adjustment is negligible. In Fig. 7 are plotted together the optimum shapes with and without the singular terms. The values of K are so chosen that the elevation of the leading edges is the same as that of the centerline for those shapes with the singularities removed and that the elevation of the leading edges is unchanged from the previous case for those shapes with the singularities kept.

It is to be emphasized that the optimum shapes obtained from the five-term approximation give values of minimum C_D/C_L^2 which are sufficiently accurate for engineering purposes, although they cannot be considered as the exact optimum shapes.

Results

Minimum values of C_D/C_L^2, the corresponding lift distributions and wing shapes, under various assumptions have been computed for $m = 0.5, 0.8, 1.0$. Flat-plate data are included for comparison.

(1) *Minimum Drag Coefficients*

Table 1

	Case	Minimum C_D/C_L^2	Minimum $m(C_D/C_L^2)$	Flat Plate C_D/C_L^2	Flat Plate $m(C_D/C_L^2)$
$m = 0$	(a)				0.0796*
	(b)				0.1592*
$m = 0.5$	(a)	0.2476	0.1238	0.2477	0.1239
	(b)	0.2486	0.1243	0.3855	0.1928
	(c)	0.2491			
$m = 0.8$	(a)	0.2214	0.1771	0.2224	0.1779
	(b)	0.2216	0.1773	0.2821	0.2257
	(c)	0.2221			
$m = 1.0$	(a) and (b)	0.2298	0.2298	0.2500	0.2500
	(c)	0.2310			

* Obtained from reference 2.

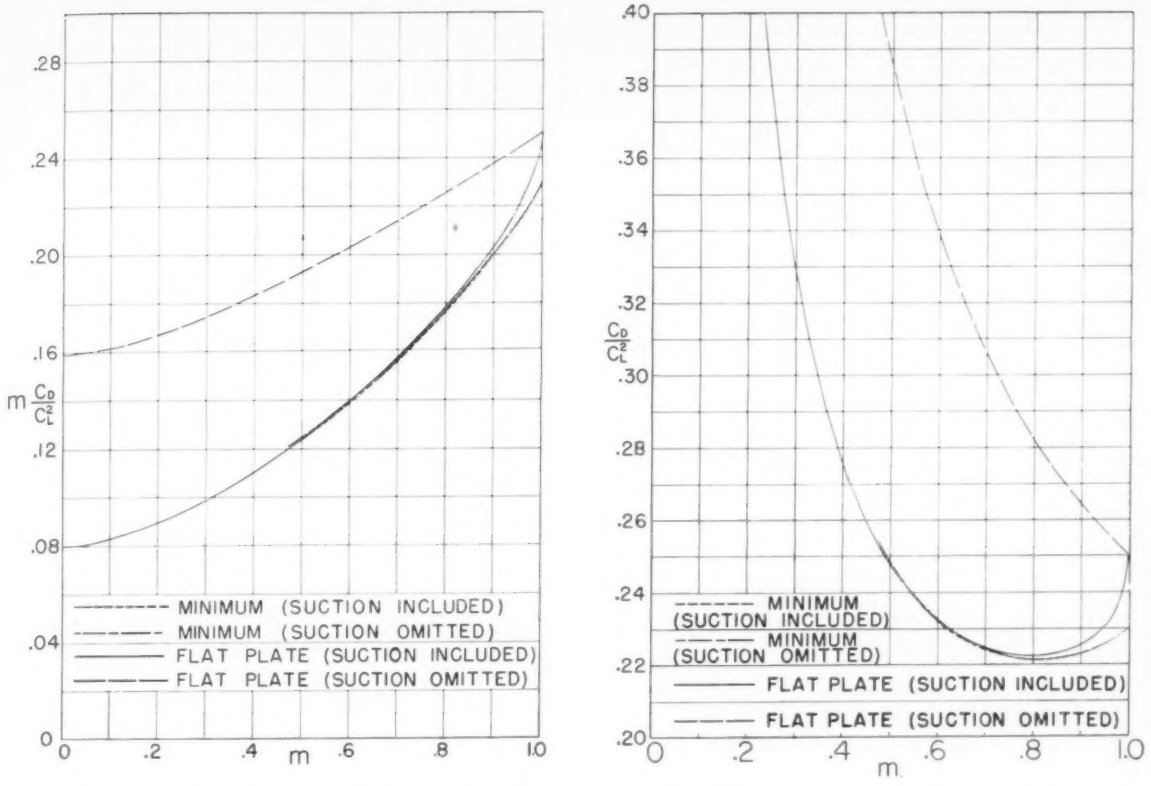

FIG. 5. Minimum C_D/C_L^2 and minimum C_D/C_L^2 multiplied by leading-edge slope for wings with conical camber at $M = \sqrt{2}$. Comparison with flat plate.

(2) *Lift Distributions*

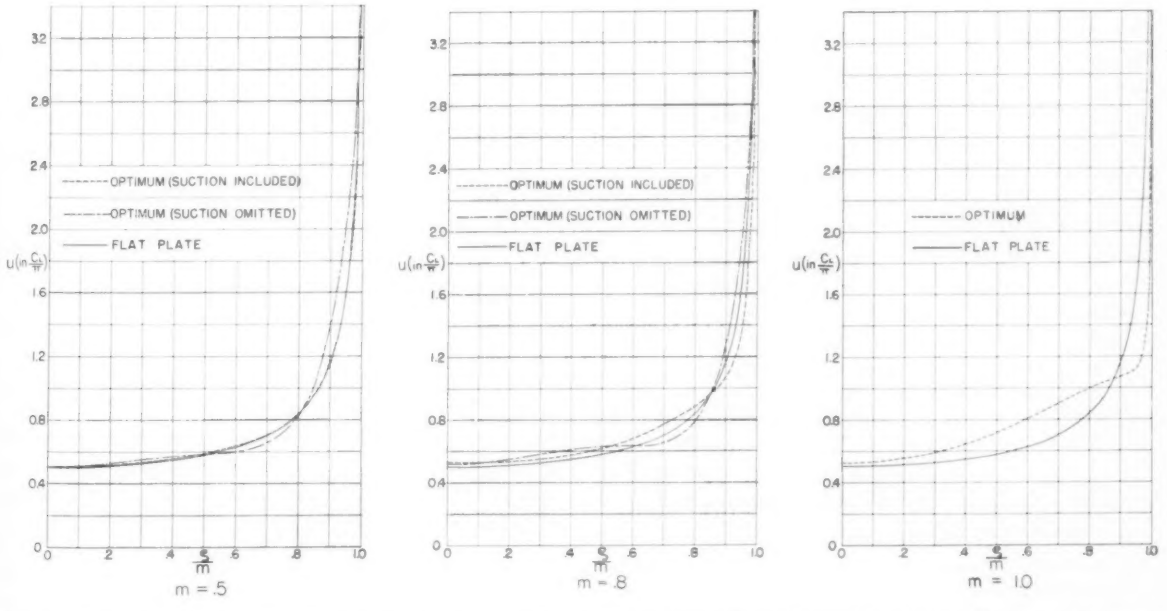

FIG. 6. Optimum lift distributions (based on five-term approximation) for wings with conical camber at $M = \sqrt{2}$. Comparison with flat plate.

(3) *Camber Shapes*

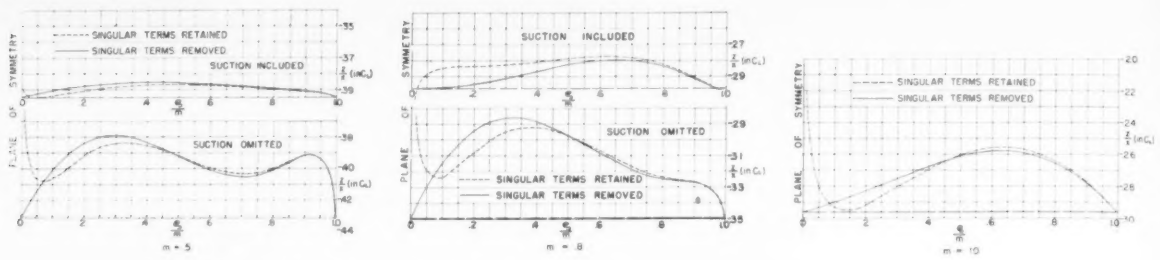

FIG. 7. Optimum conical cambers (based on five-term approximation) at $M = \sqrt{2}$.

CONCLUSION AND DISCUSSION

The theoretical minimum of C_D/C_L^2 for a thin, cambered, conical, delta wing with subsonic leading edges, including the full effect of suction forces, is found to be very nearly equal to the value for a flat plate.* Only when the leading edges are very close to the Mach cone is there noticeable improvement in drag by use of the optimum shape. The maximum gain in the limiting case of sonic leading edges is still only 8 per cent. The conclusion may be drawn that in this case no appreciable reduction of the induced drag of a flat delta wing will be obtained by using "conical" camber.

However, the theoretical calculation sometimes falls short of the truth for wings moving in real fluid. Unless the leading edge is sufficiently rounded, there will be flow separation that nullifies the suction forces. As a consequence, the theoretical minimum C_D/C_L^2 estimated by assuming full effect of suction forces is not always attainable, and the corresponding optimum camber may not be the "genuine" one.

The results for minimum C_D/C_L^2 with suction force omitted show an appreciable improvement over the corresponding case of the flat plate (with suction force omitted). In fact, the minimum values without suction are only very slightly higher than the minima of the former case *with* suction. In other words, the use of proper camber will almost entirely overcome the unfavorable effect of the loss of suction force.

The lift distribution for minimum drag with suction omitted includes only a very small component of the type that would produce suction if flow separation were absent. The suction force, according to Eq. (34), is proportional to $(b_1' - b_1'')^2$, and the optimum lift distribution (say for $m = 0.8$) leads to $|b_1' - b_1''| = 0.0052\ C_L/\pi$. A "restricted" minimum (case of no separation) was also determined with the condition $b_1' = b_1''$, and the results show very small differences from the foregoing case, where the restriction was not applied but the favorable suction force was omitted.

It appears natural that if the suction force is not taken into account, then the corresponding optimum lift distribution will contain only a small component that would otherwise produce suction. It has even been conjectured that this component would completely vanish for the "exact" minimum if the approximation involved by the use of a finite number of terms representing the lift could be avoided. This speculation is practically of little importance, since the difference between the "restricted" and the unrestricted case is negligible, even in the present approximation.

The same method of approach in the determination of minimum drag for conical wings could be extended to nonconical wings by proper choosing of the u and w series. For illustration, the simplest case of finding the optimum combination of a parabolically-cambered wing and a flat plate has been treated in Appendix III. The results show that, for cases with suction included, there is practically no improvement in drag (maximum reduction is only 6 per cent at $m = 0.4$),† while for cases with suction omitted, the improvement is large for small m (maximum is 33.4 per cent at $m = 0$) and is small for large m. These data give some idea about the effect of chordwise camber and its comparison with conical camber.

The theoretical optimum conical shape for minimum C_D/C_L^2 by using finite number of terms for approximation shows a logarithmic singularity at the centerline of the wing. However, the removal of the "singular part" of the shape does not influence the C_D/C_L^2 essentially; this may be understood, as the singular part of the shape acts like a central "fin" with very small effects on the pressure distribution. By calculation, one finds that the effect of the singular part on minimum C_D/C_L^2 is practically negligible.

Although the values of minimum C_D/C_L^2 and the corresponding pressure distribution are insensitive to the number of terms taken for approximation, the shape of the center portion of the corresponding wing is, under certain conditions, very sensitive. In other words, the shape of the center portion of the wing has a small effect on C_D/C_L^2 and on pressure distribution, and the approximated "optimum" wing may still show very bad convergence near its center, while the number

* This result agrees with a recent investigation made by Adams and Sears[3] for relatively slender plan forms, as well as the well-known result of R. T. Jones and others for very slender plan forms.

† At $m = 1$, the improvement is zero. This agrees with Graham's conclusion[7] that, for delta wings with sonic or supersonic leading edges, a simple camber produced by bending the wing along spanwise lines gives no reduction in drag.

of terms taken is considered sufficient to give close value of minimum C_D/C_L^2.

The case in which the worst convergence for the shape has to be expected is the one with suction force omitted and m large. This was concluded from the fact that camber is very ineffective in the drag reduction for this case, as indicated by Fig. 8. The reason may be stated as follows: The "conical camber" is actually a specific combination of chordwise camber and twist, and here it is the twist that is more effective in the conical case. But, for the same slope of the wing ordinate, the twist is largest near the tip and smallest at the center. Hence, the shape of the center portion may exhibit great variations and will not be determined sufficiently if only a few terms are taken for the evaluation of minimum C_D/C_L^2.

To illustrate the accuracy of the five-term approximation, values of minimum C_D/C_L^2 for the case $m = 0.8$, with suction forces omitted, have been calculated. They are, in the order of increasing number of terms taken for approximation, 0.2821, 0.2420, 0.2257, 0.2225, and 0.2216. For other cases, the convergence is expected to be even better.

APPENDIX (I)

EVALUATION OF $\int_0^m u_{2n-1}\bar{w}_{2n'-1}d\zeta$ FOR $n = 2, 3, 4, \ldots, n' = 1, 2, 3, \ldots$

Let

$$U_{2n-1} = \int u_{2n-1}d\zeta \tag{A1}$$

Then

$$\int_0^m u_{2n-1}\bar{w}_{2n'-1}\,d\zeta = [U_{2n-1}\bar{w}_{2n'-1}]_0^m - \int_0^m U_{2n-1}\frac{d\bar{w}_{2n'-1}}{d\zeta}\,d\zeta \tag{A2}$$

From Eqs. (12) and (18),

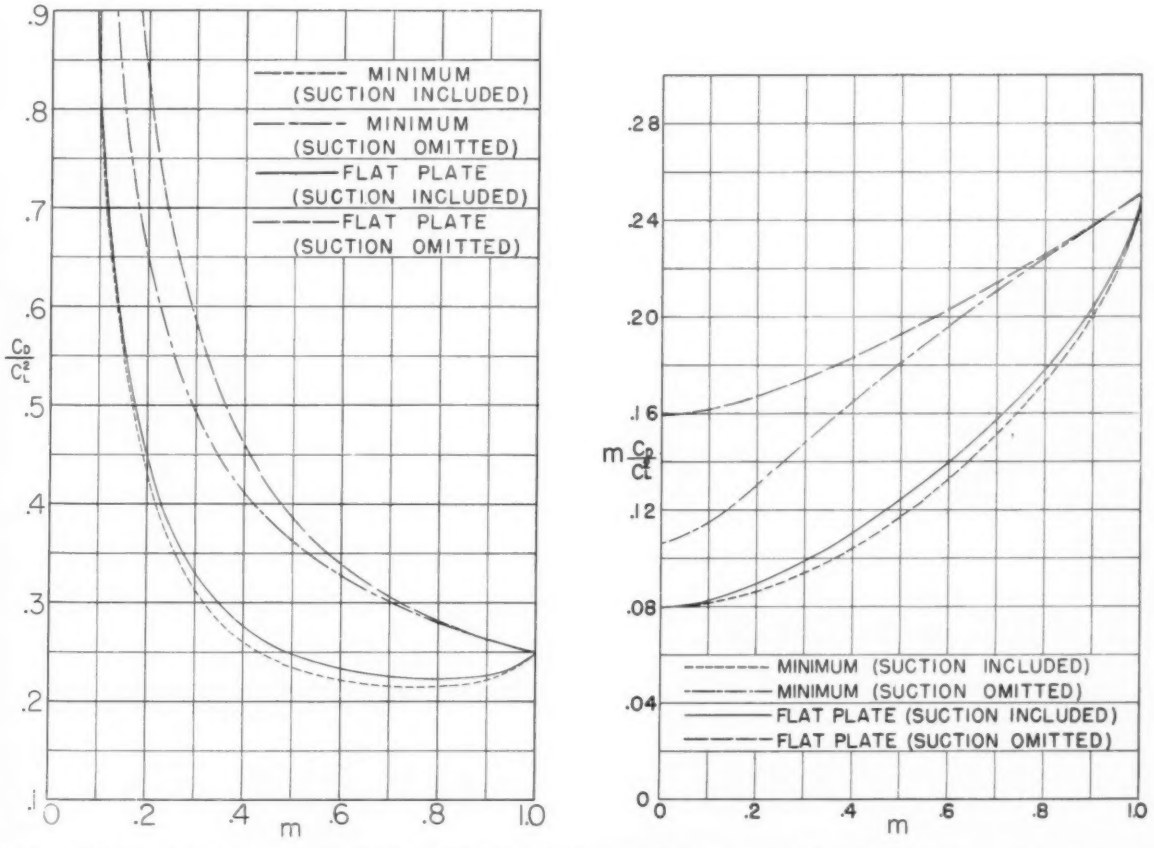

FIG. 8. Minimum C_D/C_L^2 and minimum C_D/C_L^2 multiplied by leading-edge slope for wings with parabolic chordwise camber (constant along span) at $M = \sqrt{2}$. Comparison with flat plate.

$$U_{2n'-1} = (-1)^{n-1} m \int \cos(2n-1)\theta \cos\theta d\theta$$
$$= (-1)^{n-1}(m/4)\left((\sin 2n\theta/n) + \{[\sin 2(n-1)\theta]/(n-1)\}\right) \quad \text{(A3)}$$

From Eqs. (3), (12), and (18)

$$dw_{2n'-1}/d\zeta = (-1)^{n-1}[(2n-1)/m^2]\{[\cos(2n-1)\theta]/(\sin\theta\cos\theta)\}\sqrt{1-m^2\sin^2\theta} \quad \text{(A4)}$$

Since U_{2n-1} is zero at $\zeta = 0$, m (or $\theta = 0$, $\pi/2$) and $w_{2n'-1}$ shows only logarithmic singularities at $\zeta = 0$ and is finite at $\zeta = m$, the first term in the right-hand side of Eq. (A2) vanishes. Thus,

$$\int_0^m u_{2n-1} w_{2n'-1}\, d\zeta = -\int_0^m U_{2n-1}\frac{dw_{2n'-1}}{d\zeta}\, d\zeta$$
$$= (-1)^{n+n'-1}\frac{2n'-1}{8}\left[\frac{1}{n}\int_0^{\pi/2}\frac{\sin(2n+2n'-1)}{\sin\theta}\sqrt{1-m^2\sin^2\theta}\, d\theta + \right.$$
$$\frac{1}{n}\int_0^{\pi/2}\frac{\sin(2n-2n'+1)\theta}{\sin\theta}\sqrt{1-m^2\sin^2\theta}\, d\theta + \frac{1}{n-1}\int_0^{\pi/2}\frac{\sin(2n+2n'-3)}{\sin\theta}\sqrt{1-m^2\sin^2\theta}\, d\theta +$$
$$\left.\frac{1}{n-1}\int_0^{\pi/2}\frac{\sin(2n-2n'+1)\theta}{\sin\theta}\sqrt{1-m^2\sin^2\theta}\, d\theta\right] \quad \text{(A5)}$$

The integrals $\int_0^{\pi/2}\frac{\sin\mu\theta}{\sin\theta}\sqrt{1-m^2\sin^2\theta}\, d\theta$ (μ odd) can be reduced to linear combinations of the parameters S_{2k} which are evaluated in Appendix (II).

APPENDIX (II)

Evaluation of $S_{2k} = \int_0^{\pi/2}\sin^{2k}\theta\sqrt{1-m^2\sin^2\theta}\, d\theta$

Since

$$\frac{d}{d\theta}(\sin^{2k-1}\theta\cos\theta\sqrt{1-m^2\sin^2\theta}) = (2k-1)\sin^{2k-2}\theta\sqrt{1-m^2\sin^2\theta} - 2k\sin^{2k}\theta\sqrt{1-m^2\sin^2\theta} -$$
$$\frac{m^2\sin^{2k}\theta}{\sqrt{1-m^2\sin^2\theta}} + \frac{m^2\sin^{2k+2}\theta}{\sqrt{1-m^2\sin^2\theta}} \quad \text{(A6)}$$

One has, by integrating both sides from $\theta = 0$ to $\theta = \pi/2$,

$$2k\int_0^{\pi/2}\sin^{2k}\theta\sqrt{1-m^2\sin^2\theta}\, d\theta = (2k-1)\int_0^{\pi/2}\sin^{2k-2}\theta\sqrt{1-m^2\sin^2\theta}\, d\theta -$$
$$m^2\int_0^{\pi/2}\frac{\sin^{2k}\theta}{\sqrt{1-m^2\sin^2\theta}}\, d\theta + m^2\int_0^{\pi/2}\frac{\sin^{2k+2}\theta}{\sqrt{1-m^2\sin^2\theta}}\, d\theta \quad \text{(A7)}$$

But

$$\int_0^{\pi/2}\frac{\sin^{2k}\theta}{\sqrt{1-m^2\sin^2\theta}}\, d\theta = -\frac{1}{m^{2k}}\int_0^{\pi/2}\frac{1-m^{2k}\sin^{2k}\theta}{\sqrt{1-m^2\sin^2\theta}} + \frac{K(m)}{m^{2k}} =$$
$$\{[K(m)-E(m)]/m^{2k}\} - (S_2/m^{2k-2}) - (S_4/m^{2k-4}) \ldots - (S_{2k-4}/m^4) - (S_{2k-2}/m^2) \quad \text{(A8)}$$

Hence, after rearranging terms

$$S_{2k} = \{1/[(2k+1)m^{2k}]\}\{(1-m^2)[K(m)-E(m)-m^2S_2-m^4S_4\ldots-m^{2k-4}S_{2k-4}] +$$
$$m^{2k-2}(2km^2-1)S_{2k-2}\} \quad \text{(A9)}$$

from which one can obtain

$$S_2 = [1/(3m^2)][(1-m^2)K(m) - (1-2m^2)E(m)] \quad \text{(A10)}$$
$$S_4 = [1/(5m^4)]\{(1-m^2)[K(m)-E(m)] + m^2(4m^2-1)S_2\} \quad \text{(A11)}$$
$$S_6 = [1/(7m^6)]\{(1-m^2)[K(m)-E(m)-m^2S_2] + m^4(6m^2-1)S_4\} \quad \text{(A12)}$$
$$S_8 = [1/(9m^4)]\{(1-m^2)[K(m)-E(m)-m^2S_2-m^4S_4] + m^6(8m^2-1)S_6\} \quad \text{(A13)}$$

$$S_{10} = [1/(11m^{10})]\{(1 - m^2)[K(m) - E(m) - m^2S_2 - m^4S_4 - m^6S_6 + m^8(10m^2 - 1)S_8]\} \quad \text{(A14)}$$

APPENDIX (III)

Effect of Chordwise Camber on Drag

The same method of approach for determining the minimum C_D/C_L^2 value of a conical wing can be extended to nonconical wings. This is illustrated by the following typical case—a delta wing with parabolic camber constant along span ($z \propto x^2 +$ constant) at $M = \sqrt{2}$. The results obtained will provide one with a rough idea of the relative merits of chordwise and conical cambers in drag reduction.

Similar to the conical case, one may put

$$u = a_1u_1 + a_2u_2 \quad \text{(A15)}$$

$$w = a_1w_1 + a_2w_2 \quad \text{(A16)}$$

where $u, w =$ the resultant nondimensional perturbed velocity components on top surface of the wing; $u_1, w_1 =$ the flat plate components; $u_2, w_2 =$ the components created by a wing with upwash at surface proportional to x; and $a_1, a_2 =$ arbitrary coefficients that are linear functions of C_L, coefficient of total lift. From references 15 and 9,

$$u_1 = m/\sqrt{m^2 - \zeta^2} \quad \text{(A17)}$$

$$w_1 = -(1/m)E(\sqrt{1 - m^2}) \quad \text{(A18)}$$

u_2, w_2 can be deduced from reference 18, such that, at $M = \sqrt{2}$,

$$u_2 = (x/CH)[(2m^2 - \zeta^2)/\sqrt{m^2 - \zeta^2}] \quad \text{(A19)}$$

$$w_2 = x/C \quad \text{(A20)}$$

where $C =$ root chord and

$$H = [(1 - 2m^2)/(1 - m^2)]E(\sqrt{1 - m^2}) + [m^2/(1 - m^2)]K(\sqrt{1 - m^2})$$

It can be shown that

$$C_{D_2} = \pi\left[\frac{\sqrt{1 - m^2}}{m}a_1^2 + \frac{4\sqrt{1 - m^2}}{3H}a_1a_2 + \frac{m}{2H^2}\sqrt{1 - m^2}\,a_2^2\right] \quad \text{(A21)}$$

$$C_D = \pi\left\{\left[\frac{2E(\sqrt{1 - m^2}) - \sqrt{1 - m^2}}{m}\right]a_1^2 + \left[\frac{4}{3} + \frac{2E(\sqrt{1 - m^2})}{H} - \frac{4\sqrt{1 - m^2}}{3H}\right]a_1a_2 + \frac{m}{2H}\left(3 - \frac{\sqrt{1 - m^2}}{H}\right)a_2^2\right\} \text{ (suction force included)} \quad \text{(A22)}$$

and

$$C_D = \pi\left\{\frac{2E(\sqrt{1 - m^2})}{m}a_1^2 + \left[\frac{4}{3} + \frac{2E(\sqrt{1 - m^2})}{H}\right]a_1a_2 + \frac{3m}{2H}a_2^2\right\} \text{ (suction force omitted)} \quad \text{(A23)}$$

at a lift coefficient

$$C_L = 2\pi[a_1 + (m/H)a_2] \quad \text{(A24)}$$

With Eqs. (A22), (A23), and (A24), one can determine the appropriate set of a_1 and a_2 for each case by certain minimization procedure.

Results are plotted in Fig. 8.

References

[1] Jones, R. T., *The Minimum Drag of Thin Wings in Frictionless Flow*, Journal of the Aeronautical Sciences, Vol. 18, No. 2, pp. 75–81, February, 1951.

[2] Jones, R. T., *Properties of Low-Aspect-Ratio Pointed Wings at Speeds Below and Above the Speed of Sound*, NACA TR 835, 1946.

[3] Adams, M. C., and Sears, W. R., *Slender-Body Theory—Review and Extension*, Journal of the Aeronautical Sciences, Vol. 20, No. 2, pp. 85–98, February, 1953.

[4] Pucket, A. E., *Supersonic Wave Drag of Thin Airfoils*, Journal of the Aeronautical Sciences, Vol. 13, No. 9, pp. 475–484, September, 1946.

[5] Henderson, A., Jr., *Supersonic Wave Drag of Nonlifting Delta Wings with Linearly Varying Thickness Ratio*, NACA TN 2858, December, 1952.

[6] Rott, N., *Minimum Drag Cambered Rectangular Wing for Supersonic Speeds*, Journal of the Aeronautical Sciences, Vol. 20, No. 9, p. 642, September, 1953.

(*Continued on page 843*)

An Investigation of the Bending of Angle Beams in the Plastic Range*

H. NORMAN ABRAMSON,† HARRY A. WILLIAMS,‡ AND BRUCE G. WOOLPERT**

Stanford University

SUMMARY

An earlier investigation[16] revealed the necessity for further study of the bending of unsymmetrical beams in the plastic range, inasmuch as twist occurs and has a marked effect.

Angle cross-section beams of 24 S-T aluminum-alloy material were subjected to bending in the plastic range with the plane of loading at various angles to the minor principal axis of the cross section. The moment was applied by means of an eccentric load with a relatively long moment arm.

For a simplified approach, it was found that Cozzone's method of plastic bending analysis[5] and an analysis based on an exponential relationship between stress and strain both gave reasonable correlation between theoretical and experimental bending moments in the plastic range beyond the yield strength. Both methods are approximate since they assume that the neutral axis does not rotate or translate and the cross section does not rotate. The exponential method is not valid in the range below the yield strength.

Other factors concerned with the general behavior of angle beams subjected to plastic bending are also considered.

SYMBOLS

a	= constant dependent upon the material for the exponential equation
a_c	= distance to point on neutral axis, in.
Δa_c	= change in a_c, in.
b	= length of short leg, in.
c	= general symbol for distances from neutral axis, in.
c_c, c_t	= distance from neutral axis to outer compressive and tensile fibers, respectively, in.
d, g	= symbols for particular cross-section dimensions, in.
e	= general symbol for strain, in./in.
e_c, e_t	= outer fiber compressive and tensile strain, respectively, in./in.
e_1 to e_{12}	= strains determined experimentally, in./in.
f_c, f_t	= stress determined from compression and tension tests, respectively, lbs. per sq.in.
f_p, f_y	= proportional limit stress and yield strength, respectively, from average stress strain curve, lbs. per sq.in.
f_m	= outer fiber bending stress, lbs. per sq.in.
f_{mc}, f_{mt}	= outer fiber compressive and tensile stress, respectively, lbs. per sq.in.
f_o	= Cozzone's intercept stress, lbs. per sq.in.
f_{oc}, f_{ot}	= intercept stress for compressive and tensile area, respectively, lbs. per sq.in.
k_c, k_t	= Cozzone's beam section constants
K	= constant in exponential equation, lbs. per sq.in.
x_n, y_n	= distance to point on rotated neutral axis, in.
E	= Young's modulus of elasticity, lbs. per sq.in.
I_x, I_y, I_{xy}	= moments and product of inertia of cross section with respect to x and y axes, in.^{4}
I_x', I_y'	= moment of inertia with respect to principal axis, in.^{4}
I_{N_c}, I_{N_t}	= moment of inertia of compressive and tensile areas, respectively, with respect to neutral axis, in.^{4}
K_f	= plastic stress function based on average stress-strain curve, lbs. per sq.in.
K_{fc}, K_{ft}	= plastic stress function based on compression and tensile stress-strain curves, respectively, lbs. per sq.in.
L	= moment arm to centroid at mid-span, in.
M_t	= experimental bending moment, in.-lbs.
M_{th}	= bending moment computed analytically, in. lbs.
M_{th}', M_{th}''	= bending moments computed analytically for compressive and tensile areas, respectively, in.-lbs.
n	= power to which e and ρ are raised in the exponential equation
P	= dynamometer load, lbs.
Q_{mc}, Q_{mt}	= statical moment of compressive and tensile areas, respectively, in.^{3}
r	= distance from neutral axis to an element in the beam cross section used in the derivation of the exponential equation, in.
t	= thickness of angle beam leg, in.
ΔT_c	= $\Delta a_c \sin \gamma$, in.
α	= angle between principal axis and neutral axis, deg.
$\Delta\alpha$	= change in angle α, deg.
θ	= angle between plane of loading and y axis, deg.
ϕ	= angle between plane of loading and normal to neutral axis, deg.
ρ	= radius of curvature, in.
γ	= angle between x-axis and neutral axis, deg.

Received August 27, 1954.

* The work reported in this paper was carried out under Air Force Contract W35-038 AC-16697 at Stanford University. The authors wish to express their appreciation to the Air Material Command for granting permission to publish these results.

† Formerly Research Assistant and student, Stanford University. Now, Associate Professor of Aeronautical Engineering, The A & M College of Texas.

‡ Professor of Civil Engineering, Stanford University.

** Formerly Assistant Professor of Civil Engineering, Stanford University.

INTRODUCTION

PURE BENDING in the plastic range when the applied loads are parallel to a principal plane of bending has been studied by a number of investigators.[1–10] When the loads are not parallel to a principal plane, the complexity of the problem increases many fold. The complexity is further increased when the beam cross section is not symmetrical with respect to a principal axis. Goodier's general solution of the problem for open sections[11] indicates the difficulties encountered even in the elastic case. It is seen at once that pure bending, as it is usually understood, does not prevail except under very restricted conditions.†† If the ap-

†† This general subject is discussed further in another paper.[12]

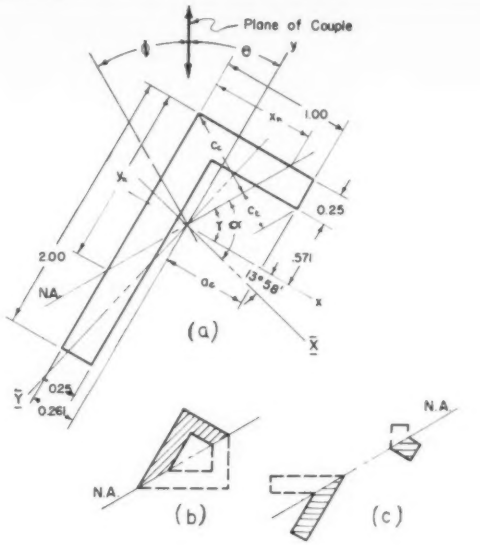

SECTION PROPERTIES								
Rectangular Axes				Principal Axes				
I_x = 0.2706				I_ξ = 0.2854				
I_y = 0.0456				I_η = 0.0308				
I_{xy} = 0.0600								
θ	α	Φ	I_ξ	I_η	Q_{max}	Q_{max}	C_ξ	C_η
0°	66°33'	52°35'	0.0330	0.0385	0.0929	0.0862	0.670	0.744
30°	83°37'	39°39'	0.0167	0.0173	0.0635	0.0622	0.507	0.518
60°	88°13'	14°15'	0.0140	0.0177	0.0581	0.0558	0.457	0.572
76° 07'	90°00'	-0°07'	0.0127	0.0183	0.0570	0.0537	0.434	0.592

FIG. 1 — ANGLE BEAM CROSS SECTION PROPERTIES

plied torsion and axial thrust are eliminated from Goodier's solution, it is evident that a torsion couple must still act at any cross section except the midpoint of the length unless all of the deflection is parallel to a principal plane. This couple produces twist, and it is evident that the relationship between components causing normal stress must vary along the length of the beam. Hence, the neutral axis must rotate also.

If plastic action prevails to any large extent, the various parts of an open section must be relatively heavy and the usual assumptions for shear flow might be questioned. The major obstacle to the solution of the plastic bending problem results, however, from the nonlinear relationship between stress and strain. This leads to even more complex relationships between moment and stress and eliminates the use of super position. Except in special cases, pronounced curvature results in considerable rotation.

It is evident that a rigorous solution of the problem of plastic bending of unsymmetrical beams must be developed from the concepts of pure plasticity[7–9]—e.g., Phillips presents the exact theory of combined pure bending and axial force for a prismatical bar[7] using the equations of the theory of plastic deformations. The solution of the differential equations is extremely difficult. Hence, it appears wise, for the benefit of the designer, to seek approximate but practical solutions which will give reasonably accurate results. Some attempts in this direction have already been made.[13–16]

In a previous investigation,[16] by one of the authors, of plastic bending when loads were not parallel to a principal plane, some exploratory tests of angle beams were made. A modification of Cozzone's approach[5] gave a resisting moment at the mid-span which was less than 15 per cent larger than the applied end moment until plastic instability occurred at which time the per cent difference increased rapidly.

The present investigation is an extension of the previous work. In planning the program it was decided to test beams of rather long span in order to accentuate rotation and to apply the end moments by means of a small eccentric load with a relatively large moment arm.* The primary purpose is to determine to what extent a relationship between bending moment at the mid-span and outer fiber stress will agree with the applied end moment if a simplified theoretical approach is used in the analysis. The resisting moment is computed by a modification of Cozzone's graphical method[5] and by an analytical method based on an exponential relationship between stress and strain. Both methods neglect rotation and other variables in the interests of simplicity. Data on rotation of the cross section and movement of the neutral axis are also presented to add information regarding the general behavior of the tested beams.

Apparatus and Test Procedures

Test Specimens and Stress-Strain Characteristics

The test specimens were machined to the dimensions shown in Fig. 1 from 24 S-T aluminum-alloy stock, 1 by 2 in. in cross section. Each beam had a clear span of 24 in. Photographs of some specimens after testing are shown in Fig. 2.

Considerable difference between the stress-strain curves in tension and compression exists for 24 S-T aluminum alloy, but inasmuch as this material is commonly used in practice, it was decided to use it rather than some other material which might have tension and compression curves that are in better agreement. All analytical computations were based upon an average stress-strain curve. Tension and compression samples from the original stock gave stress-strain data as indicated in Fig. 3. The curves of Fig. 3 were selected as being representative of the material and were used for all computations. Cozzone's intercept stress, f_o, is also shown in the figure.

Loading and Strain Apparatus and Testing Procedure

The arrangement of the loading apparatus used for bending the angle beams is shown in Figs. 4 and 5. The two lever arms, machined from 3/4-in. steel plate, were supported at one end by cables from an overhead beam

* As used in this report, rotation refers to twist and not to changes in end slope of the longitudinal axis.

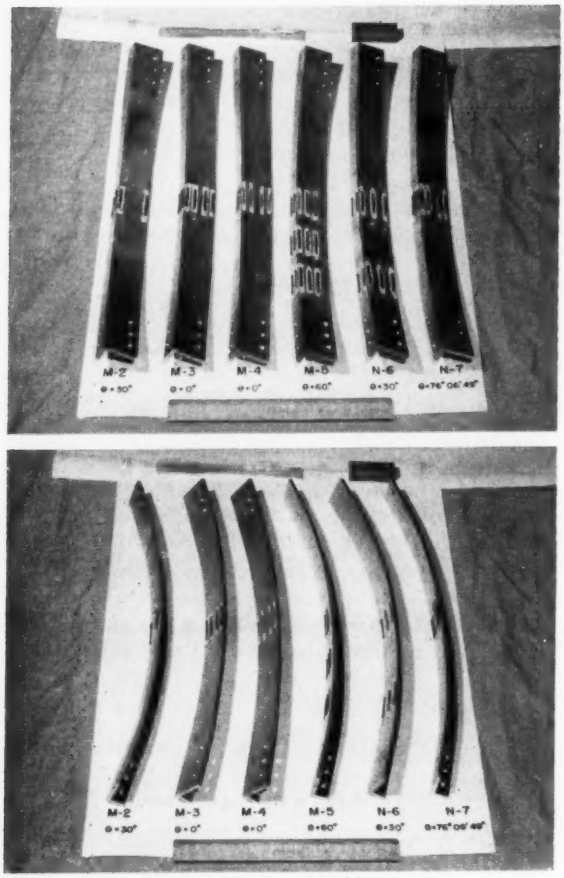

FIG. 2. Photographs of beams.

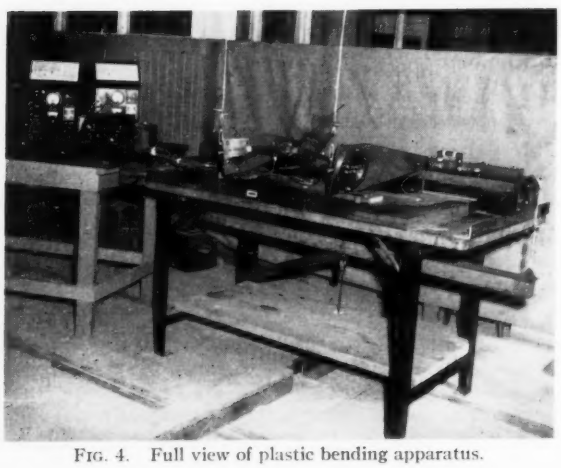

FIG. 4. Full view of plastic bending apparatus.

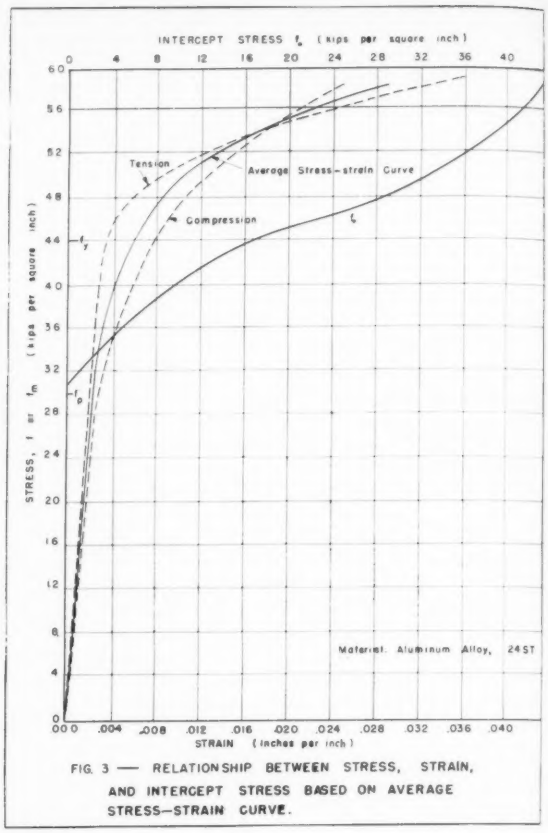
INTERCEPT STRESS f_o (kips per square inch)
Tension
Average Stress–strain Curve
Compression
STRESS, f or f_n (kips per square inch)
Material: Aluminum Alloy, 24ST
STRAIN (inches per inch)

FIG. 3 — RELATIONSHIP BETWEEN STRESS, STRAIN, AND INTERCEPT STRESS BASED ON AVERAGE STRESS–STRAIN CURVE.

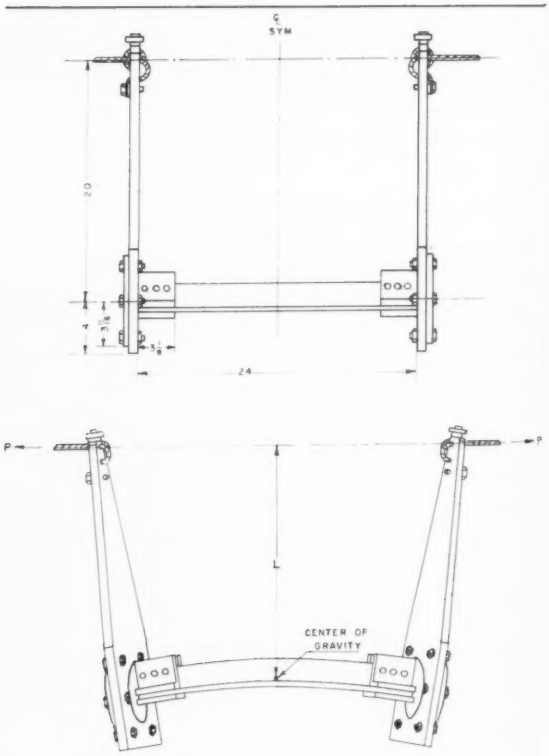

FIG. 5 — PLAN VIEW OF PLASTIC BENDING APPARATUS

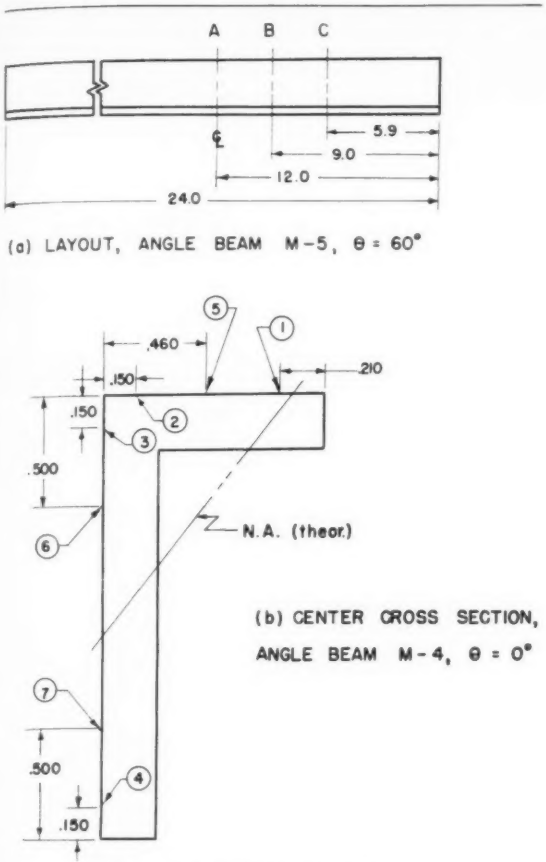

FIG. 6. Location of electric strain gages.

and at the other end by ball bearing rollers. Tracks for the rollers were attached to a heavy table immediately below the suspended arms and so arranged as to constrain the movement of the fore-end of the arms in a path perpendicular to the center line of the apparatus.

The arms at the cable end were provided with fittings which securely held the specimen in a position perpendicular to the two arms and parallel to the tracks, thus forming a rigid frame. The specimen fittings were further designed, by means of a movable disc which could be secured with a retaining ring, so that the specimen could be rotated about its lengthwise axis to provide any angle of bending desired. The load was applied through cables attached to the arms as shown. It is obvious from the loading arrangement that pure bending was only approximated, due to the presence of a small axial load.

Strain readings were taken with an SR-4 type indicator which is shown to the left of the bending apparatus in Fig. 4. The strains were measured at various points around the center cross section by SR-4 type A-12 electrical strain gages cemented to the specimen, as shown typically in Fig. 6.

The specimen was placed in the bending apparatus and adjusted to the desired angle of rotation. The normal testing procedure was to apply an increment of load, stop the testing machine, and immediately record the strain indicator readings; particular attention was given to the latter step, when in the plastic range, because of creep.

As the plastic range was reached, the decrease in moment arm resulting from the curvature of the beam was measured, at the same time that the strain readings were recorded. Rotation of the beam was also measured at that time.

Specimens were removed when the reduction in moment arm was sufficient to tend to prevent any increase in bending moment when additional load was applied. Generally, one or more of the electric strain gages had become inoperative at this point, and the maximum outer fiber strain was on the order of 2 per cent.

Analytical Procedures

Cozzone's Method

From reference 16, Cozzone's method[5] may be modified to apply to an angle beam if the rotation of the beam in the plastic range is neglected and the neutral axis is assumed to remain stationary. Neglecting these factors, an approximate solution may be found by dividing the cross section into a compression area and a tension area. The resisting moment of the compression area is obtained by assuming the symmetrical cross section shown in Fig. 1(b). The resisting moment of this beam is computed and divided by two. This is equivalent to computing I_{Nc} for one-half the cross section only. Then $k_c = [Q_{mc}/(I_{Nc}/c_c)]$ and the moment becomes

$$M'_{th} = (I_{Nc}/c_c)(1/\cos\phi)[f_{mc} + f_{oc}(k_c - 1)] \quad (1)$$

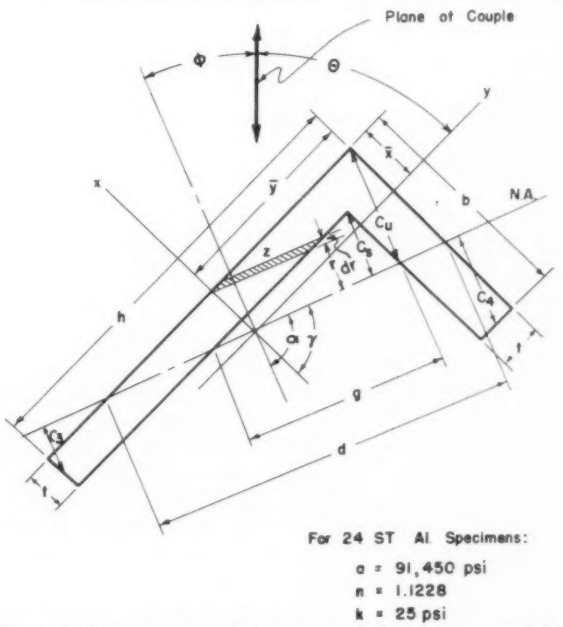

FIG. 7. Cross-section notation as used in the exponential solution for M_{th}.

A similar approach for the tension area Fig. 1(c) results in the equation

$$M''_{th} = (I_{Nt}/c_t)(1/\cos\phi)[f_{mt} + f_{ot}(k_c - 1)] \quad (2)$$

The final restraining moment is

$$M_{th} = M'_{th} + M''_{th} \quad (3)$$

The relationship between stress, strain, and intercept stress (f_o) based on an average stress-strain curve is presented in Fig. 3.

Exponential Method

An exponential relationship between stress and strain may be formulated which will closely approximate the stress-strain curve in the range of higher strains. This relationship takes the form

$$fe = ae^n - K \quad (4)$$

But it must be noted that when stress equals zero, strain is not zero although it may be made small through proper selection of the constant K.

If $e = r/\rho$ then Eq. (4) becomes

$$f = (ar^{n-1}/\rho^{n-1}) - (K\rho/r) \quad (5)$$

Table No. 1 - LOAD AND STRAIN DATA
Angle Beam M-4
$\theta = 0°$

Total Load	Mom. arm	Expt. bend. mom.	Measured strains						
P	L	M_t	e_1	e_2	e_3	e_4	e_5	e_6	e_7
(kips)	(in)	(in-kips)	(+)	(-)	(+)	(+)	(-)	(-)	(+)
			(in/in x 10^{-4})						
0	20.00	0	0	0	0	0	0	0	0
0.315	19.85	6.21	3.1	27.4	28.5	23.0	14.9	13.6	7.8
0.435	19.75	8.56	4.2	39.9	41.6	32.0	21.5	20.4	10.4
0.50	19.67	9.81	4.0	47.8	50.2	38.5	25.7	25.1	12.1
0.565	19.60	10.72	4.0	56.4	59.4	45.4	29.6	29.5	14.4
0.59	19.48	11.45	3.5	66.3	70.3	53.2	34.7	35.2	16.9
0.60	19.43	11.63	3.7	69.8	74.2	55.3	36.4	37.0	17.5
0.615	19.37	11.90	3.3	75.4	80.0	59.8	39.0	39.8	19.0
0.625	19.32	12.12	3.1	80.4	86.0	64.2	41.9	43.0	20.2
0.635	19.25	12.23	3.4	83.5	89.0	66.0	43.5	44.6	20.7
0.645	19.22	12.38	3.0	87.9	94.0	69.6	45.3	46.9	21.8
0.655	19.13	12.57	2.4	94.6	102	75.2	48.6	50.7	23.4
0.67	19.08	12.79	1.8	103	111	81.0	52.3	55.5	24.8
0.675	19.00	12.87	1.2	111	119	86.0	55.8	59.6	26.2
0.685	18.88	12.96	0	117	126	90.8	58.7	63.4	27.2
0.695	18.75	13.03	-2.0	128	139	98.2	63.0	70.1	28.5

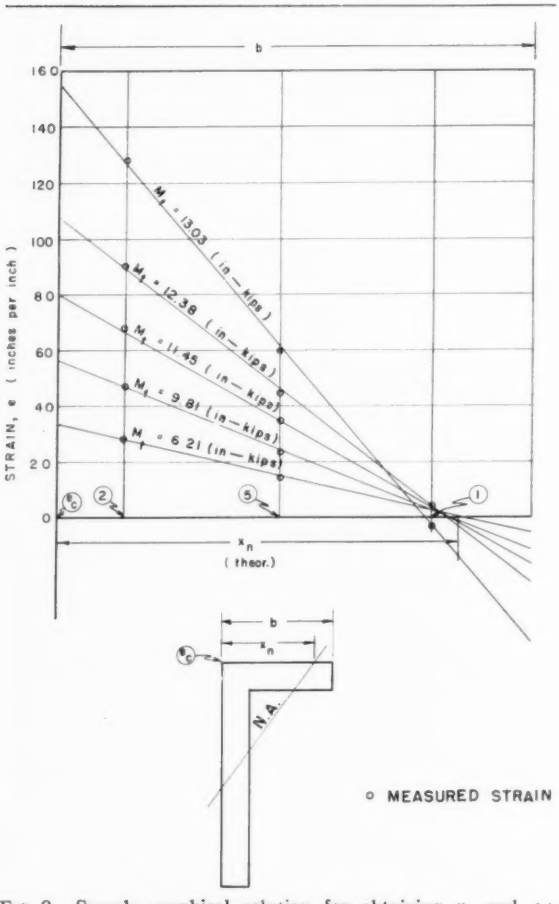

FIG. 8. Sample graphical solution for obtaining x_n and e_c; angle beam M-4, $\theta = 0°$.

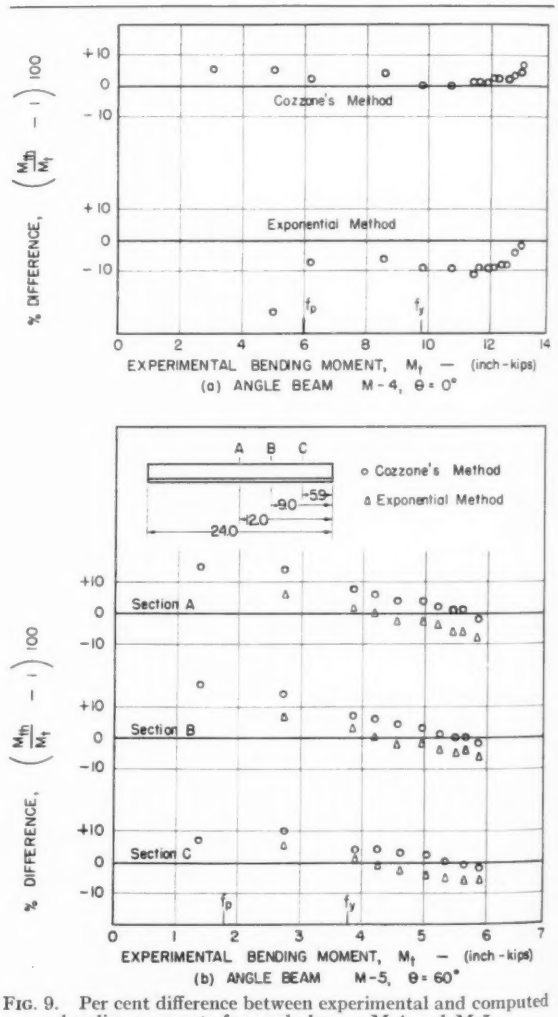

FIG. 9. Per cent difference between experimental and computed bending moments for angle beams M-4 and M-5.

Table No. 2 - THEORETICAL BENDING MOMENT
Angle Beam M - 4
$\theta = 0$

Expt. bend. mom.	[e]Rotation	[a]Neutral axis location		[a]Outer fiber strain		[b]Compression area			[b]Tension area			[b]Theoret bending moment (Cozz.)	[c]Radius of curvature	[c]Theoret bending moment (Expon.)
M_t		x_n	y_n	e_c	e_t	f_{mc}	f_{oc}	M'_{th}	f_{mt}	f_{ot}	M''_{th}	M_{th}	ρ	M_{th}
(in-kips)	(deg.)	(in)	(in)	(in/in x 10^{-4})		(ksi)	(ksi)	(in-kips)	(ksi)	(ksi)	(in-kips)	(in-kips)	(in)	(in-kips)
0	0	[d]0.840	[d]1.100	0	0	0	0	0	0	0	0	0	-	0
6.21	0.7	0.860	1.075	32.9	37.5	31.50	3.00	2.79	36.6	7.3	3.53	6.32	204	5.78
8.56	1.4	0.850	1.105	48.0	52.8	41.05	14.30	4.36	42.6	15.5	4.50	8.86	140	8.01
9.81	1.9	0.850	1.110	58.0	64.0	44.0	18.0	4.86	45.3	20.5	5.02	9.88	116	8.92
10.72	-	0.840	1.110	68.0	75.5	46.0	22.0	5.31	47.0	24.8	5.42	10.73	98.5	9.75
11.45	3.3	0.825	1.110	80.0	88.0	47.6	26.5	5.76	48.4	28.8	5.75	11.51	83.8	10.25
11.63	3.7	0.810	1.110	85.3	91.6	48.1	28.0	5.91	48.7	29.5	5.82	11.73	78.5	10.55
11.90	4.0	0.810	1.110	92.5	99.0	48.8	29.8	6.10	49.4	31.1	5.96	12.06	72.5	10.80
12.12	4.5	0.810	1.110	98.0	106.8	49.2	30.9	6.21	50.0	32.5	6.10	12.31	68.3	11.05
12.23	4.8	0.808	1.120	102.2	109.5	49.8	32,0	6.35	50.2	32.8	6.13	12.48	65.5	11.22
12.38	5.2	0.808	1.115	107.2	115.5	50.0	32.5	6.39	50.6	33.7	6.22	12.61	62.5	11.39
12.57	5.8	0.800	1.110	116.0	125.5	50.6	33.8	6.53	51.3	35.0	6.36	12.89	57.8	11.59
12.79	6.5	0.795	1.110	126	135	51.3	35.0	6.66	51.9	36.0	6.46	13.12	45.8	12.30
12.87	7.0	0.790	1.120	136	144	52.0	36.1	6.72	52.4	36.8	6.55	13.28	42.4	12.55
12.96	7.5	0.785	1.130	143	152	52.4	37.0	6.90	52.8	37.7	6.64	13.54	40.3	12.72
13.03	8.6	0.775	1.120	157	165	53.2	38.1	7.05	53.6	38.8	6.76	13.81	36.7	12.90

[a]From graphical solution assuming linear variation of strain.

[b]Resisting moment of compression and tension areas computed separately by Cozzone's method assuming neutral axis stationary:

$$M'_{th} = \frac{I_c}{c_c}\frac{1}{\cos\phi}\left[f_{mc} + f_{oc}(k_c - 1)\right] = 0.081(f_{mc} + 0.890\, f_{oc})$$

$$M''_{th} = \frac{I_t}{c_t}\frac{1}{\cos\phi}\left[f_{mt} + f_{ot}(k_t - 1)\right] = 0.0852(f_{mt} + 0.667\, f_{ot})$$

$$M_{th} = M'_{th} + M''_{th}$$

[c]Exponential equation: $M_{th} = \frac{21700}{\rho^{n-1}} - 27.05\,\rho$

[d]Theoretical value.

[e]Counterclockwise, referred to Figure 1.

In the case of angle beams, an expression for bending moment may be found as follows:

$$M_{th} = \frac{1}{\cos\phi}\left[\frac{a}{\rho^{n-1}}\frac{1}{(n+1)(n+2)}(d\,c_u^{n+1} - g\,c_s^{n+1}) - \frac{K\rho}{2}(d\,c_u - g\,c_s) + \frac{tc_3}{\cos\gamma}\times\left(\frac{a}{\rho^{n-1}}\frac{c_3^{n}}{n+1} - K\rho\right) + \frac{tc_4}{\sin\gamma}\left(\frac{a}{\rho^{n-1}}\frac{c_4^{n}}{(n+1)} - K\rho\right)\right] \tag{6}$$

where all notation is referred to Fig. 7. A derivation of Eq. (6) may be found in the Appendix.

Comparison of Bending Moments

It is easier to compare experimental and computed bending moments in the plastic range than to compare outer fiber stresses; hence, the general procedure of this paper has been to take the experimental strain corresponding to a given load, determine the necessary stress values from a representative stress-strain curve and then insert these in the appropriate formula to compute the so-called "theoretical bending moment."

The ratio of M_{th}/M_t has been taken as the criterion for comparison of bending moments.

Results and Discussion

In the interest of brevity, detailed information is presented for a single typical angle beam—namely, M-4, $\theta = 0°$—and only the important results for certain of the other specimens tested are given. In particular, results are shown for beams tested with the plane of loading at angles of 0°, 30°, 60°, and 76° 07′ to the minor principal axis of the cross section.

Strain Measurements

Typical load and strain data are presented in Table 1, where the particular strain gage locations are shown in Fig. 6(b).

In general, strain readings agreed reasonably well for two specimens tested under the same conditions. With some exceptions, the difference was not more than 5 per cent in the elastic range and 10 per cent in the plastic range. The latter might be partially explained by the nonuniformity of the material itself and by the difficulty in locating SR-4 gages exactly the same on duplicate specimens. Such discrepancies, however, did not greatly effect the computed bending moment because even large differences in outer fiber strain did not affect the stress values when working on the higher range of the stress-strain curve, where the slope is small.

Maximum Strains and Neutral Axis Locations

Maximum compressive strain (e_c), maximum tensile strain (e_t), location of neutral axis intersection with the outside of the short leg (x_n), and location of neutral axis intersection with the outside of the long leg (y_n) were all found by a graphical method which assumes a linear variation of strain across each face of the beam. A sample solution—for beam M-4, $\theta = 0°$—illustrating the method is given in Fig. 8. The procedure was to lay out to scale a leg of the beam with proper gage locations and for a given load plot the strains for each gage perpendicular to the leg. A straight line connecting all strains for a particular bending moment was drawn, from which e_c (or e_t) and x_n (or y_n) could be read directly. Table 2 presents these data for beam M-4.

One would expect the outer fiber strains to become less exact when determined as described above as the rotation and warping increases. However, such errors should have little effect on bending moment in the plastic range.

The x_n and y_n values are approximations only because these distances are quite sensitive to small change in strain. When a gage was near the neutral axis and the strains were relatively small, the effect of errors in the strain was quite pronounced. However, the results when considered collectively indicate definite trends.

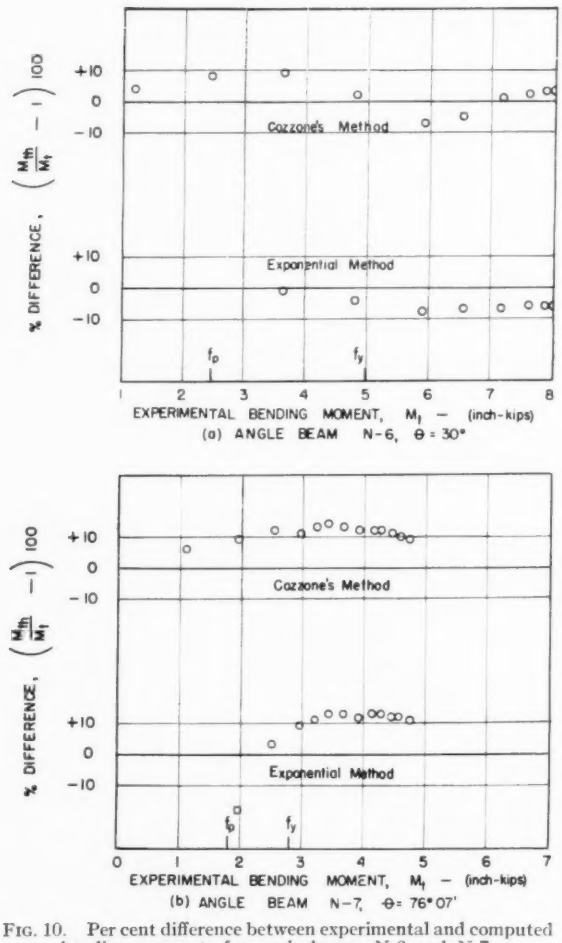

FIG. 10. Per cent difference between experimental and computed bending moments for angle beams N-6 and N-7.

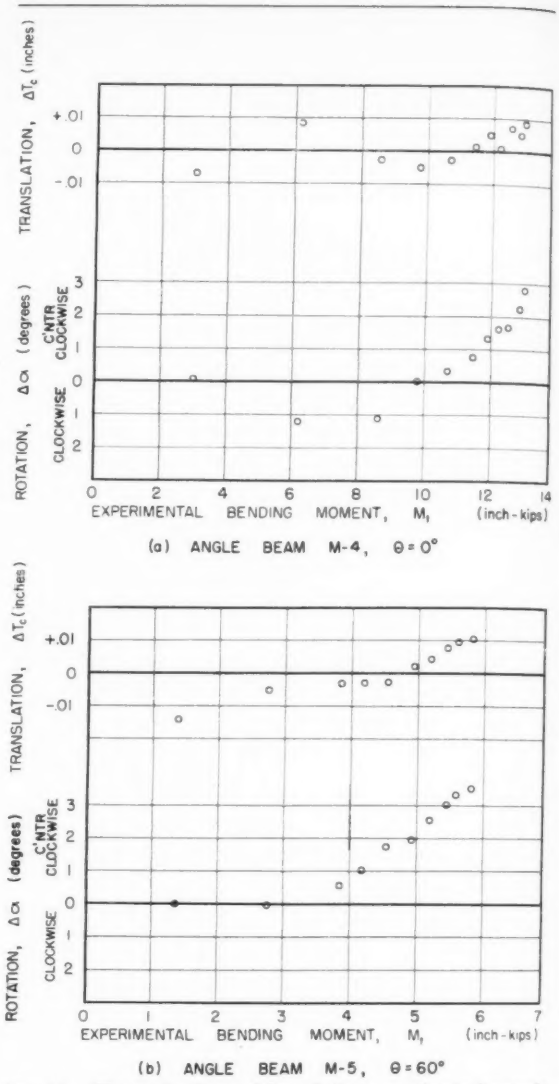

FIG. 11. Change in the position of the neutral axis for angle beams M-4 and M-5.

Theoretical Versus Experimental Bending Moments

Theoretical bending moments were computed from Eqs. (3) and (6). The per cent differences between theoretical and experimental bending moments were computed from the expression $(M_{th}/M_t - 1) \times 100$ per cent. A computation table for theoretical bending moment by both Cozzone's method and the exponential method is presented for the typical angle beam M-4 in Table 2. The values for all beams are presented graphically in Figs. 9 and 10. For comparative purposes, results for different angles of loading are shown on the same figures. The elastic, partially-elastic, and plastic ranges are shown on these graphs by indicating on the moment scale the approximate values of the experimental moment at which the proportional limit, f_p, and

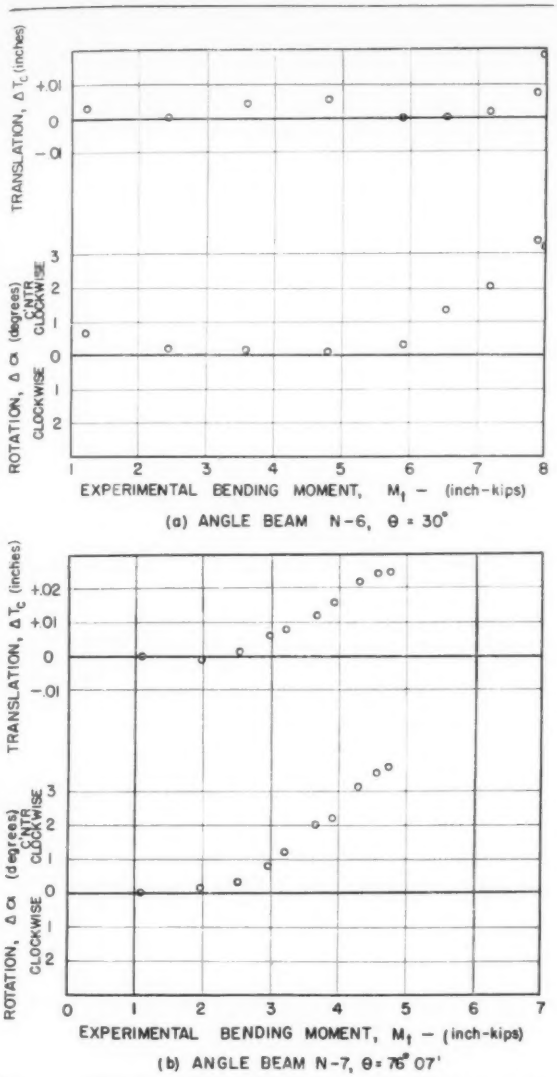

FIG. 12. Change in the position of the neutral axis for angle beams N-6 and N-7.

the 0.2 per cent offset yield strength, f_y, were reached in the outer fibers of the beam in question.

An inspection of Figs. 9 and 10 shows that theoretical bending moment was generally within approximately 10 per cent of the experimental moment in the plastic range beyond the yield strength for both Cozzone's method and the exponential method. The differences in the range below the yield strength were approximately the same for Cozzone's method but very much greater for the exponential method, which is to be expected in view of the fact that the exponential relationship between stress and strain should not be used below the yield strength. In certain cases where the twist was large, the differences were slightly greater.

Beam M-5 which was tested at 60° gave results consistent with other specimens. It is seen from Fig. 1 that the neutral axis makes an angle of less than 2° with the principal axis. There was little rotation of the cross section. It was then decided to test beam N-7 in such a position that the neutral axis coincided with the principal axis ($\theta = 76° 07'$). The results showed negligible rotation of the cross section although the rotation and translation of the neutral axis were consistent with other specimens. However, the difference between the computed and experimental bending moment appears out of line with the results for the 60° beam, M-5.

Change in Position of the Neutral Axis

Figs. 11 and 12 show the rotation and translation of the neutral axis for the various beams. The values of $\Delta\alpha$ and ΔT_c may be computed from the expressions

$$\Delta\alpha = (90° - \alpha) - \tan^{-1}(x_n/y_n) + 13° 58' \quad (7)$$

$$\Delta a_c = 0.261 + 0.760(x_n/y_n) - x_n \quad (8)$$

$$\Delta T_c = \Delta a_c \sin(\alpha - 13° 58') \quad (9)$$

These expressions are derived from simple geometrical

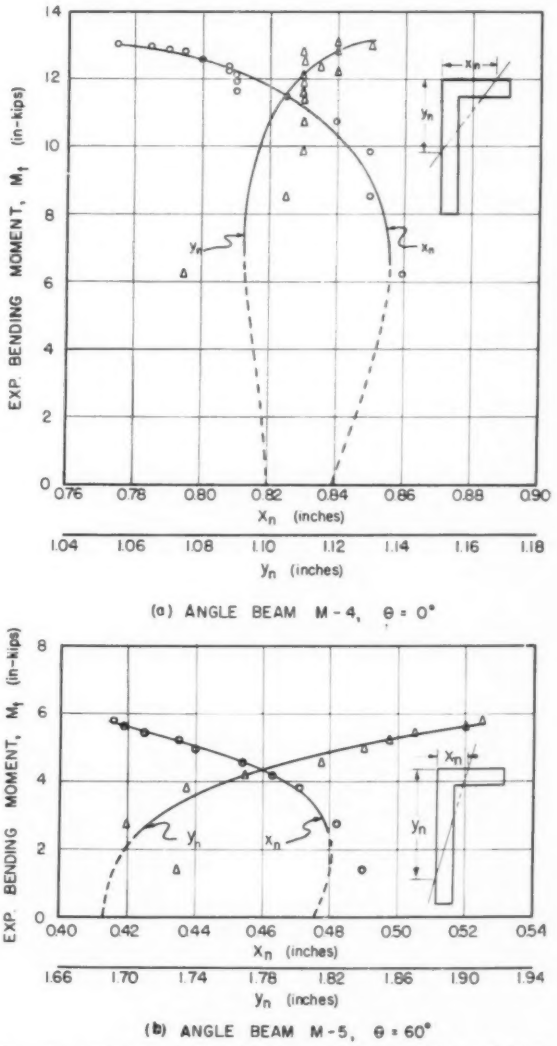
EXP. BENDING MOMENT, Mf (in-kips)
Xn (inches)
yn (inches)
(a) ANGLE BEAM M-4, θ = 0°
EXP. BENDING MOMENT, Mf (in-kips)
Xn (inches)
yn (inches)
(b) ANGLE BEAM M-5, θ = 60°

FIG. 13. Neutral axis location for angle beams M-4 and M-5.

relationships referred to in Fig. 1. The angle $\Delta\alpha$ is considered positive when the neutral axis rotates clockwise. Δa_c is positive if it represents an increase in a_c. When $\Delta T_c = \Delta a_c \sin\alpha$ is positive, it indicates that the neutral axis is translating toward the compression side of the beam. It should be noted that all of these changes are with respect to the axes of the cross section. Obviously they are intimately related to the cross-section rotation as will be discussed in the next section.

In general, rotations were all counterclockwise and were of the order of magnitude of 3° to 4° for all beams. The translations were all positive and of an order of magnitude of 0.01 in. except for angle beam N-7 for which it was approximately 0.02 in.

The same information is presented in another manner in Figs. 13 and 14 by plotting the values of x_n and y_n against applied moment. Since x_n and y_n were obtained by graphical methods, the values are approximate only. Curves have been indicated to show general trends. When the curves move in the same direction, translation is indicated; when they move in opposite directions and cross over, rotation is indicated.

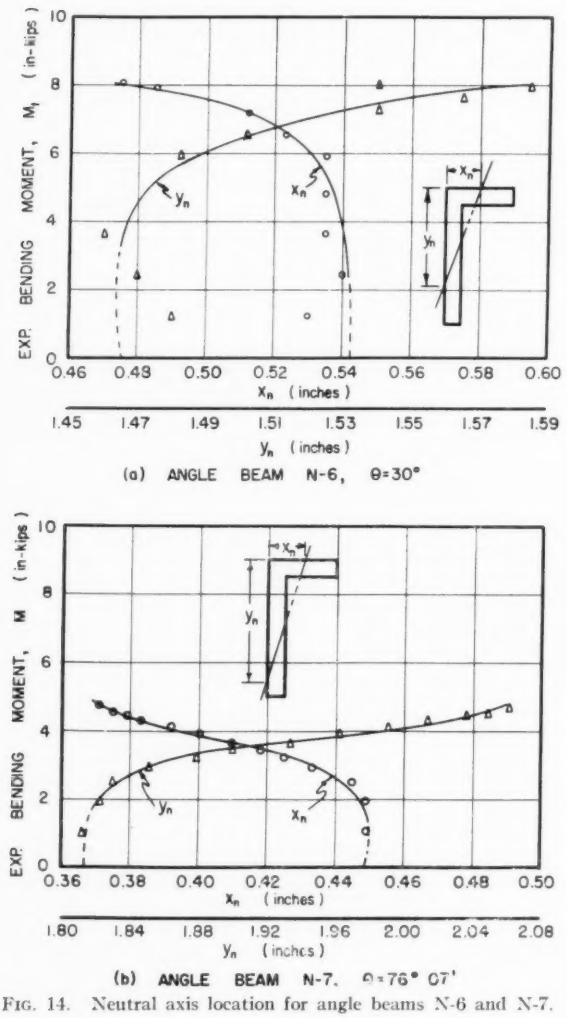

FIG. 14. Neutral axis location for angle beams N-6 and N-7.

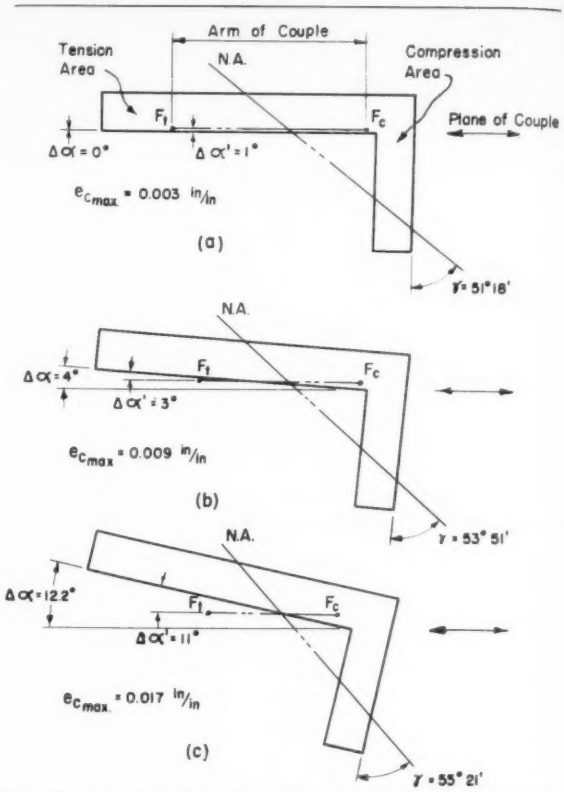

FIG. 15. Location of resisting couple at mid-span for three stages of rotation. Angle beam M-4, $\theta = 0°$.

Behavior of Resisting Couple at Mid-Span as Cross Section Rotates

The torsion couple which causes the beam to rotate must be equal to zero at the mid-span because of symmetry. Hence, the only couple acting at this section is the conventional bending moment couple. Also, equilibrium conditions demand that it be equal in magnitude and opposite in direction to the external couple. It must also lie in a plane which is parallel to that of the latter.

The location of the resisting couple for beam M-4 is shown in Fig. 15 for three stages of loading. The resultant tensile and compressive forces are F_t and F_c, respectively, and are located approximately to scale. The forces are evaluated and located by graphical integration. The difference in magnitudes was as follows:

	External Moment (in.-kips)	F_t (kips)	F_c (kips)	Arm (in.)	Resisting Couple (in.-kips)
(a)	6.21	5.0	4.7	1.24	5.52
(b)	11.90	10.3	10.6	1.00	10.45
(c)	13.03	13.7	13.2	0.86	11.55

It is seen that the percentage difference remains essentially constant with increasing load. Some error is introduced by the graphical solution, and also by the fact that the true external moment couple does not remain in a horizontal plane but rotates slightly as the

beam deflects vertically. Hence, its magnitude becomes increasingly larger than PL and the rotation is counterclockwise in Fig. 15. It will be noted that the resisting couple rotates in the same direction.

The sketches of Fig. 15 also show that the neutral axis rotates considerably less with respect to the cross section than the latter rotates with respect to its original position. This difference depends on the shape of the cross section and on the degree of plasticity. In this case, when the left-hand tip of the tension leg becomes stressed beyond the proportional limit, a "softening" results and the resultant, F_t, moves toward the neutral axis and away from the "soft" area. When the stress at the outer compressive corner moves into the plastic range, a similar shift is made by F_c. Since the resisting couple must remain parallel to the plane of the external couple, the neutral axis rotation must be adjusted with the cross-section rotation so that the stress distribution satisfies equilibrium conditions.

Deviation from Pure Bending

As mentioned earlier, the bending apparatus used only roughly approximated pure bending. Actually, an axial stress having a maximum value of approximately 1000 lbs. per sq. in. existed. Quite often in practice combined loadings of this type are encountered; to this extent, the investigation of this paper more nearly approaches practical applications. In contrast, a rigorous method of analysis for the loading used is considerably more difficult than for pure bending. However, it has been shown that an analysis which assumes pure bending gave fairly consistent results nonetheless. Since rotation was neglected, the agreement resulted, to a certain extent, from the fact that errors were partially compensating and that moment was not particularly sensitive to strain variations in the plastic range.

As a matter of interest, strain gages were placed on beam M-5 at the stations A, B, C, shown in Fig. 6(a). The detailed results are not shown, however the moment arm was corrected for the different degrees of curvature existing at stations B and C. Inspection of the data shows that strains were essentially constant at the three stations. This is partially accounted for by the fact that while the resultant moment couple increased from A to C, the bending couple about the neutral axis remained approximately constant after the tension component was subtracted. However, the x_n and y_n values show that the neutral axis location was different at each station as might be expected. The per cent difference in bending moment for the three stations are shown in Fig. 9(b); they are in close agreement.

Conclusions

Since rotation of the beam cross section and of the neutral axis were neglected in the analysis, any conclusion must be confined to the particular beam shape used in the experiments. If the analysis is extended to shapes having essentially different proportions from the one reported in this investigation, the differences between a theoretically computed bending moment and the actual moment might easily be several times as large as these reported.* This statement also applies if another type of loading is used. The method should be extended with caution to materials having essentially different stress-strain characteristics.

The following conclusions can be drawn from the results of this particular investigation:

(1) A modification of Cozzone's method of plastic bending analysis[5] gave approximate but reasonable results. For the particular material and configuration investigated, the correlation between computed and experimental bending moments in the semiplastic and plastic ranges was within 10 per cent.

(2) An exponential relationship between stress and strain also gave reasonable results. For the particular material investigated, the correlation between computed and experimental bending moments in the plastic range beyond the yield strength was within 10 per cent. The method is not valid for the range below the yield strength. Simplification of the method appears to be possible but requires further study.

(3) Rotation of the cross section was the primary factor limiting the ultimate strength of the beams. This rotation cannot be included in a simplified analysis such as was used in this investigation.

Appendix

Derivation of the Exponential Equation for Theoretical Bending Moment of an Angle Beam†

A number of equations relating stress to strain beyond the proportional limit have been suggested. Several of these were investigated by the authors with the view of developing a suitable flexure formula for an angle cross section. Many of the expressions lend themselves quite readily to a simple formula for a rectangular beam with loads in a principal plane but become quite complicated for more general solutions.

It was noticed that when the product fe was plotted against e for a number of materials, the outer portion of the curve approximated the form

$$fe = ae^n$$

It was noticed further that this expression could be modified by conventional methods[17] so that it also roughly approximated the straight line portion of the stress-strain curve by writing it in the form

$$fe = ae^n - K \quad \text{or} \quad f = ae^{n-1} - K/e \qquad \text{(A1)}$$

It is evident that this curve does not pass through the origin when $e = 0$; however, K can be adjusted so that

* Some results for rectangular and I-section beams are given in another paper.[12]

† The exponential equation has been derived for beams of rectangular and I-section in another paper.[12]

it passes quite close to the origin. Using this equation as a basis, approximate expressions can be derived for an angle beam.

If no warping of cross sections occurs (all notation referred to Fig. 7)

$$\epsilon = (r/\rho) \qquad \text{and} \qquad f = (ar^{n-1}/\rho^{n-1}) - (K\rho/r) \quad \text{(A2)}$$

Considering the area above the neutral axis—i.e., the compression area:

$$\left.\begin{aligned} &\text{Outer triangle:}\\ &M'_\Delta = \int frzdr, \quad \text{where} \quad z/d = (c_u - r/c_u)\\ &\quad = d\left[\frac{ac_u^{n+1}}{\rho^{n-1}}\left(\frac{1}{(n+1)(n+2)} - \frac{K\rho c_u}{2}\right)\right] \end{aligned}\right\} \quad \text{(A3)}$$

$$\text{Inner triangle: } M''_\Delta = g\left[\frac{ac_s^{n+1}}{\rho^{n-1}}\left(\frac{1}{(n+1)(n+2)} - \frac{K\rho c_s}{2}\right)\right] \quad \text{(A4)}$$

and

$$M_\Delta = M'_\Delta - M''_\Delta = \frac{a}{\rho^{n-1}}\frac{1}{(n+1)(n+2)}(dc_u^{n+1} - gc_s^{n+1}) - \frac{K\rho}{2}(d\,c_u - gc_s) \quad \text{(A5)}$$

Considering the area below the neutral axis—i.e., the tension area:

$$\left.\begin{aligned} &h - \text{leg:}\\ &M_h = \int frzdr\\ &\quad = t/\cos\gamma\,[(a/\rho^{n-1})(c_3^{n+1}/n+1) - K\rho c_3] \end{aligned}\right\} \quad \text{(A6)}$$

$$b - \text{leg:}\quad M_b = (t/\sin\gamma)\{(a/\rho^{n-1})[c_4^{n+1}/(n+1)] - K\rho c_4\} \quad \text{(A7)}$$

The component $M_{th}\cos\phi$ of the bending moment resisted by bending about the neutral axis is the sum of Eqs. (A5), (A6), and (A7). This leads to the value of M_{th} given as Eq. (6) in the body of the paper.

Discussion of the Exponential Method

Values of n and K for materials similar to the one of the present investigation are not difficult to determine, by the method of reference 17, when applied to the stress-strain curve of the material in question.

An exploratory investigation aimed at simplifying the exponential method would appear to indicate that for the portion of the stress-strain curve beyond the yield strength, Eq. (6) may be modified by setting $K = 0$. The effect is to increase slightly the value of the computed bending moment. Again, such a generality applies only to the particular conditions of this report.*

References

[1] Timoshenko, S., *Strength of Materials*, Part II, 2nd Ed., Chapt. 8; D. Van Nostrand Co., Inc., New York, 1941.

[2] Beilschmidt, J. L., *The Stresses Developed in Sections Subjected to Bending Moment*, Journal of the Royal Aeronautical Society, Vol. XLVI, No. 379, pp. 161–182, July, 1942.

[3] Osgood, W. R., *Plastic Bending*, Journal of the Aeronautical Sciences, Vol. 11, No. 3, pp. 213–226, July, 1944.

[4] Rappleyea, F. A., and Eastman, E. J., *Flexural Strength in the Plastic Range of Rectangular Magnesium Extrusions*, Journal of the Aeronautical Sciences, Vol. 11, No. 4, pp. 373–377, October, 1944.

[5] Cozzone, F. P., *Bending Strength in the Plastic Range*, Journal of the Aeronautical Sciences, Vol. 10, No. 5, pp. 137–151, May, 1943.

[6] Williams, H. A., *Pure Bending in the Plastic Range*, Journal of the Aeronautical Sciences, Vol. 14, No. 8, pp. 457–469, August, 1947.

[7] Phillips, A., *Pure Bending with Axial Force in the Theory of Plastic Deformations*, Stanford University Technical Report No. 3, January, 1949.

[8] Phillips, A., *On Symmetrical Pure Bending of Beams*, Stanford University Technical Report No. 4, August, 1949.

[9] Phillips, A., *A General Method of Calculating the Me_{max}. Diagrams in Plastic Bending of Beams*, Journal of Applied Mechanics, Vol. 18, No. 4, pp. 353–358, December, 1951.

[10] Horowicz, M. I., *Moment of Resistance of Beams Stressed Beyond the Elastic Limit*, Aircraft Engineering, Vol. 23, No. 263, pp. 9–14, January, 1951.

[11] Goodier, J. N., *Flexural-Torsional Buckling of Bars of Open Section Under Bending, Eccentric Thrust or Torsional Loads*, Cornell University Experiment Station, Bull. No. 28, January, 1942.

[12] Williams, H. A., *Stability of Rectangular and I Section Beams in the Plastic Range*, Technical Report No. 8, Air Forces Contract W33-038 Ac-16697, June 1, 1949.

[13] Aghbabian, M. S., and Popov, E. P., *Unsymmetrical Bending of Rectangular Beams Beyond the Elastic Limit*, Proc. First U. S. National Congress of Applied Mechanics, pp. 579–587, ASME, 1952.

[14] Barrett, A. J., *The Bending of Some Common Beam Sections into the Plastic Range*, Journal of the Royal Aeronautical Society, Vol. 57, No. 506, pp. 110–115, February, 1953.

[15] Barrett, A. J., *Unsymmetrical Bending and Bending Combined with Axial Loading of a Beam of Rectangular Cross Section into the Plastic Range*, Journal of the Royal Aeronautical Society, Vol. 57, No. 512, pp. 503–509, August, 1953.

[16] Williams, H. A., *An Investigation of Pure Bending in the Plastic Range When Loads Are Not Parallel to a Principal Plane*, NACA TN 2287, February, 1951.

[17] Davis, D. S., *Empirical Equations and Nomography*, 1st Ed., pp. 11–14; McGraw-Hill Book Co., Inc., New York, 1943.

* Inasmuch as the unmodified exponential Eq. (6) usually gives values for the computed bending moment which are less than the experimental moment, the modification just mentioned would apparently tend to bring the computed and experimental moments into closer agreement.

Transient Temperature Distributions and Thermal Stresses in a Skin-Shear Web Configuration at High-Speed Flight for a Wide Range of Parameters*

H. SCHUH†

Royal Institute of Technology, Stockholm, Sweden

ABSTRACT

The temperature distribution and thermal stresses are calculated in a configuration consisting of a skin and identical webs equally spaced for which only particular examples have hitherto been calculated. The basic differential equations for the temperature distribution are brought into a suitable dimensionless form, and it is shown that the variables determining the problem can be grouped into two dimensionless parameters provided the distance between the webs is not much smaller than about half their height, which is the case in most practical applications. By this reduction of variables a general solution of the problem is made practicable. Further, two asymptotic solutions of the temperature distributions are shown to exist which are well known from certain heat flow problems. For cases with the same material in the web and the skin, diagrams are given for the thermal stresses as functions of the two parameters mentioned above and of an additional parameter which comes in when calculating the stresses. Diagrams are also given of the temperature distribution, and, with their help, complete stress distributions can be calculated by a simple formula even if the skin and the web are of different materials.

SYMBOLS

a = length in Fig. 1(c), see also Eq. (1)
A = constant occurring in Eqs. (25) and (26)
b = length in Fig. 1(c), see also Eq. (2)
c = specific heat, skin-friction coefficient (c_f)
d = thickness of skin or web
g = parameter defined in Eq. (17)
h = $\alpha/(\rho_2 c_2 d_2)$
H = altitude above sea level
k = heat conductivity
l = length of turbulent boundary layer on aircraft surface
L = half the pitch of the web in Fig. 1(b)
M = Mach Number
N = half the height of the web in Fig. 1(b)
p = defined in Eq. (30)
Pr = Prandtl Number
R = parameter defined in Eq. (21)
Re = Reynolds Number of boundary layer based on boundary-layer length l
t = time
T = temperature
u = speed of aircraft
x = distance from middle of web
α = coefficient of heat transfer from aircraft surface to air
β = coefficient of linear thermal expansion
γ = ratio of specific heat at constant pressure and constant volume
δ = thickness of heat insulating layer
ϵ = strain; emissivity
ϑ = dimensionless temperature
θ = dimensionless mean temperature defined in Eq. (31)
κ = diffusivity
ξ = dimensionless distance defined in Eqs. (11) and (13)
ρ = density
σ = stress
τ = dimensionless time
φ = constant defined in Eq. (29)

Subscripts

1 = web
2 = skin
a = air
f = boundary layer, friction
g = total (at heat-transfer coefficient)
i = initial values
l = heat insulating layer
m = maximum
p = constant pressure
r = occurring in Eq. (34)
s = static temperature

Received September 17, 1954.

* This paper is essentially identical with KTH AERO RAPPORT FL 161, issued by Royal Institute of Technology, Division of Aeronautics, Stockholm, Sweden.

† Now with Svenska Aeroplan Aktiebolaget (SAAB), Linköping, Sweden.

(1) INTRODUCTION

SERIOUS PROBLEMS arise in supersonic flight due to the heat produced by friction of the air. One of these is thermal stresses that occur through temperature differences within the aircraft structure. These stresses may be due to steady temperature differences—for instance, those produced by the heat of the engine—or they may be of a transient kind, occurring through temperature differences set up by a change in aircraft speed or altitude. Because it takes only a short time to change the speed of an aircraft in comparison with the time required for leveling temperature differences in solids by heat conduction, the temperatures of different parts of the aircraft structure may differ appreciably, giving rise to thermal stresses. The present paper deals with some aspects of these transient phenomena. Evidently the first step is to determine the temperature distribution within the aircraft structure. To do this for a whole aircraft is a time-consuming task and results will have little general value because of the number of parameters involved. General information can be obtained if simple models are investigated. As such, an airfoil section is assumed here consisting of a skin reinforced by shear webs [see Fig.

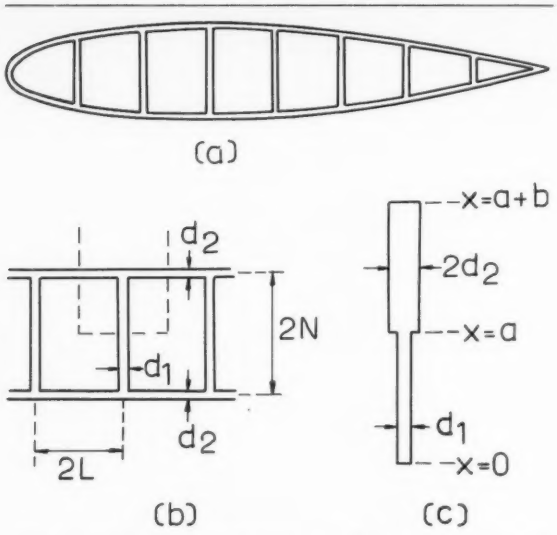

FIG. 1. (a) Wing structure consisting of skin with reinforcing webs. (b) Wing structure of section (a) replaced by identical webs equally spaced. (c) Simplified model used for analysis corresponding to parts of section (b) lying within dotted line.

1(a)]; it is further simplified for the present purpose by assuming the webs to be identical and equally spaced as shown in Fig. 1(b). This model was previously treated in references 1, 2, and 3 and a number of solutions have been obtained for certain particular values of relevant parameters. Altogether about nine examples have been investigated, however the variation of the parameters has been limited, so that general conclusions drawn from these examples are rather uncertain. For instance, only one value of the heat-transfer coefficient has been assumed in all the examples. In this paper solutions have been obtained for a continuous variation of the parameters within such a range as appears of practical importance. In the present case the great majority of the work is involved in the calculation of the temperature distribution: once this is known the thermal stresses can be calculated by a simple formula.

(2) Analytical Treatment of the Problem

It is assumed that the same amount of heat is exchanged at the upper and the lower surface, hence the temperature distribution will be symmetrical and only half the model need be considered. Further, the model is replaced by a bar [see Fig. 1(c)] consisting of two parts with different cross sections: one (from $x = 0$ to $x = a$) corresponding to the web and the other (from $x = a$ to $x = a + b$) to the skin. The temperature is assumed constant in the direction normal to the surface of the skin and the web. In the immediate neighborhood of the junction of both this assumption does not hold and in order to account for it, if necessary, the relation of the quantities a and b in Fig. 1(c) to half the height of the web N and half the pitch of the web L is left open. For most purposes it is sufficient to assume

$$a = N - (d_1/4) \tag{1}$$

$$\text{and} \qquad b = L \tag{2}$$

where d_1 is the thickness of the web.

The differential equations for the heat flow in the simplified skin-shear web configuration are[2, 3]

$$\partial T_1/\partial t = \kappa_1(\partial^2 T_1/\partial x^2) \qquad 0 \le x \le a \tag{3}$$

and

$$\partial T_2/\partial t = \kappa_2(\partial^2 T_2/\partial x^2) + h(T_f - T_2) \qquad a \le x \le a + b \tag{4}$$

T_1 and T_2 are the temperatures, κ_1 and κ_2 the thermal diffusivities in the shear web and the skin, respectively, T_f is the boundary-layer friction temperature, x the distance from the middle of the web, t the time, and $h = \alpha/(\rho_2 c_2 d_2)$, where α is the external heat-transfer coefficient due to convection, ρ_2, c_2, and d_2 the density, the specific heat, and the thickness of the skin respectively. The heat transfer to the inside of the wing has been neglected since it is usually sufficiently small. The heat transfer due to radiation has also been neglected and this point will be referred to later. The boundary and initial conditions are [see also Fig. 1(c)]

$$x = 0; \qquad \partial T_1/\partial x = 0 \tag{5}$$

$$x = a; \qquad T_1 = T_2; \qquad d_1 k_1(\partial T_1/\partial x) = 2d_2 k_2(\partial T_2/\partial x) \tag{6}$$

$$x = a + b; \qquad \partial T_2/\partial x = 0 \tag{7}$$

$$t = 0; \qquad T_1 = T_2 = T_i \tag{8}$$

Since the heat-transfer coefficient α changes with speed and altitude, α is in any particular case a function of the time, as is also the boundary-layer friction temperature T_f. In order to obtain general solutions, instantaneous start of movement with constant speed and horizontal flight is assumed, so that constant values of T_f and α can be used. The same assumption has also been made in references 1, 2, and 3. It has been shown[2, 4] that the temperature distribution and the size of the thermal stresses are not much affected by the times of acceleration which occur in high-speed flight, although the time when the maximum stresses are reached may depend on the time history of the aircraft. In an acceleration assisted by rockets or afterburners, instantaneous start is at any rate a good approximation for both maximum stresses and their time history. On the other hand top speed can often be maintained only for a short time and then the speed decreases; in such cases the present solution in its simple form can be used only during the time when the top speed is maintained. With guided missiles it should be noted that the projectile may hit its target before thermal stresses have reached their maximum value. Cases where the speed or the altitude of the aircraft changes during the major part of the flight cannot be covered by the solutions of this paper.

In an aircraft structure, rivets and screws are generally used to join the web and the skin. The thermal

contact in such junctions is not perfect, so that a temperature jump occurs across the interface between the two parts, which may influence the temperature distribution in the structure. However, such cases will not be treated here and instead perfect thermal contact is assumed between different parts of the structure.

It has already been observed in refernce 2 that in any of the particular examples calculated the temperature gradient in the skin vanishes with sufficient accuracy at a distance from the junction of the skin and the web which is much smaller than b. In view of this fact, the boundary condition Eq. (7) at $x = a + b$ is replaced by

$$x \to \infty; \qquad \partial T_2/\partial x = 0 \tag{9}$$

which is general and does not refer to a particular case. After obtaining general solutions, the minimum permissible size of $b = L$ will be determined for which Eq. (9) holds; anticipating a later result, this size of L does not limit the applicability of the present solution in most cases. One advantage of this modification of the boundary condition is that one of the parameters of the original problem as determined by Eqs. (3) to (7) disappears and hence a general solution of the problem is made practical. Another is that the same solution covers also cases with different materials for the skin and the web.

The following dimensionless temperatures, coordinates, and time are introduced:

$$\left.\begin{aligned} \vartheta_1 &= (T_f - T_1)/(T_f - T_i) \\ \xi_1 &= x/a \end{aligned}\right\} \quad 0 \leq x \leq a \tag{10, 11}$$

$$\left.\begin{aligned} \vartheta_2 &= (T_f - T_2)/(T_f - T_i) \\ \xi_2 &= [(x - a)/a]\sqrt{\kappa_1/\kappa_2} \end{aligned}\right\} \quad a \leq x \leq a + b \tag{12, 13}$$

$$\tau = t\kappa_1/a^2 \tag{14}$$

Introducing these quantities in Eqs. (3) and (4) one obtains

$$\partial\vartheta_1/\partial\tau = \partial^2\vartheta_1/\partial(\xi_1)^2 \qquad 0 \leq \xi_1 \leq 1 \tag{15}$$

$$\partial\vartheta_2/\partial\tau = [\partial^2\vartheta_2/\partial(\xi_2)^2] - g^2\vartheta_2 \qquad 0 \leq \xi_2 \leq \infty \tag{16}$$

where a parameter

$$g^2 = a^2(h/\kappa_1) = a^2(\alpha\rho_1 c_1/d_2 k_1 \rho_2 c_2) \tag{17}$$

has been introduced, which appears to be of general importance in problems of heat flow in structures whose solidity is small. The boundary conditions are rewritten and read:

$$\xi_1 = 0; \qquad \partial\vartheta_1/\partial\xi_1 = 0 \tag{18}$$

$$\xi_1 = 1 \quad \text{and} \quad \xi_2 = 0; \qquad \vartheta_1 = \vartheta_2; \quad \partial\vartheta_1/\partial\xi_1 = R(\partial\vartheta_2/\partial\xi_2) \tag{19}$$

$$\xi_2 \to \infty; \qquad \partial\vartheta_2/\partial\xi_2 = 0 \tag{20}$$

where

$$R = 2(d_2/d_1)\sqrt{k_2\rho_2 c_2/k_1\rho_1 c_1} \tag{21}$$

The initial conditions become

$$\tau = 0; \qquad \vartheta_1 = \vartheta_2 = 1 \tag{22}$$

On inspecting Eqs. (15) to (21) it follows that the solution is only determined by two parameters* besides the two independent variables and is of the form

$$\vartheta_1 = \vartheta_1(\xi_1, \tau; R, g) \tag{23a}$$

$$\vartheta_2 = \vartheta_2(\xi_2, \tau; R, g) \tag{23b}$$

Attention is drawn to two asymptotic solutions, which can easily be found. The first asymptotic solution is obtained when $g \to \infty$, provided that $d_2 \neq 0$. If $d_2 = 0$, there would be no external heat transfer as inspection of Fig. 1(c) shows. For large values of g the second term on the right-hand side of Eq. (16) is greater than the first term, and the solution of Eq. (16) is

$$\vartheta_2 = \exp.\ (-g^2\tau) \tag{24}$$

Consequently ϑ_2 is independent of ξ_2 and—because of the boundary conditions Eq. (19)—the solutions of ϑ_1 and ϑ_2 are independent of R—i.e., the thickness ratio of web and skin. From Eq. (24) it follows that, for $g \to \infty$, ϑ_2 becomes zero before ϑ_1 has appreciably departed from its initial values. Hence this asymptotic solution is equal to the temperature distribution in a slab of thickness $2N$ which is initially (at $t = 0$) at a constant temperature different from zero and which is kept at a surface temperature equal to zero for all times $t \geq 0$. The solution of this problem is well known.[5] The second asymptotic solution is obtained when $L \to 0$; then the skin-shear web configuration becomes a solid wing or—in the simplified model of Fig. 1(b)—a slab with thickness $2N$, as in the first asymptotic solution, but with external heat transfer taking place from the surfaces of the slab with a coefficient α to a medium whose temperature is T_f. The solution of this problem is also known.[5] The solid wing can be considered as a extreme case of the skin-shear web configuration shown in Fig. 1(*b*); however it does not fit the simplified model of Fig. 1(*c*), since there would be no external heat transfer for $b = L \to 0$ according to Eq. (4). The parameter determining the temperature distribution is $g^2 = (\alpha a)/k$ as follows from Eq. (17) by putting $d_2 = a$ there, but R disappears as parameter. This asymptotic solution will not be discussed here although it could be a valuable supplement to the solutions presented later, since these require values of L to be bigger than a certain lower limit.

In references 2 and 3, solutions have been obtained in the form of a series expansion with the help of a Laplace transformation. However, in any particular case the computing work seems to be rather time-consuming, particularly since the convergence of the series is rather poor at small times. This point seems to be confirmed when observing that only one numerical example has been calculated in reference 3 and 8 examples in reference 2, although in preparing the latter

* Parkes[2] found also by a somewhat different approach that two parameters determine the temperature distribution in the examples he calculated.

paper a computing staff was available. It has been shown in reference 4 that the computational work can be considerably reduced by using a suitable numerical method. Essentially, that method consists in replacing the differential Eqs. (15) and (16) by finite difference equations and using a step-by-step procedure. Good accuracy can be obtained with this method, even for rather large spatial steps. This numerical method becomes the more accurate the smaller the finite differences of space and time are, but at the same time the amount of numerical work increases; hence a reasonable compromise has to be made. A high degree of accuracy is not necessary in the present problem, because certain errors are unavoidable in applying to actual aircraft structures the results of the simplified model treated here. In order to save time a maximum error of about ± 0.03 for temperatures and thermal stresses was allowed for in the present solution.

The thermal stresses are, according to reference 6,

$$\sigma_1 = E_1\beta_1(T_i - T_1 + A_1) \qquad 0 \leq \xi_1 \leq 1 \qquad (25)$$

$$\sigma_2 = E_2\beta_2(T_i - T_2 + A_2) \qquad 0 \leq \xi_2 < \infty \qquad (26)$$

σ_1, σ_2, E_2, E_1, and β_1, β_2 are thermal stresses, Young's modulus, and the thermal coefficients of linear expansion for the web and the skin respectively; A_1 and A_2 are two constants to be determined by the following conditions: (a), that the strain ϵ_1 and ϵ_2 for web and skin is the same—i.e.,

$$\epsilon_1 = A_1\beta_1 = \epsilon_2 = A_2\beta_2 \qquad (27)$$

and (b), that there are no external forces at the ends—i.e.,

$$d_1 \int_0^a \sigma_1\, dx + 2d_2 \int_a^{a+b} \sigma_2\, dx = 0 \qquad (28)$$

It is convenient to introduce the following quantities

$$\varphi = 2(d_2E_2b/d_1E_1a) \qquad (29)$$

$$p = (b/a)\sqrt{\kappa_1/\kappa_2} \qquad (30)$$

$$\theta_1 = \int_0^1 \vartheta_1\, d\xi_1, \quad \theta_2(\xi_2) = \frac{1}{\xi_2}\int_0^{\xi_2} \vartheta_2\, d\xi_2 \qquad (31)$$

Eqs. (25) and (26) can be rewritten as

$$\sigma_1 = E_1\beta_1(T_f - T_i)\left\{\vartheta_1 - \frac{\theta_1 + \varphi(\beta_2/\beta_1)\theta_2(p) + \varphi[1 - (\beta_2/\beta_1)]}{1 + \varphi}\right\} \qquad (32)$$

$$\sigma_2 = E_2\beta_2(T_f - T_i)\left[\vartheta_2 - \frac{\varphi\theta_2(p) + (\beta_1/\beta_2)\theta_1 + 1 - (\beta_1/\beta_2)}{1 + \varphi}\right] \qquad (33)$$

The stresses can therefore be easily found, if the temperatures ϑ_1, ϑ_2, θ_1, and θ_2 are known.

(3) Results

Numerical solutions have been obtained of Eqs. (15) and (16) with the boundary and initial conditions Eqs. (18) to (22) for values of $g = 0.923$, 1.85, 3.70, 7.38 and for values of $R = 7.5$, 2.0, and 1.0. The result of calculations for $R = 2.0$ are presented in Figs. 2–8 where each figure refers to a certain time τ; the temperatures ϑ_1 and ϑ_2 are plotted against g with dimensionless distances ξ_1 (measured from the middle of the web) and ξ_2 (measured from the junction of the web and skin) as parameters; the figures contain also θ_1, the mean temperature of the web, and $\theta_1(\xi_{2r})$, and the mean temperature of ϑ_2 between 0 and ξ_{2r}. The value of ξ_{2r} in the diagrams has been chosen so that within the accuracy of present solutions

$$\theta_2(\xi_2) = (\xi_{2r}/\xi_2)\theta_2(\xi_{2r}) + [1 - (\xi_{2r}/\xi_2)]\vartheta_2(\infty) \qquad (34)$$

for any values of $\xi_2 \geq \xi_{2r}$.

The temperatures for large values of g were obtained from the first asymptotic solution discussed previously. From these and similar figures for $R = 7.5$ and 1.0, which owing to lack of space are not reproduced here, an estimate can be made of the minimum size of L, for which the present solutions are valid. The temperatures ϑ_2 differ at $\xi_2 = 1$ only a little or in some figures not at all from those at $\xi_2 \to \infty$. Hence the exact boundary condition for any particular case Eq. (7) can be replaced by the simplified boundary condition Eq. (9) if $\xi_2 \geq 1$; this condition can be relaxed to $\xi_2 \geq 1/2$ for reasons given later. Hence it follows that

$$p = (b/a)\sqrt{\kappa_1/\kappa_2} \geq 1/2 \qquad (35)$$

and thus the smallest size of $b = L$ is determined for which the present solutions are valid.

With the help of these figures the stress distribution can be found for any time τ. If φ is not too small, the maximum stress occurs in the middle of the web, hence it suffices to calculate stresses for that point and plot them against time in order to find the maximum. These curves are rather flat near their maximums, which can thus be determined with sufficient accuracy from those times to which Figs. 2–8 refer.

If the web and the skin are of the same material, further simplifications are possible. Because the position of the maximums of the stress-time curves does not vary much with φ and because these curves are rather flat, the time τ_m at which these maximums occur can be assumed approximately the same for all values of the parameter φ ranging from $\varphi = \infty$ down to the lowest corresponding to the smallest possible size of L. Values of dimensionless time τ_m vs. parameter g are shown in Fig. 9 for $R = 7.5$, 2.0, and 1.0. It is important to know these times τ_m for judging whether the present solution for constant speed after the start can be applied to cases where the operational diagrams appreciably differ, for instance, when the top speed can be maintained only for a short time, as occurs with many high-speed aircraft.

Again for cases with the same material of the web and the skin, diagrams can be given for the maximum stresses occurring in the middle of the web as a function of the parameter g for various values of φ and three values of R. The times taken to reach maximums of stresses being independent of the parameter φ greatly

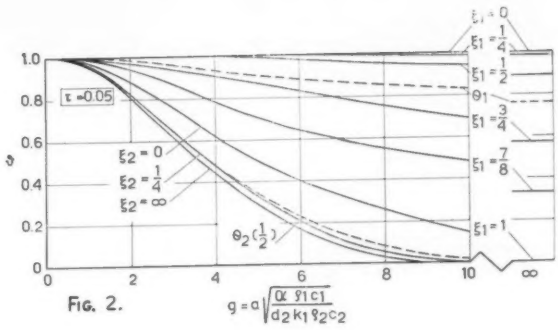

Fig. 2.

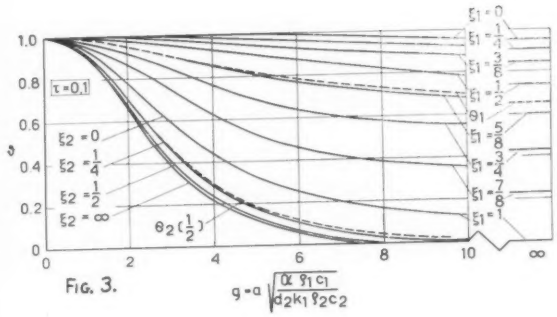

Fig. 3.

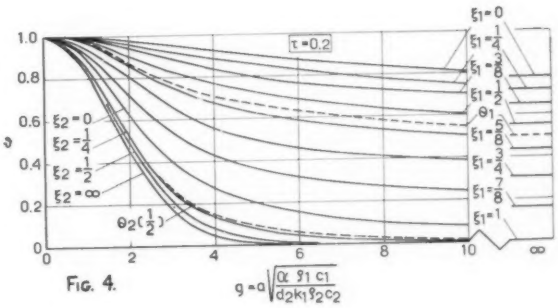

Fig. 4.

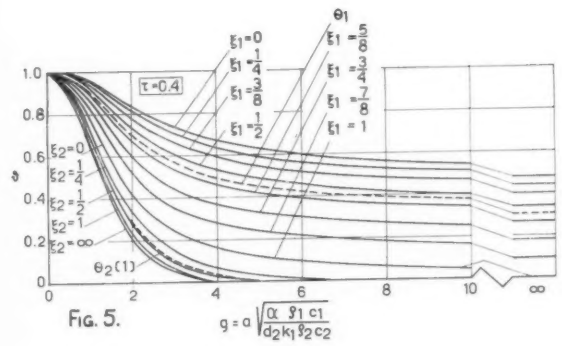

Fig. 5.

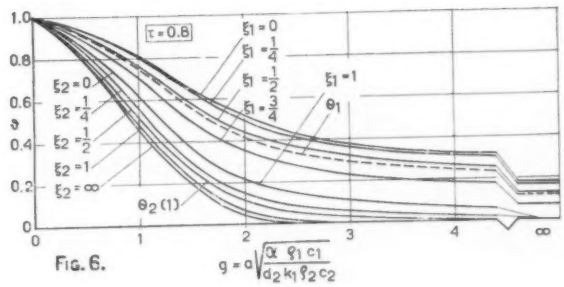

Fig. 6.

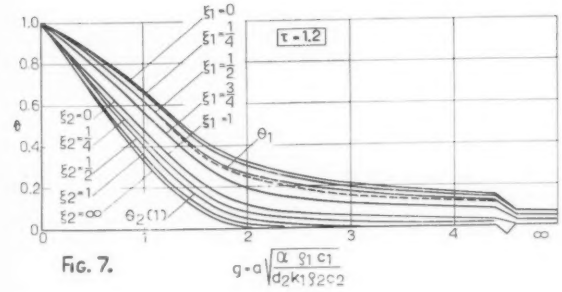

Fig. 7.

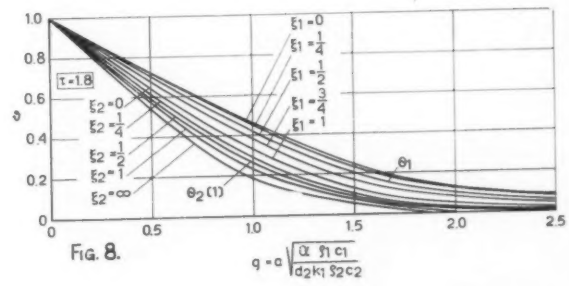

Fig. 8.

FIGS. 2–8. Temperature distributions in the structure of Fig. 1(b) as a function of the parameter g for various dimensionless distances ξ_1(web) and ξ_2(skin). Dimensionless thickness ratio of skin and web $R = 2.0$. The dimensionless times in the figures are 0.05, 0.1, 0.2, 0.4, 0.8, 1.2, and 1.8, respectively.

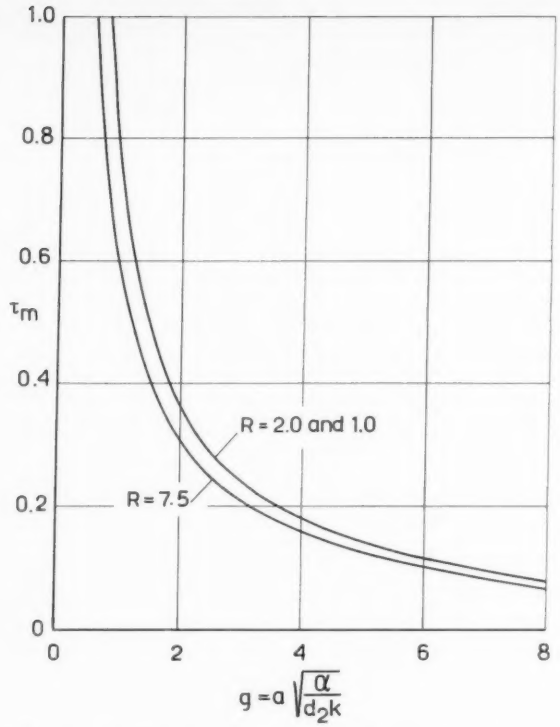

FIG. 9. Dimensionless times τ_m at which maximum thermal stresses occur as functions of parameter g for three values of the dimensionless thickness ratio of the skin and the web R. Web and skin are of the same material.

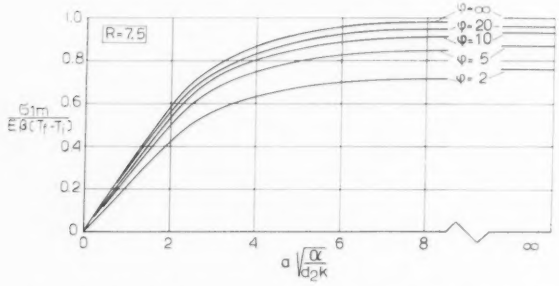

FIG. 10. In Figs. 10–12 maximum thermal stresses of the structure of Fig. 1(b) with the same material in the web and the skin as functions of the parameters g and φ. The maximum stresses occur in the middle of the web for values of parameters given in the figures. The dimensionless thickness ratio is 7.5.

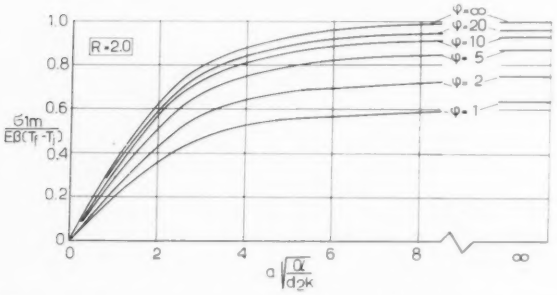

FIG. 11. The dimensionless thickness ratio is 2.0 (*see caption Fig. 10*).

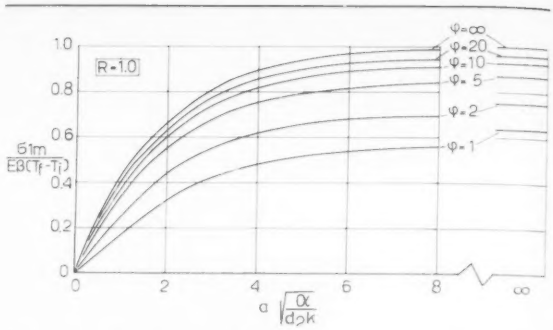

FIG. 12. The dimensionless thickness ratio is 1.0 (*see caption Fig. 10*).

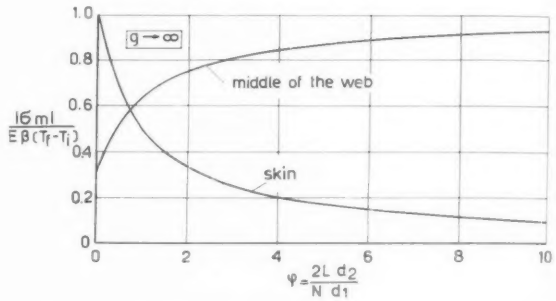

FIG. 13. The maximum thermal stresses occurring in the middle of the web and in the skin as functions of the parameter φ for values of the parameter $g \to \infty$.

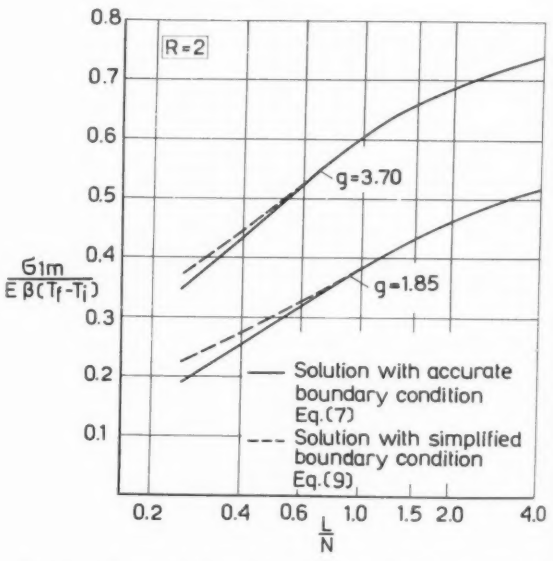

FIG. 14. Some solutions for maximum thermal stresses as functions of the dimensionless pitch L/N obtained with the accurate boundary condition in the skin Eq. (7) compared with those obtained with the simplified boundary condition according to Eq. (9). The skin and the shear web are of the same material. Stresses at $\xi_1 = 0$ (middle of the web). Parameters $R = 2.0$, $g = 1.85$ and 3.70.

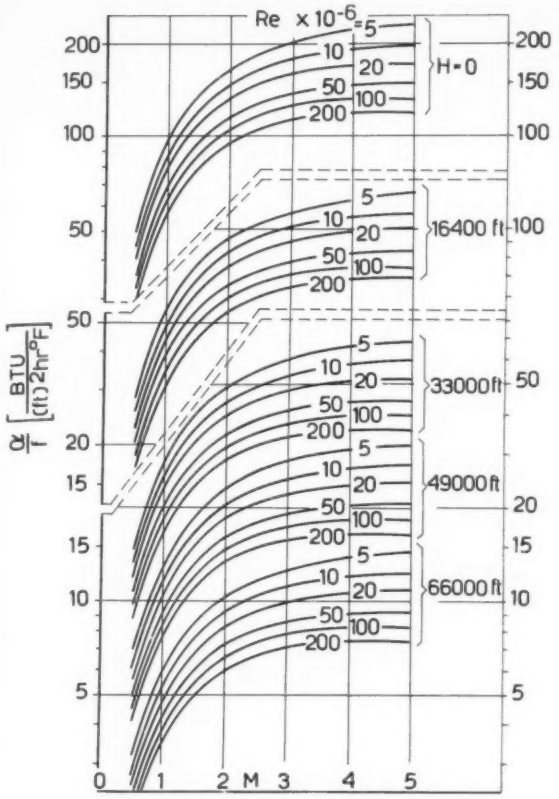

FIG. 15(a). Diagram for predicting the local external heat transfer coefficient due to convection in air for a turbulent boundary layer as a function of altitude above sea level H, Mach Number M and Reynolds Number Re of boundary layer based on boundary layer length l. f is a function of the Prandtl Number, its value for air not yet accurately known. A value of $f = 1.10$ is tentatively proposed in this paper.

simplifies preparation of these diagrams. The results can be seen in Figs. 10–12, which were obtained for $R = 2.0$ from Figs. 2–8 and for $R = 7.5$ and 1.0 from calculated temperature distributions not published in this paper. The influence of R on the stresses is small, particularly at bigger values of g. For values of $g > 6$ the maximum stresses are independent of g—i.e., independent of the heat-transfer coefficient α, height of web a, and thickness of skin d_2. For $g < 3$ they are about proportional to the square root of the heat-transfer coefficient, to the height of the web and inversely proportional to the square root of the thickness of the skin. The decrease of maximum stresses with decreasing parameter φ can, however, not be extrapolated beyond those values given in the Figs. 10–12, since for sufficiently small values of φ the maximum stress occurs in the skin. This is illustrated by Fig. 13, in which the maximum stresses in the middle of the skin and in the junction of the skin and the web are plotted vs. φ for the parameter $g \to \infty$; below a certain value of φ the maximum stresses in the skin become greater than those in the web. Besides, the times taken to reach the maximum stresses are appreciably different for both the skin and the web.

Previously the minimum size of L was estimated, which is permissible when using the standard solutions derived in this paper. This estimate has been checked by calculations for $R = 2.0$, $g = 1.70$ and 3.55, and values of $L/N \approx b/a = 0.25$, 0.50, 1.25 in which the exact boundary condition at $x = a + b$, Eq. (7), was used instead of the simplified boundary condition Eq. (9). These solutions were compared with the standard solutions and little difference between the two was found for values of L/N larger than 0.50 and even for $L/N = 0.25$ a value not altogether wrong is obtained. In view of these results a value of $1/2$ was chosen for the lower limit of p in Eq. (35).

For predicting temperature distributions and thermal stresses, the variation of the heat-transfer coefficient α with altitude above sea level H and Mach Number M has to be known, and this information may be obtained in a convenient form from Fig. 15(a) which refers to a turbulent boundary layer. The heat-transfer coefficient for air was assumed as follows[7]*

$$\alpha = f(Pr)\rho_a c_{pa} u(c_f/2) \tag{36}$$

where ρ_a and c_{pa} are the density and specific heat of air, u the aircraft speed, and c_f the coefficient of friction for a turbulent boundary layer which has been taken from reference 8. The factor $f(Pr)$ allows for the influence of the Prandtl Number Pr on heat transfer; $f = 1$ for $Pr = 1$. According to the well-known Colburn formula[9] $f(Pr) = (Pr)^{-2/3}$; however there are not sufficient experiments available to decide whether this formula gives accurate values for air ($Pr = 0.72$) as a medium. Some recent experiments[10] seem to indicate that $f(0.72) = 1.10$, which value is about 10 per cent

* Except for a region near the leading edge the pressure gradient on airfoils is sufficiently small to be neglected in determining the heat transfer coefficient. Further it is assumed that the boundary layer remains attached and is undisturbed by shock waves.

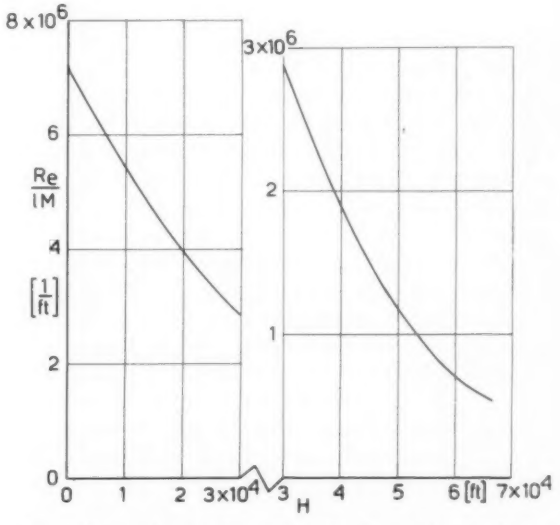

FIG. 15(b). Diagram for calculating Reynolds Number as used in Fig. 15(a) as a function of altitude H above sea level, Mach Number M and boundary layer length l.

TABLE 1

Ratio of Maximum Thermal Stresses σ_{1ml}/σ_{1m} with and Without a Heat-Insulating Layer of Thickness δ and of Heat Conductivity k_l. Characteristic Parameters: $g = 3.0$ (bare wing), $R = 2.0$, and $\varphi = 10$

(a) Flight conditions: $H = 50{,}000$ ft., $M = 2$, and $Re = 1 \times 10^8$

δ (in.)	$k_l = 0.134$	0.0336	0.0134	$\frac{\text{B.t.u.}}{\text{ft.hr.°F.}}$
0.002	1.00	0.99	0.96	
0.01	0.98	0.91	0.82	
0.02	0.96	0.85	0.71	
0.1	0.82	0.56	0.39	

(b) Flight conditions: $H = 15{,}000$ ft., $M = 2$, and $Re = 1 \times 10^8$

δ (in.)	$k_l = 0.134$	0.0336	0.0134
0.002	0.98	0.93	0.85
0.01	0.91	0.74	0.55
0.02	0.85	0.60	0.43
0.1	0.55	0.31	0.21

lower than that of Colburn. The heat-transfer coefficient in Fig. 15(a) decreases appreciably with increasing altitude, but does not change much between $M = 3$ and $M = 5$ at constant altitude. Fig. 15(b) facilitates the estimate of Reynolds Number, where l means the length of the turbulent boundary layer on an aircraft surface.

For completeness' sake, the temperature differences occurring in the formula for the stresses are given.

$$T_f - T_i = T_s\{1 + [(\gamma - 1)/2](Pr)^{1/3}M^2\} - T_{si}\{1 + [(\gamma - 1)/2](Pr)^{1/3}(M_f)^2\} \quad (37)$$

provided the aircraft was initially in equilibrium with the surrounding air. γ is the ratio of the specific heats at constant pressure and constant volume. Indices f, i and s refer to boundary-layer friction temperature, initial temperature, and static temperature, respectively. Again, a turbulent boundary layer is assumed.

In order to estimate the effect of a heat-insulating layer mounted on the outside of the aircraft skin, the heat-transfer coefficient α is to be replaced by α_g in calculating the value of the parameter g, where α_g is

$$1/\alpha_g = (1/\alpha) + (\delta/k_l) \quad (38)$$

δ is the thickness of the heat-insulating layer whose thermal conductivity is k_l. The thermal capacity of the heat insulating layer has been neglected, which is correct for thin, but not for thick layers. The values of k_l for three typical heat-insulating materials are: (a) plastics with asbestos fibers, 0.134; (b) best inorganic heat-insulating material, 0.0336; (c) air at +32°F., 0.0134 (B.t.u.)/ft. hr. °F.). Air has been given since it is the best heat insulator and the effective component of porous materials. The influence of the thickness of layers of these heat-insulating materials on maximum stresses can be estimated from Table 1(a), which refers to a typical example of flight at 50,000 ft. altitude and $Re = 1 \times 10^8$. It can be seen that appreciable effects can be obtained at altitudes of 50,000 ft. with layers of about 0.05-in. thickness and the best of heat-insulating materials. However, at lower altitudes heat-transfer coefficients are higher and the thicknesses of the insulating layer can be less for the same stress reduction [see Table 1(b).]

TABLE 2

Maximum Thermal Stresses for the Examples Calculated in References 2 and 3 Compared with the Corresponding Results of Present Solution

Source (reference)	Example	g	φ	β_2/β_1	R	$\frac{\sigma_{1m}}{E_1\beta_1(T_f - T_i)}$ other authors	present author
1	1	3.56	20	1	7.5	0.79	0.80
2	2	3.56	5.33	1	2.0	0.72	0.73
2	3	6.89	5.33	1	2.0	0.85	0.85
2	4	6.89	2.755	1	2.0	0.76	0.76
2	5	6.88	5.33	1	2.0	0.85	0.85
2	6*	3.97	5.33	1	2.0	0.73	0.76
2	7*	3.25	16.00	0.5	1.414	0.76	0.74
2	8	3.56	5.33	1	2.0	0.72	0.73
3	1	3.56	20	1	7.5	0.79	0.80

* In the original paper obtained by interpolation.

Lastly, the maximum stresses of the nine examples calculated in references 2 and 3 are compared in Table 2 with those obtained by the present analysis. Comparison is very good, particularly when noting that the biggest deviations occur in cases where the solutions of reference 2 have been obtained by extrapolation and it is therefore possible that they are less accurate.

It should be noted that in references 1, 2, and 3 a heat-transfer coefficient of 90 (B.t.u.)/(ft.²hr.°F.) has been assumed in all cases. In references 1 and 2 this value was stated to correspond to an altitude of 50,000 ft. and a Mach Number of 3.1. However, this is erroneous.† The heat-transfer coefficient at the above flight condition (see Fig. 15) would be 21 (B.t.u.) ÷ (ft.²hr.°F.).‡ Alternatively, the heat-transfer coefficient used in references 1, 2, and 3 corresponds to an altitude of 15,000 ft. and the same Mach Number of 3.1. Consequently the stresses found in references 1, 2, and 3 would be reduced by between 15 to 40 per cent if the correct heat-transfer coefficient for an altitude of 50,000 ft. were assumed. For the same reasons the prospects of reducing stresses by insulating layers at altitudes of about 50,000 ft. or above are less favorable than appeared in reference 2.

The influence of radiation can be easily considered for the asymptotic solution when $g \to \infty$; then the temperature of the skin reaches equilibrium before an appreciable heat flow occurs into the web. The skin can therefore be treated separately and its equilibrium temperature T_w due to convection and radiation can be calculated from the following equation:

$$\epsilon C_S(T_w^4 - T_s^4) = \alpha(T_f - T_w) \quad (39)$$

C_S is the constant of radiation for a black body, ϵ is the emissivity and T_s the static air temperature. The radiation from the body is assumed the same as from a "gray"

(*Continued on page 866*)

† In reference 2 Hoff's value for the heat-transfer coefficient was checked by estimating it from the drag of aircrafts by using Reynolds' analogy. However only the frictional part of the drag can be used for that purpose and that part is much less than the total drag in modern high-speed aircraft.

‡ Assuming a boundary-layer length of about 10 ft.

Computation of Vibration Modes and Frequencies on SEAC

WILLIAM F. CAHILL* AND SAMUEL LEVY†
National Bureau of Standards

SUMMARY

A description is given of several codes developed for use in the Standards Eastern Automatic Computer for computing the free vibration modes and frequencies of aircraft structures. The codes are general in nature and apply without modification to any aircraft structure whose influence coefficients, mass distribution, and geometry are specified. The codes are applicable when no more than 63 mass points are needed to define the displacement of the half-wing. In an example with seven mass points along the fuselage axis and 24 mass points for each half-wing, the computing time for the first six symmetric and the first six antisymmetric modes was 6 hours.

INTRODUCTION

KNOWLEDGE of the vibration modes and frequencies of aircraft is of primary importance in determining their flutter speeds and in making dynamic analyses of the response of the structure to landing impact and other shock loads. A great deal of effort has therefore been expended in developing convenient methods for carrying out the tedious computations involved.

The method of computing vibration mode shapes and natural frequencies by matrix iteration is a systematic procedure which has been gradually developed from the initial work by W. J. Duncan and A. R. Collar.[1] This procedure converges to the lowest frequency mode. To obtain the higher frequency modes, use has been made of the orthogonality relationship to (a) reduce the size of the matrix successively by one and thus obtain convergence to the higher modes,[1, 2] (b) "sweep" lower modes from the trial modes and thus obtain convergence to higher modes,[3, 4] or (c) modify the original matrix without changing its size so that the lower modes are successively removed.[5]

The codes to be described in this paper are based on the matrix iteration scheme together with a variation of the matrix modification scheme given by Kincaid in reference 5. The rigid body modes are eliminated as described in Appendix III of reference 6. This overall choice is particularly well suited to a high-speed computer such as SEAC because it results in highly repetitive computations where speed and accuracy are of primary importance.

The Standards Eastern Automatic Computer, SEAC,[7] is an electronic digital computer containing a 512-word mercury delay line memory and a 512-word electrostatic memory (not used in this problem). It also has internal auxiliary tape storage units which make it possible to store the many numbers required in the present problem. It computes at an average rate of about 500 operations per second.

METHOD

The method used in setting up the code follows that given in reference 6, Appendix III, but treats the symmetric and antisymmetric modes separately so that only a half-wing need be considered at a time. This limits the applicability of the code to symmetrical structures.

Consider a frame of reference coordinates x, y, z, fixed in space and oriented with respect to the airplane as shown in Fig. 1. Let the mass of the wing be represented by a moderate number of lumped masses. Let x_n, y_n, z_n be the coordinates of mass n. Let the origin be at mass 1. The influence coefficient $\delta_{m,n}$ between two lumped mass points m and n on the airplane is here defined as the vertical displacement at m due to a vertical unit load at n when point 1 is clamped and when, for determining symmetrical modes, the slope dy/dx,

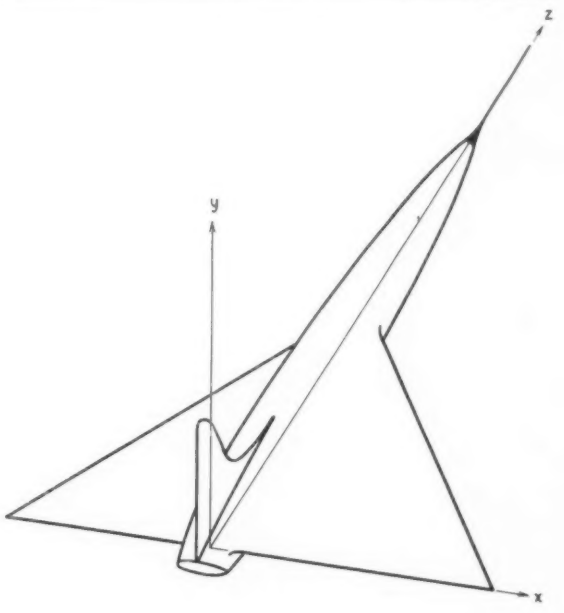

Figure 1. - Coordinate system.

Received October 7, 1954.

* Mathematician.

† Formerly, Chief of Aircraft Structures Group, National Bureau of Standards. Now, Manager, Stress Analysis Engineering, Special Defense Projects Division, General Electric Co.

normal to the fuselage axis, is taken as zero all along the fuselage axis; while, for determining antisymmetrical modes, the deflection y is taken as zero all along the fuselage axis. (As the relative fuselage rigidity increases, the symmetric and antisymmetric influence coefficients tend to equality.) Let the motion of the clamped point 1 be described by λ, θ, α; where λ is the upward displacement of point 1, θ the roll from x to y about the z axis, and α the pitch from z to y about the x axis.

Antisymmetric Modes

Consider the fundamental antisymmetric mode with a frequency ω. More accurate values, y_1', y_2', . . . y_n', of the displacements parallel to the y axis may be computed by iteration from assumed values y_1, y_2, . . . y_n in terms of the antisymmetric influence coefficients and the inertia forces due to vibratory motion of masses M_1, M_2, . . . M_n by:

$$\left.\begin{aligned}
\frac{1}{\omega^2}(y_1' - \theta x_1) &= \sum_{r=1}^{n} M_r y_r \delta_{1r} = \sum_{r=1}^{n} B_{1r}^{(1)} y_r \\
\frac{1}{\omega^2}(y_2' - \theta x_2) &= \sum_{r=1}^{n} M_r y_r \delta_{2r} = \sum_{r=1}^{n} B_{2r}^{(1)} y_r \\
&\cdot \\
&\cdot \\
&\cdot \\
\frac{1}{\omega^2}(y_n' - \theta x_n) &= \sum_{r=1}^{n} M_r y_r \delta_{nr} = \sum_{r=1}^{n} B_{nr}^{(1)} y_r
\end{aligned}\right\} \quad (1)$$

The B coefficients are frequently referred to as terms in the dynamic matrix. The superscript (1) indicates they apply for the fundamental mode. To determine θ we form the sum

$$\frac{1}{\omega^2}\sum_{s=1}^{n} x_s M_s (y_s' - \theta x_s) = \sum_{s=1}^{n} x_s M_s \sum_{r=1}^{n} B_{sr}^{(1)} y_r \quad (2)$$

and make use of the fact that if the airplane is not being accelerated as a rigid body

$$\sum_{s=1}^{n} x_s M_s y_s' = 0 \quad (3)$$

giving on substitution in Eq. (2)

$$\frac{\theta}{\omega^2} = -\frac{\sum_{s=1}^{n} x_s M_s \sum_{r=1}^{n} B_{sr}^{(1)} y_r}{\sum_{s=1}^{n} x_s^2 M_s} \quad (4)$$

The more accurate values y_1'/ω^2, y_2'/ω^2, . . . , y_n'/ω^2 are obtained from Eq. (1) using the value of θ/ω^2 given by Eq. (4):

$$\left.\begin{aligned}
\frac{y_1'}{\omega^2} &= \frac{\theta}{\omega^2} x_1 + \sum_{r=1}^{n} B_{1r}^{(1)} y_r \\
\frac{y_2'}{\omega^2} &= \frac{\theta}{\omega^2} x_2 + \sum_{r=1}^{n} B_{2r}^{(1)} y_r \\
&\cdot \\
&\cdot \\
&\cdot \\
\frac{y_n'}{\omega^2} &= \frac{\theta}{\omega^2} x_n + \sum_{r=1}^{n} B_{nr}^{(1)} y_r
\end{aligned}\right\} \quad (5)$$

The ratio $y_r/(y_r'/\omega^2)$ gives an approximate value of the square of the fundamental frequency ω_1^2 while the ratios $(y_1'/\omega^2)/(y_r'/\omega^2)$, etc., give deflections in the fundamental antisymmetric mode normalized with respect to a preselected station r. These displacements describe the mode shape more accurately than the originally assumed values. By repeating this cycle of computations, in each case starting the new cycle with the more accurate values just obtained, convergence to the fundamental mode is obtained.

To obtain convergence to the next higher mode, it is necessary to modify the right-hand side of Eqs. (1). Following reference 5, this is done as follows:

$$\left.\begin{aligned}
\frac{1}{\omega^2}(y_1' - \theta x_1) &= \sum_{r=1}^{n} B_{1r}^{(1)} y_r - \frac{\sum_{r=1}^{n} M_r y_1^{(1)} y_r^{(1)} y_r}{\omega_1^2 \sum_{r=1}^{n} M_r [y_r^{(1)}]^2} = \sum_{r=1}^{n} B_{1r}^{(2)} y_r \\
&\cdot \\
&\cdot \\
&\cdot \\
\frac{1}{\omega^2}(y_n' - \theta x_n) &= \sum_{r=1}^{n} B_{nr}^{(1)} y_r - \frac{\sum_{r=1}^{n} M_r y_n^{(1)} y_r^{(1)} y_r}{\omega_1^2 \sum_{r=1}^{n} M_r [y_r^{(1)}]^2} = \sum_{r=1}^{n} B_{nr}^{(2)} y_r
\end{aligned}\right\} \quad (6)$$

Eqs. (6) make use of the orthogonality principle to eliminate from any trial mode $y_1, y_2, \ldots, y_n$ the portion which is fundamental mode, and thus bring convergence to the next higher mode of the iteration process represented by Eqs. (1) to (5) with $B^{(2)}$ replacing $B^{(1)}$.

To obtain the third and higher modes, the successive dynamic matrix terms are obtained from

$$B_{sq}^{(t+1)} = B_{sq}^{(t)} - \frac{M_q y_s^{(t)} y_q^{(t)}}{\omega_t^2 \sum_{r=1}^{n} M_r [y_r^{(t)}]^2} \tag{7}$$

and the iteration process represented by Eqs. (1) to (5) is repeated.

Symmetric Modes

Consider the fundamental symmetric mode with a frequency ω. More accurate values $y_1', y_2', \ldots, y_n'$ of the displacements parallel to the y axis may be computed by iteration from assumed values $y_1, y_2, \ldots, y_n$ in terms of the symmetric influence coefficients and the inertia forces by

$$\left.\begin{aligned}
\frac{1}{\omega^2}(y_1' - \lambda - \alpha z_1) &= \sum_{r=1}^{n} M_r y_r \delta_{1r} = \sum_{r=1}^{n} B_{1r}^{(1)} y_r \\
\frac{1}{\omega^2}(y_2' - \lambda - \alpha z_2) &= \sum_{r=1}^{n} M_r y_r \delta_{2r} = \sum_{r=1}^{n} B_{2r}^{(1)} y_r \\
&\cdots \\
\frac{1}{\omega^2}(y_n' - \lambda - \alpha z_n) &= \sum_{r=1}^{n} M_r y_r \delta_{nr} = \sum_{r=1}^{n} B_{nr}^{(1)} y_r
\end{aligned}\right\} \tag{8}$$

To determine λ and α we form the sums

$$\left.\begin{aligned}
\frac{1}{\omega^2}\sum_{s=1}^{n} z_s M_s (y_s' - \lambda - \alpha z_s) &= \sum_{s=1}^{n} M_s z_s \sum_{r=1}^{n} B_{sr}^{(1)} y_r \\
\frac{1}{\omega^2}\sum_{s=1}^{n} M_s (y_s' - \lambda - \alpha z_s) &= \sum_{s=1}^{n} M_s \sum_{r=1}^{n} B_{sr}^{(1)} y_r
\end{aligned}\right\} \tag{9}$$

and make use of the fact that if the airplane is not being accelerated as a rigid body,

$$\sum_{s=1}^{n} z_s M_s y_s' = 0; \qquad \sum_{s=1}^{n} M_s y_s' = 0. \tag{10}$$

Substituting Eq. (10) in Eq. (9) and solving for λ/ω^2 and α/ω^2 gives

TABLE 1

Mass, x and z Station Coordinates, and Antisymmetric Mode Shapes and Frequencies

Station	Mass lb sec²/in.	x in.	z in.	Mode 1	Mode 2	Mode 3	Mode 4	Mode 5	Mode 6
1	0.01548656	49.497474	0	0.1053281	-0.2994552	0.2696731	1.2337046	1.8963363	0.7571406
2	0.02353352	91.923881	0	0.2487737	-0.6269135	0.6068175	1.1105324	3.0521377	1.5830190
3	0.03005745	134.350288	0	0.3784546	-0.7872769	0.7848211	-0.4930628	1.5104221	0.8791356
4	0.08446276	176.776695	0	0.5048352	-0.6894540	0.8096368	-2.2153784	-1.2517404	-0.8962385
5	0.05782825	280.862813	0	1.0000000	1.0000000	1.0000000	1.0000000	0.0002480	0.2433830
6	0.03844221	49.497474	52.325902	0.0303468	-0.1327213	0.1280213	0.7012243	0.8076222	0.2196500
7	0.05315167	91.923881	↕	0.0648433	-0.2419023	0.1353407	1.0086383	0.8656522	0.5417335
8	0.06155684	134.350288	↕	0.1047606	-0.3083052	-0.0186641	0.8459477	0.1979509	0.7227621
9	0.07419415	176.776695	↕	0.1469578	-0.2855751	-0.4161736	0.2403583	-0.6053820	0.5805288
10	0.11244671	250.457221	52.325902	0.2629954	0.0525995	-2.1532393	-1.2127619	1.0000000	-0.4135302
11	0.30318519	49.497474	108.894444	-0.0048429	-0.0521661	0.0789027	0.4340894	0.3614473	-0.1112689
12	0.26769497	91.923881	↕	-0.0119559	-0.0864503	0.0581000	0.7980655	0.2799138	-0.0836652
13	0.27562399	134.350288	↕	-0.0182794	-0.1024706	-0.0840490	1.0210447	-0.2527450	0.1374960
14	0.15552180	176.776695	↕	-0.0225724	-0.0847514	-0.3719861	0.9786777	-1.0727818	0.5751473
15	0.06074808	217.930309	108.894444	-0.0261044	-0.0171589	-0.7701349	0.7307846	-1.8185453	1.0000000
16	0.90096093	49.497474	171.119841	-0.0258761	-0.0064673	0.0651073	0.1182361	0.1512490	-0.1197875
17	0.68739492	91.923881	↕	-0.0535989	-0.0030001	0.1065604	0.2307441	0.1756180	-0.3590327
18	0.55464004	134.350288	↕	-0.0838845	0.0107528	0.0996684	0.3266008	-0.0380381	-0.5844872
19	0.13027820	176.776695	171.119841	-0.1160221	0.0388201	0.0539281	0.2545818	-0.3468054	-0.5258171
20	1.44840038	49.497474	233.345238	-0.0373266	0.0173477	0.0689152	-0.1383700	0.0754152	0.0330894
21	0.92140026	91.923881	↕	-0.0737608	0.0407854	0.1307565	-0.3362522	0.1180312	0.0542682
22	0.31614511	134.350288	233.345238	-0.1130376	0.0710664	0.1777964	-0.5746732	0.0767416	0.1038077
23	1.18136199	49.497474	295.570634	-0.0437203	0.0305001	0.0693467	-0.2954392	0.0236840	0.1845587
24	0.60981791	91.923881	295.570634	-0.0846868	0.0644032	0.1306468	-0.6651949	0.0080449	0.4989885
ω (rad/sec)				41.971	110.637	169.813	238.643	351.901	399.850

$$\frac{\lambda}{\omega^2} = -\frac{\left(\sum_{s=1}^{n} M_s z_s^2\right)\left[\sum_{s=1}^{n} M_s \sum_{r=1}^{n} B_{sr}^{(1)} y_r\right] - \left(\sum_{s=1}^{n} M_s z_s\right)\left[\sum_{s=1}^{n} M_s z_s \sum_{r=1}^{n} B_{sr}^{(1)} y_r\right]}{\left(\sum_{s=1}^{n} M_s\right)\left(\sum_{s=1}^{n} M_s z_s^2\right) - \left(\sum_{s=1}^{n} M_s z_s\right)^2} \tag{11}$$

$$\frac{\alpha}{\omega^2} = -\frac{\left(\sum_{s=1}^{n} M_s\right)\left[\sum_{s=1}^{n} M_s z_s \sum_{r=1}^{n} B_{sr}^{(1)} y_r\right] - \left(\sum_{s=1}^{n} M_s z_s\right)\left[\sum_{s=1}^{n} M_s \sum_{r=1}^{n} B_{sr}^{(1)} y_r\right]}{\left(\sum_{s=1}^{n} M_s\right)\left(\sum_{s=1}^{n} M_s z_s^2\right) - \left(\sum_{s=1}^{n} M_s z_s\right)^2} \tag{12}$$

It should be noted that in the special case of a thin straight line beam, where z is zero at all stations, Eqs. (11) and (12) are replaced by

$$\frac{\lambda}{\omega^2} = -\frac{\sum_{s=1}^{n} M_s \sum_{r=1}^{n} B_{sr}^{(1)} y_r}{\sum_{s=1}^{n} M_s}, \text{ if } z_1 = z_2 = \ldots z_n = 0 \tag{11'}$$

$$\frac{\alpha}{\omega^2} = 0, \text{ if } z_1 = z_2 = \ldots z_n = 0 \tag{12'}$$

The more accurate values y_1'/ω^2, y_2'/ω^2, . . . , y_n'/ω^2 are obtained from Eq. (8) using the values of λ/ω^2 and α/ω^2 given by Eqs. (11) and (12). Rewriting Eq. (8),

$$\left.\begin{aligned} \frac{y_1'}{\omega^2} &= \frac{\lambda}{\omega^2} + \frac{\alpha}{\omega^2} z_1 + \sum_{r=1}^{n} B_{1r}^{(1)} y_r \\ \frac{y_2'}{\omega^2} &= \frac{\lambda}{\omega^2} + \frac{\alpha}{\omega^2} z_2 + \sum_{r=1}^{n} B_{2r}^{(1)} y_r \\ &\cdot \\ &\cdot \\ &\cdot \\ \frac{y_n'}{\omega^2} &= \frac{\lambda}{\omega^2} + \frac{\alpha}{\omega^2} z_n + \sum_{r=1}^{n} B_{nr}^{(1)} y_r \end{aligned}\right\} \tag{13}$$

The ratio $y_r/(y_r'/\omega^2)$ gives an approximate value of the square of the fundamental symmetric frequency ω_1^2 while the ratios $(y_1'/\omega^2)/(y_r'/\omega^2)$, etc. give deflections in the fundamental symmetric mode normalized with respect to a preselected station r which are more accurate than the originally assumed values. Iteration of this cycle of computations converges to the fundamental mode.

To obtain convergence to the second mode and higher modes, $B_{sr}^{(1)}$ in Eq. (8) is replaced successively by $B_{sr}^{(2)}$, $B_{sr}^{(3)}$, etc., given by Eq. (7), and the iteration process represented by Eqs. (8) to (13) is repeated.

Machine Computation

The problem is broken down into three parts for purposes of programming due to the limitation of memory space in SEAC. The function of the first code is to form the dynamic matrix [$B_{sr}^{(1)}$ coefficients] and store it on tape and also to determine the constants used in eliminating the rigid body motions and print them for use with the second code. The second code computes the frequency and mode by the iteration scheme presented in the previous section. The third code modifies the dynamic matrix and stores it on tape for use in computing the mode of next higher frequency.

Formation of Dynamic Matrix and Constants for Removing Rigid Body Motions

The first code reads in, converts into binary form, and stores the mass constants, M_1, M_2, . . . , M_n, and the geometric constants,

$$u_1, u_2, \ldots, u_n = x_1, x_2, \ldots, x_n \tag{14}$$

(for antisymmetric modes)

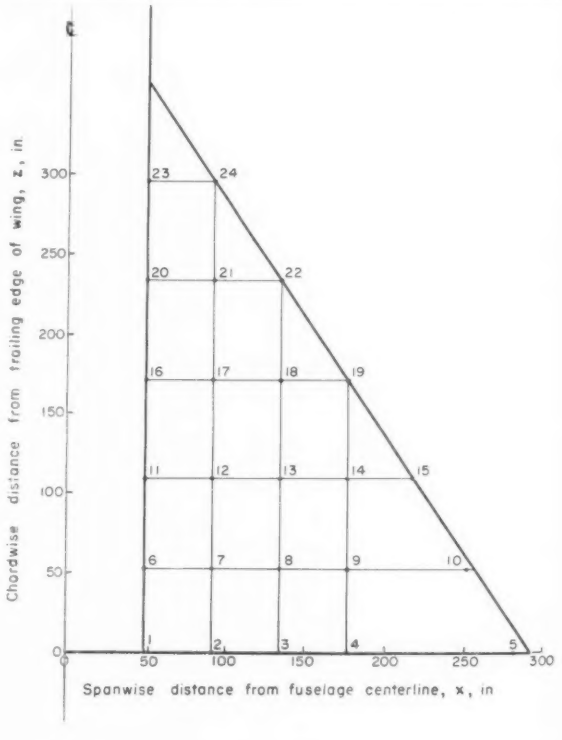

Figure 2 - Locations of stations on one wing

$$u_1, u_2, \ldots, u_n = z_1, z_2, \ldots, z_n \qquad (14')$$

(for symmetric modes)

It sums the elements of the above vectors as a check that they have been read in correctly and stores them internally. The code then computes the products

$$v_1, v_2, \ldots, v_n = M_1u_1, M_2u_2, \ldots, M_nu_n \qquad (15)$$

and the constants D, E, F, and G, where, for antisymmetric modes,

$$D = \sum_{r=1}^{n} v_r u_r \qquad (16)$$

$$E = 0 \qquad (17)$$

$$F = 0 \qquad (18)$$

$$G = 1 \quad D \qquad (19)$$

and, for symmetric modes,

$$D = \left(\sum_{r=1}^{n} M_r\right)\left(\sum_{r=1}^{n} v_r u_r\right) - \left(\sum_{r=1}^{n} v_r\right)^2 \qquad (16')$$

$$E = (1 \quad D)\left(\sum_{r=1}^{n} v_r\right), \qquad \text{one or more } u\text{'s} \neq 0 \qquad (17')$$

$$= 0, \qquad \text{all } u\text{'s} = 0$$

$$F = (1 \quad D)\left(\sum_{r=1}^{n} v_r u_r\right), \qquad \text{one or more } u\text{'s} \neq 0 \qquad (18')$$

$$= 1 \quad \left(\sum_{r=1}^{n} M_r\right), \qquad \text{all } u\text{'s} = 0$$

$$G = (1 \quad D)\left(\sum_{r=1}^{n} M_r\right), \qquad \text{one or more } u\text{'s} \neq 0 \qquad (19')$$

$$= 0, \qquad \text{all } u\text{'s} = 0$$

The numbers obtained in Eqs. (17) to (19) are printed out for use by the second code. The first code then reads in the influence coefficient matrix a row at a time, converts it into binary form, computes the rows of corresponding terms $B_{sr}^{(1)}$ in the dynamic matrix, and stores them together with their row sums on magnetic tape for use by the second code. A running sum of the terms in the influence coefficient matrix is also computed to be printed at the end as a check on "read in."

Iteration

The second code chooses as a starting vector, $y_1 = 1, y_2 = 1, \ldots, y_n = 1$. It then reads the dynamic matrix a row at a time from magnetic tape, checking the row sum, and performs the summation indicated

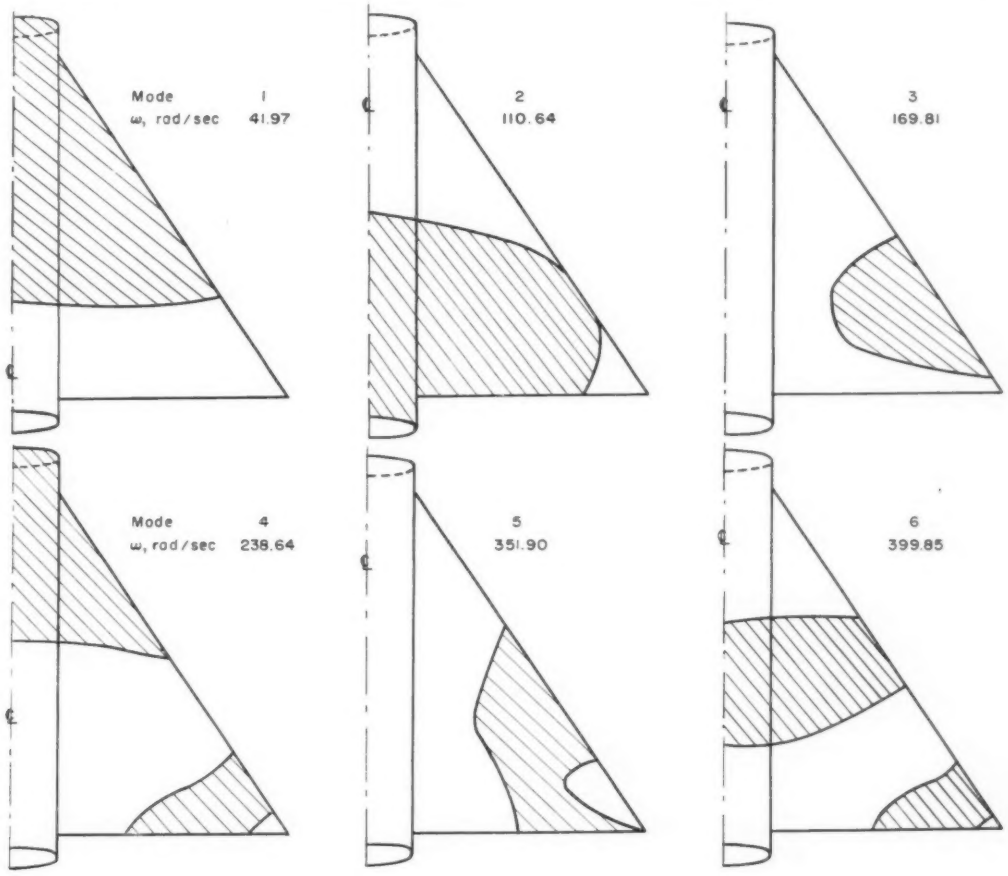

Figure 3– Nodal lines and frequencies of antisymmetric vibration modes of delta wing.

TABLE 2
Antisymmetric Influence Coefficient Matrix (10^3 in./lb.)

Station	1	2	3	4	5	6	7	8	9	10	11
1	.4130	.7403	.9581	1.1276	1.6164	.2474	.4351	.5975	.7368	.9796	.1766
2	.7403	1.4935	1.9705	2.3084	3.2803	.4588	.8366	1.1722	1.4572	1.9431	.3328
3	.9581	1.9705	2.7850	3.3395	4.7735	.6071	1.1291	1.6190	2.0448	2.7567	.4473
4	1.1276	2.3034	3.3395	4.2408	6.2804	.7234	1.3552	1.9718	2.5394	3.5005	.5392
5	1.6164	3.2803	4.7735	6.2804	11.9258	1.0510	1.9709	2.8950	3.8208	5.7745	.7962
6	.2474	.4588	.6071	.7234	1.0510	.1618	.2843	.3911	.4834	.6451	.1193
7	.4351	.8366	1.1291	1.3552	1.9709	.2843	.5212	.7256	.8990	1.2013	.2133
8	.5975	1.1722	1.6190	1.9718	2.8950	.3911	.7256	1.0374	1.3010	1.7510	.2965
9	.7368	1.4572	2.0448	2.5394	3.8208	.4834	.8990	1.3010	1.6721	2.2960	.3687
10	.9796	1.9431	2.7567	3.5005	5.7745	.6451	1.2013	1.7510	2.2960	3.4662	.4953
11	.1766	.3328	.4473	.5392	.7962	.1193	.2133	.2965	.3687	.4953	.0940
12	.3112	.5903	.7984	.9662	1.4293	.2093	.3789	.5304	.6612	.8886	.1640
13	.4331	.8281	1.1285	1.3737	2.0463	.2903	.5303	.7500	.9415	1.2716	.2268
14	.5436	1.0463	1.4364	1.7610	2.6618	.3636	.6674	.9520	1.2081	1.6525	.2840
15	.6397	1.2358	1.7058	2.1066	3.2597	.4277	.7864	1.1266	1.4415	2.0183	.3342
16	.1368	.2585	.3489	.4222	.6279	.0929	.1670	.2332	.2910	.3924	.0743
17	.2432	.4596	.6204	.7510	1.1168	.1650	.2970	.4153	.5184	.6986	.1318
18	.3409	.6449	.8719	1.0570	1.5764	.2311	.4169	.5841	.7306	.9867	.1843
19	.4309	.8161	1.1049	1.3420	2.0123	.2921	.5272	.7399	.9274	1.2589	.2329
20	.1158	.2188	.2953	.3576	.5325	.0786	.1414	.1976	.2468	.3330	.0629
21	.2072	.3913	.5281	.6393	.9520	.1407	.2530	.3535	.4413	.5956	.1127
22	.2920	.5517	.7446	.9017	1.3439	.1984	.3567	.4985	.6226	.8408	.1588
23	.1039	.1962	.2648	.3206	.4776	.0705	.1268	.1773	.2213	.2988	.0565
24	.1865	.3523	.4755	.5758	.8578	.1267	.2278	.3183	.3975	.5366	.1014

by the right-hand side of Eq. (1) for antisymmetric modes [or Eq. (8) for symmetric modes].

Using Eqs. (14), (15), and (17) to (19), it is seen that both Eq. (5) for removing rigid body modes from the tth antisymmetric mode and Eq. (13) for removing rigid body modes from the tth symmetric mode can be written for the deflection at station q as

$$\frac{y_q'}{\omega^2} = E\sum_{s=1}^{n} v_s \sum_{r=1}^{n} B_{sr}^{(t)} y_r - F\sum_{s=1}^{n} M_s \sum_{r=1}^{n} B_{sr}^{(t)} y_r + Eu_q \sum_{s=1}^{n} M_s \sum_{r=1}^{n} B_{sr}^{(t)} y_r - Gu_q \sum_{s=1}^{n} v_s \sum_{r=1}^{n} B_{sr}^{(t)} y_r + \sum_{r=1}^{n} B_{qr}^{(t)} y_r \quad (20)$$

The second code carries out the computation indicated by Eq. (20), normalizes the resulting mode shape to give unit deflection at a preselected station and compares the improved mode with the starting mode. It repeats this iteration cycle until the initial and final modes agree to a preset small value indicating that convergence is complete. The frequency ω_t is then computed, and the frequency and mode shape are converted from binary to decimal notation and printed.

Modification of Dynamic Matrix

The third code computes the terms in the new dynamic matrix for higher modes as indicated by Eq. (7), using the numbers already stored on magnetic tape. It stores this new dynamic matrix on magnetic tape together with row sums for checking purposes. The machine is then ready to take the second code and compute the next higher mode. This process is continued until all the desired modes have been obtained.

EXAMPLE

An example of the computation carried out by SEAC using these codes is given in Table 1 for the antisymmetric modes of a delta wing airplane. In column (1) of Table 1 is given the station number (only the half-wing stations 1 to 24 are given) column (2) gives the mass at the station, columns (3) and (4) give the x- and z-coordinates respectively and columns (5)–(10) give the mode shapes and natural frequencies for the first six modes. Fig. 2 shows the location of stations on one wing. The nodal lines for antisymmetric wing vibration are shown in Fig. 3. Similar results have been obtained for symmetric modes. The influence coefficient matrix used in the computation of the antisymmetric modes is given in Table 2. The computing time for six symmetric and six antisymmetric modes for this delta wing airplane having seven stations on the fuselage and 24 stations on each half-wing was 6 hours. This time is sufficiently short to make such computations practicable, where they could not be undertaken at all with desk computers.

CONCLUSIONS

It is concluded that the computation of vibration modes by high-speed electronic digital computers such as SEAC can be done for structures with many degrees of freedom. The computation time is relatively short and the data preparation time is moderate since it merely involves tabulation of the mass values and locations in addition to the influence coefficient matrix.

TABLE 2
(*Continued*)

12	13	14	15	16	17	18	19	20	21	22	23	24
.3112	.4331	.5436	.6397	.1368	.2432	.3409	.4309	.1158	.2072	.2920	.1039	.1865
.5903	.8281	1.0463	1.2358	.2585	.4596	.6449	.8161	.2188	.3913	.5517	.1962	.3523
.7984	1.1285	1.4364	1.7058	.3489	.6204	.8719	1.1049	.2953	.5281	.7446	.2648	.4755
.9662	1.3737	1.7610	2.1066	.4222	.7510	1.0570	1.3420	.3576	.6393	.9017	.3206	.5758
1.4293	2.0463	2.6618	3.2597	.6279	1.1168	1.5764	2.0123	.5325	.9520	1.3439	.4776	.8578
.2093	.2903	.3636	.4277	.0929	.1650	.2311	.2921	.0786	.1407	.1984	.0705	.1267
.3789	.5303	.6674	.7864	.1670	.2970	.4169	.5272	.1414	.2530	.3567	.1268	.2278
.5304	.7500	.9520	1.1266	.2332	.4153	.5841	.7399	.1976	.3535	.4985	.1773	.3183
.6612	.9415	1.2081	1.4415	.2910	.5184	.7306	.9274	.2468	.4413	.6226	.2213	.3975
.8886	1.2716	1.6525	2.0183	.3924	.6986	.9867	1.2589	.3330	.5956	.8408	.2988	.5366
.1640	.2268	.2840	.3342	.0743	.1318	.1843	.2329	.0629	.1127	.1588	.0565	.1014
.2919	.4058	.5078	.5971	.1301	.2319	.3253	.4105	.1103	.1975	.2784	.0990	.1778
.4058	.5730	.7223	.8510	.1805	.3223	.4542	.5742	.1533	.2744	.3870	.1375	.2470
.5078	.7223	.9275	1.1039	.2264	.4040	.5706	.7251	.1924	.3444	.4861	.1727	.3102
.5971	.8510	1.1039	1.3548	.2668	.4753	.6723	.8595	.2269	.4060	.5735	.2036	.3658
.1301	.1805	.2264	.2668	.0601	.1065	.1488	.1881	.0512	.0917	.1293	.0460	.0826
.2319	.3223	.4040	.4753	.1065	.1909	.2667	.3351	.0909	.1632	.2299	.0817	.1467
.3253	.4542	.5706	.6723	.1488	.2667	.3772	.4747	.1272	.2282	.3222	.1143	.2053
.4105	.5742	.7251	.8595	.1881	.3351	.4747	.6089	.1607	.2879	.4074	.1444	.2596
.1103	.1533	.1924	.2269	.0512	.0909	.1272	.1607	.0446	.0796	.1122	.0403	.0723
.1975	.2744	.3444	.4060	.0917	.1632	.2282	.2879	.0796	.1441	.2025	.0721	.1298
.2784	.3870	.4861	.5735	.1293	.2299	.3222	.4074	.1122	.2025	.2893	.1015	.1833
.0990	.1375	.1727	.2036	.0460	.0817	.1143	.1444	.0403	.0721	.1015	.0374	.0668
.1778	.2470	.3102	.3658	.0826	.1467	.2053	.2596	.0723	.1298	.1833	.0668	.1235

REFERENCES

[1] Duncan, W. J , and Collar, A. R., *A Method for the Solution of Oscillation Problems by Matrices*, Philos. Mag., Series 7, Vol. 17, No. 115, pp. 866–909, May, 1934.

[2] von Karman, Theodore, and Biot, Maurice A., *Mathematical Methods in Engineering*, p. 199; McGraw-Hill Book Co., New York, 1940.

[3] Beskin, L., and Rosenberg, R. M., *Higher Modes of Vibration by a Method of Sweeping*, Journal of the Aeronautical Sciences, Vol. 13, No. 11, pp. 597–604, November, 1946.

[4] Houbolt, John C., and Anderson, Roger A., *Calculation of Uncoupled Modes and Frequencies in Bending or Torsion of Nonuniform Beams*, NACA TN 1522, February, 1948.

[5] Kincaid, W. M., *Numerical Methods for Finding Characteristic Roots and Vectors of Matrices*, Quart. of Appl. Math., Vol. 5, No. 3, pp. 320–345, October, 1947.

[6] Levy, Samuel, *Computation of Influence Coefficients for Aircraft Structures with Discontinuities and Sweepback*, Journal of the Aeronautical Sciences, Vol. 14, No. 10, pp. 547–560, October, 1947.

[7] *The Operating Characteristics of the SEAC*, (anonymous), Mathematical Tables & Aids to Computation, Vol. 4, No. 32, pp. 229–230, October, 1950.

The Supersonic Conical Wing of Minimum Drag

(*Continued from page 817*)

[7] Graham, E. W., *A Drag Reduction Method for Wings of Fixed Plan Form*, Journal of the Aeronautical Sciences, Vol. 19, No. 12, pp. 823–825, December, 1952.

[8] Jones, R. T., *Wing Plan Forms for High-Speed Flight*, NACA TN 1033, 1946.

[9] Baldwin, B. S., Jr., *Triangular Wings Cambered and Twisted to Support Specified Distributions of Lift at Supersonic Speeds*, NACA TN 1816, 1949.

[10] Jones, R. T., *The Use of Conical and Cylindrical Fields in Supersonic Wing Theory*, NACA University Conference on Aerodynamics, Langley Aero. Lab., June 21–23, 1948.

[11] Goldstein, S., and Ward, G. N., *The Linearized Theory of Conical Field in Supersonic Flow, with Application to Plane Airfoils*, Aeronautical Quarterly, Vol. II, pp. 39–84, 1950.

[12] Durand, W. F., (Ed.), *Aerodynamic Theory;* von Kármán, Th., and Burgers, J. M., "General Aerodynamic Theory—Perfect Fluids," Vol. II, pp. 48–53; Springer, Berlin, 1953.

[13] Brown, C. E., *Theoretical Lift and Drag of Thin Triangular Wings at Supersonic Speeds*, NACA TN 1183, 1946.

[14] Jones, R. T., *Estimated Lift-Drag Ratios at Supersonic Speed* , NACA TN 1350, 1947.

[15] Stewart, H. J., *The Lift of a Delta Wing at Supersonic Speeds*, Quar. App. Math., Vol. IV, No. 3, pp. 246–254, October, 1946.

[16] McCullough, G. B., and Gault, D. E., *Examples of Three Representative Types of Airfoil-Section Stall at Low Speed*, NACA TN 2502, 1951.

[17] Vincenti, W. G., *Comparison Between Theory and Experiment for Wings at Supersonic Speeds*, NACA TR 1033, 1951.

[18] Brown, C. E., and Adams, M. C., *Damping in Pitch and Roll of Triangular Wings at Supersonic Speeds*, NACA TN 1566, 1948.

The Flat Plate with an Angle of Attack in a Choked Wind Tunnel

K. GOTTFRIED GUDERLEY*
Wright Air Development Center

Introduction

Recently, B. Marschner[1] has shown, that in a choked wind tunnel, the wall influence on the pressure distribution over a wedge is rather small. This is of interest for the question of transonic wind-tunnel testing. It appears desirable to extend the investigations to a body with an angle of attack.

This is done in the present paper for an inclined plate. By repeated application of an idea used previously[2] to determine the flow over this body at Mach Number one, the numerical work can be kept within reasonable bounds.

Aside from the numerical result which illustrates the wall influence on the pressure distribution over the plate, the general approach also deserves some interest as an example for the treatment of unsymmetric flow patterns in the vicinity of Mach Number one; this theory was developed in reference 3.

Some details of the investigations which might have interrupted the general line of thought have been relagated to a second part. The first part contains the leading ideas and a discussion of the results. Although only loosely related to the present subject, some remarks have been added which show in principle how the flow in a choked closed tunnel can be interpreted as the flow with a slightly changed angle of attack at a Mach Number different from one.

Part I—The Principal Ideas of the Investigations and the Results

(1) *The Basic Equations of the Hodograph*

Let w and θ be the absolute valute value of the velocity vector and its angle with a fixed axis. They are the independent variables of the hodograph. In transonic work the variable w is frequently replaced by another variable η defined by the equation

$$w = w^*[1 + (\gamma + 1)^{-1/3} \cdot \eta] \qquad \text{(I, 1)}$$

here w^* is the value of w at the sonic velocity and γ is the ratio of the specific heats. By a limiting process in which the deviations from the sonic velocity are assumed to be small—the details of which are carried out in reference 4—the equation for the stream function ψ in the η, θ-plane is simplified to

$$\psi_{\eta\eta} - \eta \cdot \psi_{\theta\theta} = 0 \qquad \text{(I, 2)}$$

Consistent with this approximation the pressure coefficient for sonic condition is expressed by

$$c_p = (p - p^*)/(\rho^* w^{*2}/2) = -2(\gamma + 1)^{-1/3} \cdot \eta \quad \text{(I, 3a)}$$

Here p is the pressure, p^* the sonic pressure, and ρ^* the density at sonic speed. Similarly, one finds for the Mach Number M

$$M - 1 = (1/2) \cdot (\gamma + 1)^{2/3} \cdot \eta \qquad \text{(I, 3b)}$$

After ψ is found, the coordinates x and y in the physical plane are determined from the relations

$$x_\eta = (\gamma + 1)^{1/3} \cdot \eta \cdot \psi_\theta \qquad \text{(I, 4a)}$$

$$x_\theta = (\gamma + 1)^{1/3} \cdot \psi_\eta \qquad \text{(I, 4b)}$$

$$y = \psi \qquad \text{(I, 4c)}$$

Here the stream density at the sonic speed is put equal to one.

(2) *The Boundary Value Problem*

The flow over an inclined plate in a choked wind tunnel is shown in Fig. 1. Sonic lines start at the trailing edge and at the leading edge and extend to the walls. A stagnation point is obtained at the pressure side (the lower side in Fig. 1) of the plate; it lies close to the leading edge. Streamlines that lie slightly above the stagnation streamline experience first a reversal of the flow direction and then spill over the leading edge. The Meyer expansion that arises at the leading edge propagates into these streamlines. This explains the shape of the sonic line, which starts at the leading edge on the lower side of the plate in a direction normal to its surface and then bends upward to reach the upper wall. Theoretically, one obtains at the suction side of the plate, right behind the leading edge, a complete vacuum. Naturally, other physical effects will interfere here, but their influence on the subsonic part of the field is negligible.

Since the pressure on the suction side is lower than the sonic pressure, a Meyer expansion will also start at the trailing edge. The sonic line extends into the lower part of the flow field and finally reaches the lower wind-tunnel wall.

The hodograph is shown in Fig. 2. Corresponding points in Figs. 1 and 2 have the same notation. Point D is the leading edge, point C the stagnation point, point B the trailing edge. The free-stream velocity is marked by point P; at this point all streamlines origi-

Received August 31, 1954.

* Applied Mechanics Branch, Aeronautical Research Laboratory.

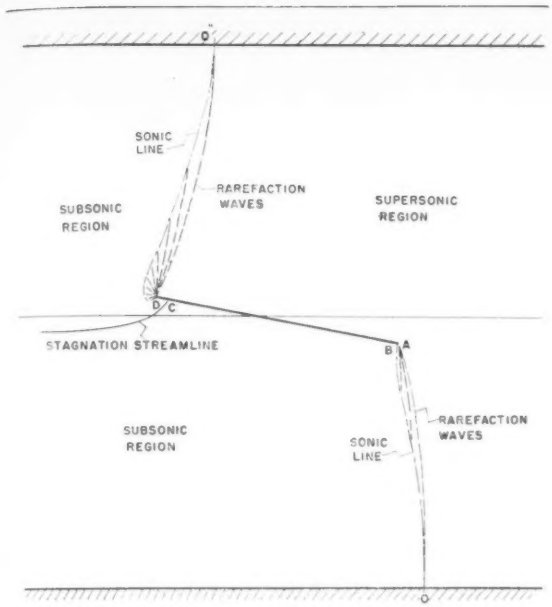

FIG. 1. Flow over a flat plate in a closed tunnel at choking.

nate. For the streamline that runs from infinity (point P) to the stagnation point C and then follows the surface of the body, we set $\psi = 0$. Part of the streamlines that lie, in the hodograph, as well as in the physical plane, above the stagnation streamline, will spill over the leading edge.

The map of the lower wind-tunnel wall is given by PQO′, the map of the upper wall by PO″. It is important that the points P and Q do not coincide (as they do for symmetric bodies for reasons of symmetry). At the present we do not know whether point P lies at the upper or lower side of OQ. Our description of the flow field refers to a location of the point P as shown in Figs. 2 and 3. The relative location of points P and Q is an additional parameter of the problem. It is determined during the computations by the requirement that at zero velocity, there is a branch point of the streamlines. From the physical point of view it appears so natural that a branch point of the streamlines must lie at zero velocity, that one might expect this condition to be fulfilled automatically. A counterexample is given by the incompressible hodograph for which, from the mathematical point of view, the stagnation point is equivalent to all other points of the hodograph. Moreover, flow patterns with a hodograph according to Fig. 2, possess a physical significance—although only little practical importance—even in the case where the branch point of the streamlines does not coincide with the stagnation point.

Fig. 3 shows the boundary value problem in the η, θ-plane. The origin of the coordinate system is placed into point B. By the simplifications made in the derivation of differential Eq. (2), the boundary CDE moves to infinity. Along the line ABC we have $\psi = 0$, and the boundary condition along CDE expresses itself now as the requirement that ψ vanishes at infinity. For the Mach wave EO″, one obtains the condition that no singularity propagates along it, and that it does not map to infinity. The condition that point C is a branch point of the streamlines is now expressed by the requirement that infinity is a branch point of the streamlines. As a consequence of the approximation, the stagnation point coincides in the physical plane with the leading edge of the airfoil—i.e., the region of reversed flow becomes smaller and smaller as the angle of attack is reduced.

The width of the wind tunnel may be unity, and we allow for the possible displacement of the model in the direction toward the upper wall by an amount c. Then we have as boundary conditions along the wall: $\psi = \text{const.} = 1/2 - c$ for O′QP and $\psi = \text{const.} = -1/2 - c$ along PO″.

(3) *Method of Solution*

In the following computations, the assumption will be made that the choking Mach Number is very close to one—i.e., that for a given angle of attack, QO′ is very short. This requires that the wind tunnel is sufficiently wide. The future computations will show that the ratio $|\eta_Q|/(3\theta_0/2)^{2/3}$ must be small, where η_Q is the value of η at point Q and θ_0 is the angle of attack.

Under this assumption one can expect the pressure distribution over the plate to be expressible as a development with respect to η_Q—i.e., the solution will appear as the solution at Mach one with certain correction terms added.

The calculation proceeds in the following steps.

Step 1. One determines a family of particular solutions that fulfill the boundary conditions at the map of the plate and are free of singularities within the region bounded by EOABC. Naturally, they will then disregard the boundary condition along O′QPO″. Since the boundary condition along ABC and at infinity is

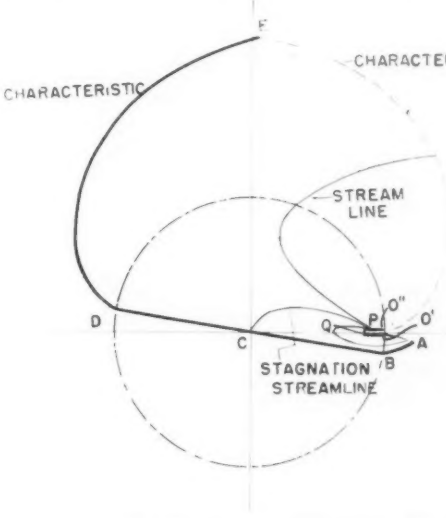

FIG. 2. Hodograph representation of Fig. 1.

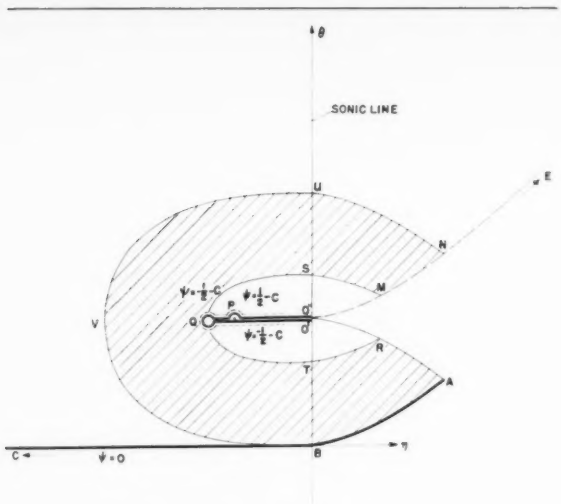

FIG. 3. Flow in the η, θ plane.

homogeneous, there must be at least one singularity in the flow field. This singularity will be placed into the point $O \equiv O' \equiv O''$. Actually in each particular solution, three singularities will be superimposed on each other at point O in order to fulfill the additional conditions that infinity is branch point of the streamlines and that the plate has a given length.

The most general solution that fulfills the boundary conditions at the plate can be obtained by a superposition of these particular solutions—within a region in which this superposition converges. The map of the wall will lie outside of the region of convergence, but the map of the plate is within this region provided that OQ is sufficiently small. The coefficients by which these solutions are multiplied are naturally undetermined at this point of the calculations. The shape of the body in consideration enters only this part of the computations.

Step 2. We determine the most general solution that fulfills the boundary condition along $O'QPO''$, but is otherwise free of singularities within the subsonic regime. Here the boundary condition at the plate is disregarded. For this purpose, one finds first an expression which fulfills the inhomogeneous boundary condition prescribed along $O'QPO''$, and then superimposes expressions which have $\psi = 0$ along this line. These latter expressions must have at least one singularity in the flow field which will be placed to infinity. The solution that fulfills the inhomogeneous boundary condition will have the location of point P and of point Q as parameters. The most general expression that fulfills the boundary conditions at the wall is obtained by superimposing the particular solutions which have $\psi = 0$ along OQ, on the solution which fulfills the inhomogeneous boundary conditions along OQ.

Step 3. If OQ is sufficiently small, the solutions found in Steps 1 and 2 have a common region of validity. There they must coincide. This yields an infinite system of equations for the coefficients that were left undetermined in the previous steps. This system can be solved by a development with respect to the length OQ—i.e., with respect to the deviation of the choking Mach Number from 1.

Details of Steps 1 and 2 are found in the second part. In the following paragraphs we derive the form that the results of these investigations will assume, from a reasoning of plausibility, and then proceed to calculate the final results.

(4) *Certain Particular Solutions of Eq. (I, 2)*

The particular solutions which are obtained by the steps described previously, appear as the superposition of other particular solutions which have been investigated in references 3 and 4. Some of their properties will be described subsequently. We introduce new independent variables

$$\rho = -\eta^3 + (9/4)\theta^2 \qquad \text{(I, 5a)}$$

$$\xi = \eta/[(3/2)\theta]^{2/3} \qquad \text{(I, 5b)}$$

If one makes the product hypothesis

$$\psi = \rho^{-(1/12) \pm \sqrt{\lambda}/3} G(\xi, \lambda) \qquad \text{(I, 6)}$$

where λ is an arbitrary parameter, one is led to the following differential equation for G.

$$\frac{\partial}{\partial \xi}\left[(1-\xi^3)^{5/6}\frac{\partial G}{\partial \xi}\right] + \left(-\lambda + \frac{1}{16}\right)\times \frac{\xi}{(1-\xi^3)^{7/6}}\cdot G = 0 \qquad \text{(I, 7)}$$

For a given value of λ, the differential equation has two linearly independent solutions. They can be chosen such that the expressions ψ which arise from Eq. (I, 6) are either symmetric or antisymmetric with respect to the line $\xi = -\infty$. This will be indicated by the notation $G^{(s)}$ or $G^{(a)}$ respectively. We impose the condition that, for $\xi = -\infty$, $G^{(s)} = 1$ and $G^{(a)}$ behaves as $(-\xi)^{-3/2}$. Obviously, if an expression $\psi(\eta, \theta)$ fulfills Eq. (I, 2), then also $\psi(\eta, \bar{\theta})$, where $\bar{\theta} = \theta -$ const., is a solution. We shall use $\bar{\theta} = \theta - \theta_0$—i. e., the origin of the η, $\bar{\theta}$-system will be placed at point O. The variables ρ and ξ [Eq. (I, 5)] will then be denoted by $\bar{\rho}$ and $\bar{\xi}$.

As can be found from the character of the functions G for large values of λ (reference 4, Part 3j), the boundary for the region in which a superposition of the particular solutions found in the first step will converge, is given in the subsonic region by the line $\bar{\rho} =$ const. through point Q (line SQT) and in the supersonic region by the characteristics TR and MS. The region of convergence for the superposition of the particular solutions found in the second step is bounded in the subsonic region by the line $\bar{\rho} =$ const. through point B (line UVB), and in the supersonic region by the characteristics BA and UN. The shaded region in Fig. 3 is common to both representations.

Now we ask which solution of the form (I, 6) taken for the $\bar{\rho}$, $\bar{\xi}$-system will occur in the representation of the solution in the shaded region. The conditions

imposed are that along AO and EO no singularities propagate and that these Mach waves do not map to infinity. The particular solutions can be symmetric as well as antisymmetric with respect to the line $\bar{\xi} = -\infty$. This discussion is carried out in the second part. One finds the following values of $\sqrt{\lambda}$:

For the antisymmetric solutions:

$$\left.\begin{aligned}\sqrt{\lambda} &= (3/4) + h\\ \sqrt{\lambda} &= -(9/4) - 3h\end{aligned}\right\} \quad h = 0, 1 \ldots$$

For the symmetric solutions:

$$\left.\begin{aligned}\sqrt{\lambda} &= (1/4) + h\\ \sqrt{\lambda} &= -(3/4) - 3h\end{aligned}\right\} \quad h = 0, 1 \ldots$$

The value of ρ for point O may be denoted by ρ_0. Expressed by the angle of attack θ_0, we have $\rho_0 = (9/4)\cdot\theta_0^2$. The particular solutions (I, 6) obtained by the last discussion will be multiplied with suitable powers of ρ_0 and then denoted in the following manner.

Antisymmetric solutions:

$$\psi_{-(5/6)-h} = \pm(\bar{p}/\rho_0)^{-(5/6)-h}\cdot G^{(a)}\{\xi,[(9/4)+3h]^2\} \quad \text{(I, 8a)}$$

$$\psi_{(1/6)+(h/3)} = \pm(\bar{p}/\rho_0)^{(1/6)+(h/3)} \times G^{(a)}\{\xi,[(3/4)+h]^2\} \quad \text{(I, 8b)}$$

Symmetric solutions:

$$\psi_{-(1/3)-h} = (\bar{p}/\rho_0)^{-(1/3)-h}\cdot G^{(s)}\{\xi,[(3/4)+3h]^2\} \quad \text{(I, 8c)}$$

$$\psi_{h/3} = (\bar{p}/\rho_0)^{h/3}\cdot G^{(s)}\{\xi,[(1/4)+h]^2\} \quad \text{(I, 8d)}$$

The upper and lower signs apply for $\theta > 0$ and $\theta < 0$ respectively. The subscripts of ψ give the power to which $\bar{p}/\rho_0$ is raised.

(5) *Solutions Fulfilling the Boundary Conditions at the Plate*

Among the particular solutions just listed, those with a negative subscript are singular at point O. The particular solutions which fulfill the boundary conditions at the plate will be denoted by capital Ψ with a superscript which corresponds to the strongest singularity which occurs at point O.

Let us first consider the expression which describes the flow with a free stream Mach Number one. Here the singularity which occurs at point O is given by $\psi_{-5/6}$. To fulfill the additional condition that infinity is a branch point of the streamlines, one needs another solution which has $\psi = 0$ along the map of the plate. The only singularity which can be used in this case is $\psi_{-1/3}$, (reference 3, p. 50, or reference 5, p. 760). Furthermore, the length of the plate in the physical plane is prescribed; this condition will be fulfilled by multiplying the hodograph expression with a suitable factor. Thus, the flow with a free-stream Mach Number one has in principle the form

$$\psi = (L/l)\cdot\Psi^{-5/6} \quad \text{(I, 9a)}$$

where

$$\Psi^{-5/6} = \psi_{-5/6} + \alpha_{-1/3}{}^{-5/6}\psi_{-1/3} + \sum_{k=0}^{\infty}\alpha_{(1/6)+(k/3)}{}^{-5/6}\cdot\psi_{(1/6)+(k/3)} + \sum_{k=0}^{\infty}\alpha_{k/3}{}^{-5/6}\cdot\psi_{k/3} \quad \text{(I, 9b)}$$

Here L is the length of the plate, and l and the α's are constants—l is the length obtained from the solution $\psi^{-5/6}$. The α will be determined in the second part. Their superscripts are those of the functions ψ in whose representation they occur; their subscripts are those of the function ψ whose coefficients they are. The terms in the sum give the regular terms which will naturally occur in the representation of the solution in the vicinity of point O.

The other particular solutions which fulfill the boundary conditions at the plate are constructed in a similar manner. One first finds a solution which has $\psi = 0$ along the map of the plate surface and is singular at point O. The singularity may be given by $\psi_{-(5/6)-h}$, or by $\psi_{(-1/3)-h}$ $(h = 1, 2, \ldots)$. One superimposes to this particular solution of the same type with $\psi_{-1/3}$ as singularity at point O, in order to make infinity a branch point of the streamlines. The expression thus obtained will in general change the length of the plate when it is superimposed to the basic flow at Mach Number one. Therefore, the expression (I, 9b) multiplied with a suitable constant is superimposed on it, such that the resulting expression does not give a contribution to the length of the plate. Thus these particular solutions have the form

$$\Psi^{-(5/6)-h} = \psi_{-(5/6)-h} + \alpha_{-5/6}{}^{-(5/6)-h}\cdot\psi_{-5/6} + \alpha_{-(1/3)}{}^{-(5/6)-h}\cdot\psi_{-1/3} + \sum_{k=0}^{\infty}\alpha_{(1/6)+(k/3)}{}^{-(5/6)-h} \times \psi_{(1/6)+(k/3)} + \sum_{k=0}^{\infty}\alpha_{k/3}{}^{-(5/6)-h}\cdot\psi_{k/3} \quad \text{(I, 9c)}$$

$$\Psi^{-(4/3)-h} = \psi_{-(4/3)-h} + \alpha_{-5/6}{}^{-(4/3)-h}\cdot\psi_{-5/6} + \alpha_{-1/3}{}^{-(4/3)-h}\cdot\psi_{-1/3} + \sum_{k=0}^{\infty}\alpha_{(1/6)+(k/3)}{}^{-(4/3)-h} \times \psi_{(1/6)+(k/3)} + \sum_{k=0}^{\infty}\alpha_{(k/3)}{}^{-(4/3)-h}\cdot\psi_{k/3} \quad \text{(I, 9d)}$$

(6) *Remarks Concerning a Body of a More General Shape*

For a more general body, the solutions which fulfill the boundary conditions at its surface have, in principle, the same form. The quantity ρ_0 which occurs in the definition (I, 8) can be fixed arbitrarily. L is a characteristic length of the body; l is the value of this length as obtained from the solution $\Psi^{-5/6}$. One starts the calculation of such flow patterns with the flow over the body at Mach Number one. At point O the same singularities will occur as for the flat plate.[3] Thus the solution will have the form (I, 9a) and (I, 9b); naturally the constants in Eq. (I, 9) will be different. Next those particular solutions are determined, which, if superimposed to the basic flow, leave the surface of the body unchanged. Here a linearization of the boundary condition in the hodograph is required.[3]

The solutions thus obtained have the form of the expressions (I, 9c) and (I, 9d).

These considerations yield a simple interpretation for the solution $\Psi^{-4/3}$ in the case of a body of an arbitrary shape. Let us assume that the flow over an arbitrary body at Mach Number one is known, and also that the angle of attack is changed by a small amount. The change of the angle of attack is conveniently expressed in the hodograph by the shift of point O along the sonic line. Denoting the change of the angle of attack by $\Delta\alpha$, and considering for a moment the function $\Psi^{-5/6}$ as function of η and $\bar{\theta}$, we can write the strongest singularity of Eq. (I, 9b) in the form

$$[L/l(\Delta\alpha)]\cdot\psi_{-5/6}(\eta,\ \bar{\theta}-\Delta\alpha)$$

Consider now the first order terms in a development with respect to $\Delta\alpha$. The predominating term is found from the last equation as

$$-[L/l(\Delta\alpha)]\cdot(\partial\psi_{-5/6}/\partial\bar{\theta})$$

Thus the change of the angle of attack is equivalent to the superposition of a solution which leaves the surface of the body unchanged and has at point O a singularity given by $(\partial\psi_{-5/6}/\partial\bar{\theta})$ together with other singularities $\psi_{-5/6}$ and $\psi_{-1/3}$ which appear automatically in the solution of the boundary value problem.

Now $(\partial\psi_{-5/6}/\partial\bar{\theta})$ is proportional to $\psi_{-4/3}$ as can be seen from reference 4 where the same particular solutions are discussed in a slightly different form. The factor of proportionality is best obtained from the behavior of the functions along the line $\bar{\xi}=-\infty$. There, according to Eq. (I, 8a) and (I, 8b) and the definitions for $G^{(a)}$,

$$\psi_{-5/6}=(\bar{p}/\rho_0)^{-5/6}\cdot(-\bar{\xi})^{-3/2}=(\bar{p}/\rho_0)^{-5/6}\times[(3/2)\bar{\theta}/(-\eta)^{3/2}]$$

Because of the definition of $\bar{p}$, [Eq. (I, 5a)]

$$(\partial\bar{p}/\partial\bar{\theta})=0\quad\text{for }\bar{\theta}=0$$

and thus, $(\partial\psi_{-5/6}/\partial\bar{\theta})=(3/2)\cdot(\bar{p}/\rho_0)^{-4/3}\cdot\rho_0^{-1/2}$

According to Eq. (I, 8c), this is the behavior of

$$(3/2)\cdot\rho_0^{-1/2}\cdot\psi_{-4/3}\qquad\text{at }\bar{\xi}=-\infty$$

Thus it follows that the effect of a small change of the angle of attack $\Delta\alpha$ is expressed in the vicinity of the body by a superposition of

$$-(3/2)\cdot(L/l)\cdot\Psi^{-4/3}\cdot\rho_0^{-1/2}\cdot\Delta\alpha\qquad\text{(I, 9e)}$$

One is tempted to interpret also the other particular solutions $\Psi^{-11/6}$, $\Psi^{-7/3}$, Eqs. (I, 9c), and (I, 9d) in a similar manner—i.e., as higher order terms in a development with respect to the angle of attack. For a general body this leads to difficulties because of the linearization required in fulfilling the boundary conditions at the surface of the body. In the case of the plate where the boundary condition is *linear*, and where the solution is known for any angle of attack, the particular solutions $\Psi^{-(5/6)-k}$ and $\Psi^{-(1/3)-k}$ are in principle contained in the expression for the flow at Mach Number one. Obviously, expressions of the form (II, 16) which are used for the determination of the particular solutions $\Psi^{-(5/6)-k}$ etc., arise by repeated differentiation of the expression (II, 16a), which gives the flow over a flat plate at Mach Number one.

(7) *Solutions Fulfilling the Boundary Conditions at the Wind Tunnel Walls*

The solutions which fulfill the homogeneous boundary condition $\psi=0$ along O′QO″, have one singularity at infinity, given by a particular solution—Eq. (I, 8)—with a positive subscript. Besides, they contain a superposition of functions with a negative subscript which are regular at infinity. Particular solutions which are antisymmetric with respect to $\bar{\xi}=-\infty$, fulfill the condition $\psi=0$ along O′QO″ immediately. Denoting particular solutions which have $\psi=0$ along O′QO″ by capital Ψ with a superscript corresponding to the subscript of the particular solution which is singular at infinity, we thus have

$$\Psi^{(1/6)+(h/3)}=\psi_{(1/6)+(h/3)}\qquad\text{(I, 10a)}$$

For a singularity which is symmetric with respect to $\bar{\xi}=-\infty$, the entire expression ψ will be symmetric with respect to this line. In such particular solutions no antisymmetric terms (I, 8a) will appear.

$$\Psi^{h/3}=\psi_{h/3}+\sum_{k=0}^{\infty}\beta_{(-1/3)-k}^{h/3}(\bar{p}_Q/\rho_0)^{h/3+1/3+k}\times\psi_{(-1/3)-k}\qquad\text{(I, 10b)}$$

Here $\bar{p}_Q$ is the value of $\bar{p}$ at point Q. The constants β play a role similar to that of the α. It is not surprising that in these particular solutions the ratio $(\bar{p}_Q/\rho_0)$ appears as a parameter.

The determination of the inhomogeneous particular solutions is simplified by the fact that for a sufficiently small model, the ratio of the length PQ to the length OQ is small. In the vicinity of point Q, the differential Eq. (2) for ψ can be simplified to

$$\psi_{\eta\eta}+|\eta_Q|\cdot\psi_{\theta\theta}=0$$

η_Q is the value of η at point Q. This is Laplace's equation. In a region where this equation is applicable, an expression which fulfills the inhomogeneous boundary conditions along OQ can be represented by

$$\psi=(1/2)-c-(1/\pi)\times Im\log\left(\sqrt{\eta+i\bar{\theta}/|\eta_Q|^{-1/2}+|\eta_Q|}-\sqrt{|\eta_Q|-|\eta_P|}\right)\qquad\text{(I, 11)}$$

Here η_P is the value of η at point P. The second root in the argument of the logarithm is positive; for the path O″PQ, the first root is positive, too. The sign of the difference between the two roots is positive between P and O″, negative between Q and P. As one travels around point P on the path indicated in Fig. 3 by the dashed line, the argument of

$$\sqrt{\eta+i\bar{\theta}/\eta_Q|^{-1/2}+|\eta_Q|}-\sqrt{|\eta_Q|-|\eta_P|}$$

increases from 0 to π. Thus we have $\psi=(1/2)-c$

along PO″, and $\psi = -(1/2) - c$ along PQ. As one travels around point Q along the path indicated, the first root changes its sign and the expression

$$\sqrt{\eta + i\bar{\theta}\,|\eta_Q|^{-1/2} + |\eta_Q|} - \sqrt{|\eta_Q| - |\eta|_P}$$

remains negative, thus $\psi = -(1/2) - c$ along QO′.

If $\left|\sqrt{|\eta_Q| - |\eta_P|}\right| < \left|\sqrt{\eta + i\bar{\theta}\,|\eta_Q|^{-1/2} + |\eta_Q|}\right|$

then the expression (I, 11) can be developed with respect to $\sqrt{|\eta_Q| - |\eta_P|}$.

$$\psi = (1/2) - c - (1/2\pi)\, Im \log (\eta + i\bar{\theta}\,|\eta_Q|^{-1/2} + |\eta_Q|) - (1/\pi)\cdot\sqrt{|\eta_Q| - |\eta_P|}\times Im\,(\eta + |\eta_Q| + i\bar{\theta}\cdot|\eta_Q|^{-1/2})^{-1/2} \quad \text{(I, 12)}$$

Thus the desired inhomogeneous expression is represented for small values of the distance PQ by the superposition of two singular expression whose local behavior is described by the analytic functions occurring in Eq. (I, 12).

The logarithmic singularity in Eq. (I, 12) combined with the constant 1/2 fulfills the boundary conditions $\psi = 1/2$ along O″Q and $\psi = -1/2$ along O′Q. This solution (except for a factor 1/2) has been considered in reference 1 in conjunction with the flow over a symmetrical body in a choked tunnel. For $\bar{p} > \bar{p}_Q$, this expression is represented by

$$\psi_I = \pm \sum_{h=0}^{\infty} \gamma_{-(5/6)-h}\cdot(\bar{p}_Q/\rho_0)^{(5/6)+h}\cdot\psi_{-(5/6)-h} \quad \text{(I, 13)}$$

The upper sign is valid for $\bar{\theta} > 0$, the lower one for $\bar{\theta} < 0$. The constants γ can be found from reference 1 as

$$\gamma_{-(5/6)-h} = \frac{1}{\pi\cdot\sqrt{3}}\,\frac{\Gamma[(5/3)+h]}{\Gamma(2/3)}\cdot\frac{\Gamma[(4/3)+h]}{\Gamma(1/3)}\times\frac{\Gamma(5/6)}{\Gamma[(11/6)+h]}\cdot\frac{\Gamma(1/6)}{\Gamma[(7/6)+h]}$$

$$= \frac{1}{\pi\sqrt{3}}\cdot\frac{2/3\cdot 5/3\ldots(2/3)+h}{5/6\cdot 11/6\ldots(5/6)+h}\times\frac{1/3\cdot 4/3\ldots(1/3)+h}{1/6\cdot 7/6\ldots(1/6)+h} \quad \text{(I, 13a)}$$

The expression (I, 13) does not contain terms which are singular at infinity.

The other singular term in (I, 12) yields $\psi = 0$ along O′Q and O″Q. A representation for it will be derived in the second part. It can be characterized by its behavior for $\bar{\theta} = 0$, $\eta < -|\eta_Q|$:

$$(1/\pi)\cdot(|\eta_Q| - |\eta_P|)^{1/2}\cdot(|\eta| - |\eta_Q|)^{-1/2}$$

This particular solution is symmetric with respect to the line $\xi = -\infty$. It will not contain terms which are singular at infinity. Thus one will expect it to have the form

$$\psi_{II} = \sum_{h=0}^{\infty} \delta_{-(1/3)-h}\cdot(\bar{p}_Q/\rho_0)^{(1/3)+h}\cdot\psi_{-(1/3)-h} \quad \text{(I, 14)}$$

The expression ψ_{II} derived in the second part behaves for $\bar{\theta} = 0$ and $\rho > \rho_Q$ as

$$(1/\sqrt{3})\cdot|\eta_Q|^{1/2}(|\eta| - |\eta_Q|)^{-1/2}$$

(8) *Solution of the Boundary Value Problem*

The most general expression which fulfills the conditions at the plate surface is given by a superposition of the solution (I, 9), which may be written in the form

$$\psi = (L/l)\left[\Psi^{-5/6} + \sum_{h=1}^{\infty} A^{-(5/6)-h}\cdot\Psi^{-(5/6)-h} + \sum_{h=0}^{\infty} A^{-(4/3)-h}\cdot\Psi^{-(4/3)-h}\right] \quad \text{(I, 15)}$$

Here the A's are constants which will be determined subsequently. The most general expression which fulfills the conditions at the wind-tunnel wall is given by a superposition of ψ_I (Eq. I, 13), of ψ_{II} (Eq. I, 14), of the expressions (I, 10), and of a constant $-c$ which takes into account a possible displacement of the model from the centerline of the wind tunnel.

$$\psi = \psi_I + C'\cdot\psi_{II} + \sum_{h=0}^{\infty} B^{(1/6)+(h/3)}\cdot\Psi^{(1/6)+(h/3)} + \sum_{h=0}^{\infty} B^{h/3}\,\Psi^{h/3} - c \quad \text{(I, 16)}$$

where $C' = (\sqrt{3}/\pi)\,|\eta_Q|^{-1/2}\,(|\eta_Q| - |\eta_P|)^{1/2}$ (I, 16b)

The coefficient C' of the second term and the B's are unknown. In the common region of validity the expressions (I, 15) and (I, 16) must coincide. A sufficient condition is that the coefficients of the individual particular solutions (I, 8) are the same. This yields the following equations:

terms with $\psi_{-(5/6)-h}$, $(h = 1,2\ldots)$

$$(L/l)\cdot A^{-(5/6)-h} = \gamma_{-(5/6)-h}\cdot(\bar{p}_Q/\rho_0)^{(5/6)+h} \quad \text{(I, 17a)}$$

terms with $\psi_{-(5/6)}$

$$(L/l)\left[1 + \sum_{k=1}^{\infty} A^{-(5/6)-k}\cdot\alpha_{-5/6}{}^{-(5/6)-k} + \sum_{k=0}^{\infty} A^{-(4/3)-k}\cdot\alpha_{-5/6}{}^{-(4/3)-k}\right] = \gamma_{-5/6}(\bar{p}_Q/\rho_0)^{5/6} \quad \text{(I, 17b)}$$

terms with $\psi_{-(4/3)-h}$, $h = 0, 1\ldots$

$$(L/l)\cdot A^{-(4/3)-h} = C'\cdot\delta_{-(4/3)-h}\cdot(\bar{p}_Q/\rho_0)^{(4/3)+h} + \sum_{k=0}^{\infty} B^{k/3}\cdot\beta_{-(4/3)-h}{}^{k/3}\cdot(\bar{p}_Q/\rho_0)^{(k/3)+(4/3)+h} \quad \text{(I, 17c)}$$

terms with $\psi_{-1/3}$

$$(L/l)\left[\alpha_{-1/3}{}^{-5/6}+\sum_{k=1}^{\infty}A^{-(5/6)-k}\cdot\alpha_{-1/3}{}^{-(5/6)-k}+\sum_{k=0}^{\infty}A^{-(4/3)-k}\cdot\alpha_{-1/3}{}^{-(4/3)-k}\right]=$$
$$C'\cdot\delta_{-1/3}\,(\bar{p}_Q/\rho_0)^{1/3}+\sum_{k=0}^{\infty}B^{k/3}\cdot\beta_{1/3}{}^{k/3}\,(\bar{p}_Q/\rho_0)^{(k/3)+(1/3)} \qquad \text{(I, 17d)}$$

terms with $\psi_{h/3}$, $h = 1,2\ldots$

$$(L/l)\left[\alpha_{h/3}{}^{-5/6}+\sum_{k=1}^{\infty}A^{-(5/6)-k}\cdot\alpha_{h/3}{}^{-(5/6)-k}+\sum_{k=0}^{\infty}A^{-(4/3)-k}\cdot\alpha_{h/3}{}^{-(4/3)-k}\right]=B^{h/3} \qquad \text{(I, 17e)}$$

Since $\psi_0 \equiv 1$ [see the definition (I, 8d) and the first paragraph of Part II], the coefficients of ψ_0 give

$$(L/l)\left[\alpha_0{}^{-5/6}+\sum_{k=1}^{\infty}A^{-(5/6)-k}\cdot\alpha_0{}^{-(5/6)-k}+\sum_{k=0}^{\infty}A^{-(4/3)-k}\cdot\alpha_0{}^{-(4/3)-k}\right]=-c+B^0 \qquad \text{(I, 17f)}$$

Finally the terms with $\psi^{1/6+h/3}$ yield

$$(L/l)\cdot\left[\alpha_{(1/6)+(h/3)}{}^{-5/6}+\sum_{k=1}^{\infty}A^{-(5/6)-k}\cdot\alpha_{(1/6)+(h/3)}{}^{-(5/6)-k}+\right.$$
$$\left.\sum_{k=0}^{\infty}A^{-(4/3)-k}\cdot\alpha_{(1/6)+(h/3)}{}^{-(4/3)-k}\right]=B^{(1/6)+(h/3)} \qquad \text{(I, 17g)}$$

The first of these equations gives directly the $A^{-(5/6)-h}$ ($h = 1,2\ldots$). Furthermore, the quantities $B^{(1/6)+h}$ appear only in Eq. (I, 17g), thus they can disregarded until the other unknowns have been determined.

Important for the pressure distribution over the plate are the quantities A—they yield the correction terms to the basic flow given by $\Psi^{-5/6}$. Among the value of A obtained from Eq. (I, 17a), the one with the lowest power of $\bar{p}_Q/\rho_0$ is $A^{-11/6}$; it is proportional to $|\bar{p}_Q/\rho_0|^{11/6}$, the other terms are presently unimportant.

For further computations we make the assumption, justified by later results, that the coefficients $A^{-(4/3)-h}$ are multiplied with powers of $\bar{p}_Q/\rho_0$ larger than 5/6, Then Eq. (I, 17b) yields

$$L/l = \gamma_{-5/6}\cdot(\bar{p}_Q/\rho_0)^{5/6} + \text{higher order terms} \qquad \text{(I, 18a)}$$

or
$$\bar{p}_Q/\rho_0 = (\gamma_{-5/6})^{-6/5}\cdot L^{6/5}\cdot l^{-6/5} + \text{higher order terms} \qquad \text{(I, 18b)}$$

Accordingly L/l can be considered in the following computations as $O(\bar{p}_Q/\rho_0)^{5/6}$. One obtains from Eq. (I, 17e)

$$B^{h/3} = O[(\bar{p}_Q/\rho_0)^{5/6}]$$

and from Eq. (I, 17f)

$$B^0 = c + O[(\bar{p}_Q/\rho_0)^{5/6}]$$

With these results and Eq. (I, 18a) one finds as the lowest order terms in Eq. (I, 17d)

$$\gamma_{-5/6}(\bar{p}_Q/\rho_0)^{5/6}\cdot\alpha_{-1/3}{}^{-5/6} = C'\delta_{-1/3}(\bar{p}_Q/\rho_0)^{1/3} + c\beta_{-1/3}{}^{0}(\bar{p}_Q/\rho_0)^{1/3}$$

Hence
$$C' = \frac{[(\bar{p}_Q/\rho_0)^{1/2}\cdot\gamma_{-5/6}\cdot\alpha_{-1/3}{}^{-5/6}]}{\delta_{-1/3}} - \frac{c\cdot\beta_{-1/3}{}^{0}}{\delta_{-1/3}}$$

Inserting this into Eq. (I, 17c) one obtains

$$\frac{L}{l}A^{-(4/3)-h} = \left(\frac{\bar{p}_Q}{\rho_0}\right)^{(11/6)+h}\frac{\gamma_{-5/6}\cdot\alpha_{-1/3}{}^{-5/6}\cdot\delta_{-(4/3)-h}}{\delta_{-1/3}} - \left(\frac{\bar{p}_Q}{\rho_0}\right)^{(4/3)+h}\cdot c\left(\beta_{-1/3}{}^{0}\frac{\delta_{-(4/3)-h}}{\delta_{-1/3}} - \beta_{-(4/3)-h}{}^{0}\right) \qquad \text{(I, 18)}$$

Presently this expression is of importance for $h = 0$. The solution for the flow over the plate with the lowest order terms for the wall influence included, is obtained by inserting these results into Eq. (I, 15). The quantity $\bar{p}_Q/\rho_0$ is given in formula (I, 18b)

$$\psi = \frac{L}{l}\left[\Psi^{-5/6}+\frac{\bar{p}_Q}{\rho_0}\left(\frac{\gamma_{-11/6}}{\gamma_{-5/6}}\cdot\Psi^{-11/6}+\alpha_{-1/3}{}^{-5/6}\cdot\frac{\delta_{-4/3}}{\delta_{-1/3}}\cdot\Psi^{-4/3}\right)\times\right.$$
$$\left.-\left(\frac{\bar{p}_Q}{\rho_0}\right)^{1/2}\cdot\frac{c}{\gamma_{-5/6}}\left(\beta_{-1/3}{}^{0}\cdot\frac{\delta_{-4/3}}{\delta_{-1/3}}-\beta_{-4/3}{}^{0}\right)\cdot\Psi^{-4/3}\right] \qquad \text{(I, 19)}$$

If higher order terms for the solution were determined, then one would expect fractional powers of $\bar{p}_Q/\rho_0$ to occur, even if the displacement of the model from the wind-tunnel axis is disregarded. The values of the γ are given in Eq. (I, 13a), and the other constants are derived in the second part—one has

$$\gamma_{-5/6} = \frac{8}{5\pi\cdot\sqrt{3}};\quad \frac{\gamma_{-11/6}}{\gamma_{-5/6}} = \frac{80}{77};\quad \alpha_{-1/3}{}^{-5/6} = -\frac{19}{16} \qquad \text{(II, 48)}$$

$$\frac{\delta_{-4/3}}{\delta_{-1/3}} = \frac{1}{2} \tag{II, 57}$$

$$\beta_{-1/3}{}^{0} = -\frac{3\Gamma(5/6)}{\Gamma(1/3)\Gamma(1/2)} \tag{II, 61a}$$

$$\beta_{-4/3}{}^{0} = -\frac{3}{8}\frac{\Gamma(5/6)}{\Gamma(1/3)\Gamma(1/2)} \tag{II, 61b}$$

$$l = \left(\frac{9}{8}\right)\sqrt{3}\left\{(\gamma+1)^{1/3}\left(\frac{3}{2}\right)^{4/3}\cdot\theta_0{}^{1/3}\,\frac{\Gamma(5/6)\cdot\Gamma(5/3)}{\Gamma(5/2)}\right\} \tag{II, 47}$$

and thus finds

$$\psi = \frac{L}{l}\left\{\Psi^{-5/6} + \frac{\bar{p}_Q}{\rho_0}\left(\frac{80}{77}\Psi^{-11/6} - \frac{19}{32}\Psi^{-4/3}\right) + \left(\frac{\bar{p}_Q}{\rho_0}\right)^{1/2} c\,\frac{45}{64}\cdot\frac{\sqrt{\pi}\cdot\sqrt{3}\Gamma(5/6)}{\Gamma(1/3)}\cdot\Psi^{-4/3}\right\}$$

and

$$\frac{\bar{p}_Q}{\rho_0} = \left[(\gamma+1)^{1/3}\left(\frac{3}{2}\right)^{4/3}\frac{9}{5\pi}\cdot\frac{\Gamma(5/6)\cdot\Gamma(5/3)}{\Gamma(5/2)}\right]^{-6/5}\theta_0{}^{-2/5}\,L^{6/5}$$

For simplicity numerical values may be inserted as far as practical. We choose $\gamma = 1.4$. Then

$$\psi = \frac{L}{l}\left[\Psi^{-5/6} + \frac{\bar{p}_Q}{\rho_0}\left(\frac{80}{77}\cdot\Psi^{-11/6} - \frac{19}{32}\Psi^{-4/3}\right) + \left(\frac{\bar{p}_Q}{\rho_0}\right)^{1/2}\cdot c\cdot 0.9094\,\Psi^{-4/3}\right] \tag{I, 20a}$$

$$\bar{p}_Q/\rho_0 = 0.988\cdot\theta_0{}^{-2/5}L^{6/5} \tag{I, 20b}$$

Since
$$\rho_0 = (9/4)\theta_0{}^2 \tag{I, 20c}$$

we have
$$\bar{p}_Q = 2.223\cdot\theta_0{}^{8/5}\cdot L^{6/5}$$

and
$$|\eta_Q| = \sqrt[3]{\bar{p}_Q} = 1.305\,\theta_0{}^{8/15}L^{6/15} \tag{I, 20d}$$

Furthermore, because of Eq. (I, 3b), we obtain for the choking Mach Number $M_{\text{chok.}}$

$$1 - M_{\text{chok.}} = 1.170\,\theta_0{}^{8/15}\cdot L^{6/15} \tag{I, 20e}$$

(9) *The Pressure Distribution Over the Plate*

According to Eq. (I, 4), the coordinates in the physical plane arise from a given ψ by a linear operation. Therefore, if one superimposes different expressions ψ on each other, then the corresponding values of the coordinates which belong to a given value of η and θ are also added. We apply this to the coordinates x which are found along the side of the plate BC for a given value of η. The contribution to x belonging to a particular solution $\Psi^{-(5/6)-h}$ may be denoted by $x^{(-5/6)-h}$. The point $x = 0$ is assumed to be the leading edge of the plate which is, in the present approximation, identical with the stagnation point ($\eta = -\infty$). With these notations one obtains

$$x = \frac{L}{l}\left\{x^{-5/6} + \frac{\bar{p}_Q}{\rho_c}\left(\frac{80}{77}x^{-11/6} - \frac{19}{32}x^{-4/3}\right) + \left(\frac{\bar{p}_Q}{\bar{p}_0}\right)^{1/2}\cdot c\cdot 0.9094\cdot x^{-4/3}\right\} \tag{I, 21}$$

The solutions $x^{-(5/6)-h}$ have been constructed in such a manner that only $x^{-5/6}$ gives a contribution to the total length of the plate. The total length of the plate is obtained if one sets $\eta = 0$—i.e., determines the value of x for the rearward starting point of the sonic line. The length l, introduced previously, is given by the value of $x^{-5/6}$ for $\eta = 0$.

The last equation can be written as

$$\frac{x}{L} = \frac{x^{-5/6}}{l} + \frac{\bar{p}_Q}{\rho_i}\left(\frac{80}{77}\cdot\frac{x^{-11/6}}{l} - \frac{19}{32}\cdot\frac{x^{-4/3}}{l}\right) + c\left(\frac{\bar{p}_Q}{\rho_0}\right)^{1/2}\cdot 0.9094\cdot\frac{x^{-4/3}}{l}$$

The quantities $x^{-(5/6)-h}$ depend only upon $\eta/(3\theta_0/2)^{2/3}$ as can be seen from the second part. Introducing for brevity

$$\bar{\eta} = \eta/(3\theta_0/2)^{2/3} \tag{I, 22}$$

and
$$f_1(\bar{\eta}) = x^{-5/6}/l$$

$$\epsilon\cdot f_2(\bar{\eta}) = \frac{\bar{p}_Q}{\rho_0}\left[\frac{80}{77}\cdot\frac{x^{-11/6}}{l} - \frac{19}{32}\cdot\frac{x^{-4/3}}{l}\right] + c\left(\frac{\bar{p}_Q}{\rho_0}\right)^{1/2}0.9094\,\frac{x^{-4/3}}{l} \tag{I, 23}$$

(where ϵ is a small quantity, introduced to show that the expression $\epsilon\cdot f_2$ is a correction to f_1), Eq. (I, 21) is written as

$$x/L = f_1(\bar{\eta}) + \epsilon\cdot f_2(\bar{\eta}) \tag{I, 24}$$

Since $\bar{\eta}$ is related to the pressure coefficient by Eq. (I, 3a), we are interested in a result of the form

$$\bar{\eta} = g_1(x/L) + \epsilon\cdot g_2(x/L) \tag{I, 25}$$

For this purpose the last equation is inserted into Eq. (I, 24)

$$\frac{x}{L} = f_1\left[g_1\left(\frac{x}{L}\right) + \epsilon g_2\left(\frac{x}{L}\right)\right] + \epsilon f_2\left[g_1\left(\frac{x}{L}\right) + \epsilon g_2\left(\frac{x}{L}\right)\right]$$

This equation is developed with respect to ϵ. The zero order terms yield $x/L = f_1[g_1(x/L)]$—i.e., g_1 is the inverse of f_1.

The first order terms yield

$$\left.\begin{aligned} f_1'\left[g_1\left(\frac{x}{L}\right)\right]\cdot\epsilon\cdot g_2\left(\frac{x}{L}\right) + \epsilon\cdot f_2\left[g_1\left(\frac{x}{L}\right)\right] = 0 \\ \epsilon\cdot g_2\frac{x}{L} = -\epsilon\frac{f_2(g_1[x/L])}{f_1'(g_1[x/L])} \end{aligned}\right\} \quad \text{(I, 26)}$$

According to the results of the second part we have

$$f_1(\tilde{\eta}) = \frac{x}{L} = -\frac{3\cdot\Gamma(5/2)}{\Gamma(5/6)\cdot\Gamma(5/3)}\cdot\int_{\infty}^{-\tilde{\eta}} u^{3/2}(1+u^3)^{-5/2}du$$

The solid line in the upper part of Fig. 4 shows the inverse function g thus obtained. Furthermore, we find

$$\frac{\epsilon\cdot f_2(\tilde{\eta})}{f_1'(\tilde{\eta})} = \left(\frac{\bar{p}_Q}{\rho_0}\right)\cdot(-\tilde{\eta})\left[-\frac{30}{77}\frac{(-\tilde{\eta})^3}{1+(-\tilde{\eta})^3}+\frac{35}{48}\right] + c\left(\frac{\bar{p}_Q}{\rho_0}\right)^{1/2} 0.9094\left(\frac{-2}{3}\right)(-\tilde{\eta})$$

In this expression one must, according to Eq. (I, 26), replace $\tilde{\eta}$ by g_1 and then insert the result into Eq. (I, 25). One thus obtains an expression for the pressure distribution

$$\tilde{\eta} = \frac{\eta}{(3\theta_0/2)^{2/3}} = g_1\left(\frac{x}{L}\right)\left[1+\frac{\bar{p}_Q}{\rho_0}\left(\frac{30}{77}\frac{g_1^3}{1-g_1^3}+\frac{35}{48}\right) - c\left(\frac{\bar{p}_Q}{\rho_0}\right)^{1/2} 0.606\right]$$

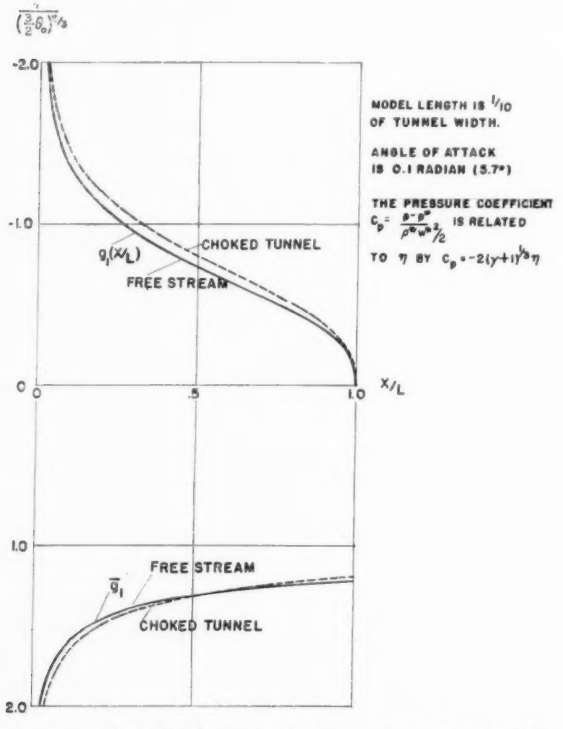

FIG. 4. $\eta/[(3/2)\theta_0]^{2/3}$ versus X/L for flow over plate at Mach one and for flow in a choked tunnel.

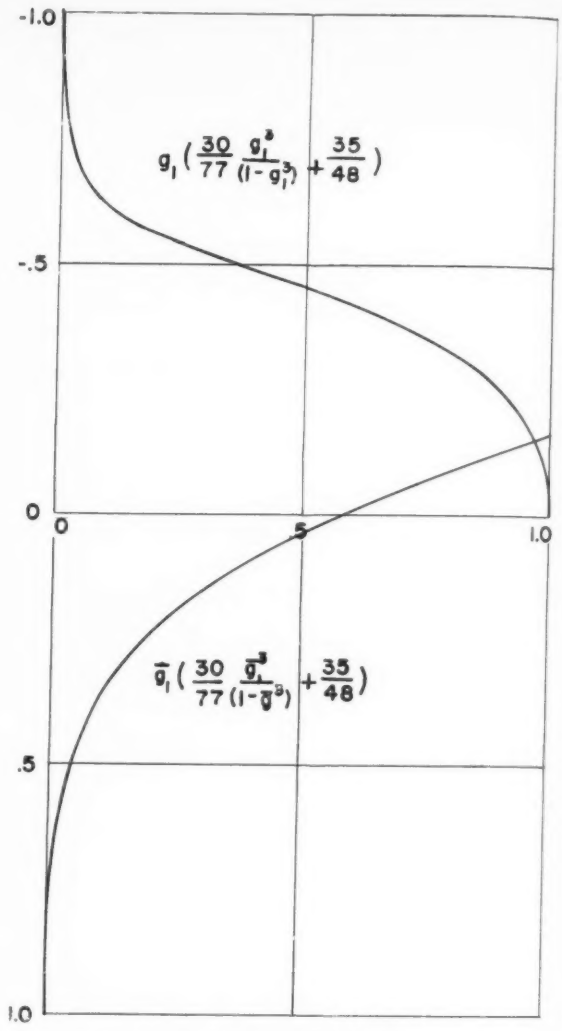

FIG. 5. Functions needed for the evaluation of the pressure change caused by the wind tunnel walls.

The value of $\bar{p}_Q/\rho_0$ is obtained from Eq. (I, 20b). The expression $g_1\{(30/77)[g_1^3/(1-g_1^3)]+(35/48)\}$, which occurs here, is shown in Fig. 5.

These formulas give the pressure distribution on the subsonic side of the plate. It has been found previously that the free stream pressure distribution on the suction side is obtained with sufficient accuracy by analytic continuation of the solution obtained to supersonic speeds; we assume that the same is true in the present case.

Accordingly, we have for the suction side:

$$\bar{f}_1(\tilde{\eta}) = \frac{x}{L} = -\frac{3\Gamma(5/2)}{\Gamma(5/6)\cdot\Gamma(5/3)}\cdot\int_{\infty}^{\tilde{\eta}} u^{3/2}(1-u^3)^{-5/2}\,du \quad \tilde{\eta}>1$$

The function $\bar{g}_1(x/L)$ is then the inverse of this expression (solid line in the lower part of Fig. 4). The pressure distribution on the suction side is expressed by

$$\bar{\eta} = \frac{\eta}{(3\theta_0/2)^{2/3}} = \bar{g}_1 \frac{x}{L}\left[1 + \frac{\bar{p}_Q}{\rho_0}\left(\frac{30}{77}\cdot\frac{\bar{g}_1{}^3}{1-\bar{g}_1{}^3} + \frac{35}{48}\right) - c\left(\frac{\bar{p}_Q}{\rho_0}\right)^{1/2}\cdot 0.606\right] \quad \text{(I, 27)}$$

The expression $\bar{g}_1\{(30/77)[\bar{g}_1{}^3/(1-\bar{g}_1{}^3)] + (35/48)\}$ is included in Fig. 5.

Discussion

The results obtained here can be discussed from two different points of view. First, the computations give some data which illustrate the effect of the wall on a plate in a choked wind tunnel. Secondly, the present investigations illustrate for an unsymmetric body the treatment of a flow field which deviates slightly from a flow field with a free stream Mach Number one. It thus can serve to illustrate the essential features of such flows.

Fig. 4 gives a comparison of the pressure distribution at Mach one with the pressure distribution in a choked tunnel for a plate whose length is equal to 0.1 of the wind-tunnel width and with an angle of attack of 0.1 radian (5.7°). Actually the quantity $\eta/(3\theta_0/2)^{2/3}$ is plotted; according to Eq. (I, 3a) it is proportional to the pressure coefficient. The solid lines give the pressures in a free stream at Mach one, the dashed lines give the results from the choked tunnel. The difference in the pressure distributions is rather small, which shows that even unsymmetric bodies can be measured in a choked tunnel without too strong an influence of the wall.

According to Eq. (I, 19), the angle of attack and the plate length enters the correction by means of the value of $\bar{p}_Q/\rho_0$, which is determined by Eq. (I, 20b). It is natural that the increase of the plate length at a fixed wind-tunnel size will increase the wall influence. That a reduction of the angle of attack will increase the relative error may be somewhat surprising, but it is actually clear from the transonic similarity law.

The expression for the choking Mach Number has the form found in reference 1 for a symmetric wedge in a choked tunnel. If one denotes by L the length of the wedge from the nose to the shoulder, then the expression found in reference 1 assumes the form

$$1 - M_{\text{chok.}} = 1.488\cdot\theta_0{}^{8/15}\cdot L^{6/15}$$

Even the coefficients at the right side of this equation are quite close to the value given in Eq. (I, 20e). That the symmetrical wedge chokes at a slightly lower Mach Number than the flat plate can be ascribed to the influence of the spill-over which occurs at the leading edge of the plate.

Within the approximation, a displacement of the body from the wind-tunnel centerline is exactly equivalent to a change of the angle of attack. A general formula will be given in connection with the flow over a body of a more general form.

The flat plate set at a fixed angle of attack may be considered as an example for an unsymmetric body. Eq. (I, 19) can immediately be considered as the solution for a general body if the proper expressions $\Psi^{-5/6}$, $\Psi^{-4/3}$, and $\Psi^{-11/6}$ are inserted. The properties of the body enter this solution in the form of these particular solutions, by the quantity l which is a characteristic length of the body and in the form of the coefficient $\alpha_{-1/3}{}^{-5/6}$ which is related to the unsymmetry of the body. The latter quantities are immediately connected with the solutions $\Psi^{-5/6}$, etc. (For the plate, the unsymmetry is caused by the angle of attack.) Thus the extension of the present approach to other bodies would require only the determination of the function $\Psi^{-5/6}$, $\Psi^{-4/3}$, and $\Psi^{-11/6}$.

One general conclusion can be drawn. The expression (I, 9e) together with Eq. (I, 20a) show that the displacement from the wind-tunnel axis is exactly equivalent to a change of the angle attack, $\Delta\alpha$, which is given by

$$\Delta\alpha = -(2/3)\cdot 0.9094\cdot\bar{p}_Q{}^{1/2}\cdot c$$

Here $\bar{p}_Q$ can be expressed by the choking Mach Number and one obtains for a body of an arbitrary shape

$$\Delta\alpha = -(2/3)\cdot 0.9094[2^{2/3}/(\gamma+1)](1 - M_{\text{chok.}})^{3/2}\cdot c = -0.716\cdot c(1 - M_{\text{chok.}})^{3/2}$$

This effect is quite small—e.g., for a model with a choking Mach Number 0.9 and a displacement from the centerline of 0.1 times the tunnel width, one finds

$$\Delta\alpha = -0.00227$$

or

$$\Delta\alpha = -0.13°$$

In reference 3, the flow in a choked tunnel has been used as an illustration for flow patterns which are close to a flow with a free stream Mach Number one. It appeared plausible that no matter which boundary conditions are imposed at a distance from the body, the solution would always appear in the form (I, 19)—naturally with different values of the constants which depend upon the boundary conditions imposed at a distance from the model. The flow pattern which is most interesting in this regard is the flow at a high subsonic Mach Number. Naturally, a displacement from a fictitious center line will be without influence in a flow field which extends to infinity, thus the solution for a flow with a high subsonic Mach Number can be expected to have the form

$$\psi = (L/l)[\Psi^{-5/6} + (\bar{p}_M/\rho_0)(c_1\Psi^{-11/6} + c_2\cdot\alpha_{-1/3}{}^{-5/6}\times\Psi^{-4/3})] \quad \text{(I, 28)}$$

The constants c_1 and c_2 are independent of the form of the body considered. $\bar{p}_M$ is the value of $\bar{p}$ which belongs to the free stream Mach Number. ρ_0 can be chosen arbitrarily—e.g., it can be defined by a characteristic angle of the body, then it would be possible to apply afterwards the transonic similarity law. It can also be set to equal unity. A direct evaluation of this formula is impossible in most cases, even if the constants c_1 and c_2 were known, since for each body configuration one needs the functions $\Psi^{-5/6}$, $\Psi^{-11/6}$, and $\Psi^{-4/3}$. But it is useful if we compare the influence of different boundary conditions imposed at a distance

from the given body, for then these functions Ψ are the same. In particular the question can be answered as to which free flow corresponds to the flow in a choked wind tunnel.

For a symmetrical contour, the second terms in Eqs. (I, 19) and (I, 28) are zero, and the expressions will agree if

$$c_1 \cdot \bar{p}_M = \bar{p}_Q \cdot \gamma_{-11/6} / \gamma_{-5/6}$$

Naturally, this formula is applicable only if the constants c_1 and $\gamma_{-11/6}/\gamma_{-5/6}$ have the same sign; then we have the relation

$$1 - M = (1 - M_{\text{chok.}}) \cdot [(\gamma_{-11/6}/(c_1 \cdot \gamma_{-5/6})]^{1/3}$$

To obtain agreement for an unsymmetrical contour, a change of the angle of attack must be admitted. If both the deviation of the free stream Mach Number from one and the angle of attack change are small, we expect a simple superposition of the effect, and one obtains them by a combination of Eqs. (I, 19) and (I, 9e)

$$\psi = \frac{L}{l}\left[\Psi^{-5/6} + \frac{\bar{p}_Q}{\rho_0}\left(\frac{\gamma_{-11/6}}{\gamma_{-5/6}} \cdot \Psi^{-11/6} + \alpha_{-1/3}{}^{-5/6} \times \frac{\delta_{-4/3}}{\delta_{-1/3}} \cdot \Psi^{-4/3}\right) - \frac{3}{2} \rho_0{}^{-1/2} \cdot \Delta\alpha \cdot \Psi^{-4/3}\right] \quad \text{(I, 29)}$$

The expressions (I, 28) and (I, 29) will agree if

$$c_2 \cdot \alpha_{-1/3}{}^{-5/6} \cdot \bar{p}_M = \frac{\bar{p}_Q \cdot \alpha_{-1/3}{}^{-5/6} \cdot \delta_{-4/3}}{\delta_{-1/3}} - \frac{3}{2} \rho_0{}^{-1/2} \cdot \Delta\alpha$$

$$\Delta\alpha = -\left(\frac{2}{3}\right) \rho_0{}^{1/2} \cdot \alpha_{-1/3}{}^{-5/6} \cdot \bar{p}_Q \left(\frac{c_2}{c_1} \frac{\gamma_{-11/6}}{\gamma_{-5/6}} - \frac{\delta_{-4/3}}{\delta_{-1/3}}\right)$$

In these relations the constants c_1 and c_2 are unknown but they can be determined once and for all by experiments. But furthermore, the quantity $\alpha_{-1/3}{}^{-5/6}$ enters the solution, and this quantity is determined by the body contour. On the other hand, this quantity is the lowest order term which causes the pressure distribution along the lower and upper wall of the wind tunnel to be different. Thus if the pressure distributions along the walls agree for two different bodies, then these bodies have the same value of $\alpha_{-1/3}{}^{-5/6}$, and, therefore, the same Mach Number and angle of attack correction. Thus the corrections to be applied can be found from the wall pressure distributions. The Mach Number correction is found from the average of the pressure distribution along the lower and upper wall, and the angle of attack correction from the difference of the pressure distribution.

Practically, one will measure the pressure distribution over a sample body in a choked tunnel and also the wall pressures. Furthermore, one determines for the same body the pressure distributions in a free flight (or in a much larger wind tunnel) at different Mach Numbers and for slightly changed angles of attack. The Mach Number and that angle of attack for which the pressure distribution over the body in free flight agrees best with the pressure distribution in the tunnel gives first, the coordination between the wall pressures and second, the effective Mach Number and the angle of attack correction.

If one accepts the linear dependence of $\Delta\alpha$ on $\alpha_{-1/3}{}^{-5/6}$, one does not need further experiments. An important extension is obtained by the application of the transonic similarity law.

Naturally, the procedure of determining Mach Number and angle of attack corrections described here is not restricted to a choked flow but can be applied also for other Mach Numbers.[6]

The corrections considered here are the lowest order terms in a development with respect to the model size. Even if the first order effects are equal to zero, the higher order effects will differ. In the present case one must keep in mind that the lowest order terms are proportional to $\bar{p}_Q$, while higher order terms would—according to the form of the system (I, 17)—contain powers of $\bar{p}_Q{}^{4/3}$, etc. Since the powers of $\bar{p}_Q$ are thus rather closely spaced, it may happen that higher order terms have an influence comparable with the lowest order expressions. Here it is rather reassuring that even the lowest order influence is within reasonable bounds for a body of technically acceptable dimensions; otherwise there might be doubt if the results of a wind-tunnel test, even when corrected in the manner described above, would have a practical significance.

Part II—Details of the Investigations

(1) *Formulas for the Particular Solutions of Eq.* (5)

(a) In Eq. (I, 6) of the main text, particular solutions for ψ were given by the hypothesis

$$\psi = \rho^{-(1/12) + (\sqrt{\lambda}/3)} G(\xi, \lambda)$$

Depending upon whether the function ψ which arises from this hypothesis is symmetric or antisymmetric with respect to the line $\xi = -\infty$, the functions G will be denoted by $G^{(s)}$ or $G^{(a)}$. As mentioned in the first part, we impose at $\xi = -\infty$ the condition that $G^{(s)} = 1$ and that $G^{(a)}$ behaves as $(-\xi)^{-3/2}$. The values of $\sqrt{\lambda}$ which are used in the present analysis are determined by requirements imposed to the function ψ at $\xi = -\infty$ and along the Mach wave $\xi = 1$.

According to Eq. (19d) of reference 3, the function $G^{(s)}$ is given along $\xi = 1$ by

$$G^{(s)} = \Gamma\left(-\frac{1}{2}\right) \cdot \left(\frac{\Gamma[(2/3)\sqrt{\lambda}] \cdot \sin\{\pi[(\sqrt{\lambda}/3) - (1/4)]\}}{\Gamma[(\sqrt{\lambda}/3) + (5/12)] \cdot \Gamma[(\sqrt{\lambda}/3) + (1/12)]} (1 - \xi^3)^{-(\sqrt{\lambda}/3) + (1/12)} [1 + O(1 - \xi^3)] + \frac{\Gamma[-(2/3)\sqrt{\lambda}] \cdot \sin\{\pi[-(\sqrt{\lambda}/3) - (1/4)]\}}{\Gamma[-(\sqrt{\lambda}/3) + (5/12)] \cdot \Gamma[-(\sqrt{\lambda}/3) + (1/12)]} (1 - \xi^3)^{(\sqrt{\lambda}/3) + (1/12} [1 + O(1 - \xi^3)]\right)$$

Using the definitions for ρ and ξ, Eqs. (I, 5) one finds

$$\psi = \eta^{-(1/4)+\sqrt{\lambda}} \cdot \Gamma\left(-\frac{1}{2}\right)\left(\frac{\Gamma[(2/3)\cdot\sqrt{\lambda}]\cdot\sin\{\pi[(\sqrt{\lambda}/3)-(1/4)]\}}{\Gamma[(\sqrt{\lambda}/3)+(5/12)]\cdot\Gamma[(\sqrt{\lambda}/3)+(1/12)]}\cdot[1+O(1-\xi^3)]+\right.$$
$$\left.\frac{\Gamma[-(2/3)\cdot\sqrt{\lambda}]\cdot\sin\{\pi[-(\sqrt{\lambda}/3)-(1/4)]\}}{\Gamma[-(\sqrt{\lambda}/3)+(5/12)]\cdot\Gamma[-(\sqrt{\lambda}/3)+(1/12)]}(1-\xi^3)^{(2/3)\cdot\sqrt{\lambda}}[1+O(1-\xi^3)]\right) \quad \text{(II, 1)}$$

Similarly one finds for the functions $G^{(a)}$ the following representation in the vicinity of $\xi = 1$

$$\psi = \eta^{-(1/4)+\sqrt{\lambda}} \cdot \Gamma\left(\frac{1}{2}\right)\left(\frac{\Gamma[(2/3)\sqrt{\lambda}]\cdot\sin\{\pi[(\sqrt{\lambda}/3)+(1/4)]\}}{\Gamma[(\sqrt{\lambda}/3)+(11/12)]\cdot\Gamma[(\sqrt{\lambda}/3)+(7/12)]}[1+O(1-\xi^3)]+\right.$$
$$\left.\frac{\Gamma[-(2/3)\cdot\sqrt{\lambda}]\cdot\sin\{\pi[-(\sqrt{\lambda}/3)+(1/4)]\}}{\Gamma[-(\sqrt{\lambda}/3)+(11/12)]\cdot\Gamma[-(\sqrt{\lambda}/3)+(7/12)]}(1-\xi^3)^{(2/3)\cdot\sqrt{\lambda}}[1+O(1-\xi^3)]\right) \quad \text{(II, 2)}$$

(b) For the particular solutions which represent the solution in the vicinity of point O, we have the requirement that along the characteristic $\xi = 1$, neither a singularity propagates nor this line is mapped to infinity. Obviously, the second term in the parentheses of Eqs. (II, 1) and (II, 2) describes such a behavior because of the presence of the factor $(1-\xi^3)^{(2/3)\sqrt{\lambda}}$, so we obtain the condition that the coefficient of this term must vanish. This happens if either the sine function in the numerator is zero or the Γ-functions in the denominator are infinite. One thus obtains the following values of $\sqrt{\lambda}$

$$(3/4)+h \quad \text{and} \quad -(9/4)-3h \qquad (h = 0, 1, 2\ldots) \text{ for the antisymmetric solutions} \qquad \text{(II, 3)}$$
$$(1/4)+h \quad \text{and} \quad -(3/4)-3h \qquad (h = 0, 1, 2\ldots) \text{ for the symmetric solutions} \qquad \text{(II, 4)}$$

These are the same values as given in the main text.

For these values of $\sqrt{\lambda}$ we need the behavior of the functions G along the sonic line. Formulas (18c) and (19d) of reference 3 give

$$G^{(a)} = \frac{3\,\Gamma(4/3)\cdot\Gamma(1/2)}{2\Gamma[(\sqrt{\lambda}/3)+(11/12)]\cdot\Gamma[-(\sqrt{\lambda}/3)+(11/12)]}(1-\xi^3)^{(1/12)-(\sqrt{\lambda}/3)}\times$$
$$F\left(-\frac{\sqrt{\lambda}}{3}+\frac{1}{12},-\frac{\sqrt{\lambda}}{3}+\frac{7}{12},\frac{2}{3},\xi^2\right)+\frac{3\,\Gamma(2/3)\cdot\Gamma(1/2)}{2\Gamma[(\sqrt{\lambda}/3)+(7/12)]\cdot\Gamma[-(\sqrt{\lambda}/3)+(7/12)]}\times$$
$$(1-\xi^3)^{(1/12)-(\sqrt{\lambda}/3)}\cdot\xi\cdot F\left(-\frac{\sqrt{\lambda}}{3}+\frac{5}{12},-\frac{\sqrt{\lambda}}{3}+\frac{11}{12},\frac{4}{3},\xi^2\right) \quad \text{(II, 5)}$$

and

$$G^{(s)} = -\frac{3\cdot\Gamma(4/3)\cdot\Gamma(-1/2)}{2\Gamma[(\sqrt{\lambda}/3)+(5/12)]\cdot\Gamma[-(\sqrt{\lambda}/3)+(5/12)]}(1-\xi^3)^{(1/12)-(\sqrt{\lambda}/3)}\times$$
$$F\left(-\frac{\sqrt{\lambda}}{3}+\frac{1}{12},-\frac{\sqrt{\lambda}}{3}+\frac{7}{12},\frac{2}{3},\xi^3\right)-\frac{3\,\Gamma(2/3)\cdot\Gamma(-1/2)}{2\Gamma[(\sqrt{\lambda}/3)+(1/12)]\cdot\Gamma[-(\sqrt{\lambda}/3)+(1/12)]}\times$$
$$(1-\xi^3)^{(1/12)-(\sqrt{\lambda}/3)}\cdot\xi\cdot F\left(-\frac{\sqrt{\lambda}}{3}+\frac{5}{12},-\frac{\sqrt{\lambda}}{3}+\frac{11}{12},\frac{4}{3},\xi^3\right) \quad \text{(II, 6)}$$

Inserting the above values of $\sqrt{\lambda}$ one obtains, with some simplifications in the Γ-functions, as representations in the vicinity of the sonic line

$$G^{(a)}\left\{\xi,\left[-\left(\frac{9}{4}\right)-3h\right]^2\right\} = (-)^h\cdot(3/8)\cdot 2^{1/3}\frac{\Gamma[(5/6)+h]/\Gamma(5/6)}{\Gamma[(5/3)+h]/\Gamma(5/3)}-(-)^h\cdot(3/8)\cdot 2^{2/3}\cdot\xi\times$$
$$\frac{\{\Gamma[(7/6)+h]/\Gamma(7/6)\}}{\{\Gamma[(4/3)+h]/\Gamma(4/3)\}} \quad \text{(II, 7a)}$$

$$G^{(a)}\left\{\xi,\left[\left(\frac{3}{4}\right)+3h\right]^2\right\} = -(-)^h\cdot(3/2)\cdot 2^{1/3}\frac{\Gamma[(1/3)+h]/\Gamma(1/3)}{\Gamma[(7/6)+h]/\Gamma(7/6)}-(-)^h(3/4)\cdot 2^{2/3}\cdot\xi\times$$
$$\frac{\{\Gamma[(2/3)+h]/\Gamma(2/3)\}}{\{\Gamma[(5/6)+h]/\Gamma(5/6)\}} \quad \text{(II, 7b)}$$

$$G^{(a)}\left\{\xi,\left[\left(\frac{7}{4}\right)+3h\right]^2\right\} = (-)^h\frac{\Gamma[(2/3)+h]/\Gamma(2/3)}{\Gamma[(3/2)+h]/\Gamma(3/2)} \quad \text{(II, 7c)}$$

$$G^{(a)}\left\{\xi,\left[\left(\frac{11}{4}\right)+3h\right]^2\right\} = -(-)^h\cdot\xi\frac{\Gamma[(4/3)+h]/\Gamma(4/3)}{\Gamma[(3/2)+h]/\Gamma(3/2)} \quad \text{(II, 7d)}$$

$$G^{(s)}\left\{\xi, \left[-\left(\frac{3}{4}\right) - 3h\right]^2\right\} = \frac{1}{2}\cdot 2^{1/3}\,(-)^h\,\frac{\Gamma[(5/6)+h]/\Gamma(5/6)}{\Gamma[(2/3)+h]/\Gamma(2/3)} - \frac{1}{4}\cdot(2)^{2/3}(-)^h\cdot\xi\,\frac{\Gamma[(7/6)+h]/\Gamma(7/6)}{\Gamma[(1/3)+h]/\Gamma(1/3)} \qquad \text{(II, 8a)}$$

$$G^{(s)}\left\{\xi, \left[\left(\frac{1}{4}\right) + 3h\right]^2\right\} = (-)^h\,\frac{\Gamma[(2/3)+h]/\Gamma(2/3)}{\Gamma[(1/2)+h]/\Gamma(1/2)} \qquad \text{(II, 8b)}$$

$$G^{(s)}\left\{\xi, \left[\left(\frac{5}{4}\right) + 3h\right]^2\right\} = -(-)^h\cdot\xi\,\frac{\Gamma[(4/3)+h]/\Gamma(4/3)}{\Gamma[(1/2)+h]/\Gamma(1/2)} \qquad \text{(II, 8c)}$$

$$G^{(s)}\left\{\xi, \left[\left(\frac{9}{4}\right) + 3h\right]^2\right\} = -(-)^h\cdot 2^{1/3}\,\frac{\Gamma[(4/3)+h]/\Gamma(4/3)}{\Gamma[(7/6)+h]/\Gamma(7/6)} - (-)^h\cdot 2^{2/3}\cdot\xi\,\frac{\Gamma[(5/3)+h]/\Gamma(5/3)}{\Gamma[(5/6)+h]/\Gamma(5/6)} \qquad \text{(II, 8d)}$$

Eqs. (II, 7a), (II, 7b), (II, 8a), and (II, 8d) originate from each other by a suitable choice of h. The values of $\sqrt{\lambda}$ given in the first parts of Eqs. (II, 3) and (II, 4) lead to the expressions (II, 7b), (II, 7c), (II, 7d), and to (II, 8b), (II, 8c), and (II, 8d).

In (II, 7c), (II, 7d), (II, 8b), and (II, 8c), either the value of G or its derivative with respect to ξ vanishes at $\xi = 0$. Actually the corresponding solutions ψ are polynomial in ξ or also in η and θ, as can be seen by inserting ρ, ξ, and the proper values of $\sqrt{\lambda}$ into Eqs. (II, 5) and (II, 6).

One obtains for $G^{(s)}$ and $\sqrt{\lambda}/3 = (1/12) + h$

$$\psi = (-)^h\,\frac{\Gamma[(2/3)+h]/\Gamma(2/3)}{\Gamma[(1/2)+h]/\Gamma(1/2)}\cdot\left(\frac{3}{2}\theta\right)^{2h}\cdot F\left[-h, \frac{1}{2}-h, \frac{2}{3}, \frac{\eta^3}{(9/4)\theta^2}\right] \qquad \text{(II, 9a)}$$

for $G^{(s)}$ and $\sqrt{\lambda}/3 = (5/12) + h$

$$\psi = -(-)^h\,\frac{\Gamma[(4/3)+h]/\Gamma(4/3)}{\Gamma[(1/2)+h]/\Gamma(1/2)}\,\eta\left(\frac{3}{2}\theta\right)^{2h}\cdot F\left[-h, \frac{1}{2}-h, \frac{4}{3}, \frac{\eta^3}{(9/4)\theta^2}\right] \qquad \text{(II, 9b)}$$

for $G^{(a)}$ and $\sqrt{\lambda}/3 = (7/12) + h$

$$\psi = (-)^h\,\frac{\Gamma[(2/3)+h]/\Gamma(2/3)}{\Gamma[(3/2)+h]/\Gamma(3/2)}\cdot\left(\frac{3}{2}\theta\right)^{2h+1}\cdot F\left[-\frac{1}{2}-h, -h, \frac{2}{3}, \frac{\eta^3}{(9/4)\theta^2}\right] \qquad \text{(II, 9c)}$$

and for $G^{(a)}$ and $\sqrt{\lambda}/3 = (11/12) + h$

$$\psi = -(-)^h\,\frac{\Gamma[(4/3)+h]/\Gamma(4/3)}{\Gamma[(3/2)+h]/\Gamma(3/2)}\cdot\eta\left(\frac{3}{2}\theta\right)^{2h+1}\cdot F\left[-\frac{1}{2}-h, -h, \frac{4}{3}, \frac{\eta^3}{(9/4)\theta^2}\right] \qquad \text{(II, 9d)}$$

(c) Another family of particular solutions is determined by the condition $\psi = 0$ along $\xi = -\infty$ and along $\xi = 1$. The first condition requires that the particular solution be antisymmetric with respect to $\xi = -\infty$. The second condition requires that in Eq. (II, 2) $\sqrt{\lambda}$ be positive and that the first term in the parentheses should vanish. This leads to $\sqrt{\lambda} = (9/4) + 3h$. The behavior of the corresponding functions G along the sonic line is given in Eq. (II, 7a).

(d) We need furthermore asymptotic expressions for the function G at high negative values of λ. They are obtained from the differential equation (I, 7) for G by the method of R. E. Langer.[7] Some details of the derivation of the following formulas are given in reference 4. For large negative values of λ, the differential equation (I, 7) is integrated asymptotically by

$$G \sim (1-\xi^{-3})^{1/12}\,\nu(\xi)^{1/2}\cdot e^{-i\pi/6}\cdot I_{1/3}[i(\sqrt{|\lambda|}/3)\cdot v(\xi)] \qquad \text{(II, 10a)}$$

and

$$G \sim (1-\xi^{-3})^{1/12}\nu(\xi)^{1/2}\cdot e^{i\pi/6}\cdot I_{-1/3}[i(\sqrt{|\lambda|}/3)v(\xi)] \qquad \text{(II, 10b)}$$

with

$$v(\xi) = 2\cdot tg^{-1}[(-\xi)^{3/2}] \qquad \text{(II, 11)}$$

These expressions represent those exact solutions which agree with them asymptotically with respect to the value of the functions and the first derivative at $\xi = 0$. There the above expressions give

$$-[|\lambda|^{1/6}\cdot 2^{1/2}\cdot 3^{-1/3}/\Gamma(4/3)]\cdot\xi \qquad \text{(II, 12a)}$$

and

$$[|\lambda|^{-1/3}\cdot 3^{1/3}2^{1/2}/\Gamma(2/3)] \qquad \text{(II, 12b)}$$

For $\xi < 0$ and large values of $|\lambda|$ the Bessel functions can be represented by their asymptotic series and thus one obtains other asymptotic expressions for the same functions G. One finds in either case

$$G \sim [(1-\xi^{-3})^{1/12}\cdot\sqrt{3}/\sqrt{2\pi}\cdot|\lambda|^{1/4}]\cdot e^{(\sqrt{|\lambda|}/3)\cdot v(\xi)} \qquad \text{(II, 13)}$$

(2) *Particular Solutions Which Fulfill the Boundary Conditions Along the Map of the Plate*

We seek particular solutions of Eq. (I, 2) that fulfill the following conditions:

(1) $\psi = 0$ along the line ABC of Fig. 3.
(2) $\psi = 0$ at infinity.
(3) infinity is a branch point of the streamlines.
(4) point O is a singular point.
(5) The characteristics EO does not map to infinity.

Except for the character of the singularity at point O the problem is the same as that in reference 2. The

treatment is also quite analogous except for some simplifications in the representation.

First one determines particular solutions of the form (I, 6) which are suitable for the representation of the solution in the vicinity of the point B and at infinity. In the vicinity of point B, the boundary conditions $\psi = 0$ along BC and AB are prescribed. This is the problem treated in Part II, 1c, and one obtains as a possible set of particular solutions

$$\psi = \rho^{2/3 + h} \cdot G^{(a)}\{\xi, [(9/4) + 3h]^2\} \quad \text{(II, 14)}$$

For the representation of the solutions at infinity, the condition $\psi = 0$ along BC restricts us to solutions which are antisymmetric with respect to the line $\xi = -\infty$, condition 2 restricts us to negative values of $\sqrt{\lambda}$, and the condition that no singularity in ψ or in the higher derivatives propagates along EO leads us to the problem treated in Section II, 1b. The values of $\sqrt{\lambda}$ given in the second part of Eq. (II, 3) are then applicable, and one obtains as a possible set of particular solutions

$$\psi = \rho^{-(5/6) + h} \cdot G^{(a)}\{\xi, [(9/4) + 3h]^2\} \quad \text{(II, 15)}$$

Condition 3 imposes a further restriction. At a large value of ρ, the one particular solution with the absolutely largest power of ρ will prevail. Now one can see that among the particular solutions (II, 15) only the expression $\rho^{-5/6} \cdot G^{(a)}[\xi, (9/4)^2]$ has no branch point of the streamlines at infinity. If this particular solution is excluded, infinity will always be a branch point of the streamlines.

The solution investigated in reference 2 is represented along the line BC by the expression

$$\psi = (-\xi)^{-3/2} \left(\frac{\rho}{\rho_0}\right)^{2/3} \left[1 + \left(\frac{\rho}{\rho_0}\right)\right]^{-5/2} \quad \text{(II, 16a)}$$

here ρ_0 is the value of ρ at point O. For the present purpose this expression may be generalized in the following manner

$$\psi^{m,n} = (-\xi)^{-3/2} \cdot \left(\frac{\rho}{\rho_0}\right)^{(2/3) + m} \left[1 + \left(\frac{\rho}{\rho_0}\right)\right]^{-5/2 - n} \quad \text{(II, 16b)}$$

m and n being integral numbers. Since

$$\left(\frac{\rho}{\rho_0}\right)^{(2/3) + m + 1} \left[1 + \left(\frac{\rho}{\rho_0}\right)\right]^{-(5/2) - n} = \left(\frac{\rho}{\rho_0}\right)^{2/3 + m} \times \left[1 + \left(\frac{\rho}{\rho_0}\right)\right]^{-(5/2) - n + 1} - \left(\frac{\rho}{\rho_0}\right)^{(2/3) + m} \times \left[1 + \left(\frac{\rho}{\rho_0}\right)\right]^{-(5/2) - n}$$

solutions obtained by changing either m or n are not independent from each other.

We must show that the analytic continuation of the expression fulfills the conditions given at the beginning of the paragraph, and we must study the character of the singularities which arise at point O. The final aim is to determine the coefficients α which occur in the expressions (I, 9), to compute the change of the x-coordinate caused by these particular solutions, and finally to determine their influence on the pressure distribution.

That the analytic continuation of the expression (II, 16) is free of singularities in the entire subsonic region can be shown with the method of reference 2—i.e., by means of the particular solutions (I, 6) with negative values of λ and asymptotic expressions for large values of $|\lambda|$. This part of the work will not be repeated here. The remaining computation, however, will be carried out since the numerical results are needed.

Developing Eq. (II, 16) with respect to ρ or ρ^{-1}, one obtains

$$\psi^{m,n} = (-\xi)^{-3/2} \sum_{h=0}^{\infty} (-)^h \frac{\Gamma[(5/2) + n + h]}{\Gamma[(5/2 + n) \cdot \Gamma(h + 1)]} \cdot \left(\frac{\rho}{\rho_0}\right)^{(2/3) + m + h} \quad \text{(II, 17)}$$

for $\rho < \rho_0$ and $\psi^{m,n} = (-\xi)^{-3/2} \sum_{h=0}^{\infty} (-)^h \frac{\Gamma[(5/2) + n + h]}{\Gamma[(5/2) + n]\Gamma(h + 1)} \cdot \left(\frac{\rho}{\rho_0}\right)^{-(11/6) + m - n - h}$ (II, 18)

for $\rho < \rho_0$.

From these expressions one obtains as analytic continuation

$$\psi^{m,n} = \sum_{h=0}^{\infty} (-)^h \frac{\Gamma[(5/2) + n + h]}{\Gamma[(5/2) + n] \cdot \Gamma(h + 1)} \cdot G^{(a)}\left\{\xi, \left[\left(\frac{9}{4}\right) + 3(m + h)\right]^2\right\} \cdot \left(\frac{\rho}{\rho_0}\right)^{(2/3) + m + h}$$

for $\rho < \rho_0$ and $\psi^{m,n} = \sum_{h=0}^{\infty} (-)^h \frac{\Gamma[(5/2) + n + h]}{\Gamma[(5/2) + n] \cdot \Gamma(h + 1)} \cdot G^{(a)}\left\{\xi, \left[\left(\frac{9}{4}\right) + 3(1 + n - m + h)\right]^2\right\} \times \left(\frac{\rho}{\rho_0}\right)^{-(11/6) + m - n - h}$

for $\rho > \rho_0$.

Then Eq. (II, 7a) yields the following representations of $\psi^{m,n}$ along the sonic line

$$\psi^{m,n} = (-)^m \cdot \frac{3}{8}\left\{2^{1/3}\sum_{h=0}^{\infty}\left(\frac{\rho}{\rho_0}\right)^{(2/3)+m+h}\frac{\Gamma[(5/2)+h+n]\cdot\Gamma[(5/6)+m+h]\cdot\Gamma(5/3)}{\Gamma[(5/2)+n]\cdot\Gamma(h+1)\cdot\Gamma(5/6)\cdot\Gamma[(5/3)+m+h]} - 2^{2/3}\cdot\xi\sum_{h=0}^{\infty}\left(\frac{\rho}{\rho_0}\right)^{(2/3)+m+h}\frac{\Gamma[(5/2)+n+h]\cdot\Gamma[(7/6)+m+h]\cdot\Gamma(4/3)}{\Gamma[(5/2)+n]\Gamma(h+1)\cdot\Gamma(7/6)\cdot\Gamma[(4/3)+m+h]}\right\}$$

for $\rho < \rho_0$, and

$$\psi^{m,n} = (-)^{n+m+1}\cdot\frac{3}{8}\left\{2^{1/3}\sum_{h=0}^{\infty}\left(\frac{\rho}{\rho_0}\right)^{-(11/6)+m-n-h}\frac{\Gamma[(5/2)+n+h]\cdot\Gamma[(11/6)+n-m+h]\cdot\Gamma(5/3)}{\Gamma[(5/2)+n]\Gamma(h+1)\cdot\Gamma(5/6)\cdot\Gamma[(8/3)+n-m+h]} - 2^{2/3}\cdot\xi\sum_{h=0}^{\infty}\left(\frac{\rho}{\rho_0}\right)^{-(11/6)+m-n-h}\frac{\Gamma[(5/2)+n+h]\cdot\Gamma[(13/6)+n-m+h]\cdot\Gamma(4/3)}{\Gamma[(5/2)+n]\cdot\Gamma(h+1)\cdot\Gamma(7/6)\cdot\Gamma[(7/3)+n-m+h]}\right\}$$

for $\rho > \rho_0$.

This can be written as

$$\psi^{m,n} = (-)^n\cdot\frac{3}{8}\cdot\left(\frac{\rho}{\rho_0}\right)^{(2/3)+m}\cdot\left\{2^{1/3}\frac{\Gamma[(5/6)+m]\cdot\Gamma(5/3)}{\Gamma(5/6)\cdot\Gamma[(5/3)+m]}\cdot F\left(\frac{5}{2}+n,\frac{5}{6}+m,\frac{5}{3}+m,\frac{\rho}{\rho_0}\right) - 2^{2/3}\cdot\xi\frac{\Gamma[(7/6)+m]\cdot\Gamma(4/3)}{\Gamma(7/6)\cdot\Gamma[(4/3)+m]}\cdot F\left(\frac{5}{2}+n,\frac{7}{6}+m,\frac{4}{3}+m,\frac{\rho}{\rho_0}\right)\right\} \quad \text{(II, 19)}$$

for $\rho < \rho_0$, and

$$\psi^{m,n} = (-)^{n+m+1}\cdot\frac{3}{8}\left(\frac{\rho}{\rho_0}\right)^{-(11/6)+m-n}\cdot\left\{2^{1/3}\frac{\Gamma[(11/6)+n-m]\cdot\Gamma(5/3)}{\Gamma(5/6)\cdot\Gamma[(8/3)+n-m]}\cdot F\left[\frac{5}{2}+n,\frac{11}{6}+n-m,\frac{8}{3}+n-m,\left(\frac{\rho}{\rho_0}\right)^{-1}\right] - 2^{2/3}\frac{\Gamma[(13/6)+n-m]\cdot\Gamma(4/3)}{\Gamma(7/6)\cdot\Gamma[(7/3)+n-m]}\cdot F\left[\frac{5}{2}+n,\frac{13}{6}+n-m,\frac{7}{3}+n-m,\left(\frac{\rho}{\rho_0}\right)^{-1}\right]\right\} \quad \text{(II, 20)}$$

for $\rho > \rho_0$.

From these equations we shall derive representations for ψ in the vicinity of point O and thus study the singularity arising there. By means of the following relation for hypergeometric functions (see e.g., reference 8, p. 257).

$$\frac{\Gamma(a)\cdot\Gamma(b)}{\Gamma(c)}\cdot F(a,b,c,z) = \frac{\Gamma(a)\cdot\Gamma(b-a)}{\Gamma(c-a)}(-z)^{-a}\cdot F(a,1+a-c,1+a-b,z^{-1}) + \frac{\Gamma(b)\Gamma(a-b)}{\Gamma(c-b)}(-z)^{-b}\cdot F(b,1+b-c,1+b-a,z^{-1}) \quad \text{(II, 21)}$$

one finds that the expressions $\left(\frac{\rho}{\rho_0}\right)^{(2/3)+m}\cdot F\left[\frac{5}{2}+n,\frac{5}{6}+m,\frac{5}{3}+m,\frac{\rho}{\rho_0}\right]$

and $\left(\frac{\rho}{\rho_0}\right)^{-(11/6)+m-n}\cdot F\left[\frac{5}{2}+n,\frac{11}{6}+n-m,\frac{8}{3}+n-m,\left(\frac{\rho}{\rho_0}\right)^{-1}\right]$

which occur in Eqs. (II, 19) and (II, 20) fulfill the same hypergeometric differential equation. The same holds for the expression

$\left(\frac{\rho}{\rho_0}\right)^{(2/3)+m}\cdot F\left[\frac{5}{2}+n,\frac{7}{6}+m,\frac{4}{3}+m,\left(\frac{\rho}{\rho_0}\right)\right]$ from (II, 19)

and $\left(\frac{\rho}{\rho_0}\right)^{-(11/6)+m-n}\cdot F\left[\frac{5}{2}+n,\frac{13}{6}+n-m,\frac{7}{3}+m,\left(\frac{\rho}{\rho_0}\right)^{-1}\right]$ from (II, 20)

As a consequence the expressions (II, 19) and (II, 20), if developed at $\rho/\rho_0 = 1$, will be represented by linear combinations of the same hypergeometric series. To establish that the inner and outer representation "fit" at point O, one must merely show that the coefficients of corresponding hypergeometric series are the same.

By means of the formula (reference 8, p. 252)

$$F(a,b,c,z) = \frac{\Gamma(c)\Gamma(c-a-b)}{\Gamma(c-a)\cdot\Gamma(c-b)}\cdot F(a,b,1+a+b-c,1-z) + \frac{\Gamma(c)\Gamma(a+b-c)}{\Gamma(a)\cdot\Gamma(b)}(1-z)^{c-a-b}\cdot F(c-a,c-b,1+c-a-b,1-z) \quad \text{(II, 22)}$$

one obtains, using known relations for the Γ-function,

$$\psi^{m,n} = (-)^m \cdot \frac{3}{8} \cdot \left(\frac{\rho}{\rho_0}\right)^{(2/3)+m} \cdot \left\{ 2^{1/3} \frac{\Gamma(5/3)\Gamma[(5/6)+m]\cdot\Gamma[(-5/3)-n]}{\Gamma(5/6)^2\cdot\Gamma[-(5/6)+m-n]} \cdot F\left(\frac{5}{2}+n, \frac{5}{6}+m, \frac{8}{3}+n, 1-\frac{\rho}{\rho_0}\right) + \right.$$
$$2^{1/3} \frac{\Gamma(5/3)\cdot\Gamma[(5/3)+n]}{\Gamma(5/6)\cdot\Gamma[(5/2)+n]} \left(1-\frac{\rho}{\rho_0}\right)^{-(5/3)-n} \cdot F\left(-\frac{5}{6}+m-n, \frac{5}{6}, -\frac{2}{3}-n, 1-\frac{\rho}{\rho_0}\right) -$$
$$\xi \cdot 2^{2/3} \frac{\Gamma(4/3)\cdot\Gamma[(7/6)+m]\cdot\Gamma[(-7/3)-n]}{\Gamma(7/6)\cdot\Gamma(1/6)\cdot\Gamma[-(7/6)+m-n]} \cdot F\left(\frac{5}{2}+n, \frac{7}{6}+m, \frac{10}{3}+n, 1-\frac{\rho}{\rho_0}\right) -$$
$$\left. \xi \cdot 2^{2/3} \frac{\Gamma(4/3)\cdot\Gamma[(7/3)+n]}{\Gamma(7/6)\Gamma[(5/2)+n]} \left(1-\frac{\rho}{\rho_0}\right)^{-(7/3)-n} \cdot F\left(-\frac{7}{6}+m-n, \frac{1}{6}, -\frac{4}{3}-n, 1-\frac{\rho}{\rho_0}\right) \right\} \quad \text{(II, 23)}$$

and $\rho < \rho_0$ and

$$\psi^{m,n} = (-)^m \cdot \frac{3}{8} \cdot \left(\frac{\rho}{\rho_0}\right)^{-11/6+m-n} \left\{ 2^{1/3} \frac{\Gamma(5/3)\cdot\Gamma[(5/6)+m]\cdot\Gamma[-(5/3)-n]}{\Gamma(5/6)^2\cdot\Gamma[-(5/6)+m-n]} \cdot F\left(\frac{5}{2}+n, \frac{11}{6}+n-m, \right.\right.$$
$$\left. \frac{8}{3}+n, 1-\frac{\rho_0}{\rho}\right) + (-)^{n+1} \cdot 2^{1/3} \frac{\Gamma(5/3)\cdot\Gamma[(5/3)+n]}{\Gamma(5/6)\cdot\Gamma[(5/2)+n]} \left(1-\frac{\rho_0}{\rho}\right)^{-(5/3)-n} \cdot F\left(\frac{1}{6}-m, \frac{5}{6}, -\frac{2}{3}-n, 1-\frac{\rho_0}{\rho}\right) -$$
$$\xi \cdot 2^{2/3} \frac{\Gamma(4/3)\cdot\Gamma[(7/6)+m]\cdot\Gamma[-(7/3)-n]}{\Gamma(7/6)\cdot\Gamma(1/6)\cdot\Gamma[-(7/6)+m-n]} \cdot F\left(\frac{5}{2}+n, \frac{13}{6}+n-m, \frac{10}{3}+n, 1-\frac{\rho_0}{\rho}\right) -$$
$$\left. (-)^{n+1} \cdot \xi \cdot 2^{2/3} \frac{\Gamma(4/3)\cdot\Gamma[(7/3)+n]}{\Gamma(7/6)\cdot\Gamma[(5/2)+n]} \left(1-\frac{\rho_0}{\rho}\right)^{-(7/3)-n} \cdot F\left(-\frac{1}{6}-m, \frac{1}{6}, -\frac{4}{3}-n, 1-\frac{\rho_0}{\rho}\right) \right\} \quad \text{(II, 24)}$$

for $\rho > \rho_0$.

The coefficients of the hypergeometric expressions which correspond to each other in the representation for $\rho < \rho_0$ and for $\rho > \rho_0$ are the same. The factor $(-)^{n-1}$ which occurs in the second and fourth line of Eq. (II, 24) is caused by the fact that the particular solutions ψ which can be used to represent the solutions in the vicinity of point O are either symmetric or antisymmetric with respect to the line $\theta = \theta_0$, depending upon the power of $[1 - (\rho/\rho_0)]$ which occurs in front of the hypergeometric functions.

For the determination of the α occurring in Eqs. (I, 9) we need the development of $\psi^{m,n}$ in the vicinity of point O in terms of the particular solutions (I, 6). Here the following difficulty arises: The particular solutions (I, 6) are defined in the $\bar{p}$, $\bar{\xi}$-system—i.e., in a system which has point O as its origin. According to the definition of ρ given in Eq. (I, 5) we have along the sonic line

$$\rho/\rho_0 = (\theta/\theta_0)^2 \quad \text{and} \quad (\bar{p}/\rho_0) = (1 - \theta/\theta_0)^2 = (1 - \sqrt{\rho/\rho_0})^2$$

Thus in order to find the desired development in particular solutions (I, 6) we need a development of $\psi^{m,n}$ along the sonic line in terms of $(1 - \sqrt{\rho/\rho_0})$.

We proceed in the following manner. Along the sonic line the function $\psi^{m,n}$ fulfills a hypergeometric differential equation. We make in this differential equation a transformation of the independent variable

$$1 - \sqrt{\rho/\rho_0} = u \quad \text{(II, 25)}$$

Then $u = 0$ is the point O. The expression $\psi^{m,n}$ represented as a power series development with respect to u has the desired form. The coefficients can then be determined by a recurrence relation. Along the sonic line, the expression for $\psi^{m,n}$ is given (except for a constant) in Eq. (II, 19) as

$$\psi = (\rho/\rho_0)^{(2/3)+m} \cdot F[(5/2)+n, (5/6)+m, (5/3)+m, \rho/\rho_0]$$

It fulfills the differential equation

$$\psi'' \rho(1-\rho) + \psi'[(1/3) - m - \rho(3 - m + n)] - \psi \cdot (1/6) \cdot [(11/6) + n - m] = 0$$

By the transformation (II, 25), one obtains the differential equation

$$(d^2\psi/du^2)(-u^3 + 3u^2 - 2u) + (d\psi/du)\{-u^2 + 2u - 2(3 - m + n)(u^2 - 2u + 1) + [(2/3) - 2m]\} -$$
$$\psi(2/3)\cdot[(11/6) + n - m](u - 1) = 0$$

With a hypothesis

$$\psi = \sum_{k=0}^{\infty} a_k{}^{\nu} u^{\nu+k} \quad \text{(II, 26)}$$

where ν is a constant which will be determined subsequently, and the $a_k{}^{\nu}$ are suitable constants, one obtains the following recurrence relation for the $a_k{}^{\nu}$:

$$a_k^{\nu}(k+\nu)[-2(k+\nu)-(10/3)-2n]+ a_{k-1}^{\nu}\{3[k+\nu+(1/6)+(2/3)(n-m)]^2-(103/36)-4(n-m)-(4/3)(n-m)^2\}- a_{k-2}^{\nu}[k+\nu-(5/3)][k+\nu+(5/3)+2(n-m)]=0 \quad \text{(II, 27)}$$

The series starts for such values of ν, for which the coefficient of the term a_k vanishes for $k = 0$. This happens for $\nu = 0$ and $\nu = -(5/3) - n$. The lowest powers for u which occur then in Eq. (II, 26) are naturally the same as the powers of $(1 - \rho/\rho_0)$ in Eq. (II, 23). For $\nu = 0$, the first line of Eq. (II, 23) yields directly

$$a_0^0 = (-)^m \cdot \frac{3}{8} \cdot 2^{1/3} \frac{\Gamma(5/3)\cdot\Gamma[(5/6)+m]\cdot\Gamma[-(5/3)-n]}{\Gamma(5/6)^2\cdot\Gamma[-(5/6)+m-n]} \quad \text{(II, 28a)}$$

For $\nu = -(5/3) - n$, we transform the expression which occurs in the second line of Eq. (II, 23), in the following manner

$$(1-\rho/\rho_0)^{-(5/3)-n} = (1+\sqrt{\rho/\rho_0})^{-(5/3)-n}\cdot(1-\sqrt{\rho/\rho_0})^{-(5/3)-n}$$

and thus obtain

$$a_0^{-(5/3)-n} = 2^{-(5/3)-n}(-)^m \cdot \frac{3}{8}\cdot 2^{1/3} \frac{\Gamma(5/3)\cdot\Gamma[(5/3)+n]}{\Gamma(5/6)\cdot\Gamma[(5/2)+n]} \quad \text{(II, 28b)}$$

The second term in Eq. (II, 19) is essentially given by

$$\xi\cdot(\rho/\rho_0)^{(2/3)+m}\cdot F[(5/2)+n,\ (7/6)+m,\ (4/3)+m,\ \rho/\rho_0] \quad \text{(II, 29)}$$

The corresponding expression in a development around point O will contain a factor $\bar{\xi}$. Along the sonic line we have

$$\xi = \eta/\rho^{1/3} = (\eta/\bar{\rho}^{1/3})(\bar{\rho}/\rho_0)^{1/3}\cdot(\rho_0/\rho)^{1/3} = \bar{\xi}\cdot(\bar{\rho}/\rho_0)^{1/3}(\rho_0/\rho)^{1/3} \quad \text{(II, 30)}$$

Thus we consider now the expression $y = (\rho/\rho_0)^{(1/3)+m}\cdot F[(5/2)+n,\ (7/6)+m,\ (4/3)+m,\ \rho/\rho_0]$ (II, 31)

It fulfills the differential equation

$$y''(1-\rho)\cdot\rho + y'[(2/3)-m-(4+n-m)\cdot\rho] + y(-5/6)[(13/6)+n-m] = 0$$

which, by the transformation Eq. (II, 25), assumes the form

$$(d^2y/du^2)(-u^3+3u^2-2u)+(dy/du)\{-(2u-u^2)+(4/3)-2m+(-u^2+2u-1)[8+2(n-m)]\}+ y(-10/3)[(13/6)+(n-m)(u-1)]=0$$

With a hypothesis

$$y = \sum_{k=0}^{\infty} b_k^{\mu}\, u^{\mu+k} \quad \text{(II, 32)}$$

one obtains the recurrence relation

$$b_k^{\mu}(k+\mu)[-2(k+\mu)-2n-(14/3)]+ b_{k-1}^{\mu}\{3[(k+\mu)+(5/6)+(2/3)(n-m)]^2-(103/36)-4(n-m)-(4/3)(n-m)^2\}- b_{k-2}^{\mu}[k+\mu-(1/3)]\{k+\mu+(7/3)+2(n-m)[k+\mu-(1/3)]\}=0 \quad \text{(II, 33)}$$

The values of μ are found as $\mu = 0$ and $\mu = -n - (7/3)$. If one replaces in Eq. (II, 23) ξ by $\bar{\xi}$ by means of Eq. (II, 30), and also inserts the expression for Eq. (II, 31) just found together with Eq. (II, 30), into Eq. (II, 29)—then the results have the same form. The initial coefficients b are obtained from Eq. (II, 23) as

$$b_0^0 = (-)^{m+1}\cdot\left(\frac{3}{8}\right)\cdot 2^{2/3}\cdot\frac{\Gamma(4/3)\cdot\Gamma[(7/6)+m]\cdot\Gamma[-(7/3)-n]}{\Gamma(7/6)\cdot\Gamma(1/6)\cdot\Gamma[-(7/6)+m-n]} \quad \text{(II, 34a)}$$

$$b_0^{-(7/3)-n} = (-)^{m+1}\cdot\left(\frac{3}{8}\right)\cdot 2^{2/3}\cdot 2^{-(7/3)-n}\frac{\Gamma(4/3)\cdot\Gamma[(7/3)+n]}{\Gamma(7/6)\cdot\Gamma[(5/2)+n]} \quad \text{(II, 34b)}$$

Since the representations for $\psi^{m,n}$ fulfills for $\rho > \rho_0$ the same differential equation as for $\rho < \rho_0$, an investigation of the expression occurring in Eq. (II, 20) would have given the same results. Since $u = \sqrt{\bar{\rho}/\rho_0}$ we have as representation for $\psi^{m,n}$ in the vicinity of the sonic line, if $\theta < \theta_0$

$$\psi^{m,n} = \sum_{k=0}^{\infty} a_k^0\,(\bar{\rho}/\rho_0)^{k/2} + (\bar{\rho}/\rho_0)^{-(5/6)-(n/2)}\cdot\sum_{k=0}^{\infty} a_k^{-(5/3)-n}\,(\bar{\rho}/\rho_0)^{k/2} + \bar{\xi}(\bar{\rho}/\rho_0)^{1/3}\sum_{k=0}^{\infty} b_k^0\,(\bar{\rho}/\rho_0)^{k/2} + \bar{\xi}(\bar{\rho}/\rho_0)^{-(5/6)-(n/2)}\cdot\sum_{k=0}^{\infty} b_k^{-(7/3)-n}\,(\bar{\rho}/\rho_0)^{k/2} \quad \text{(II, 35)}$$

The particular solutions of the form (I, 6) that are suitable to represent the solution in the vicinity of point O have been discussed in Part II, 1b. One must only replace the quantities ρ and ξ by $\bar{\rho}$ and $\bar{\xi}$. The powers of occurring in the last equation correspond to the values given in Eqs. (II, 3) and (II, 4). The behavior of the corresponding functions G along the sonic line is expressed in Eqs. (II, 7) and (II, 8). Thus it is possible to find from Eq. (II, 35) the superposition of particular solutions (I, 7) by which the solutions $\psi^{m,n}$ are represented in the vicinity of point O.

Here the following fact is remarkable. The terms with $a_k{}^{-(5/3)-n}$ and with $b_k{}^{-(7/3)-n}$ in Eq. (II, 35) have the same power of $\bar{\rho}$ and belong therefore to the same particular solutions (I, 6). The coefficient of these particular solutions are determined independently by the two different equations. It appears desirable to show that the results are the same. We proceed in the following manner: Using the definitions (I, 6) and the expression for G, Eqs. (II, 7) and (II, 8a), one finds that for symmetric as well as for antisymmetric particular solutions

$$\frac{(\psi\bar{\xi})_{-(5/6)-(k/2)}}{\psi_{-(5/6)-(k/2)}} = -2^{-2/3}\,\frac{\Gamma(2/3)\cdot\Gamma[(7/3)+k]}{\Gamma(4/3)\cdot\Gamma[(5/3)+k]} \tag{II, 36}$$

Hence it follows that

$$b_k{}^{-(7/3)-n} = -a_k{}^{-(5/3)-n}\cdot 2^{-2/3}\times\frac{\Gamma(2/3)\cdot\Gamma[(7/3)+n-k]}{\Gamma(4/3)\cdot\Gamma[(5/3)+n-k]} \tag{II, 37}$$

This relation is fulfilled for $a_0{}^{-(5/3)-n}$ and $b_0{}^{-(7/3)-n}$ Eqs. (II, 28b) and (II, 33b). Furthermore, one can show without difficulty, that the recurrence relation (II, 33) for $b_k{}^{-(7/3)-n}$ originates from that for the $a_k{}^{-(5/3)-n}$, Eq. (II, 27), by inserting into these relations Eq. (II, 37) and the values $\nu = -(5/3) - n$ and $\mu = -(7/3) - n$.

For the future determination of the functions $\Psi^{-5/6}$, $\Psi^{-4/3}$ and $\Psi^{-11/6}$ we list here the first terms of the development of some of the expressions $\psi^{m,m}$ along the sonic line.

$$\psi^{0,0} = \frac{1}{9\cdot\sqrt{3}}\cdot 2^{1/3}\left[\left(\frac{\bar{\rho}}{\rho_0}\right)^{-5/6} + \left(\frac{19}{12}\right)\left(\frac{\bar{\rho}}{\rho_0}\right)^{-1/3} + \text{higher order terms}\right] \tag{II, 38a}$$

$$\psi^{1,1} = \frac{1}{9\cdot\sqrt{3}}\cdot 2^{1/3}\left[-\left(\frac{1}{3}\right)\cdot\left(\frac{\bar{\rho}}{\rho_0}\right)^{-4/3} + \text{higher order terms}\right] \tag{II, 38b}$$

$$\psi^{2,2} = -\frac{1}{9\cdot\sqrt{3}}\cdot 2^{1/3}\left[\left(\frac{8}{63}\right)\left(\frac{\bar{\rho}}{\rho_0}\right)^{-11/6} - \left(\frac{143}{378}\right)\times\left(\frac{\bar{\rho}}{\rho_0}\right)^{-4/3} + \text{higher order terms}\right] \tag{II, 38c}$$

Furthermore, we mention the following relations, valid along the sonic line which originate from the definition (I, 6) and the formulas (II, 7) and (II, 8)

$$\psi_{-5/6} = \pm\left(\frac{3}{8}\right)\cdot 2^{1/3}\left(\frac{\bar{\rho}}{\rho_0}\right)^{-5/6} \tag{II, 39a}$$

$$\psi_{-11/6} = \pm\left(\frac{3}{8}\right)\cdot 2^{1/3}\left(\frac{\bar{\rho}}{\rho_0}\right)^{-11/6} \tag{II, 39b}$$

$$\psi_{-1/3} = 2^{-2/3}\left(\frac{\bar{\rho}}{\rho_0}\right)^{-1/3} \tag{II, 39c}$$

$$\psi_{-4/3} = -2^{-2/3}\cdot\left(\frac{5}{4}\right)\left(\frac{\bar{\rho}}{\rho_0}\right)^{-4/3} \tag{II, 39d}$$

To determine the final expression for the functions $\Psi^{-5/6}$, $\Psi^{-4/3}$, etc., we need the x-coordinates along the plate. Their evaluation is based upon Eq. (I, 4a). According to this equation, a certain linear combination of functions ψ leads to the same linear combination for the corresponding function x and y.

Thus we determine first the contributions to x caused by the functions $\psi^{0,0}$, $\psi^{1,1}$ etc. They may be denoted by $x^{0,0}$, $x^{1,1}$ or in general by $x^{n,n}$. According to Eq. (II, 16), we have along the side of the plate

$$\psi^{n,n} = (-\xi)^{-3/2}(\rho/\rho_0)^{(2/3)+n}[1 + (\rho/\rho_0)]^{-(5/2)-n} \tag{II, 40}$$

or in terms of η and θ

$$\psi^{n,n} = \frac{3\theta}{2\,(-\eta)^{3/2}}\cdot\left(\frac{-\eta}{[(3/2)\theta_0]^{2/3}}\right)^{2+3n}\times\left[1+\left(\frac{-\eta}{[(3/2)\theta_0]^{2/3}}\right)^{3}\right]^{-(5/2)-n}$$

Hence with Eq. (I, 4a)

$$\frac{\partial x^{n,n}}{\partial\eta} = -(\gamma+1)^{1/3}\cdot\left(\frac{3}{2}\right)\left(\frac{3\theta_0}{2}\right)^{-1/3}\times\left(\frac{-\eta}{[(3/2)\theta_0]^{2/3}}\right)^{(3/2)+3n}\cdot\left[1+\left(\frac{-\eta}{[(3/2)\theta_0]^{2/3}}\right)^{3}\right]^{-(5/2)-n}$$

It is practical to introduce a new variable by

$$\bar{\eta} = \eta/(3\theta_0/2)^{2/3} \tag{II, 41}$$

The last equation is then written as

$$\frac{dx^{n,n}}{d(-\bar{\eta})} = \left[(\gamma+1)^{1/3}\cdot\left(\frac{3}{2}\right)^{4/3}\cdot\theta_0{}^{1/3}\right]\times(-\bar{\eta})^{(3/2)+3n}\,[1+(-\bar{\eta})^3]^{-(5/2)-n}$$

and thus, denoting a variable of integration by u

$$x^{n,n} = \left[(\gamma+1)^{1/3}\cdot\left(\frac{3}{2}\right)^{4/3}\cdot\theta_0{}^{1/3}\right]\times\int_{-\infty}^{-\bar{\eta}} u^{3/2+3n}\,(1+u^3)^{-(5/2)-n}\,du \tag{II, 42}$$

Here the constant of integration is chosen such that the stagnation point and, in the present approximation, the leading edge lies at $x = 0$. The contribution to the plate length of these expressions is found, if one evaluates the integral from $\bar{\eta} = -\infty$ (equivalent to $u = \infty$) to $\bar{\eta} = 0$ ($\bar{\eta} = 0$ gives the point on the pressure side where the sonic line starts—i.e., the trailing edge) Let us introduce

$$I^{n,n} = \int_{\infty}^{0} u^{(3/2)+3n}(1+u^3)^{-(5/2)-n}\,du \qquad \text{(II, 43)}$$

By the transformation $u^3 = (v/1-v)$ this expression assumes the form of a B-integral and one finds

$$I^{n,n} = -(1/3)\{\Gamma[(5/6)+n]\cdot\Gamma(5/3)/\Gamma[(5/2)+n]\} \qquad \text{(II, 44)}$$

In particular we have

$$I^{0,0} = -(1/3)\cdot[\Gamma(5/6)\cdot\Gamma(5/3)/\Gamma(5/2)] \qquad \text{(II, 45a)}$$

$$I^{1,1} = (1/3)\cdot I^{0,0} \qquad \text{(II, 45b)}$$

$$I^{2,2} = (11/63)\cdot I^{0,0} \qquad \text{(II, 45c)}$$

After these preparations, one can find the expressions for $\Psi^{-5/6}$, $\Psi^{-4/3}$ etc. $\Psi^{-5/6}$ fulfills the boundary condition at the surface of the plate and possesses as strongest singularity at point O the solution $\psi_{-5/6}$ with a coefficient one. Thus, from Eqs. (II, 38a) and (II, 39a)

$$\Psi^{-5/6} = -(27/8)\cdot\sqrt{3}\cdot\psi^{0,0} \qquad \text{(II, 46)}$$

The constant l is the plate length obtained for this solution, it is found by means of Eq. (II, 45a) as

$$l = \left(\frac{9}{8}\right)\cdot\sqrt{3}\,\frac{\Gamma(5/6)\cdot\Gamma(5/3)}{\Gamma(5/2)}\times(\gamma+1)^{1/3}\cdot\left(\frac{3}{2}\right)^{1/3}\cdot\theta_0^{1/3} \qquad \text{(II, 47)}$$

Furthermore, one needs for the evaluation of Eq. (II, 19) the quantity $\alpha_{-1/3}{}^{-5/6}$ which is found from Eqs. (II, 46), (II, 38a), and (II, 39c) as

$$\alpha_{-1/3}{}^{-5/6} = -19/16 \qquad \text{(II, 48)}$$

$\Psi^{-4/3}$ has as strongest singularity at point O the expression $\psi_{-4/3}$ with a coefficient one, and, furthermore, its contribution to the plate length is zero. Hence from Eqs. (II, 38b), (II, 39d), and (II, 45)

$$\Psi^{-4/3} = [(135\cdot\sqrt{3})/8][\psi^{1,1} - (1/3)\psi^{0,0}] \qquad \text{(II, 49)}$$

Finally, the solution $\Psi^{-11/6}$ is characterized by its strongest singularity given by $\psi_{-11/6}$ with a coefficient one, by the absence of the singularity $\psi_{-4/3}$ and by the fact that its contribution to the over-all length of the plate is zero.

$$\psi^{-11/6} = \frac{27\cdot 63\cdot\sqrt{3}}{128}\left[\psi^{2,2} - \frac{143}{126}\cdot\psi^{1,1} + \frac{11}{54}\cdot\psi^{0,0}\right] \qquad \text{(II, 50)}$$

Then the corresponding values of x (along the plate) are given by replacing the functions ψ by the expressions (II, 42). The results are listed subsequently (the expressions for $x^{-4/3}$ and $x^{-11/6}$, actually all the higher x's, can be evaluated by integrations by parts):

$$x^{-5/6} = -\frac{27}{8}\cdot\sqrt{3}\left[(\gamma+1)^{1/3}\left(\frac{3}{2}\right)^{4/3}\cdot\theta_0^{1/3}\right]\times\int_{\infty}^{-\bar\eta} u^{3/2}(1+u^3)^{-5/2}\,du$$

$$x^{-4/3} = -\frac{9}{4}\cdot\sqrt{3}\left[(\gamma+1)^{1/3}\left(\frac{3}{2}\right)^{4/3}\cdot\theta_0^{1/3}\right]\times(-\bar\eta)^{5/2}[1+(-\bar\eta)^3]^{5/2}$$

$$x^{-11/6} = \frac{27}{128}\cdot 63\cdot\sqrt{3}\left[(\gamma+1)^{1/3}\cdot\left(\frac{3}{2}\right)^{4/3}\cdot\theta_0^{1/3}\right]\times(-\bar\eta)^{5/2}[1+(-\bar\eta)^3]^{5/2}\left(-\frac{2(-\bar\eta)^3}{21[1+(-\bar\eta)^3]}+\frac{11}{135}\right) \qquad \text{(II, 51)}$$

Because of their simplicity we mention furthermore the following expressions which are needed in evaluating Eq (I, 26)

$$\frac{x^{-4/3}}{(d/d\bar\eta)(x^{-5/6})} = -\left(\frac{2}{3}\right)(-\bar\eta);\quad \frac{x^{-11/6}}{(d/d\bar\eta)(x^{-5/6})} = \frac{63}{16}(-\bar\eta)\left(-\frac{2}{21}\cdot\frac{(-\bar\eta)^3}{1+(-\bar\eta)^3}+\frac{11}{135}\right) \qquad \text{(II, 52)}$$

The form of the first of these expressions is not surprising after the interpretation which has been given to $\Psi^{-4/3}$ in part I, 6. There we found that for a change of the angle of attack by $\Delta\alpha$, the solution for the flow field is given by

$$(L/l)\cdot[\Psi^{-5/6} - (3/2)\cdot\Psi^{-4/3}\rho_0{}^{-1/2}\cdot\Delta\alpha]$$

On the basis of the considerations of part I, 9, the change of the pressure distribution is then given by

$$\Delta\bar\eta = (3/2)\rho_0{}^{-1/2}\cdot\Delta\alpha\,[x^{-4/3}/(d/d\bar\eta)(x^{-5/6})]$$

or with Eq. (II, 51a) and $\rho_0 = (9/4)\theta_0{}^2$

$$\Delta\bar\eta = (2/3)\cdot\bar\eta\cdot(\Delta\alpha/\theta_0) \qquad \text{(II, 53)}$$

On the other hand the pressure distribution over a flat plate can, in principle, be written in the form

$$\eta = \bar\eta(x)\cdot(3\theta_0/2)^{2/3}$$

If one changes the angle of attack θ_0 by $\Delta\alpha$ then one obtains

$$[\Delta\eta/(3\theta_0/2)^{2/3}] = \bar\eta(x)\cdot(2/3)(\Delta\alpha/\theta_0)$$

This is Eq. (II, 53).

(3) *Particular Solutions Which Have $\psi = 0$ Along OQ and Are Singular at O or Q*

We seek particular solutions which are symmetric with respect to the line $\bar\xi = -\infty$ and have $\psi = 0$ along OQ. Naturally one will have along OQ a change of the sign of ψ_θ. Along the line $\bar\xi = -\infty$ from Q to $\eta = -\infty$, ψ_θ will be zero. The solutions will be singular either at point Q or at point O. The second possibility is a generalization which is not needed in the present applications.

We start with an assumed form of ψ along $\bar\xi = -\infty$ for $\bar p > \bar p_Q$

$$\psi = (\bar p/\bar p_Q)^{-1/3}[1-(\bar p/\bar p_Q)^{-1}]^{-(1/2)-k} \qquad \text{(II, 54)}$$

here k is a positive or negative integral number.

This expression will be continued analytically through the subsonic region and it will be shown that the continuation fulfills the desired boundary conditions.

Along the line $\bar{\xi} = -\infty$ and for $\bar{p}/\bar{p}_Q > 1$, Eq. (II, 54) is developed in the form

$$\psi = \left(\frac{\bar{p}}{\bar{p}_Q}\right)^{-1/3} \cdot \sum_{h=0}^{\infty} \frac{\Gamma[(1/2) + h + k]}{\Gamma[(1/2) + k] \cdot \Gamma(h+1)} \cdot \left(\frac{\bar{p}}{\bar{p}_Q}\right)^{-h} \qquad \text{(II, 55)}$$

By means of the particular solutions given in Eq. (I, 8c) and with the aid of Eqs. (II, 9a) one finds as the representation along the sonic line

$$\psi = (1/2)(\bar{p}/\bar{p}_Q)^{-1/3}\{2^{1/3} \cdot F[(1/2) + k, 5/6, 2/3, (-\bar{p}/\bar{p}_Q)^{-1}] - \bar{\xi} \cdot 2^{-1/3} \cdot F[(1/2) + k, 7/6, 1/3, (-\bar{p}/\bar{p}_Q)^{-1}]\} \qquad \text{(II, 56)}$$

As a series representation the expression converges for $\bar{p} > \bar{p}_Q$ only, but as a hypergeometric function the representation along the entire sonic line is obvious.

From here on we shall proceed in the following manner: By a development of the expression found along the sonic line with respect to particular solutions (I, 6) for negative values of λ, we form a representation for the subsonic region which shows that no singularities will occur except at the line $\bar{\xi} = -\infty$. Since this procedure differs somewhat from the one applied in reference 2, some of its details will be shown. In a further step we develop the solutions for $\bar{p} < \bar{p}_Q$ in terms of the particular solutions (I, 8b) and thus show that along OQ the boundary condition $\psi = 0$ is fulfilled.

But first, before we carry out these investigations whose sole purpose is to justify the assumption, Eq. (II, 54), we derive the expression $\delta_{-4/3}/\delta_{-1/3}$ needed for the evaluations of the first part. The function to be represented is shown in Eq. (I, 14); it is characterized by its behavior along $\bar{\xi} = -\infty$—i.e., $\psi \sim (\bar{p} - \bar{p}_Q)^{-1/2}$ for $\bar{p} > \bar{p}_Q$. To obtain this solution we choose in Eq. (II, 54) $k = 0$. Then one finds by a comparison of Eq. (I, 14) with Eq. (II, 55), using Eq. (I, 8c)

$$\delta_{-4/3}/\delta_{-1/3} = 1/2 \qquad \text{(II, 57)}$$

To show the convergence of the expression through the subsonic region, we use the particular solutions (I, 6) for negative values of λ. The two terms on the right side of Eq. (II, 56) will be treated separately. For negative values of λ the particular solutions (I, 6) have along the sonic line, the form

$$\bar{p}^{-1/12} \cos[(\sqrt{|\lambda|}/3) \cdot \log \bar{p}] \quad \text{or} \quad \bar{p}^{-1/12} \times \sin[(\sqrt{|\lambda|}/3) \cdot \log \bar{p}]$$

Accordingly, we develop the expression $\bar{p}^{1/12} \cdot \psi$ taken from Eq. (II, 56) with respect to $\cos[(\sqrt{|\lambda|}/3) \log \bar{p}]$ and $\sin[(\sqrt{|\lambda|}/3) \log \bar{p}]$ and then replace each term by the corresponding particular solution (I, 6). Assume that $\bar{p}^{1/12} \cdot \psi$ is represented along the sonic line in the following form

$$\bar{p}^{1/12} \cdot \psi = \int_0^{\infty} g_1(u) \cdot \cos(uw) du + \int_0^{\infty} g_2(u) \cdot \sin(uw) \cdot du \qquad \text{(II, 58)}$$

where $w = \log \bar{p}$, where u replaces $\log \bar{p}$ and where the g are functions which arise by the development. If $\bar{p}^{1/12} \cdot \psi$ does not fulfill the conditions necessary for the convergence of the Fourier integral then a finite number of suitable particular solutions must be subtracted beforehand. In the complex $\bar{p}$-plane, $\bar{p}^{1/12}\psi$ has the singular points $-\infty$, 0, and $-\bar{p}_\theta$ since it is represented by hypergeometric series Eq. (II, 56). Therefore the representation (II, 58) converges in the complex w-plane in a strip $-\pi < Imw < \pi$. This gives an estimation for the g. For $|Imw| < \pi - \epsilon$ the expression (II, 58) can be written as

$$\int_0^{\infty} \{g_1(u)[\cos(u\,Rew) \cdot \cosh(u \cdot Imw) + i \sin(u\,Rew) \cdot \sinh(u\,Imw)] + g_2(u)[\sin(u \cdot Rew) \cdot \cosh(u\,Imw) - i \cos(u\,Rew) \cdot \sinh(u\,Imw)]\} du$$

This expression would diverge if the coefficients of $\cos(u\,Rew)$ and of $\sin(u\,Rew)$ were unbounded for large values of u. Using the approximation for hyperbolic function of a large argument, one finds

$$\sqrt{g_1^2(u) + g_2^2(u)} \cdot e^{u\,Imw} \leq M \qquad g_1(u) \leq M \cdot e^{-u(\pi - \epsilon)} \qquad g_2(u) \leq M \cdot e^{-u(\pi - \epsilon)}$$

Now it follows from Eqs. (II, 12) and (II, 13), that a function $G(\xi, \lambda)$ which assumes the value of $G(0, \lambda)$ along the sonic line, and for which $dG/d\xi$ is zero, is represented for large negative values of λ and for $\xi < 0$ by an expression

$$G(\xi, \lambda) \backsimeq G(0, \lambda) \cdot \text{const.} \cdot |\lambda|^{-1/12} \cdot e^{(\sqrt{|\lambda|}/3) \cdot \nu(\xi)}$$

or, using $\lambda = -9u^2$

$$[G(\xi, -9u^2)/G(0, -9u^2)] \backsimeq \text{const.} \cdot |\lambda|^{-1/12} \cdot e^{u \cdot \nu(\xi)}$$

The analytic continuation of the expression ψ from the sonic line through the subsonic region will be free of singularities, if

$$\psi = \bar{p}^{-1/12} \cdot \int_0^{\infty} \left[g_1'(u) \cdot \cos(uw) \frac{G(\xi, -9u^2)}{G(0, -9u^2)} + g_2(u) \cdot \sin(uw) \frac{G(\xi, -9u^2)}{G(0, -9u^2)}\right] du \leq \bar{p}^{-1/12} \int_0^{\infty} M \cdot |\lambda|^{-1/12} \cdot \text{const.} \cdot e^{u[\nu(\xi) - \pi + \epsilon]} du$$

converges. This is the case for $\nu(\xi) < \pi - \epsilon$ where $\epsilon > 0$ but can be taken arbitrarily small. According to Eq. (II, 11), $\nu(\xi) = \pi$ corresponds to $\bar{\xi} = -\infty$. This completes the proof of the convergence. For the contribution due to ψ_ξ along the sonic line one proceeds analogously.

To show that the analytic continuation of expression (II, 56) fulfills the condition $\psi = 0$ along OQ, we use the development for

$$\psi = 2^{-2/3}\left\{\left(\frac{\bar{p}}{\bar{p}_Q}\right)^{(1/6)+k}\frac{\Gamma[(1/3)-k]\cdot\Gamma(2/3)}{\Gamma[(1/6)-k]\cdot\Gamma(5/6)}\cdot F\left[\left(\frac{1}{2}\right)+k,\left(\frac{5}{6}\right)+k,\left(\frac{2}{3}\right)+k,\left(-\frac{\bar{p}}{\bar{p}_Q}\right)\right]-\left(\frac{\bar{p}}{\bar{p}_Q}\right)^{1/2}\frac{\Gamma[k-(1/3)]\cdot\Gamma(2/3)}{\Gamma[-(1/6)]\cdot\Gamma[(1/2)+k]}\cdot F\left[\left(\frac{5}{6}\right),\left(\frac{7}{6}\right),\left(\frac{4}{3}\right)-k,\left(-\frac{\bar{p}}{\bar{p}_Q}\right)\right]\right\}-$$

$$\xi\cdot 2^{-4/3}\left\{\left(\frac{\bar{p}}{\bar{p}_Q}\right)^{(1/6)+k}\frac{\Gamma[(2/3)-k]\cdot\Gamma(1/3)}{\Gamma[-(1/6)-k]\cdot\Gamma(7/6)}\cdot F\left[\left(\frac{1}{2}\right)+k,\left(\frac{7}{6}\right)+k,\left(\frac{1}{3}\right)+k,\left(-\frac{\bar{p}}{\bar{p}_Q}\right)\right]+\left(\frac{\bar{p}}{\bar{p}_Q}\right)^{5/6}\frac{\Gamma[k-(2/3)]\cdot\Gamma(1/3)}{\Gamma(-5/6)\Gamma[(1/2)+k]}\cdot F\left[\left(\frac{7}{6},\frac{11}{6},\left(\frac{5}{3}\right)-k,\left(-\frac{\bar{p}}{\bar{p}_Q}\right)\right]\right\}$$

The powers of $\bar{p}/\bar{p}_Q$ occurring here are those of the particular solutions which have $\psi = 0$ along OQ and are regular along the Mach wave EO, Eq. (I, 8b). The continuation of the second and fourth term of the last equation to OQ is obvious. The first and third terms contain the same powers of $\bar{p}/\bar{p}_Q$, it can be shown by a straightforward computation that these terms are represented by the same particular solutions (I, 8b).

(4) *Particular Solutions Which Have $\psi = 0$ Along OQ and Are Singular at Infinity*

The particular solutions in question are obtained by a generalization of the assumption, Eq. (II, 54). Denoting momentarily the expression (II, 54) evaluated for $k = 0$, by $\hat{\psi}$, they are given along $\bar{\xi} = -\infty$ by

$$\psi = \left(\frac{\bar{p}}{\bar{p}_Q}\right)^h\int\left(\frac{\bar{p}}{\bar{p}_Q}\right)^{-h-1}\cdot\hat{\psi}\cdot d\left(\frac{\bar{p}}{\bar{p}_Q}\right)$$

$$= \left(\frac{\bar{p}}{\bar{p}_Q}\right)^h\cdot\int\left(\frac{\bar{p}}{\bar{p}_Q}\right)^{-(1/3)-h-1}\left[1-\left(\frac{\bar{p}}{\bar{p}_Q}\right)^{-1}\right]^{-1/2}\cdot d\left(\frac{\bar{p}}{\bar{p}_Q}\right) \qquad \text{(II, 59)}$$

The choice of the constant of integration is an important part of this analysis; it will be discussed later.

If one writes the last expressions as a series, then the powers of $(\bar{p}/\bar{p}_Q)^{-1}$ which occur in it will be the same as in Eq. (II, 55), but the coefficients will be changed by the integration, depending upon the powers of $\bar{p}/\bar{p}_Q$ occurring in the various terms. Thus, the analytic continuation of this function (II, 59) is accomplished by the same particular solutions (I, 8c) as previously and the representation along the sonic line is obtained by carrying out in Eq. (II, 56) the operation corresponding to Eq. (II, 59). Naturally, the operation can also be carried out on the individual terms of the powers series representations of the hypergeometric functions occurring in Eq. (II, 56). Here the constant of integration which will occur, will cause a term with a power $(\bar{p}/\bar{p}_Q)^h$ to be present which was not contained in the original series (II, 56). This term will represent the desired singularity at infinity; it is the main task to determine its coefficients.

In the previous analysis, it was important that for the hypergeometric expressions of Eq. (II, 56) that describe the behavior along the sonic line, there exists a relation between the representation at $\bar{p}/\bar{p}_Q = 0$ and at $\bar{p}/\bar{p}_Q = \infty$. This relation can be derived by means of Barnes' contour integral for the hypergeometric function. Here Barnes' representation will be useful for the determination of the constant of integration.

According to Barnes' formula (see, for instance, reference 8, p. 256) we have

$$\frac{\Gamma(a)\cdot\Gamma(b)}{\Gamma(c)}\cdot F(a,b,c,z) = \frac{1}{2\pi i}\int_{-i\infty}^{+i\infty}\frac{\Gamma(a+s)\Gamma(b+s)\cdot\Gamma(-s)}{\Gamma(c+s)}(-z)^s ds$$

where the path of integration runs essentially along the imaginary s-axis with such loops, if necessary, that the poles of $\Gamma(-s)$ lie to the right and the poles of $\Gamma(a+s)$ and $\Gamma(b+s)$ lie to the left of the path. The behavior of the integrand at infinity of the complex s-plane is such that the path of integration can be closed at will through either the right or left half plane.

We obtain for the hypergeometric functions occurring in Eq. (II, 56)

$$F\left[\frac{1}{2},\frac{5}{6},\frac{2}{3},\left(-\frac{\bar{p}}{\bar{p}_Q}\right)^{-1}\right] = \frac{\Gamma(2/3)}{\Gamma(1/2)\cdot\Gamma(5/6)}\cdot\frac{1}{2\pi i}\int_{-i\infty}^{+i\infty}\frac{\Gamma[(1/2)+s]\Gamma[(5/6)+s]\Gamma(-s)}{\Gamma[(2/3)+s]}\cdot\left(\frac{\bar{p}}{\bar{p}_Q}\right)^{-s}ds \qquad \text{(II, 60a)}$$

and

$$F\left[\frac{1}{2},\frac{7}{6},\frac{1}{3},\left(-\frac{\bar{p}}{\bar{p}_Q}\right)^{-1}\right] = \frac{\Gamma(1/3)}{\Gamma(1/2)\cdot\Gamma(7/6)}\cdot\frac{1}{2\pi i}\int_{-i\infty}^{+i\infty}\frac{\Gamma[(1/2)+s]\cdot\Gamma[(7/6)+s]\cdot\Gamma(-s)}{\Gamma[(1/3)+s]}\cdot\left(\frac{\bar{p}}{\bar{p}_Q}\right)^{-s}ds \qquad \text{(II, 60b)}$$

If one closes the path of integration in the right half plane, then the calculus of residues gives the series representation

in powers of $(\bar{p}/\bar{p}_Q)^{-1}$ if one closes it in the left half plane then one obtains the series representation in powers of $(\bar{p}/\bar{p}_Q)$. In the first case, the residues are formed at the poles of $\Gamma(-s)$; in the second case, at the poles of $\Gamma[(1/2) + s]$ and $\Gamma[(5/6) + s]$ or $\Gamma[(7/6) + s]$. If we carry out in Eq. (II, 60) the operation indicated in Eq. (II, 5g) then we obtain for ψ along the sonic line

$$\psi = -2^{-2/3}\cdot\frac{1}{2\pi i}\,\frac{\Gamma(2/3)\cdot(\bar{p}/\bar{p}_Q)^{-1/3}}{\Gamma(1/2)\cdot\Gamma(5/6)}\int_{-i\infty}^{+i\infty}\frac{\Gamma[(1/2)+s]\cdot\Gamma[(5/6)+s]\cdot\Gamma(-s)}{\Gamma[(2/3)+s]\cdot[s+(1/3)+h]}\cdot(\bar{p}/\bar{p}_Q)^{-s}\,ds +$$

$$\xi\cdot 2^{-4/3}\,\frac{1}{2\pi i}\cdot\frac{\Gamma(1/3)\cdot(\bar{p}/\bar{p}_Q)^{-1/3}}{\Gamma(1/2)\cdot\Gamma(7/6)}\cdot\int_{-i\infty}^{+i\infty}\frac{\Gamma[(1/2)+s]\cdot\Gamma[(7/6)+s]\cdot\Gamma(-s)}{\Gamma[(1/3)+s]\,[s+(1/3)+h]}\,(\bar{p}/\bar{p}_Q)^{-s}\,ds$$

The integrands have besides the poles which occurred in the original expressions (II, 60), a pole at $s = -(1/3) - h$. The residues at the original poles are changed because of the factor $[s + (1/3) + h]$ occurring in the denominator because of the integration. The contribution of these poles give the integrated terms of the hypergeometric series proceeding in powers of either $\bar{p}/\bar{p}_Q$ or $(\bar{p}/\bar{p}_Q)^{-1}$.

We choose the path of integration in such a manner that point $s = (-1/3) - h$ lies to its right. Then this pole lies outside of the contour which leads to the representation in powers of $\bar{p}/\bar{p}_Q$—i.e., around point O, the representation contains solely the integrated terms of the hypergeometric series. This shows immediately that the analytic continuation of this representation will give $\psi = 0$ along OQ.

The representation for large values of $\bar{p}/\bar{p}_Q$ will contain an additional term caused by the residue at point $s = -1/3 - h$. It is found to be

$$\psi = -2^{-2/3}\,\frac{\Gamma(2/3)}{\Gamma(1/2)\cdot\Gamma(5/6)}\cdot\frac{\Gamma[(1/6)-h]\cdot\Gamma[(1/2)-h]\cdot\Gamma[(1/3)+h]}{\Gamma[(1/3)-h]}\cdot\left(\frac{\bar{p}}{\bar{p}_Q}\right)^h +$$

$$\xi\cdot 2^{-4/3}\,\frac{\Gamma(1/3)}{\Gamma(1/2)\cdot\Gamma(7/6)}\cdot\frac{\Gamma[(1/6)-h]\cdot\Gamma[(5/6)-h]\cdot\Gamma[(1/3)+h]}{\Gamma(-h)}\cdot\left(\frac{\bar{p}}{\bar{p}_Q}\right)^h$$

The next question concerns the analytic continuation of this term through the subsonic region. Obviously, the analytical continuation is given by a particular solution of the form (I, 6) with $\sqrt{\lambda}/3 = 1/12 + h$; in general it will be represented by a linear combination of the symmetrical and antisymmetrical expression ψ. The coefficient of the symmetrical and antisymmetric particular solutions can be found by means of Eqs. (II, 5) and (II, 6). One finds for the coefficient of the symmetrical portion

$$\{\Gamma[(1/3)+h]\cdot\Gamma(1/2)/\Gamma[(5/6)+h]\}$$

and for the coefficient of the antisymmetrical portion

$$-(2/\sqrt{3})\cdot\pi^{1/2}\{\Gamma[(1/2)-3h]/\Gamma(-3h)\}$$

The antisymmetric coefficient is zero, if $3h$ is a non-negative integral number. Then the solutions are entirely symmetric with respect to $\bar{\xi} = -\infty$. These are the particular solutions used in Eq. (I, 10b). If $(1/2 - 3h)$ is a non-positive integral number, the ratio of the antisymmetric coefficient and the symmetric coefficient is infinite—this gives the particular solutions (I, 10a).

The present approach defined first the function ψ along the line $\bar{\xi} = -\infty$ by Eq. (II, 59) and then used the idea of analytic continuation. One can also carry out the operation indicated in Eq. (II, 59) in the entire $\bar{p}$, $\bar{\xi}$-plane with an additional condition regarding the behavior of the constant of integration in its dependence upon $\bar{\xi}$; one thus finds a solution of the original differential equation for ψ. Since the function ψ defined by Eq. (II, 59) is regular along the Mach wave OE, the function originating by the operation Eq. (II, 59) will also be regular along this Mach wave. This condition applies also to the term with $(\bar{p}/\bar{p}_Q)^h$ and thus determines independently the ratio of the coefficients of the antisymmetric and symmetric portions.

The idea just presented leads also to an independent determination of the coefficient of the symmetrical particular solution, at least in a heuristic manner. The solution gives $\psi = 0$ along OQ. This determines the constant of integration in Eq. (II, 59); one obtains for large values of $\bar{p}/\bar{p}_Q$

$$\psi = \left(\frac{\bar{p}}{\bar{p}_Q}\right)^h\cdot\int_1^\infty\left(\frac{\bar{p}}{\bar{p}_Q}\right)^{-1/3-h-1}\times$$

$$\left[1-\left(\frac{\bar{p}}{\bar{p}_Q}\right)\right]^{-1/2}\cdot d\left(\frac{\bar{p}}{\bar{p}_Q}\right)$$

The integral which occurs here can be transformed into a B-integral.
Thus

$$\psi = (\bar{p}/\bar{p}_Q)^h\,\{\Gamma(1/2)\cdot\Gamma[(1/3)+h]/\Gamma[(5/6)+h]\}$$

Remembering that along $\bar{\xi} = -\infty$ on the contribution of the antisymmetric particular solution to ψ is zero, we find immediately the symmetrical coefficient given above.

The procedure just described gives the necessary results quite rapidly, but the author feels that the previous method is more suitable to derive these results rigorously.

For the evaluation of the results of the first part we need the function (II, 59) for $h = 0$.
Here one finds for the representation at infinity

$$\psi = \frac{\Gamma(1/3)\cdot\Gamma(1/2)}{\Gamma(5/6)} - 3\left(\frac{\bar{p}}{\bar{p}_Q}\right)^{-1/3} - \left(\frac{3}{8}\right)\left(\frac{\bar{p}}{\bar{p}_Q}\right)^{-4/3}$$

or with the notation of Eq. (I, 10b)

$$\beta_{-1/3}{}^0 = -3\cdot\Gamma(5/6)/[\Gamma(1/3)\cdot\Gamma(1/2)]$$
$$\beta_{-4/3}{}^0 = -3\cdot\Gamma(5/6)/[8\Gamma(1/3)\cdot\Gamma(1/2)].$$

REFERENCES

[1] Marschner, Bernard W., *The Flow Over a Body in a Choked Wind Tunnel and in a Sonic Free Jet*, Thesis, California Institute of Technology, 1954. (To be published in the Journal of the Aeronautical Sciences.)

[2] Guderley, Gottfried, *The Flow Over a Flat Plate With a Small Angle of Attack at Mach Number 1*, Journal of the Aeronautical Sciences, Vol. 21, No. 4, pp. 261–274, April, 1954.

[3] Guderley, Gottfried, *Two-Dimensional Flow Patterns With a Free Stream Mach Number Close to One*, AF Technical Report 6343, May, 1951.

[4] Guderley, Gottfried, *Singularities at the Sonic Velocity*, AF Technical Report F-TR-1171 ND, Wright-Patterson AFB.

[5] Guderley, Gottfried, and Yoshihara, Hideo, *Two-Dimensional Unsymmetric Flow Patterns at Mach Number 1*, Journal of the Aeronautical Sciences Vol. 20, No. 11, pp. 757–768, November, 1954.

[6] Guderley, Gottfried, *On Wind-Tunnel Corrections in Transonic Range*, WADC Technical Report 53-506, December 1953.

[7] Langer, R. E., *Asymptotic Solutions of Ordinary Differential Equations with an Application to Bessel Functions of Large Order Transactions*, American Math Society, pp. 23–64, 1931.

[8] Copson, E. T., *An Introduction to the Theory of a Complex Variable;* Oxford University Press.

Transient Temperature Distributions...

(*Continued from page 836*)

body and the energy received from the surroundings by radiation is assumed equal to $\epsilon C_S T_s^4$, which is in most cases sufficiently accurate for the present purpose. In cases where the thermal stresses are nearly equal to their asymptotic value for $g \to \infty$, it is only necessary to replace in the previous formulas the fluid friction temperature T_f by the wall temperature T_w as calculated from Eq. (39). In other cases—i.e., if $g < 6$—the maximum thermal stresses occur before the skin has reached its equilibrium temperature and consequently at a time when the temperature level in the whole structure is lower than for the asymptotic case. Since the heat radiated from the surface is proportional to the fourth power of the absolute temperature, the radiation effects will be less at lower temperature levels and consequently they will also be less for values of $g < 6$ than for the asymptotic case $g \to \infty$. Thus an upper limit of the radiation effects on thermal stresses can be found as regards the effective temperature difference $T_f - T_i$ in the formulas for the stresses.

The influence of radiation on the parameter g can be determined approximately by using an effective heat-transfer coefficient

$$\alpha_{\text{eff.}} = \alpha_{\text{con.}} + \alpha_{\text{rad.}} \qquad (40)$$

where the first and second term refer to convection and radiation respectively. The second term in Eq. (40) is equal to the left-hand side of Eq. (39) divided by $T_w - T_0$.

In the case treated in reference 1 the material of the wing was steel and the flight data were $M = 3.1$ and $H = 50{,}000$ ft. Assuming the emissivity of steel as $\epsilon = 0.80$, the upper limit of the error due to neglecting radiation would be 10 per cent as regards the effective temperature difference $T_f - T_i$ and $\alpha_{\text{eff.}}$ would be about 14 per cent higher than $\alpha_{\text{con.}}$ Hence in this case the thermal stresses would not be materially effected by taking radiation into account.

REFERENCES

[1] Hoff, N. J., *Structural Problems of Future Aircraft*, Third Anglo-American Aeronautical Conference at Brighton, England, 1951, the Royal Aeronautical Society, pp. 77–114. Appendix I, "Aerodynamic Heating and Thermal Stresses," by Paul Torda and N. J. Hoff, pp. 103–110.

[2] Parkes, E. W., *Transient Thermal Stresses in Wings*, Aircraft Engineering XXV, No. 298, pp. 373–378, December, 1953.

[3] Pohle, F. V., and Oliver, H., *Temperature Distribution and Thermal Stresses in a Model of a Supersonic Wing*, Journal of the Aeronautical Sciences, Vol. 21, No. 1, pp. 8–16, January, 1954.

[4] Schuh, H., *On the Calculation of Temperature Distribution and Thermal Stresses in Parts of Aircraft Structures at Supersonic Speeds*, Readers' Forum, Journal of the Aeronautical Sciences, Vol. 21, No. 8, pp. 575–576, August, 1954.

[5] Carslaw, H. S., and Jaeger, J. C., *Conduction of Heat in Solids*, Oxford University Press, England, 1947.

[6] Timoshenko, S., and Goodier, J. N., *Theory of Elasticity*, 2nd Ed., McGraw-Hill Book Company, New York, 1951.

[7] von Kàrmàn, Th., *Analogy Between Fluid Friction and Heat Transfer*, Engineering 48, pp. 210–213, 1939.

[8] R. W. Wilson, *Turbulent Boundary-Layer Characteristics at Supersonic Speeds—Theory and Experiment*, Journal of the Aeronautical Sciences, Vol. 17, No. 9, pp. 585–594, September, 1950.

[9] Colburn, A. P., *A Method for Correlating Forced-Convection Heat-Transfer Data and a Comparison with Fluid Friction*, Trans. Amer. Inst. of Chem. Engr., Vol. 29, pp. 174–210, 1933.

[10] Slack, E. G., *Experimental Investigation of Heat Transfer through Laminar and Turbulent Boundary Layers on a Cooled Flat Plate at a Mach Number of 2.4*, NACA TN 2686, 1952.

Readers' Forum

BRIEF REPORTS of investigations in the aeronautical sciences and discussions of papers published in the JOURNAL are presented in this special department. Publication is completed as soon as possible after receipt of the material. The Editorial Committee does not hold itself responsible for the opinions expressed by the correspondents.

The Load Carrying Capacity of Initially Flat Circular Steel Plates Under Reversed Loading*

R. M. Haythornthwaite and E. T. Onat†
Assistant Professor of Engineering, and Research Associate, Respectively, Division of Applied Mathematics, Brown University, Providence, R.I.

May 17, 1955

SUMMARY

The testing of a simply supported, centrally loaded mild steel plate, 20 in. diameter, is described. The plate was loaded well into the plastic range and then reloaded in the reverse sense. Under reversed loading, temporary plastic instability was observed, as predicted by applying a new large deflection theory for plates composed of rigid plastic material.[11] Earlier tests have shown that the limit load obtained by neglecting changes in geometry is often of little physical significance for a monotonically increasing load. These tests show that, in reversed loading, it becomes a measure of the minimum load carrying capacity available during a phase of plastic instability.

INTRODUCTION

LOADING TESTS of structural steel frameworks[1, 2, 3] have shown that good estimates of their load carrying capacity can be obtained by the methods of limit analysis.[4, 5] In the theory, a rigid-plastic material is usually assumed and the load carrying capacity is estimated as the load at which a structure composed of this material would begin to deform. It can be shown that, if the material is perfectly plastic—i.e., nonstrain-hardening, and if the accompanying change in geometry is disregarded, plastic flow continues under constant load.[5] If, however, changes in geometry and strain-hardening are considered, then in general plastic flow can continue only under either increasing or decreasing load.[6] Hence the methods of limit analysis may require modification before they can be applied successfully to other types of structure.

In the case of circular plates, recent tests[7, 8, 9] have shown that limit analysis based on the initial geometry and neglecting strain-hardening leads to estimates of load carrying capacity that are far too low. It has been suggested that change in geometry is probably the significant factor.[7] To investigate this point theoretically, estimates of the load carrying capacity of the plate in the deformed state must be obtained. For simply supported plates loaded centrally the shape remains close to the conical form suggested by the incipient (zero deflection) velocity field.[10] Consequently, an approximate load-deflection curve was found assuming the shape remains exactly conical. Each point on this curve represents an upper bound to the load carrying capacity of a conical shell composed of rigid ideally plastic material. This analysis has enabled the writers to predict with reasonable accuracy the load deflection curves observed for steel plates over a wide range of the thickness/diameter ratio.[11]

The theory leads also to important conclusions concerning behavior under reversed loading. These will be discussed in the light of new data obtained from tests of a plate supported freely near the outer edge and carrying a central load.

THE RIGID-PLASTIC PLATE IN REVERSE LOADING

Fig. (1) shows the theoretical load-deflection relationship for various stages in the loading and unloading of a rigid-plastic plate

When the load is smaller than a certain yield load P_A, the plate remains rigid. Above P_A, the theory for large deformations[11] leads to the locus GAB, the right-hand branch of which will be followed. The right-hand path is chosen to satisfy the condition that the plastic work done in the plate should be positive. BC is a typical unloading path.

If loading is continued in the reverse sense after C is reached, the plate will remain rigid until P_D, at which the plate will again deform plastically, but in the opposite sense. Due to assumed symmetry of the yield condition, $P_E = -P_D$. If the conical shape is again assumed, the locus obtained is DEF, which is symmetrical with BAG. When strain is controlled during a test, the locus DEF will be followed, implying a decrease in the applied load. On the other hand, when the load is maintained, as under dead weight loading, the locus jumps directly from D to F, as indicated by the dotted line in Fig. 1. Thus the decrease in load along DE indicates the possibility of a temporary plastic instability.

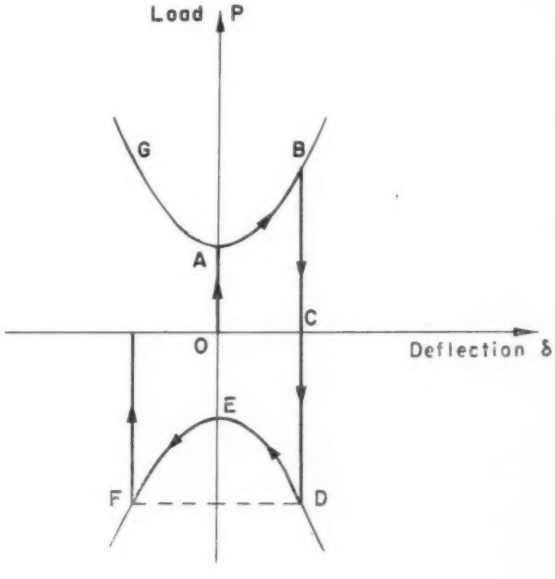

Fig. 1

* The results presented in this paper were obtained in the course of research sponsored by the Office of Ordnance Research under Contract No. DA-19-020-ORD-3172, Project No. TB2-0001 (1086).

† Now at Yenisehir, Ankara, Turkey.

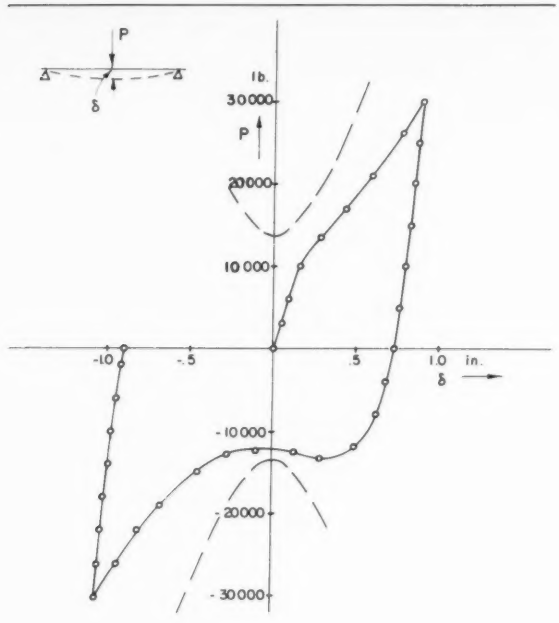

Fig. 2. Mild steel plate under reversing-load First cycle (load range ± 30,000 lb)

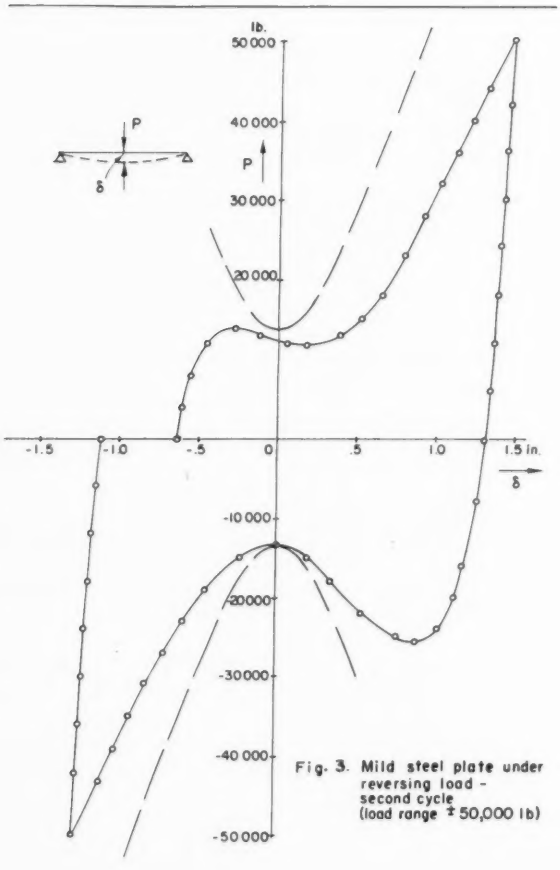

Fig. 3. Mild steel plate under reversing load - second cycle (load range ± 50,000 lb)

Fig. 1 is drawn for a material that can be considered to have an indefinitely large modulus of elasticity. If the modulus is finite, as in the case of all metals, the load-deflection cycle will be modified by the elastic deflection; but it may be expected that the general features of Fig. 1 will be preserved, since it is drawn for what can be regarded as a limiting case. Thus the reversed bending test provides what may prove to be a unique opportunity for observing temporary plastic instability under easily controlled conditions. In addition, the exact symmetry of the loci GAB and FED enables the role of strain-hardening, the Bauschinger effect, etc., to be assessed.

The Testing of a Mild Steel Plate

The theoretical considerations described above have prompted a new program of experiments. One test that serves to illustrate several important points will be described briefly. A complete report of the program will be made elsewhere when all the data are available.

The plate was cut from rolled steel $^1/_2$ in. thick. For testing, it was freely supported on a steel ring, inner radius 10 in., and loaded at the center through a 2-in. diameter hard steel punch. The test was carried out in a 120,000-lb. capacity universal testing machine fitted with continuously variable control of the displacement rate. The central deflection of the underside of the plate relative to the lower pattern of the machine was measured by means of a 0–1-in. dial gauge reading to 0.001 in.

The load-deflection curves for the first two cycles of loading are shown in Figs. 2 and 3. For the first cycle, Fig. 2, the plate was loaded monotonically to 30,000 lbs. This load was then removed, the plate turned over, and the same load applied in the opposite direction.* During both loadings, the deflection after each increment of load was recorded as soon as the time rate of defleetion had fallen to 0.001 in. per min. or less. For the second cycle, Fig. 3, the plate was loaded to 50,000 lbs. in each direction, a steady rate of displacement of approximately 0.04 in. per min. being maintained in each case. The zero deflection datum for Fig. 3 was fixed during the second half-cycle by observing the deflection reading at which the plate appeared to be most nearly flat, as judged with a straight edge.

Tensile control tests were performed on standard flat test pieces and the average tensile yield stress was found to be 32,000 lbs. per sq. in. On the basis of this yield stress, the theoretical load-deflection loci described in the previous section were computed for the known dimensions of the test plate. They are indicated by the dotted lines in Figs. 2 and 3.

Discussion

As has been anticipated, the finite elastic modulus of steel leads to substantial modification of the theoretical load-deflection cycle; however, the general features indicated by the analysis for rigid-plastic material can still be traced. Although the corners are considerably rounded off in a manner that recalls the buckling of elastic shells, quite definite instability can be observed in reverse bending. The trend of the two cycles shown suggests that the instability will be inhibited completely for cycles with lower maximum loads, but its presence at high loads is beyond question.

For the quadrants in which the plate was stable, the general shape of the experimental curve is well represented by the theory. This provides further confirmation that the dominant physical factors have been properly introduced in the theory.

In the first cycle, Fig. 2, the load at which the ordinate is crossed is of particular interest because it is less than expected. This is probably yet another example of the Bauschinger effect.[12]

* The plate was supported on a ring 20 in. in diameter internally. The plate itself was 21 in. in diameter, so it overlapped the edge of the ring by 1/2 in. When the plate was turned over after the first half cycle, it would be supported at its outer diameter. This would slightly increase the rate of deflection in the elastic range, but the ultimate carrying capacity would be unaffected. In any case, the plate would be supported again at 20 in. diameter as soon as the slope at the edges changed sign.

The discrepancy disappears after the higher load has been applied, Fig. 3. The Bauschinger effect may have been cancelled by further strain-hardening; on the other hand, it is likely that the plate was never truly flat at any stage following the application of the higher load. This would result in a slight increase of strength without the aid of changes in the properties of the steel.

It is remarkable that the large deflection imposed during the second cycle appears to produce an inconsequential increase in strength as the ordinate is crossed. The load carrying capacity remains very nearly the limit load obtained by neglecting changes in geometry (the apex of each locus). Thus this particular limit load, which is of little significance for monotonically increasing load, remains of continuing significance for reversed loading. It becomes a measure of the minimum load carrying capacity available during a phase of plastic instability.

References

[1] Maier-Leibnitz, H., *Die Bedeutung der Zähigkeit des Stahles für die Berechnung und Bemessung von Stahlhochbauwerken, insbesondere von statisch unbestimmten Konstructionen: Versuche, Ausdeutung und Anwendung der Ergebnisse*, Prelim. Pubn. Second Cong., Int. Assn. Bridge & Structural Eng., Berlin, p. 103, 1936.

[2] Baker, J. F., and Roderick, J. W., *Investigation into the Behavior of Welded Rigid Frame Structures*, Trans. Inst. Welding 1, pp. 206–226, 1938, and 3, pp. 83–92, 1940.

[3] Baker, J. F., and Roderick, J. W., *Tests on Full-Scale Portal Frames*, Proc. Instn. Civil Engineers, Vol. I (Part I) 71, 1952.

[4] Greenberg, H. J., and Prager, W., *Limit Design of Beams and Frames*, Proc. Amer. Soc. Civil Engrs., Vol. 77, Separate No. 59, 1951.

[5] Drucker, D. C., Prager, W., and Greenberg, H. J., *Extended Limit Design Theorems for Continuous Media*, Q. Appl. Math., Vol. 9, pp. 381–389, 1952.

[6] Hill, R., *On the State of Stress in a Plastic-Rigid Body at the Yield Point*, Phil. Mag. (7), Vol. 42, pp. 868–875, 1951.

[7] Haythornthwaite, R. M., *The Deflection of Plates in the Elastic-Plastic Range*, Proc. of the Second U. S. National Congress of Applied Mechanics, ASME, pp. 521–526, New York, N. Y., 1955.

[8] Cooper, R. M., and Shifrin, G. A., *An Experiment on Circular Plates in the Plastic Range*, Proc. of the Second U. S. National Congress of Applied Mechanics, ASME, pp. 527–534, New York, N. Y., 1955.

[9] Foulkes, J., and Onat, E. T., *Tests of the Behavior of Circular Plates under Transverse Load*, Brown University Technical Report, OOR-3172/3, May, 1955.

[10] Hopkins, H. G., and Prager, W., *The Load Carrying Capacities of Circular Plates*, Journal of the Mechanics and Physics of Solids, Vol. 2, pp. 1–3, 1953.

[11] Onat, E. T., and Haythornthwaite, R. M., *Load Carrying Capacity of Circular Plates at Large Deflection*, to be presented at the Diamond Jubilee Annual Meeting of the American Society of Mechanical Engineers, Chicago, Ill., November 13–18, 1955, and to appear in the Journal of Applied Mechanics as Paper No. 55-A-14.

[12] See, for instance, Nadai, A., *Theory of Flow and Fracture of Solids*, p. 28; McGraw-Hill, 1950.

On the Decay of a Flow Nonuniformity

William J. Guman

Department of Aeronautical Engineering, Rensselaer Polytechnic Institute, Troy, N.Y.

June 17, 1955

THE DECAY MECHANISM of a flow nonuniformity is a topic of considerable complexity, but a simple calculation is capable of yielding interesting information on the flow changes resulting from such decay.

Consider the case of a steady one-dimensional nonuniform compressible flow in a constant area duct with negligible wall friction. Let it be assumed that at each section the flow is nonuniform in its velocity but that the pressure and temperature are uniform.

Application of the three conservation equations to this case produces the relations

$$\frac{\bar{M}^2\left(1 + \frac{\gamma - 1}{2\eta}\bar{M}^2\right)}{(1 + \gamma\bar{M}^2)^2} = \text{const.} \qquad (1)$$

$$T\left(1 + \frac{\gamma - 1}{2\eta}\bar{M}^2\right) = \text{const.} \qquad (2)$$

$$p(1 + \gamma\bar{M}^2) = \text{const.} \qquad (3)$$

where by definition

$$\bar{M} = \bar{u}/\sqrt{\gamma g R T} \qquad \eta = (\bar{u})^2/\overline{u^2}$$

and with

$$\bar{u} = 1/m\int u\,dm \qquad \overline{u^2} = 1/m\int u^2\,dm$$

In these, u is the local instantaneous velocity, T and p the static temperature and pressure respectively, m the mass flow rate with $dm = \rho u dA$.

Inspection of relations (1), (2), and (3) shows that, under the stipulated conditions, the decay of a nonuniformity is accompanied in the subsonic domain by an increase of Mach Number and a decrease of pressure and, in the supersonic domain by a decrease of Mach Number and an increase of pressure and temperature. The static temperature in the subsonic domain may increase or decrease depending on the initial conditions. It can be seen that the parameters used vary in a similar manner as in the case of a Raleigh process with heat addition. The entropy rise reaches a maximum at a Mach Number of one.

For example, if at a section 1

$$\bar{M}_1 = 0.80 \qquad \eta_1 = 0.90$$

then at a section 2, if a complete decay occurred ($\eta_2 = 1.0$) one obtains

$$M_2 = 0.835 \qquad T_2/T_1 = 1.002 \qquad p_2/p_1 = 0.959$$

An Electrochemical Method of Visualizing the Boundary Layer*

Edward W. Geller

Assistant Professor of Aeronautical Engineering, University of Alabama, University, Ala.

July 16, 1955

A DIRECT METHOD of obtaining the velocity profile of the boundary layer is accomplished by marking a line element of fluid perpendicular to the surface over which the boundary layer is to be studied. As it moves downstream such a fluid element which has been made visible acquires the shape of the velocity profile, which can then be recorded directly on film by taking a photograph at the appropriate time.

The problem in applying this idea is to find a method to mark an element of the fluid. At the Institute for Technology at Stuttgart, Germany, Wortmann[1] accomplished this by using an

* This technique was developed by Edward W. Geller as research for a Master's thesis and under the helpful guidance of Dr. August Raspet, Aerophysics Department, Mississippi State College.

FIG. 1. Velocity profile is formed by the row of bubbles released at the wire. Wire diameter is 0.001 in. The free-stream velocity is approximately 1 1/2 ft. per sec.

electrochemical reaction along a small wire placed in water flow. This work prompted the development of a similar technique at the Aerophysics Department, Mississippi State College. A short description of the method follows.

The working fluid for this technique is necessarily water because of the chemical reaction used. A fine platinum wire is mounted perpendicular to the surface over which the velocity profile is to be obtained. The boundary layer along one wall of a water tunnel was used to demonstrate the technique. When a voltage pulse is applied between the wire and another electrode in contact with the water, a row of small bubbles is formed along the wire by the electrolysis which readily takes place if a small amount of salt has been added to the water. In this manner the necessary fluid element is marked. The row of bubbles is distorted into the shape of the velocity profile as it is swept downstream. By taking a microphotograph at the appropriate time a velocity profile such as shown in Fig. 1 is recorded.

REFERENCE

[1] Wortmann, F. X., *Ein Methode Zur Beobachtung Und Messung Von Wasserströmungen Mit Tellur*, Zeitschrift Für Angewandte Physik, Vol. 5, pp. 201–206, 1953.

Comment on "Calculation of Span Loading for Arbitrary Plan Forms"

Johannes Weissinger

Ordentlicher Professor, Institut fur Angewandte Mathematik, Technische Hochschule, Karlsruhe, Germany

June 28, 1955

A RECENT NOTE of de Young[1] begins with the statement, "The Weissinger method (for example, see NACA Rep. 921) is limited to use on wings with a quarter chord line of constant sweep" which is correct only for my preliminary report.[2] My full paper on the subject[3] contains on pp. 93–98 nearly the whole note of de Young (for instance integral equation, numerical method of solution, choice of m and M) and also some numerical tables for the aid of the computer.

REFERENCES

[1] De Young, John, *Calculation of Span Loading for Arbitrary Plan Forms*, Journal of the Aeronautical Sciences, Readers' Forum, Vol. 22, No. 3, pp. 208–210, March, 1955.

[2] Weissinger, J., *Über die Auftriebsverteilung von Pfeilflügeln*, F. B. No. 1553, Berlin-Adlershof, 1942. Also published as NACA TM 1120, March, 1947.

[3] Weissinger, J., *Über eine Erweiterung der Prandtlschen Theorie der tragenden Linie*, Mathematische Nachrichten, Vol. 2, Nos. 1 and 2, pp. 45–106, January-February, 1949.

Aerodynamic Derivatives for Both Steady and Nonsteady Motion of Slender Bodies

R. M. Wood and C. H. Murphy

Ballistic Research Laboratories, Aberdeen Proving Ground, Md.

July 1, 1955

THE APPLICATION of Munk's slender body theory to the calculation of aerodynamic coefficients describing steady motion (α, q constant) has been made by a number of authors.[1–3] Dorrance[4] has obtained slender body values of those coefficients associated with nonsteady angle of attack as a by-product of a linear analysis of the potential equation for nonsteady supersonic flow. The stability derivatives for the most general motion of slender bodies with arbitrary cross section have been calculated by Sacks.[5] This treatment is, however, quite complex. This note will present a simple derivation of all non-zero stability derivatives of a slender body of revolution.

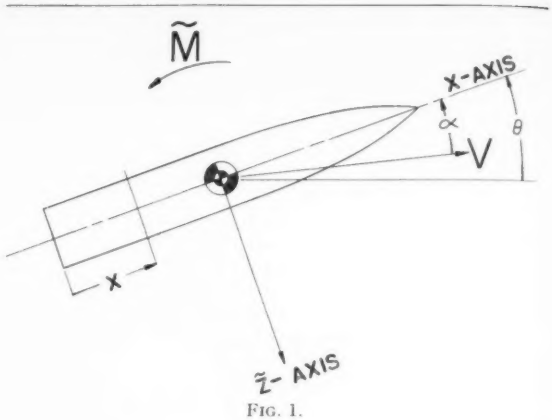

FIG. 1.

We shall make the usual assumption that the cross flow, u, at each cross section is a two-dimensional potential flow, and independent of both the axial flow and the cross flows at neighboring cross sections. For a circular cross section, the potential of the flow with respect to stationary air is that of a doublet. The kinetic energy per unit length can be found by the surface integral of a function of this potential,[6] and is of the form of $u^2/2$ multiplied by an "apparent mass," which in this case is precisely the mass of the displaced fluid. Hence,

$$\text{momentum of the fluid per unit length} = \rho A u \qquad (1)$$

where ρ = air density, A = cross-sectional area.

If we consider the momentum of the fluid at adjacent cross sections we see that it will depend on the local area and fluid velocity. Now the axial velocity, U, will move the fluid from one cross section to the next and hence from a region of higher momentum to one of lower momentum or vice versa. This local change in momentum gives rise to a differential force which can then be integrated to give the total force on the body. Since we are then actually interested in the location of the cross section of the fluid and its motion, we will interpret x to be its location with respect to the base. (See Fig. 1.)

We shall make use of a nonrolling right-handed coordinate system $X\tilde{Y}\tilde{Z}$ with X pointing forward along the missile's axis and the $\tilde{Y}$ axis initially in the horizontal plane, where a nonrolling coordinate system will mean one whose x-component of angular velocity is zero. (We make use of the tilde superscript to distinguish these axes from the standard aerodynamic missile-fixed axes. In the case of a spin-stabilized body of revolution, those axes would be spinning rapidly with respect to our nonrolling axes and, hence, with respect to air at infinity.)

As is shown in reference 7, the treatment of time derivatives of the dynamic variables—i.e., $\dot{\alpha}$, $\dot{q}$—is much more natural in nonrolling coordinates. Sacks[5] uses a missile-fixed system but specifically measures $\dot{\alpha}$ and $\dot{\beta}$ in a nonrolling system. However, he does measure $\dot{q}$ and r in the rolling system and therefore obtains a non-zero value of $C_{L_{pr}}$ and $C_{m_{pr}}$ for a body of revolution.

If we consider projections of the velocity vector and a fixed-direction vector on the $X\tilde{Z}$ plane, and with α and θ as defined in Fig. 1, then

$$u = -U\alpha + (x - x_{cg})q \qquad (2)$$

where $U = -dx/dt$ = axial component of the velocity of the missile, x_{cg} = the distance of the center of gravity from the base, x = the distance of fluid cross section from the base, $q = \dot{\theta}$. By Newton's Second Law and Eqs. (1) and (2) the force/unit length in the $\tilde{z}$ direction, $d\tilde{Z}/dx$, is the time rate of change of momentum per unit length. Hence, $d\tilde{Z}/dx = (d/dt)(\rho A u)$ and

$$\frac{dZ}{dx} = \rho U^2 \left\{ \alpha \frac{dA}{dx} - \frac{\dot{\alpha} A}{U} - \frac{q}{U}\left[A + (x - x_{cg})\frac{dA}{dx}\right] + \frac{\dot{q}}{U^2}(x - x_{cg})A \right\} \quad (3)$$

(Since we assume that the total velocity V is constant, its axial component is not necessarily constant. $\dot{U}$ is of second order, however, and is neglected.)

Integrating over the length of the missile, one obtains

$$\bar{Z} = \rho U^2 \left[-\alpha S_b - (\dot{\alpha}/U)vd^3 - (q/U)S_b x_{cg} + (\dot{q}/U^2)(x_c - x_{cg})vd^3 \right] \quad (4)$$

where

S_b = $-\int_0^L \left(\frac{dA}{dx}\right) dx$ (base area)

vd^3 = $\int_0^L A\, dx$ (v is dimensionless volume)

$(x_c - x_{cg})vd^3$ = $\int_0^L (x - x_{cg})A\, dx$ (x_c is the x-coordinate of the centroid)

d = diameter of the reference cross section

If we multiply Eq. (3) by $-(x - x_{cg})$ as is required by the indicated positive direction of $\bar{M}$ (see Fig. 1), and integrate, we can obtain the moment about the center of gravity:

$$\bar{M} = \rho U^2 \left\{ \alpha(vd^3 - x_{cg}S_b) + (\dot{\alpha}/U)\left[vd^3(x_c - x_{cg})\right] - (q/U)\left[x_{cg}^2 S_b + (x_c - x_{cg})vd^3\right] - (\dot{q}/U^2)k^2 vd^5 \right\} \quad (5)$$

where $vk^2d^5 = \int_0^L (x - x_{cg})^2 A\, dx$; ($k$ is the dimensionless transverse radius of gyration of the homogeneous model about its center of gravity).

An examination of Eqs. (4) and (5) shows that, under our assumptions, $\bar{Z}$ and $\bar{M}$ depend linearly on α, $\dot{\alpha}$, q, and $\dot{q}$. In order to obtain the relations for the various stability derivatives we first write the equations defining them.

$$\bar{Z} = (\rho V^2 S/2)\left[C_{\bar{Z}\alpha}\,\alpha + C_{\bar{Z}\dot{\alpha}}(\dot{\alpha}d/2V) + C_{\bar{Z}q}(qd/2V) + C_{\bar{Z}\dot{q}}(\dot{q}d^2/4V^2)\right] \quad (6)$$

$$\bar{M} = (\rho V^2 S d/2)\left[C_{\bar{m}\alpha}\,\alpha + C_{\bar{m}\dot{\alpha}}(\dot{\alpha}d/2V) + C_{\bar{m}q}(qd/2V) + C_{\bar{m}\dot{q}}(\dot{q}d^2/4V^2)\right] \quad (7)$$

where S = the reference area, V = the total velocity.

If Eqs. (4) and (5) are compared with Eqs. (6) and (7), the nondimensional $\hat{x} = x/d$ is introduced, and it is assumed that for small angles of attack and yaw U can be replaced by V, then the following relations are valid.

$$\left.\begin{array}{ll} C_{\bar{Z}\alpha} = -2S_b/S & C_{\bar{m}\alpha} = (-2S_b/S)\hat{x}_{cg} + 2v/(S/d^2) \\ C_{\bar{Z}\dot{\alpha}} = -4v/(S/d^2) & C_{\bar{m}\dot{\alpha}} = -4v/(S/d^2)(\hat{x}_{cg} - \hat{x}_c) \\ C_{\bar{Z}q} = -(4S_b/S)\hat{x}_{cg} & C_{\bar{m}q} = (-4S_b/S)\hat{x}_{cg}^2 + [4v/(S/d^2)](\hat{x}_{cg} - \hat{x}_c) \\ C_{\bar{Z}\dot{q}} = -[(8v)/(S/d^2)] \times (\hat{x}_{cg} - \hat{x}_c) & C_{\bar{m}\dot{q}} = -8vk^2/(S/d^2) \end{array}\right\} \quad (8)$$

The corresponding relations for Y and N can be found from symmetry considerations. It can easily be shown that

$$\left.\begin{array}{ll} C_{\bar{Y}\beta} = C_{\bar{Z}\alpha} & C_{\bar{n}\beta} = -C_{\bar{m}\alpha} \\ C_{\bar{Y}r} = -C_{\bar{Z}q} & C_{\bar{n}r} = C_{\bar{m}q} \\ C_{\bar{Y}\dot{\beta}} = C_{\bar{Z}\dot{\alpha}} & C_{\bar{n}\dot{\beta}} = -C_{\bar{m}\dot{\alpha}} \\ C_{\bar{Y}\dot{r}} = -C_{\bar{Z}\dot{q}} & C_{\bar{n}\dot{r}} = C_{\bar{m}\dot{q}} \end{array}\right\} \quad (9)$$

Since the derivation of Eqs. (9) was based on the assumption of nonviscous flow, this theory makes no prediction of Magnus force and moment derivatives. We see, however, that Munk's elementary theory based on the concept of apparent mass of each cross section will provide slender-body values of all 16 first-order nonMagnus aerodynamic coefficients.

Reference 8 includes a conversion of the above results to ballistic nomenclature for two types of motion and also gives an order-of-magnitude discussion showing that, for projectiles or missiles in air, the angular acceleration terms (arising from the $\dot{q}$ coefficients) are negligibly small and are usually neglected.

References

[1] Munk, M. M., *The Aerodynamic Forces on Airship Hulls*, NACA Report No. 184, 1924.

[2] Tsien, H. S., *Supersonic Flow Over an Inclined Body of Revolution*, Journal of the Aeronautical Sciences, Vol. 5, No. 12, pp. 480–484, October, 1938.

[3] Laitone, E. V., *Linearized Subsonic and Supersonic Flow About Inclined Slender Bodies of Revolution*, Journal of the Aeronautical Sciences, Vol. 14, No. 11, pp. 631–642, November, 1947.

[4] Dorrance, W. H., *Non-Steady Supersonic Flow About Pointed Bodies of Revolution*, Journal of the Aeronautical Sciences, Vol. 18, No. 8, pp. 505–512, August, 1951.

[5] Sacks, A. H., *Aerodynamic Forces, Moments, and Stability Derivatives for Slender Bodies of General Cross Section*, NACA TN 3283, November, 1954.

[6] Lamb, H., *Hydrodynamics*, 6th Ed.; Dover, New York, 1945.

[7] Murphy, C. H., and Nicolaides, J. D., *A Generalized Ballistic Force System*, Ballistic Research Laboratories Report No. 933, May, 1955.

[8] Wood, R. M., and Murphy, C. H., *Aerodynamic Derivatives for Both Steady and Non-Steady Motion of Slender Bodies*, Ballistic Research Laboratories Memorandum Report No. 880, April, 1955.

Comment on "Hypersonic Similarity and the Tangent-Cone Approximation for Unyawed Bodies of Revolution"[1]

V. Halbmillion
Naval Ordnance Laboratory, White Oak, Silver Spring, Md.

June 29, 1955

In reference 1, the authors have successfully attempted to combine the tangent-cone approximation with analytical solutions for the surface pressure on a slender cone in order to obtain an analytic representation of the pressure distribution on ogives. A justification for the use of the tangent-cone approximation was made by referring to a report by Halbmillion and Kulishek,[2] and the method was described as follows: each transverse section of the body is replaced by a section of the coaxial cone tangent to the body surface; the pressure is then assumed to be that which would exist on the cone at the same free-stream Mach Number, and the surface pressure on the cone is obtained by a numerical solution of the Taylor-Maccoll equations.

The implication that the method as described above was used and justified by Halbmillion and Kulishek is not quite correct. The curves of reference 2 originally presented by Halbmillion and McGraw in reference 3 are based on the following approximate law:

At a given Mach Number, the pressure ratio on the surface of an ogive at a given point is dependent only on the flow inclination—i.e., the tangent-cone angle—at that point. To a given local flow inclination for any ogive corresponds a single value of the pressure ratio. (The pressure ratio is defined as the ratio of the local static pressure to the static pressure in the undisturbed stream.)

Fowler and French[4] had made the additional assumption that this value of the pressure ratio is equal to the Taylor-Maccoll value for the tangent cone. But a check against experimental and analytical data which became available later indicated that this approximation is not fully satisfactory. Fortunately, the major discrepancies in pressure ratios occur at low angles of flow inclination and therefore do not affect substantially the wave drag calculations. Nevertheless, the writer felt that, for the purpose of predicting wave drag and pressure distributions, the Taylor-Maccoll values should be corrected. For example, at the junction between ogive and cylindrical body, where the tangent-cone angle is zero, the Taylor-Maccoll value of the pressure ratio is unity. Experimental data and computations by the method of characteristics indicate an average value of 0.83, and this was one of the key values selected in establishing the pressure ratio curves of reference 2. Other values of the pressure ratio for

various values of the Mach Number and the tangent-cone angle were similarly obtained statistically and the curves were interpolated and extrapolated by assuming functional variations similar to those derived from the Taylor-Maccoll theory.

Therefore, the curves presented in reference 2 should generally yield pressure distribution and drag values closer to the true values than those derived by Taylor-Maccoll theory without introducing experimental corrections. Since these curves appeared, a large number of experimental checks were made at Mach Numbers ranging from 1.5 to 5.0, and the results were always very satisfactory for engineering purposes. In order to secure greater accuracy, it is necessary to resort to the second order theory of Van Dyke or to the method of characteristics used with a sufficiently fine mesh. The amount and complexity of the work involved are then very considerably greater than for the case of the tangent-cone method used with the curves of reference 2.

References

[1] Probstein, Ronald, and Bray, Kenneth, Journal of the Aeronautical Sciences, Readers' Forum, Vol. 22, No. 1, p. 66, January, 1955.

[2] Halbmillion, V., and Kulishek, C. J., *Geometric and Aerodynamic Data on Ogives*, NavOrd Report 2239, U.S. Naval Ordnance Lab., White Oak, Md., January, 1952.

[3] Halbmillion, V., and McGraw, H., *A Method of Determining Approximately the Pressure Distribution on the Ogival Nose of Missiles*, NOLM 9816, U.S. Naval Ordnance Lab., White Oak, Md., 1949.

[4] Fowler, J. E., and French, D. M., *A Graphical Correlation Based on the Taylor-Maccoll Results of the Air Conditions Just Outside the Boundary-Layer of a Cone as Related to the Conditions of the Undisturbed Air*, Data Folder 85501, General Electric Company, Schenectady, N.Y., 1946.

Variation of Maximum Thermal Stress in Free Plates

P. J. Schneider

Research Associate, Department of Mechanical Engineering, University of Minnesota

April 11, 1955

Current development of high-temperature structures employing ductile and brittle materials has not only renewed past interest in the general theory of thermal stress and shock, but has stimulated, as well, a systematic study of several classes of structures with regard to susceptibility and full-range variation of maximum thermal stresses for a variety of typical operating conditions.

A technically important structure within the class of one-dimensional systems is the plane plate whose thickness 2δ is small relative to its face dimensions. In this case the plate temperature, t, varies only with x—the distance from and normal to the mid-plane of the plate. If, additionally, the plate is free of external constraints, then the nonzero normal components of thermal stress, σ_y and σ_z, away from the plate edges, are identical and equal to[1]

$$\frac{(1-\nu)}{E\beta}\,\sigma(X) = \frac{1}{2}\int_{-1}^{1} t(X)dX - t(X) + \frac{3}{2}X\int_{-1}^{1} t(X)X dX \tag{1}$$

Here ν, E, and β are the Poisson's ratio, modulus of elasticity, and coefficient of linear thermal expansion for the plate material (each considered uniform), and $X = x/\delta$ is the dimensionless distance from the plate mid-plane $X = 0$. If the temperature distribution, $t(x)$, or history, $t(x, \theta)$, is symmetric about $X = 0$, then the third term in Eq. (1) vanishes, and the local steady or instantaneous thermal stress is simply proportional to the difference between mean and local plate temperature, $(\bar{t} - t)$.

Six free plates are considered for a comparison of full-range resistance to maximum thermal stress alone. Each plate is of semithickness δ, and, in addition to assuming uniform mechanical properties ν, E, and β, the material for each is considered to be of uniform thermal conductivity k:

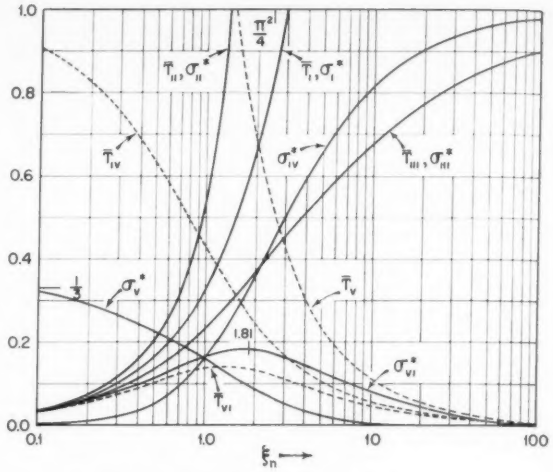

Fig. 1. Maximum thermal stress in free plates.

Case I. Solid plate; uniform unit-volume heat generation, q'''; faces $X = \pm 1$ at t_1.

Case II. Solid plate; positive linear heat generation, $q_1'''[1 + \alpha(t - t_1)]$, $\alpha \geq 0$; faces $X = \pm 1$ at t_1.

Case III. Solid plate; negative linear heat generation, $q_1'''[1 + \alpha(t - t_1)]$, $\alpha \leq 0$; faces $X = \pm 1$ at t_1.

Case IV. Porous plate; nongenerating; plate porosity P; fluid coolant of uniform thermal capacity C_f, thermal conductivity k_f, and specific mass velocity G $(-\infty \leq X \leq -1)$; coolant temperature t_{f_0} at $X = -\infty$; face $X = 1$ at t_1.

Case V. Porous plate; uniform heat generation; porosity and coolant as in *Case IV*.

Case VI. Solid plate; nuclear heating by nonuniform gamma-ray absorption, $q_1''\lambda \exp[-\lambda\delta(1 + X)]$; faces $X = \pm 1$ at t_1.

Solutions for the dimensionless temperature profile, $T_n(X)$, and mean plate temperature, $\bar{T}_n$, are given below,[2] along with the integrated dimensionless thermal-stress solutions, $\sigma_n^*(X)$, according to Eq. (1):

Case I.

$$T_I = \xi_I(1 - X^2) \tag{2}$$

$$\bar{T}_I = \xi_I/3 \tag{3}$$

$$\sigma_I^* = (\xi_I/2)\,[X^2 - (1/3)] \tag{4}$$

Case II.

$$T_{II} = \cos(\sqrt{\xi_{II}}X)/\cos(\sqrt{\xi_{II}}) - 1 \tag{5}$$

$$\bar{T}_{II} = (1/\sqrt{\xi_{II}})\tan(\sqrt{\xi_{II}}) - 1 \tag{6}$$

$$\sigma_{II}^* = (1/\sqrt{\xi_{II}})\tan(\sqrt{\xi_{II}}) - \cos(\sqrt{\xi_{II}}X)/\cos(\sqrt{\xi_{II}}) \tag{7}$$

Case III.

$$T_{III} = 1 - \cosh(i\sqrt{\xi_{III}}X)/\cosh(i\sqrt{\xi_{III}}) \tag{8}$$

$$\bar{T}_{III} = 1 - (1/i\sqrt{\xi_{III}})\tanh(i\sqrt{\xi_{III}}) \tag{9}$$

$$\sigma_{III}^* = \cosh(i\sqrt{\xi_{III}}X)/\cosh(i\sqrt{\xi_{III}}) - (1/i\sqrt{\xi_{III}})\tanh(i\sqrt{\xi_{III}}) \tag{10}$$

Case IV.

$$T_{IV} = \exp[-\xi_{IV}(1 - X)] \tag{11}$$

$$\bar{T}_{IV} = (1/2\xi_{IV})\,[1 - \exp(-2\xi_{IV})] \tag{12}$$

$$\sigma_{IV}^* = (3/2\xi_{IV})\,\{[1 + (1/\xi_{IV})]\exp(-2\xi_{IV}) + [1 - (1/\xi_{IV})]\}X - \exp[-\xi_{IV}(1 - X)] + (1/2\xi_{IV})\,[1 - \exp(-2\xi_{IV})] \tag{13}$$

Case V.

$$T_V = (1/\xi_V^2)\,\{1 - \exp[-\xi_V(1 - X)]\} + (1/\xi_V)(1 + X) \tag{14}$$

TABLE I

n	ξ_n	$\overline{T_n}$	$\sigma_{n\ \max}$ *
I	$q'''\alpha\delta^2/k$	$\alpha(\bar{t} - t_1)$	$\dfrac{(1-\nu)}{E\beta/\alpha}\ \sigma_{\delta_1 - \delta}$
II	$q_1'''\alpha\delta^2/k$	$\alpha(\bar{t} - t_1)$	$\dfrac{(1-\nu)}{E\beta/\alpha}\ \sigma_{\delta_1 - \delta}$
III	$q_1'''\alpha\delta^2/k$	$\lvert\alpha\rvert(\bar{t} - t_1)$	$\dfrac{(1-\nu)}{E\beta/\lvert\alpha\rvert}\ \sigma_{\delta_1 - \delta}$
IV	$GC_f\delta/(1-P)k$	$\dfrac{\bar{t} - t_{f_0}}{t_1 - t_{f_0}}$	$-\dfrac{(1-\nu)}{E\beta(t_1 - t_{f_0})}\ \sigma_\delta$
V	$GC_f\delta/(1-P)k$	$\dfrac{\bar{t} - t_{f_0}}{q'''\delta^2/k}$	$\dfrac{(1-\nu)}{E\beta q'''\delta^2/k}\ \sigma_\delta$
VI	$\lambda\delta$	$\dfrac{\bar{t} - t_1}{q_1''\delta/k}$	$\dfrac{1-\nu}{E\beta q_1''\delta/k}\ \sigma_{-\delta}$

$$T_V = (1/2\xi_V^2)\,[2\xi_V + \exp(-2\xi_V) - 1] + (1/\xi_V) \quad (15)$$

$$\sigma_V^* = (1/\xi_V^2)\exp[-\xi_V(1-X)] - (3/2\xi_V^2)\{[(1/\xi_V^2) + (1/\xi_V)]\exp(-2\xi_V) - [(1/\xi_V^2) - 1/\xi_V]\}X - (1/2\xi_V^3)\,[1 - \exp(-2\xi_V)] \quad (16)$$

Case VI.

$$T_{VI} = (1/\xi_{VI})\{1 - \exp[-\xi_{VI}(1+X)]\} - \{[1 - \exp(-2\xi_{VI})]/2\xi_{VI}\}(1+X) \quad (17)$$

$$\overline{T}_{VI} = (1/\xi_{VI}) - (1/2\xi_{VI})\,[(1/\xi_{VI}) + 1] \times [1 - \exp(-2\xi_{VI})] \quad (18)$$

$$\sigma_{VI}^* = (1/\xi_{VI})\exp[-\xi_{VI}(1+X)] + (3/2\xi_{VI}^3)\,[(1+\xi_{VI})\exp(-2\xi_{VI}) - (1-\xi_{VI})]X - \{[1 - \exp(-2\xi_{VI})]/2\xi_{VI}^2\} \quad (19)$$

A full-range composite plot of the mean plate temperature and corresponding thermal stress for each case is presented in Fig. 1 (see Table 1).

The well-known solution for *Case I* predicts a maximum tensile thermal stress at each face which varies directly with the heat-generation parameter ξ_I (α arbitrary). If, in *Case II*, the power production remains linear while the face temperatures are maintained at t_1, then the maximum thermal stress is again tensile at the faces, and σ_{II}^* increases indefinitely as ξ_{II} approaches $\pi^2/4$. For the opposite situation (negative α) in *Case III*, the maximum tensile stress at the plate faces approaches a limiting value of $\sigma_{III}^* = 1$. In all three of these cases, the thermal stress is independent of the face temperatures t_1. This suggests that the same stress solutions apply for any set of surface temperatures, or any combination of surface conductances and ambient temperatures.

For the porous plate in *Case IV*,† the maximum thermal stress appears at the downstream face $X = 1$. The stress is compressive, and if the downstream face is maintained at t_1, then σ_{IV}^* approaches 1 for large values of the coolant parameter ξ_{IV}. In this particular case, the stress is dependent on the difference in temperature between the downstream face of the plate and the upstream coolant. If the porous plate generates uniform heat, as in *Case V*, then the maximum thermal stress appears at the same face, but is tensile rather than compressive. The stress vanishes for large ξ_V ($X = 1$ not maintained at t_1), and approaches a limiting value of $\sigma_V^* = 1/3$ as ξ_V tends to zero. This latter limit exists because in this limiting condition the face temperatures increase indefinitely but approach an absolute difference of $q'''\delta^2/2k$.

The exponential heat source in *Case VI* produces a maximum tensile stress at the plate face $X = -1$. Limiting stresses are zero, and σ_{VI}^* reaches a peak of approximately 0.18 at a value of the absorption parameter $\xi_{VI} = 1.81$. Again the maximum stress is independent of boundary conditions.

Manson[3] has investigated thermal stresses in free power-producing plates whose thermal conductivity varies linearly with local plate temperature. In this case the solution contains the ratio of local to face conductivity as a second parameter.

† Use of Eq. (1) for porous structures assumes that the stress behavior of porous materials is substantially the same as for solid materials. Hence, without evidence to the contrary, the results of this extension must be considered to apply only to high-solidity plates

REFERENCES

[1] Timoshenko, S., *Theory of Elasticity*, McGraw-Hill Book Company, Inc., New York, 1934.

[2] Schneider, P. J., *Conduction Heat Transfer*, Addison-Wesley, Cambridge, Massachusetts, 1955.

[3] Manson, S. V., *Temperatures, Thermal Stress, and Shock in Heat-Generating Plates of Constant Conductivity and of Conductivity That Varies Linearly With Temperature*, NACA TN 2988, July, 1953.

Rapid Estimation of the Elastic-Plastic Euler Buckling Loads for Simply Supported Tapered Columns Under Varying Axial Loading

Bertram Klein

North American Aviation, Inc., Aerophysics Department, Downey, Calif.

August 3, 1955

AN IMPORTANT STRUCTURAL PROBLEM not given sufficient attention in the literature is the buckling of tapered columns attached to sheet with consequent variable axial loading. Various methods exist for the calculation of these buckling loads.[1-9] The approximate method presented here is direct, very rapid, yet sufficiently accurate and particularly suited for design. The column and its loading are shown in Fig. 1. The assumed shear flow need not be constant in magnitude.

The method concerns itself with the (P/E_tI) diagram of the column. This quantity may be looked upon as representing the buckling intensity at any section. In regions where (P/E_tI) is relatively high, deflections tend to be higher, and consequently these values should carry more weight in determining buckling. However, deflections tend to be higher around the middle of the column because of its end supports. Therefore it is suggested that the (P/E_tI) diagram be weighted according to some function which damps out at the end regions of the column. The buckling condition then becomes

$$\int_0^L \frac{P}{E_tI} f(x)dx \Big/ \int_0^L f(x)dx = \frac{\pi^2}{L^2} \quad (1)$$

In general, the function, $f(x)$, depends on the actual shape of the (P/E_tI) diagram. However, it has been found that taking $f(x) \approx \sin(\pi x/L)$ gives good results in most practical cases.

Now let it be assumed that (P/E_tI) can be represented by the power series

$$a + bu + cu^2 + du^3 + eu^4 + \ldots \quad (2)$$

where u is the nondimensional variable, x/L. Substitution of this series and the sin function into Eq. (1) and integrating yields

$$a + 0.5b + 0.297c + 0.197d + 0.139e + \ldots = \pi^2/L^2 \quad (3)$$

The left-hand side of Eq. (3) may be approximately but conveniently replaced by the expression

$$\tfrac{1}{4}\,[(P/E_tI)_{u=0.2} + 2(P/E_tI)_{u=0.5} + (P/E_tI)_{u=0.8}] = a + 0.5b + 0.295c + 0.197d + 0.136e \ldots \quad (4)$$

As mentioned previously, higher values of (P/E_tI) should count more in determining buckling. Since in general the value $(P \div E_tI)_{u=0.2} \neq (P/E_tI)_{u=0.8}$, the larger one of these two should be weighted more than the smaller one. Let u be chosen so that

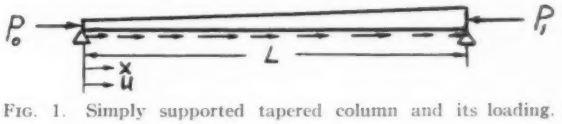

FIG. 1. Simply supported tapered column and its loading.

$(P/E_tI)_{u=0.2} \geq (P/E_tI)_{u=0.8}$. Then the proposed buckling condition takes the final form

$$\frac{1}{4}\left[1.25\left(\frac{P}{E_tI}\right)_{u=0.2} + 2\left(\frac{P}{E_tI}\right)_{u=0.5} + 0.75\left(\frac{P}{E_tI}\right)_{u=0.8}\right] = \frac{\pi^2}{L^2} \tag{5}$$

When the stress at a section is plastic, it is necessary to use the corresponding tangent modulus in Eq. (5). The procedure then becomes iterative in general. If the column has one or more steps, it may be necessary to revert back to Eq. (1).

To illustrate the ease and rapidity of the method, several problems will be worked. Comparison with known correct solutions will indicate the accuracy of the results. For the sake of simplicity all stresses will be assumed to remain elastic—i.e., $E_t = E$.

(1) $P = P_0(1 + u)$, $I = I_0(1 + u^2)$. Eq. (5) becomes

$$\frac{1}{4}\frac{P_0}{EI_0}\left[1.25\left(\frac{1.2}{1.04}\right) + 2\left(\frac{1.5}{1.25}\right) + 0.75\left(\frac{1.8}{1.64}\right)\right] = \frac{\pi^2}{L^2} \tag{6}$$

and
$$P_0 = (8.46/L^2)EI_0 \tag{7}$$

A solution obtained by another method agrees exactly with this result.

(2) $P = (1 - u)P_0$, $I = I$. Eq. (5) becomes

$$\frac{1}{4}\frac{P_0}{EI}\left[1.25\left(\frac{0.8}{1}\right) + 2\left(\frac{0.5}{1}\right) + 0.75\left(\frac{0.2}{1}\right)\right] = \frac{\pi^2}{L^2} \tag{8}$$

and
$$P_0 = (18.4/L^2)EI \tag{9}$$

A more exact solution was found to be $P_0 = (19.0/L^2)\,EI$, making the present answer in error on the safe side by about 3 per cent.

(3) $P = P_0$, $I = I_{1/2}(0.1 + 1.8u)$ for $0 \leq u \leq 1/2$, $I = I_{1/2}(1.9 - 1.8u)$ for $1/2 \leq u \leq 1$. Substitution into Eq. (5) yields

$$\frac{1}{4}\frac{P_0}{EI_{1/2}}\left[\left(\frac{1.25}{0.46}\right) + \left(\frac{2}{1}\right) + \left(\frac{0.75}{0.46}\right)\right] = \frac{\pi^2}{L^2} \tag{10}$$

$$P_0 = 6.23(EI_{1/2}/L^2) \tag{11}$$

This result agrees within less than 4 per cent on the safe side of the exact solution.[1]

(4) $P = P$, $I = uI_1$. Eq. (5) may be written

$$\frac{1}{4}\frac{P}{EI_1}[(1.25)\,(5) + 2(2) + 0.75(1.25)] = \frac{\pi^2}{L^2} \tag{12}$$

$$P = 3.53(EI_1/L^2) \tag{13}$$

The error here is less than 1 per cent since the correct solution should be

$$P = 3.50(EI_1/L^2) \tag{14}$$

Sometimes the (P/EI) diagram exhibits a maximum value around $u = (1/2)$. In such cases $f(x) = \sin^2 \pi u$ gives good results. By reasoning similar to before, the following equation is derived

$$\frac{1}{7}\left[\left(\frac{P}{EI}\right)_{u=0.2} + 5\left(\frac{P}{EI}\right)_{u=0.5} + \left(\frac{P}{EI}\right)_{u=0.8}\right] = \frac{\pi^2}{L^2} \tag{15}$$

For example, let $P/EI \propto \sin \pi u$. Then

$$(P/EI)_{1/2}\,(1/7)\,[0.588 + 5 + 0.588] = \pi^2/L^2 \tag{16}$$

and
$$P_{1/2} = (11.2/L^2)\,(EI)_{1/2} \tag{17}$$

The exact solution is

$$P_{1/2} = (11.4/L^2)\,(EI)_{1/2}$$

which makes the above approximate answer in error by less than 2 per cent on the safe side.

It should be noticed that in the derivation of Eq. (5), the damping function does not correspond exactly to the sine function. In fact, the function required to give Eq. (5) is close to $(1.5 - u) \sin \pi u$. This function will prove of use in problems involving columns with stepped taper. For example, consider the following case: $P = P$, $I = (1/2)I_1$ for $0 \leq u \leq 0.5$, and $I = I_1$ for $0.5 \leq u \leq 1$. Substitute $(1.5-u) \sin \pi u$ for $f(u)$ and the above values of I into Eq. (1) to obtain

$$\frac{\frac{P}{EI_1}\left[\int_0^{0.5}\frac{(1.5-u)\sin \pi u\,du}{1/2} + \int_{0.5}^{1}(1.5-u)\sin \pi u\,du\right]}{\int_0^1 (1.5-u)\sin \pi u\,du} = \frac{\pi^2}{L^2} \tag{18}$$

Evaluation of the integrals gives

$$\frac{P}{EI_1}\left[\frac{2\left(\frac{1.5}{\pi} - \frac{1}{\pi^2}\right) + \left(\frac{0.5}{\pi} + \frac{1}{\pi^2}\right)}{\left(\frac{3}{\pi} - \frac{1}{\pi}\right)}\right] = \frac{\pi^2}{L^2} \tag{19}$$

$$P = 6.21EI_1/L^2 \tag{20}$$

The correct solution is

$$P = 6.40EI_1/L^2$$

making the approximate answer in error by less than 3 per cent on the safe side.

References

[1] Timoshenko, S., *Theory of Elastic Stability*, Chapter II, Sections 25, 26; McGraw-Hill Book Co., Inc., New York, 1936.

[2] Newmark, N. M., *Numerical Procedure for Computing Deflections, Moments, and Buckling Loads*, Trans. ASCE, Vol. 108, p. 1161, 1943.

[3] Salvadori, M. G., *Numerical Computation of Buckling Loads by Finite Differences*, Trans. ASCE, Vol. 116, 1951.

[4] Miesse, C. C., *Determination of the Buckling Load for Columns of Variable Stiffness*, J. of Appl. Mechs., Vol. 16, pp. 406–410, December, 1949.

[5] Rasmussen, B. H., *Stability of Columns with Variable Moment of Inertia*, Frandsen Anniv. Vol., Lab. Bygn. Tekn. Medd., No. 1, pp. 100–110, 1950.

[6] Thomson, W. T., *Critical Load of Columns of Varying Cross Section*, J. of Appl. Mechs., Vol. 18, pp. 119–120, March, 1951.

[7] Bültman, W. *Buckling of a Straight Column with Variable Compressive Load and Elastic Clamping*, Bautechnik (Stahlbau), Vol. 28, pp. 50–52, April, 1951.

[8] Duncan, W. J., *Multiply-Loaded and Continuously Loaded Struts*, Engineering, Vol. 174, pp. 180–182, 202–203, August, 1952.

[9] Reinitzhuber, F., *Approximate Formulas for the Buckling of Struts with Linearly Variable Axial Loading*, Publ. Int. Bridge Struct. Engrg., Vol. 13, pp. 309–319, 1953.

Index to Volume 22

Journal of the Aeronautical Sciences

Numbers 1–12, January–December, 1955

No. 1, January, 1955, pages 1–72
No. 2, February, 1955, pages 73–144
No. 3, March, 1955, pages 145–216
No. 4, April, 1955, pages 217–288
No. 5, May, 1955, pages 289–348
No. 6, June, 1955, pages 349–444
No. 7, July, 1955, pages 445–516
No. 8, August, 1955, pages 517–588
No. 9, September, 1955, pages 589–660
No. 10, October, 1955, pages 661–732
No. 11, November, 1955, pages 733–804
No. 12, December, 1955, pages 805–884

The material has been indexed under a subject heading and by author.

*—An asterisk following an item identifies it as having appeared in the Readers' Forum section.

ABRAMSON, H. NORMAN, HARRY A. WILLIAMS, AND BRUCE G. WOOLPERT. An Investigation of the Bending of Angle Beams in the Plastic Range 818

ABZUG, MALCOLM, J. Estimation of the Lift and Moment Parameters of Leading-Edge Flaps* 655

Aerodynamics—

Acoustics in Relation to Aerodynamics, E. G. Richardson. 775

Aerodynamics of Blasts—Diffraction of Blast Around Finite Corners, H. F. Ludloff and M. B. Friedman 27

Curved Shocks in Pseudostationary Flows, Ryuma Kawamura and Hakuro Oguchi* 210

Design Charts for Transient Temperature Distribution Resulting from Aerodynamic Heating at Supersonic Speeds, Joseph Kaye and Victor C. M. Yeh 755

Difference Solution of Shock Diffraction Problem, H. F. Ludloff and M. B. Friedman* 139

Gas Dynamic Behavior of Real Gases, L. N. Tao 763

A New Method of Solution of Equation of Compressible Flow, Ezio Betti* 516

Note on Velocity Fluctuations in Equilibrium Turbulent Shear Flow Along Solid Boundaries, Heinrich B. Helmbold* 513

The Obukhoff Spectrum of Homogeneous Isotropic Turbulence, Knox Millsaps* 511

On the Determination of Local Heat-Transfer Coefficients for Bodies with Pressure Gradient in Supersonic Flow, Irving Korobkin* 283

On the Flow Behind an Attached Curved Shock, S. I. Pai* 657

On a Stress Tensor for Turbulence, Willis H. Braun* 510

Remarks on the Velocity of Sound, Max M. Munk* 795

Second-Order Pressure Law for Two-Dimensional Compressible Flow, Wallace D. Hayes* 284

A Similarity Rule for the Interaction Between a Conical Field and a Plane Shock, Y. H. Kuo* 504

The Stability of Vortex Streets with Consideration of the Spread of Vorticity of the Individual Vortices, Ulrich Domm 750

Summary of Recent GALCIT Hypersonic Experimental Investigations, Henry T. Nagamatsu 165

Wedge Pressure Coefficients in Transonic Flow by Hydraulic Analogy, Richard G. Fleddermann and Robert T. Stancil* 271

Aerodynamics, Bodies—

Application of Kelly's Theory to Cone-Cylinder-Frustum Bodies of Revolution, Robert E. Lavender* 654

Comment on "Hypersonic Similarity and the Tangent-Cone Approximation for Unyawed Bodies of Revolution," V. Halbmillion* 871

Erratum—"Wing-Body Interference at Subsonic and Supersonic Speeds—Survey and New Developments," H. S. Bluston and John B. Large* 208

The Generalized Shock-Expansion Method and Its Application to Bodies Traveling at High Supersonic Air Speeds, A. J. Eggers, Jr., Raymond C. Savin, and Clarence A. Syvertson 231

Hypersonic Similarity and the Tangent-Cone Approximation for Unyawed Bodies of Revolution, Ronald F. Probstein and Kenneth N. C. Bray* 66

Normal Force and Center of Pressure on Right Circular Cylinders, J. Leith Potter, William D. Murphree, and Norman M. Shapiro* 214

On the Wake and Drag of Bluff Bodies, Anatol Roshko ... 124

Slender Bodies of Low Wave Drag, R. N. Haskell and G. C. Grogan* 138

The Unsteady Forces on a Circular Cylinder in the Presence of Two Symmetrically Disposed Line Vortices, S. Sherman Edwards* 72

Aerodynamics, Boundary Layer & Skin Friction—

The Application of Finite Difference Methods to Boundary-Layer Type Flows, W. T. Rouleau and J. F. Osterle 249

Approximate Solutions of the Incompressible Laminar Boundary-Layer Equations for a Flat Plate in a Shear Flow, K. T. Yen* 728

The Behavior of the Boundary Layer in the Region of Transition from Laminar to Turbulent Flow, Jerome Persh* 443

Boundary-Layer Stabilization by Surface Cooling in Supersonic Flow, E. R. Van Driest and J. Christopher Boison* 70

Engineering Relations for Friction and Heat Transfer to Surfaces in High Velocity Flow, E. R. G. Eckert* 585

Errata—"Simplified Analysis of Turbulent Boundary-Layer Development Along Cylindrical Surfaces with Variable Free-Stream Mach Number," Hans U. Eckert* 70

Experimental Investigation of Turbulent Boundary Layers in Hypersonic Flow, R. Kenneth Lobb, Eva M. Winkler, and Jerome Persh 1

Forced Convection Through a Laminar Boundary Layer over an Arbitrary Surface with an Arbitrary Temperature Variation, Myron Tribus and John Klein* 62

Aerodynamics, Boundary Layer & Skin Friction (*Continued*)
Frictional Heating of Nonisothermal Walls, Myron Tribus and James E. Mahlmeister* ... 726
Further Comments on "The Effect of Boundary Layer on Sonic Flow Through an Abrupt Cross-Sectional Area Change," Robert S. Wick* ... 135
Further Comments on "Note on Boundary-Layer Transition in Supersonic Flow," A. H. Lange and R. E. Lee* ... 282
Heat Conducting Bodies in Boundary-Layer Flow, Salomon Levy* ... 440
Laminar Compressible Boundary Layer Along a Curved Insulated Surface, Arlo F. Johnson and I. Flügge-Lotz ... 445
Laminar Heat Transfer in Two-Dimensional Subsonic Effusors, Paul A. Libby and Marian Visich, Jr ... 425
Measurements of the Effect of Two-Dimensional and Three-Dimensional Roughness Elements on Boundary-Layer Transition, P. S. Klebanoff, G. B. Schubauer, and K. D. Tidstrom* ... 803
Note on the Compressible Laminar Boundary Layer with Heat Transfer and Pressure Gradient, Eli Reshotko and Clarence B. Cohen* ... 584
Note on a Formula of H. W. Emmons, J. A. Steketee* ... 578
On Compressible Laminar Boundary-Layer Characteristics in a Pressure Gradient with Heat Transfer, Morris Morduchow* ... 444
On Determining Turbulent Boundary-Layer Separation in Incompressible and Compressible Flow, H. Schuh* ... 343
On Distributed Roughness as a Means of Fixing Transition at High Supersonic Speeds, William B. Fallis* ... 339
On the Effect of Reynolds Number upon the Peak Pressure-Rise Coefficient Associated with the Separation of a Turbulent Boundary Layer in Supersonic Flow, E. S. Love* ... 345
On the Laminar Compressible Boundary Layer over a Flat Plate with Suction or Injection, H. G. Lew and J. B. Fanucci ... 589
On the Stability of the Laminar Boundary Layer in a Compressible Fluid, D. W. Dunn and C. C. Lin ... 455
Prediction of Shock-Induced Turbulent Boundary-Layer Separation, Artur Mager* ... 201
A Provisional Analysis of Turbulent Boundary Layers with Injection, Joseph H. Clarke, Hans R. Menkes, and Paul A. Libby ... 255
A Remark on "A Simple Laminar Boundary Layer with Secondary Flow," M. Z. v. Krzywoblocki* ... 582
Reversal of Skin-Friction and Heat-Transfer Trends in High-Speed Laminar Flows, George M. Low* ... 721
Separation of a Supersonic Turbulent Boundary Layer, S. M. Bogdonoff and C. E. Kepler ... 414
Similar Solutions of Compressible Boundary-Layer Equations, Ting-Yi Li and Henry T. Nagamatsu ... 607
Similar Solutions of Turbulent Boundary Layers, J. C. Rotta* ... 215
A Simple Laminar Boundary Layer with Secondary Flow, Henk G. Loos ... 35
Stability of Compressible Laminar Boundary Layer with Internal Heat Sources or Sinks, George M. Low ... 329
Summary of Existing Cone Temperature Recovery Factor Data Obtained in Continuous-Flow Wind Tunnels Plus Additional Data, Leslie M. Mack* ... 212
Turbulent Boundary Layers on Nozzle Liners, R. E. Meyer* ... 572

Aerodynamics, Internal Flow—
An Analytic Method for the Design of Two-Dimensional Asymmetric Nozzles, Hans Peter Liepman ... 701
An Approximation to the Lift of a Two-Dimensional Cascade of Airfoils, B. W. McCormick* ... 730
Comparison of Mixing Processes in Subsonic Jet Pumps, Heinrich B. Helmbold* ... 435
The Correction of Flexible Plate Supersonic Nozzle Contours by Influence Methods, William N. MacDermott ... 289
Design of Two-Dimensional Continuous-Curvature Supersonic Nozzles, James C. Sivells ... 685
Free Streamline Analysis for Slotted Two-Dimensional Supersonic Minimum-Length Nozzles, Robert Wesley Truitt* ... 658
On a Class of Two-Dimensional Channel Flows with a Straight Sonic Line, A. J. A. Morgan* ... 573
On the Decay of a Flow Nonuniformity, William J. Guman* ... 869
On the Design of Two-Dimensional Supersonic Nozzles by the Method of Characteristics, Bernard Chaix and Peter Henrici* ... 140
On the Intermittency of a Two-Dimensional Jet, William H. Hannum and Wayland Griffith* ... 202
On Some Solutions of the Hodograph Equation Which Yield Transonic Flows Through a Laval Nozzle, F. Edward Ehlers ... 107
Remark on Supersonic Nozzle Design, R. E. Meyer* ... 587
Simultaneous Measurements of Velocity and Temperature Profiles for Adiabatic Supersonic Flow of Air in a Tube, Joseph Kaye, George A. Brown, Julius C. Westmoreland, and Edward F. Kurtz, Jr.* ... 575
Simultaneous Turbulent and Laminar Flow in Ducts with Noncircular Cross Sections, E. R. G. Eckert and T. F. Irvine, Jr.* ... 65
The Static Pressure Variation in Compressible Free Jets, Walter R. Warren, Jr.* ... 205
Supersonic Diffuser Instability, Charles Lee Dailey ... 733
Temperature Field in a Laminar Incompressible Round Jet and in Convergent and Divergent Round Nozzle, Dragutin Stojanović* ... 216
Theoretical and Experimental Pressure Recovery of Sweptback Normal Shock Inlets, George D. Dickie, Jr ... 189

Aerodynamics, Turbines & Compressors—
An Approximate Relationship Between Small Radius Ratio Turbine Passage Geometry and Radial Pressure Variation, J. P. Fraser* ... 282
Conditions for the Appearance of Shock Waves in Steady Flows, Raymond Marchal* ... 275
A Note on "A Study of Surge in Compressors and Jet Engines," W. C. Randels* ... 660
Optimum Stage for Axial Flow Turbines, N. Van Le* ... 503
Propagation of Stall in a Compressor Blade Row, Frank E. Marble ... 541
Secondary Flows in Cascades of Twisted Blades, Fredric F. Ehrich ... 51
A Study of Surge in Compressors and Jet Engines, Carl E. Pearson ... 10
Surge Behavior in a Three-Stage Compressor, Carl E. Pearson* ... 799
Unsteady Aerodynamic Reactions on Airfoils in Cascade, F. Sisto ... 297
The Unsteady Forces Due to Viscous Wakes in Turbomachines, Nelson H. Kemp and W. R. Sears ... 478

Aerodynamics, Wings & Airfoils—
Aerodynamics of a Rectangular Plate with Vortex Separation in Supersonic Flow, H. K. Cheng ... 217
Calculation of Span Loading for Arbitrary Plan Forms, John DeYoung* ... 208
Comment on "Calculation of Span Loading for Arbitrary Plan Forms," Johannes Weissinger* ... 870
Comment on "Wedge Pressure Coefficients in Transonic Flow by Hydraulic Analogy," H. J. Bömelburg* ... 731
A Critique of Shock-Expansion Theory, J. J. Mahony ... 673
The Effect of Thickness on Airfoils with Constant Vertical Acceleration at Supersonic Speeds, John C. Martin and Nathan Gerber ... 179

Aerodynamics, Wings & Airfoils (*Continued*)
Equations for the Chordwise Center of Pressure for the Basic Twist Distributions on Triangular Wings Having Supersonic Leading and Trailing Edges, R. N. Haskell, J. J. Hosek, and W. S. Johnson, Jr.* 274
Equations for Loading on Triangular Wings Having Subsonic Leading Edges Due to Various Basic Antisymmetric Twist Distributions, R. N. Haskell and W. S. Johnson, Jr.* 278
Errata—Nonlinear Lift and Vortex Separation, H. K. Cheng* 660
Experimental Investigation of Influence of Edge Shape on the Aerodynamic Characteristics of Low Aspect Ratio Wings at Low Speeds, G. E. Bartlett and R. J. Vidal 517
The Flat Plate with an Angle of Attack in a Choked Wind Tunnel, K. Gottfried Guderley 844
The Lift and Moment on a Ring Concentric to a Cylindrical Body in Supersonic Flow, F. Edward Ehlers 239
The Lift of a Blowing Wing in a Parallel Stream, Heinrich B. Helmbold* 341
Lifting Pressure on Delta Wings with Subsonic Leading Edges, Symmetrical Plan Form, and Discontinuous Slope, Paul G. Kafka* 725
Limitations of Linear Theory in Predicting the Pressure Distribution on Triangular Wings, Elliott D. Katzen* 514
On the Motion of a Flat Plate at High Speed in a Viscous Compressible Fluid, II—Steady Motion, K. Stewartson 303
On the Normal Force Produced by Multifinned Tail Assemblies in Supersonic Flow, J. Leith Potter, William D. Murphree, and Norman M. Shapiro* 511
A Rigorous Method for Finding the Lift of a Certain Class of Airfoils and Remarks on the Meaning of Schrenk's Approximate Rule, Otto Laporte and Hideo Yoshihara 787
The Second-Order Thin Airfoil Theory for Compressible Flow, Isao Imai* 270
Simple Shear Flow Past a Flat Plate in a Compressible Viscous Fluid, Ting-Yi Li* 724
Simple Shear Flow Past a Flat Plate in an Incompressible Fluid of Small Viscosity, Ting-Yi Li* 651
Spanwise Variation in the Pitching-Moment Coefficient and the Center of Pressure Due to Various Basic Twist Distributions on Triangular Wings Having Supersonic Leading and Trailing Edges, Julian H. Kainer 598
The Supersonic Conical Wing of Minimum Drag, S. H. Tsien 805
On Supersonic Flow Past a Finite Wedge at the Crocco Mach Number, Kō Tamada and Yoshio Shibaoka 261
Tests of a Fairing to Reduce the Drag of a Supersonic Swept-Wing Root, W. F. Hilton 173
Transonic Lift over the Front Surface of a Two-Dimensional Diamond Airfoil, Robert Wesley Truitt* 342

Aeroelasticity—
Aerodynamic Coefficients for Cambering and Aileron Motions, E. F. Tyler* 340
Aerodynamic Flutter Derivatives for a Flexible Wing with Supersonic and Subsonic Edges, Samuel Pines, John Dugundji, and Joseph Neuringer 693
An Application of Variation Methods to the Computation of the Deformation of a Cantilever Plate Subjected to Nonuniform and Aeroelastically Induced Loads, Eugene E. Covert 555
Computation of Vibration Modes and Frequencies on SEAC, William F. Cahill and Samuel Levy 837
Determining the Mode Shapes and Frequencies of Low Aspect Ratio Multispar Wings, Marvin L. Stein* 137
The Difference Property of the Kernel of the Unsteady Lifting Surface Theory, H. G. Kuessner 227
Effect of Rotatory Inertia and Shear on Maximum Strain in Cantilever Impact Excitation, Marcel K. Newman 313
Extension of the Statistical Approach to Buffeting and Gust Response of Wings of Finite Span, H. W. Liepmann 197
A Fraction Series Solution for Characteristic Values Useful in Some Problems of Airplane Dynamics, E. L. Leppert, Jr 326
Iteration in Semidefinite Eigenvalue Problems, B. M. Fraeys de Veubeke 710
Matrix Method of Coupling Shear Flexibility and Rotatory Inertia in Bending Vibration, Marvin Stern* 276
Methods for Computing Supersonic Aerodynamic Flutter Coefficients for Two-Dimensional Flow, Ernest C. Kennedy 310
On Approximate Solutions for the Compressible Flow Around Oscillating Thin Wings, Marten Landahl, Holt Ashley, and Erik Mollo-Christensen* 581
Remarks on "An Exact Solution for Two-Dimensional Linear Panel Flutter at Supersonic Speeds," S. F. Shen* 656
A Simplified Expression for the Dihedral Effect of a Flexible Wing, W. P. Rodden* 579
Some Applications of Generalized Harmonic Analysis to Gust Loads on Airplanes, Harry Press and John C. Houbolt 17
Some Considerations on the Air Forces on a Wing Oscillating Between Two Walls for Subsonic Compressible Flow, Donald S. Woolston and Harry L. Runyan 41
Some Series Developments in Unsteady Aerodynamics, Peter F. Jordan* 722
Some Static Aeroelastic Design Considerations Relating to Flap-Type Control Surfaces, Martin Zlotnick* 580
Transient Stresses in Airfoils Under Blast Loading, H. F. Ludloff and F. J. Marshall* 508

Amer, Kenneth B., and H. Hirsch. Effect of High Advancing-Tip Mach Number on Helicopter Blade Flapping* 505
Ashley, Holt, Marten Landahl, and Erik Mollo-Christensen. On Approximate Solutions for the Compressible Flow Around Oscillating Thin Wings* 581

Barnes, Frank A., Robert C. Seamans, Jr., Theodore B. Garber, and Vincent W. Howard. Recent Developments in Aircraft Control 145
Barrett, Anthony J. Beam Strength and Curvature Under Combined Tension and Bending in the Plastic Range* 71
Bartlett, G. E., and R. J. Vidal. Experimental Investigation of Influence of Edge Shape on the Aerodynamic Characteristics of Low Aspect Ratio Wings at Low Speeds 517
Betti, Ezio. A New Method of Solution of Equation of Compressible Flow* 516
Bijlaard, P. P. On the Buckling of Stringer Panels, Including Forced Crippling 491
Birman, Joan. The Effects of Changes in Aircraft Weight on Flight Equilibrium* 61
Bluston, H. S., and John B. Large. Erratum—"Wing-Body Interference at Subsonic and Supersonic Speeds—Survey and New Developments"* 208
Bogdonoff, S. M., and C. E. Kepler. Separation of a Supersonic Turbulent Boundary Layer 414
Boison, J. Christopher, and E. R. Van Driest. Boundary-Layer Stabilization by Surface Cooling in Supersonic Flow* 70
Boley, Sara R. A Procedure for the Approximate Analysis of Buckled Plates* 337
Bömelburg, H. J. Comment on "Wedge Pressure Coefficients in Transonic Flow by Hydraulic Analogy"* 731

BRAUN, WILLIS H. On a Stress Tensor for Turbulence*.... 510
BRAY, KENNETH N. C., AND RONALD F. PROBSTEIN. Hypersonic Similarity and the Tangent-Cone Approximation for Unyawed Bodies of Revolution*..... 66
BROWN, GEORGE A., JOSEPH KAYE, JULIUS C. WESTMORELAND, AND EDWARD F. KURTZ, JR. Simultaneous Measurements of Velocity and Temperature Profiles for Adiabatic Supersonic Flow of Air in a Tube*..... 575
BYRUM, BARNEY L., AND E. RUSSELL GRADY. General Air-Frame Dynamics of a Guided Missile..... 534

CAHILL, WILLIAM F., AND SAMUEL LEVY. Computation of Vibration Modes and Frequencies on SEAC..... 837
CAMPBELL, GEORGE S. A Simplified Treatment of Partial Fractions for Dynamic-Response Calculations*..... 437
CARROL, JAMES B., AND P. F. MAEDER. On the Boundary Condition for the Flow Along a Perforated Wall*..... 203
CHAIX, BERNARD, AND PETER HENRICI. On the Design of Two-Dimensional Supersonic Nozzles by the Method of Characteristics*..... 140
CHATTERTON, JOHN B. Some General Comparisons Between the Vibratory and Conventional Rate Gyro..... 633
CHENG, H. K. Aerodynamics of a Rectangular Plate with Vortex Separation in Supersonic Flow..... 217
CHENG, H. K. Errata—Nonlinear Lift and Vortex Separation*..... 660
CICALA, PLACIDO, AND ANGELO MIELE. Brachistocronic Maneuvers of a Constant Mass Aircraft in a Vertical Plane*..... 286
CICALA, PLACIDO, AND ANGELO MIELE. Brachistocronic Maneuvers of a Variable Mass Aircraft in a Vertical Plane*..... 577
CLARK, J. W. Buckling Efficiencies of Plate Materials at Elevated Temperatures*..... 659
CLARKE, JOSEPH H., HANS R. MENKES, AND PAUL A. LIBBY. A Provisional Analysis of Turbulent Boundary Layers with Injection..... 255
COHEN, CLARENCE B., AND ELI RESHOTKO. Note on the Compressible Laminar Boundary Layer with Heat Transfer and Pressure Gradient*..... 584
COVERT, EUGENE E. An Application of Variation Methods to the Computation of the Deformation of a Cantilever Plate Subjected to Nonuniform and Aeroelastically Induced Loads..... 555
COVERT, EUGENE E. A Particular Solution of a Nonlinear Differential Equation Which Occurs in the Dynamics of Conservative Systems and Its Application to Undamped Airplane Motion*..... 134
COVERT, EUGENE E., AND L. TRILLING. Quasi-Steady Nonlinear Pitching Oscillations in Transonic Flight..... 617
COX, HUGH L., AND BERTRAM KLEIN. The Buckling of Isosceles Triangular Plates..... 321

DAILEY, CHARLES LEE. Supersonic Diffuser Instability.... 733
DECKER, JAMES L. Criteria for Longitudinal Stability Requirements..... 639
DEYOUNG, JOHN. Calculation of Span Loading for Arbitrary Plan Forms*..... 208
DICKIE, GEORGE D., JR. Theoretical and Experimental Pressure Recovery of Sweptback Normal Shock Inlets.... 189
DOMM, ULRICH. The Stability of Vortex Streets with Consideration of the Spread of Vorticity of the Individual Vortices..... 750
DORE, FRANK J., AND HANS R. FRIEDRICH. The Dynamic Motion of a Missile Descending Through the Atmosphere..... 628
DOSANJH, DARSHAN S. Some Comments on "A Theoretical and Experimental Study of Shock Tube Flows"*..... 797
DUGUNDJI, JOHN, SAMUEL PINES, AND JOSEPH NEURINGER. Aerodynamic Flutter Derivatives for a Flexible Wing with Supersonic and Subsonic Edges..... 693
DUNN, D. W., AND C. C. LIN. On the Stability of the Laminar Boundary Layer in a Compressible Fluid..... 455

ECKERT, E. R. G. Engineering Relations for Friction and Heat Transfer to Surfaces in High Velocity Flow*.... 585
ECKERT, E. R. G., AND T. F. IRVINE, JR. Simultaneous Turbulent and Laminar Flow in Ducts with Noncircular Cross Sections*..... 65
ECKERT, HANS U. Errata—"Simplified Analysis of Turbulent Boundary-Layer Development Along Cylindrical Surfaces with Variable Free-Stream Mach Number"*.... 70
EDWARDS, S. SHERMAN. The Unsteady Forces on a Circular Cylinder in the Presence of Two Symmetrically Disposed Line Vortices*..... 72
EGGERS, A. J., JR., RAYMOND C. SAVIN, AND CLARENCE A. SYVERTSON. The Generalized Shock-Expansion Method and Its Application to Bodies Traveling at High Supersonic Air Speeds..... 231
EHLERS, F. EDWARD. The Lift and Moment on a Ring Concentric to a Cylindrical Body in Supersonic Flow..... 239
EHLERS, F. EDWARD. On Some Solutions of the Hodograph Equation Which Yield Transonic Flows Through a Laval Nozzle..... 107
EHRICH, FREDRIC F. Differentiation of Experimental Data Using Least Squares Fitting*..... 133
EHRICH, FREDRIC F. Secondary Flows in Cascades of Twisted Blades..... 51
ERINGEN, A. C. Some Corrections and Further Contributions to "Ripple-Type Buckling of Sandwich Columns"*.. 142

FALLIS, WILLIAM B. On Distributed Roughness as a Means of Fixing Transition at High Supersonic Speeds*... 339
FANUCCI, J. B., AND H. G. LEW. On the Laminar Compressible Boundary Layer over a Flat Plate with Suction or Injection..... 589
FLEDDERMANN, RICHARD G., AND ROBERT T. STANCIL. Wedge Pressure Coefficients in Transonic Flow by Hydraulic Analogy*..... 271

Flight Propulsion—
The Effect of Axial Flow in a Burner on Combustion Oscillation Frequencies, R. T. Newton and J. C. Truman*..... 583
A Note on Simplified Single Spool Turbojet Equilibrium Operation, Charles A. MacGregor*..... 431
Relative Size of Turbojet Engine Components, D. Willens*..... 652

FLÜGGE-LOTZ, I., AND ARLO F. JOHNSON. Laminar Compressible Boundary Layer Along a Curved Insulated Surface..... 445
FRAEYS DE VEUBEKE, B. M. Iteration in Semidefinite Eigenvalue Problems..... 710
FRANKLAND, J. M., AND R. E. ROACH. Strength Under Combined Tension and Bending in the Plastic Range*.... 795
FRASER, J. P. An Approximate Relationship Between Small Radius Ratio Turbine Passage Geometry and Radial Pressure Variation*..... 282
FRIEDMAN, M. B., AND H. F. LUDLOFF. Aerodynamics of Blasts—Diffraction of Blast Around Finite Corners..... 27
FRIEDMAN, M. B., AND H. F. LUDLOFF. Difference Solution of Shock Diffraction Problem*..... 139
FRIEDMANN, N. E., AND D. ROSENTHAL. Solution of Combined Bending and Torsion Problems by Means of the Electrical Conducting Sheet Analogy*..... 571
FRIEDRICH, HANS R. A Method for Investigating the Influence of Flexibility of the Mounting Structure of

Hydraulic Servo Systems on the Dynamic Stability Quality of Control Systems ... 101
FRIEDRICH, HANS R., AND FRANK J. DORE. The Dynamic Motion of a Missile Descending Through the Atmosphere ... 628

GARBER, THEODORE B., ROBERT C. SEAMANS, JR., FRANK A. BARNES, AND VINCENT W. HOWARD. Recent Developments in Aircraft Control ... 145
GATEWOOD, B. E. Buckling Loads for Beams of Variable Cross Section Under Combined Loads* ... 281
GELLER, EDWARD W. An Electrochemical Method of Visualizing the Boundary Layer* ... 869
GERARD, GEORGE. Buckling Efficiencies of Piate Materials at Elevated Temperatures ... 194
GERBER, NATHAN, AND JOHN C. MARTIN. The Effect of Thickness on Airfoils with Constant Vertical Acceleration at Supersonic Speeds ... 179
GLASS, I. I., AND G. N. PATTERSON. A Theoretical and Experimental Study of Shock-Tube Flows ... 73
GRADY, E. RUSSELL, AND BARNEY L. BYRUM. General Air-Frame Dynamics of a Guided Missile ... 534
GRIFFITH, WAYLAND, AND WILLIAM H. HANNUM. On the Intermittency of a Two-Dimensional Jet* ... 202
GROGAN, G. C., AND R. N. HASKELL. Slender Bodies of Low Wave Drag* ... 138
GUDERLEY, K. GOTTFRIED. The Flat Plate with an Angle of Attack in a Choked Wind Tunnel ... 844
GUMAN, WILLIAM J. On the Decay of a Flow Nonuniformity* ... 869

HALBMILLION, V. Comment on "Hypersonic Similarity and the Tangent-Cone Approximation for Unyawed Bodies of Revolution"* ... 871
HANNUM, WILLIAM H., AND WAYLAND GRIFFITH. On the Intermittency of a Two-Dimensional Jet* ... 202
HASEGAWA, M. Errata—"On Buckling of a Clamped Rhombic Thin Plate in Shear"* ... 804
HASKELL, R. N., AND G. C. GROGAN. Slender Bodies of Low Wave Drag* ... 138
HASKELL, R. N., J. J. HOSEK, AND W. S. JOHNSON, JR. Equations for the Chordwise Center of Pressure for the Basic Twist Distributions on Triangular Wings Having Supersonic Leading and Trailing Edges* ... 274
HASKELL, R. N., AND W. S. JOHNSON, JR. Equations for Loading on Triangular Wings Having Subsonic Leading Edges Due to Various Basic Antisymmetric Twist Distributions* ... 278
HAYES, WALLACE D. Second-Order Pressure Law for Two-Dimensional Compressible Flow* ... 284
HAYTHORNTHWAITE, R. M., AND E. T. ONAT. The Load Carrying Capacity of Initially Flat Circular Steel Plates Under Reversed Loading* ... 867
HELMBOLD, HEINRICH B. Comparison of Mixing Processes in Subsonic Jet Pumps* ... 435
HELMBOLD, HEINRICH B. The Lift of a Blowing Wing in a Parallel Stream* ... 341
HELMBOLD, HEINRICH B. Note on Velocity Fluctuations in Equilibrium Turbulent Shear Flow Along Solid Boundaries* ... 513
HENRICI, PETER, AND BERNARD CHAIX. On the Design of Two-Dimensional Supersonic Nozzles by the Method of Characteristics* ... 140
HILL, JACQUES A. F. On the Calibration of Supersonic Wind Tunnels* ... 441
HILTON, W. F. Tests of a Fairing to Reduce the Drag of a Supersonic Swept-Wing Root ... 173
HIRSCH, H., AND KENNETH B. AMER. Effect of High Advancing-Tip Mach Number on Helicopter Blade Flapping* ... 505
HOFF, N. J. Rapid Creep in Structures ... 661
HOSEK, J. J., R. N. HASKELL, AND W. S. JOHNSON, JR. Equations for the Chordwise Center of Pressure for the Basic Twist Distributions on Triangular Wings Having Supersonic Leading and Trailing Edges* ... 274
HOUBOLT, JOHN C., AND HARRY PRESS. Some Applications of Generalized Harmonic Analysis to Gust Loads on Airplanes ... 17
HOWARD, VINCENT W., ROBERT C. SEAMANS, JR., FRANK A. BARNES, AND THEODORE B. GARBER. Recent Developments in Aircraft Control ... 145
HOY, WALTER W., AND JAMES E. MARTIN. An Application of the Buffon Needle Problem to the Determination of the Probability of Obtaining a Free Flight Arrested Landing in Carrier Landings* ... 68

IMAI, ISAO. The Second-Order Thin Airfoil Theory for Compressible Flow* ... 270
IRVINE, T. F., JR., AND E. R. G. ECKERT. Simultaneous Turbulent and Laminar Flow in Ducts with Noncircular Cross Sections* ... 65

JOHNSON, ARLO F., AND I. FLÜGGE-LOTZ. Laminar Compressible Boundary Layer Along a Curved Insulated Surface ... 445
JOHNSON, W. S., JR., AND R. N. HASKELL. Equations for Loading on Triangular Wings Having Subsonic Leading Edges Due to Various Basic Antisymmetric Twist Distributions* ... 278
JOHNSON, W. S., JR., J. J. HOSEK, AND R. N. HASKELL. Equations for the Chordwise Center of Pressure for the Basic Twist Distributions on Triangular Wings Having Supersonic Leading and Trailing Edges* ... 274
JORDAN, PETER F. Some Series Developments in Unsteady Aerodynamics* ... 722

KAFKA, PAUL G. Lifting Pressure on Delta Wings with Subsonic Leading Edges, Symmetrical Plan Form, and Discontinuous Slope* ... 725
KAINER, JULIAN H. Spanwise Variation in the Pitching-Moment Coefficient and the Center of Pressure Due to Various Basic Twist Distributions on Triangular Wings Having Supersonic Leading and Trailing Edges ... 598
KATZEN, ELLIOTT D. Limitations of Linear Theory in Predicting the Pressure Distribution on Triangular Wings* ... 514
KAWAMURA, RYUMA, AND HAKURO OGUCHI. Curved Shocks in Pseudostationary Flows* ... 210
KAYE, JOSEPH, GEORGE A. BROWN, JULIUS C. WESTMORELAND, AND EDWARD F. KURTZ, JR. Simultaneous Measurements of Velocity and Temperature Profiles for Adiabatic Supersonic Flow of Air in a Tube* ... 575
KAYE, JOSEPH, AND VICTOR C. M. YEH. Design Charts for Transient Temperature Distribution Resulting from Aerodynamic Heating at Supersonic Speeds ... 755
KEMP, NELSON H., AND W. R. SEARS. The Unsteady Forces Due to Viscous Wakes in Turbomachines ... 478
KENNEDY, ERNEST C. Methods for Computing Supersonic Aerodynamic Flutter Coefficients for Two-Dimensional Flow ... 310
KEPLER, C. E., AND S. M. BOGDONOFF. Separation of a Supersonic Turbulent Boundary Layer ... 414
KLEBANOFF, P. S., G. B. SCHUBAUER, AND K. D. TIDSTROM. Measurements of the Effect of Two-Dimensional and Three-Dimensional Roughness Elements on Boundary-Layer Transition* ... 803
KLEIN, BERTRAM. Interaction Equation for the Buckling of Unstiffened Cylinders Under Combined Bending, Torsion, and Internal Pressure* ... 583

KLEIN, BERTRAM. Parameters Predicting the Initial and Final Collapse Pressures of Uniformly Loaded Spherical Shells* ... 69
KLEIN, BERTRAM. Rapid Estimation of the Elastic-Plastic Euler Buckling Loads for Simply Supported Tapered Columns Under Varying Axial Loading ... 873
KLEIN, BERTRAM, AND HUGH L. COX. The Buckling of Isosceles Triangular Plates ... 321
KLEIN, JOHN, AND MYRON TRIBUS. Forced Convection Through a Laminar Boundary Layer over an Arbitrary Surface with an Arbitrary Temperature Variation* ... 62
KOROBKIN, IRVING. On the Determination of Local Heat-Transfer Coefficients for Bodies with Pressure Gradient in Supersonic Flow* ... 283
KRIVETSKY, ALEXANDER. Plasticity Coefficients for the Plastic Buckling of Plates and Shells* ... 432
KRZYWOBLOCKI, M. Z. v. A Remark on "A Simple Laminar Boundary Layer with Secondary Flow"* ... 582
KUESSNER, H. G. The Difference Property of the Kernel of the Unsteady Lifting Surface Theory ... 227
KUO, Y. H. A Similarity Rule for the Interaction Between a Conical Field and a Plane Shock* ... 504
KURTZ, EDWARD F., JR., JOSEPH KAYE, GEORGE A. BROWN, AND JULIUS C. WESTMORELAND. Simultaneous Measurements of Velocity and Temperature Profiles for Adiabatic Supersonic Flow of Air in a Tube* ... 575

LANDAHL, MARTEN, HOLT ASHLEY, AND ERIK MOLLO-CHRISTENSEN. On Approximate Solutions for the Compressible Flow Around Oscillating Thin Wings* ... 581
LANGE, A. H., AND R. E. LEE. Further Comments on "Note on Boundary-Layer Transition in Supersonic Flow"* ... 282
LAPORTE, OTTO, AND HIDEO YOSHIHARA. A Rigorous Method for Finding the Lift of a Certain Class of Airfoils and Remarks on the Meaning of Schrenk's Approximate Rule ... 787
LARGE, JOHN B., AND H. S. BLUSTON. Erratum—"Wing-Body Interference at Subsonic and Supersonic Speeds—Survey and New Developments"* ... 208
LAVENDER, ROBERT E. Application of Kelly's Theory to Cone-Cylinder-Frustum Bodies of Revolution* ... 654
LEE, R. E., AND A. H. LANGE. Further Comments on "Note on Boundary-Layer Transition in Supersonic Flow"* ... 282
LEPPERT, E. L., JR. A Fraction Series Solution for Characteristic Values Useful in Some Problems of Airplane Dynamics ... 326
LEVY, SALOMON. Heat Conducting Bodies in Boundary-Layer Flow* ... 440
LEVY, SAMUEL, AND WILLIAM F. CAHILL. Computation of Vibration Modes and Frequencies on SEAC ... 837
LEW, H. G., AND J. B. FANUCCI. On the Laminar Compressible Boundary Layer over a Flat Plate with Suction or Injection ... 589
LI, TING-YI. Simple Shear Flow Past a Flat Plate in a Compressible Viscous Fluid* ... 724
LI, TING-YI. Simple Shear Flow Past a Flat Plate in an Incompressible Fluid of Small Viscosity* ... 651
LI, TING-YI, AHD HENRY T. NAGAMATSU. Similar Solutions of Compressible Boundary-Layer Equations ... 607
LIBBY, PAUL A., HANS R. MENKES, AND JOSEPH H. CLARKE. A Provisional Analysis of Turbulent Boundary Layers with Injection ... 255
LIBBY, PAUL A., AND MARIAN VISICH, JR. Laminar Heat Transfer in Two-Dimensional Subsonic Effusors ... 425
LIEPMAN, HANS PETER. An Analytic Method for the Design of Two-Dimensional Asymmetric Nozzles ... 701
LIEPMANN, H. W. Extension of the Statistical Approach to Buffeting and Gust Response of Wings of Finite Span ... 197
LIN, C. C., AND D. W. DUNN. On the Stability of the Laminar Boundary Layer in a Compressible Fluid ... 455

LOBB, R. KENNETH, EVA M. WINKLER, AND JEROME PERSH. Experimental Investigation of Turbulent Boundary Layers in Hypersonic Flow ... 1
LOOS, HENK G. A Simple Laminar Boundary Layer with Secondary Flow ... 35
LOVE, E. S. On the Effect of Reynolds Number upon the Peak Pressure-Rise Coefficient Associated with the Separation of a Turbulent Boundary Layer in Supersonic Flow* ... 345
LOW, GEORGE M. Reversal of Skin-Friction and Heat-Transfer Trends in High-Speed Laminar Flows* ... 721
LOW, GEORGE M. Stability of Compressible Laminar Boundary Layer with Internal Heat Sources or Sinks ... 329
LUDLOFF, H. F., AND M. B. FRIEDMAN. Aerodynamics of Blasts—Diffraction of Blast Around Finite Corners ... 27
LUDLOFF, H. F., AND M. B. FRIEDMAN. Difference Solution of Shock Diffraction Problem* ... 139
LUDLOFF, H. F., AND F. J. MARSHALL. Transient Stresses in Airfoils Under Blast Loading* ... 508
LUNDBERG, BO. Fatigue Life of Airplane Structures (Eighteenth Wright Brothers Lecture) ... 349

MACDERMOTT, WILLIAM N. The Correction of Flexible Plate Supersonic Nozzle Contours by Influence Methods. 289
MACGREGOR, CHARLES A. A Note on Simplified Single Spool Turbojet Equilibrium Operation* ... 431
MACK, LESLIE M. Summary of Existing Cone Temperature Recovery Factor Data Obtained in Continuous-Flow Wind Tunnels Plus Additional Data* ... 212
MAEDER, P. F., AND JAMES B. CARROLL. On the Boundary Condition for the Flow Along a Perforated Wall* ... 203
MAGER, ARTUR. Prediction of Shock-Induced Turbulent Boundary-Layer Separation* ... 201
MAHLMEISTER, JAMES E., AND MYRON TRIBUS. Frictional Heating of Nonisothermal Walls* ... 726
MAHONY, J. J. A Critique of Shock-Expansion Theory ... 673
MARBLE, FRANK E. Propagation of Stall in a Compressor Blade Row ... 541
MARCHAL, RAYMOND. Conditions for the Appearance of Shock Waves in Steady Flows* ... 275
MARSHALL, F. J., AND H. F. LUDLOFF. Transient Stresses in Airfoils Under Blast Loading* ... 508
MARTIN, JAMES E., AND WALTER W. HOY. An Application of the Buffon Needle Problem to the Determination of the Probability of Obtaining a Free Flight Arrested Landing in Carrier Landings* ... 68
MARTIN, JOHN C., AND NATHAN GERBER. The Effect of Thickness on Airfoils with Constant Vertical Acceleration at Supersonic Speeds ... 179

Mathematics—
Differentiation of Experimental Data Using Least Squares Fitting, Fredric F. Ehrich* ... 133

MCCORMICK, B. W. An Approximation to the Lift of a Two-Dimensional Cascade of Airfoils* ... 730
MCCORMICK, B. W. The Effect of a Finite Hub on the Optimum Propeller ... 645
MENKES, HANS R., JOSEPH H. CLARKE, AND PAUL A. LIBBY. A Provisional Analysis of Turbulent Boundary Layers with Injection ... 255
MERRIAM, KENNETH G. A Short Cut in Computing Product of Inertia* ... 583
MEYER, R. E. Remark on Supersonic Nozzle Design* ... 587
MEYER, R. E. Turbulent Boundary Layers on Nozzle Liners* ... 572
MEYER, R. E., AND T. A. d'Ews Thomson. Note on the Unsteady Heat Regenerator* ... 337
MIELE, ANGELO, AND PLACIDO CICALA. Brachistocronic Maneuvers of a Constant Mass Aircraft in a Vertical Plane* ... 286

MIELE, ANGELO, AND PLACIDO CICALA. Brachistocronic Maneuvers of a Variable Mass Aircraft in a Vertical Plane* ... 577
MILLSAPS, KNOX. The Obukhoff Spectrum of Homogeneous Isotropic Turbulence* ... 511
MOLLO-CHRISTENSEN, ERIK, HOLT ASHLEY, AND MARTEN LANDAHL. On Approximate Solutions for the Compressible Flow Around Oscillating Thin Wings* ... 581
MORDUCHOW, MORRIS. On Compressible Laminar Boundary-Layer Characteristics in a Pressure Gradient with Heat Transfer* ... 444
MORGAN, A. J. A. On a Class of Two-Dimensional Channel Flows with a Straight Sonic Line* ... 573
MUNK, MAX M. Remarks on the Velocity of Sound* ... 795
MURPHREE, WILLIAM D., J. LEITH POTTER, AND NORMAN M. SHAPIRO. Normal Force and Center of Pressure on Right Circular Cylinders* ... 214
MURPHREE, WILLIAM D., J. LEITH POTTER, AND NORMAN M. SHAPIRO. On the Normal Force Produced by Multifinned Tail Assemblies in Supersonic Flow* ... 511
MURPHY, C. H., AND R. M. WOOD. Aerodynamic Derivatives for Both Steady and Nonsteady Motion of Slender Bodies* ... 870
MURPHY, J. S., AND A. M. O. SMITH. A Dust Method for Locating the Separation Point* ... 273

NAGAMATSU, HENRY T. Summary of Recent GALCIT Hypersonic Experimental Investigations ... 165
NAGAMATSU, HENRY T., AND TING-YI LI. Similar Solutions of Compressible Boundary-Layer Equations ... 607
NASH, WILLIAM A. Effect of Large Deflections and Initial Imperfections on the Buckling of Cylindrical Shells Subject to Hydrostatic Pressure ... 264
NEEDHAM, ROBERT A. The Ultimate Strength of Multiweb Box Beams in Pure Bending ... 781
NEURINGER, JOSEPH, SAMUEL PINES, AND JOHN DUGUNDJI. Aerodynamic Flutter Derivatives for a Flexible Wing with Supersonic and Subsonic Edges ... 693
NEWMAN, MARCEL K. Effect of Rotatory Inertia and Shear on Maximum Strain in Cantilever Impact Excitation ... 313
NEWTON, R. T., AND J. C. TRUMAN. The Effect of Axial Flow in a Burner on Combustion Oscillation Frequencies* ... 583
NIEDENFUHR, F. W. On the Possibility of Aeroelastic Reversal of Propeller Blades* ... 438

OGUCHI, HAKURO, AND RYUMA KAWAMURA. Curved Shocks in Pseudostationary Flows* ... 210
ONAT, E. T. On Certain Second-Order Effects in the Limit Design of Frames ... 681
ONAT, E. T., AND R. M. HAYTHORNTHWAITE. The Load Carrying Capacity of Initially Flat Circular Steel Plates Under Reversed Loading* ... 867
OSTERLE, J. F., AND W. T. ROULEAU. The Application of Finite Difference Methods to Boundary-Layer Type Flows ... 249

PAI, S. I. On the Flow Behind an Attached Curved Shock* 657
PATTERSON, G. N., AND I. I. GLASS. A Theoretical and Experimental Study of Shock-Tube Flows ... 73
PEARSON, CARL E. A Study of Surge in Compressors and Jet Engines ... 10
PEARSON, CARL E. Surge Behavior in a Three-Stage Compressor* ... 799

Performance—
An Additional Note on Rolling Pull-Out Calculations, Ralph W. Stone, Jr.* ... 211
An Application of the Buffon Needle Problem to the Determination of the Probability of Obtaining a Free Flight Arrested Landing in Carrier Landings, James E. Martin and Walter W. Hoy* ... 68
Author's Reply, Edward S. Rutowski* ... 62
Brachistocronic Maneuvers of a Constant Mass Aircraft in a Vertical Plane, Placido Cicala and Angelo Miele* ... 286
Brachistocronic Maneuvers of a Variable Mass Aircraft in a Vertical Plane, Placido Cicala and Angelo Miele* ... 577
The Effects of Changes in Aircraft Weight on Flight Equilibrium, Joan Birman* ... 61
Supplementary Remark on "Airplane Stopping Distance," B. Saelman* ... 802

PERSH, JEROME. The Behavior of the Boundary Layer in the Region of Transition from Laminar to Turbulent Flow* ... 443
PERSH, JEROME, EVA M. WINKLER, AND R. KENNETH LOBB. Experimental Investigation of Turbulent Boundary Layers in Hypersonic Flow ... 1
PINES, SAMUEL, JOHN DUGUNDJI, AND JOSEPH NEURINGER. Aerodynamic Flutter Derivatives for a Flexible Wing with Supersonic and Subsonic Edges ... 693
POTTER, J. LEITH, WILLIAM D. MURPHREE, AND NORMAN M. SHAPIRO. Normal Force and Center of Pressure on Right Circular Cylinders* ... 214
POTTER, J. LEITH, WILLIAM D. MURPHREE, AND NORMAN M. SHAPIRO. On the Normal Force Produced by Multifinned Tail Assemblies in Supersonic Flow* ... 511
PRESS, HARRY, AND JOHN C. HOUBOLT. Some Applications of Generalized Harmonic Analysis to Gust Loads on Airplanes ... 17
PROBSTEIN, RONALD F., AND KENNETH N. C. BRAY. Hypersonic Similarity and the Tangent-Cone Approximation for Unyawed Bodies of Revolution* ... 66

Propellers—
Direct Calculation of Propeller Deflection, S. M. Ramachandra* ... 726
The Effect of a Finite Hub on the Optimum Propeller, B. W. McCormick ... 645
On the Possibility of Aeroelastic Reversal of Propeller Blades, F. W. Niedenfuhr* ... 438

PRZEMIENIECKI, J. S. Transient Temperatures and Stresses in Plates Attained in High-Speed Flight* ... 345

RAMACHANDRA, S. M. Direct Calculation of Propeller Deflection* ... 726
RANDELS, W. C. A Note on "A Study of Surge in Compressors and Jet Engines"* ... 660
RESHOTKO, ELI, AND CLARENCE B. COHEN. Note on the Compressible Laminar Boundary Layer with Heat Transfer and Pressure Gradient* ... 584
RICHARDSON, E. G. Acoustics in Relation to Aerodynamics ... 775
ROACH, R. E., AND J. M. FRANKLAND. Strength Under Combined Tension and Bending in the Plastic Range* ... 795
RODDEN, W. P. On Use of the General Bending Formula* ... 516
RODDEN, W. P. A Simplified Expression for the Dihedral Effect of a Flexible Wing* ... 579
ROSÉN, JOHN. The Design and Calibration of a Variable Mach Number Nozzle ... 484
ROSENTHAL, D., AND N. E. FRIEDMANN. Solution of Combined Bending and Torsion Problems by Means of the Electrical Conducting Sheet Analogy* ... 571
ROSHKO, ANATOL. On the Wake and Drag of Bluff Bodies ... 124

Rotating Wing Aircraft—
Effect of High Advancing-Tip Mach Number on Helicopter Blade Flapping, Kenneth B. Amer and H. Hirsch* ... 505

ROTTA, J. C. Similar Solutions of Turbulent Boundary Layers* ... 215
ROULEAU, W. T., AND J. F. OSTERLE. The Application of Finite Difference Methods to Boundary-Layer Type Flows ... 249
RUETENIK, J. R. The Effect of the Temperature Dependence of King's "Constant" A on the Hot-Wire Sensitivity Coefficient* ... 502
RUNYAN, HARRY L., AND DONALD S. WOOLSTON. Some Considerations on the Air Forces on a Wing Oscillating Between Two Walls for Subsonic Compressible Flow ... 41
RUTOWSKI, EDWARD S. Author's Reply* ... 62

SAELMAN, B. Supplementary Remark on "Airplane Stopping Distance"* ... 802
SAVIN, RAYMOND C., A. J. EGGERS, JR., AND CLARENCE A. SYVERTSON. The Generalized Shock-Expansion Method and Its Application to Bodies Traveling at High Supersonic Air Speeds ... 231
SCANLAN, R. H. Comment on the Note "Electrical Resistance Networks for Beam and Column Problems"* ... 202
SCHNEIDER, P. J. Variation of Maximum Thermal Stress in Free Plates* ... 872
SCHUBAUER, G. B., P. S. KLEBANOFF, AND K. D. TIDSTROM. Measurements of the Effect of Two-Dimensional and Three-Dimensional Roughness Elements on Boundary-Layer Transition* ... 803
SCHUH, H. On Determining Turbulent Boundary-Layer Separation in Incompressible and Compressible Flow* ... 343
SCHUH, H. Transient Temperature Distributions and Thermal Stresses in a Skin-Shear Web Configuration at High-Speed Flight for a Wide Range of Parameters ... 829
SEAMANS, ROBERT C., JR., FRANK A. BARNES, THEODORE B. GARBER, AND VINCENT W. HOWARD. Recent Developments in Aircraft Control ... 145
SEARS, W. R., AND NELSON H. KEMP. The Unsteady Forces Due to Viscous Wakes in Turbomachines ... 478
SERDENGECTI, S., AND H. S. TSIEN. Analysis of Peak-Holding Optimalizing Control ... 561
SHAPIRO, NORMAN M., J. LEITH POTTER, AND WILLIAM D. MURPHREE. Normal Force and Center of Pressure on Right Circular Cylinders* ... 214
SHAPIRO, NORMAN M., J. LEITH POTTER, AND WILLIAM D. MURPHREE. On the Normal Force Produced by Multifinned Tail Assemblies in Supersonic Flow* ... 511
SHEN, S. F. Remarks on "An Exact Solution for Two-Dimensional Linear Panel Flutter at Supersonic Speeds"* 656
SHIBAOKA, YOSHIO, AND KŌ TAMADA. On Supersonic Flow Past a Finite Wedge at the Crocco Mach Number ... 261
SISTO, F. Unsteady Aerodynamic Reactions on Airfoils in Cascade ... 297
SIVELLS, JAMES C. Design of Two-Dimensional Continuous-Curvature Supersonic Nozzles ... 685
SMITH, A. M. O., AND J. S. MURPHY. A Dust Method for Locating the Separation Point* ... 273

Stability & Control—
Aerodynamic Derivatives for Both Steady and Nonsteady Motion of Slender Bodies, R. M. Wood and C. H. Murphy* ... 870
Analysis of Peak-Holding Optimalizing Control, H. S. Tsien and S. Serdengecti ... 561
Criteria for Longitudinal Stability Requirements, James L. Decker ... 639
The Dynamic Motion of a Missile Descending Through the Atmosphere, Hans R. Friedrich and Frank J. Dore ... 628
Estimation of the Lift and Moment Parameters of Leading-Edge Flaps, Malcolm J. Abzug* ... 655
Gaussian Outputs from Non-Gaussian Inputs, Leo J. Tick* ... 208
General Air-Frame Dynamics of a Guided Missile, Barney L. Byrum and E. Russell Grady ... 534
A Method for Investigating the Influence of Flexibility of the Mounting Structure of Hydraulic Servo Systems on the Dynamic Stability Quality of Control Systems, Hans R. Friedrich ... 101
A Particular Solution of a Nonlinear Differential Equation Which Occurs in the Dynamics of Conservative Systems and Its Application to Undamped Airplane Motion, Eugene Covert* ... 134
Quasi-Steady Nonlinear Pitching Oscillations in Transonic Flight, L. Trilling and E. E. Covert ... 617
Recent Developments in Aircraft Control, Robert C. Seamans, Jr., Frank A. Barnes, Theodore B. Garber, and Vincent W. Howard ... 145
A Simplified Treatment of Partial Fractions for Dynamic-Response Calculations, George S. Campbell* ... 437
Some General Comparisons Between the Vibratory and Conventional Rate Gyro, John B. Chatterton ... 633

STANCIL, ROBERT T., AND RICHARD G. FLEDDERMANN. Wedge Pressure Coefficients in Transonic Flow by Hydraulic Analogy* ... 271
STEIN, MARVIN L. Determining the Mode Shapes and Frequencies of Low Aspect Ratio Multispar Wings* ... 137
STEKETEE, J. A. Note on a Formula of H. W. Emmons* ... 578
STERN, MARVIN. Analysis of Thermal Stresses in Conical Shells* ... 506
STERN, MARVIN. Matrix Method of Coupling Shear Flexibility and Rotatory Inertia in Bending Vibration* ... 276
STEWARTSON, K. On the Motion of a Flat Plate at High Speed in a Viscous Compressible Fluid, II—Steady Motion ... 303
STOJANOVIĆ, DRAGUTIN. Temperature Field in a Laminar Incompressible Round Jet and in Convergent and Divergent Round Nozzle* ... 216
STONE, RALPH W., JR., An Additional Note on Rolling Pull-Out Calculations* ... 211

Stress Analysis & Structures—
Analysis of Thermal Stresses in Conical Shells, Marvin Stern* ... 506
Beam Strength and Curvature Under Combined Tension and Bending in the Plastic Range, Anthony J. Barrett* 71
Buckling Efficiencies of Plate Materials at Elevated Temperatures, J. W. Clark* ... 659
Buckling Efficiencies of Plate Materials at Elevated Temperatures, George Gerard ... 194
Buckling Loads for Beams of Variable Cross Section Under Combined Loads, B. E. Gatewood* ... 281
The Buckling of Isosceles Triangular Plates, Hugh L. Cox and Bertram Klein ... 321
Comment on the Note "Electrical Resistance Networks for Beam and Column Problems," R. H. Scanlan* ... 202
Effect of Large Deflections and Initial Imperfections on the Buckling of Cylindrical Shells Subject to Hydrostatic Pressure, William A. Nash ... 264
Errata—"On Buckling of a Clamped Rhombic Thin Plate in Shear," M. Hasegawa* ... 804
Fatigue Life of Airplane Structures (Eighteenth Wright Brothers Lecture), Bo Lundberg ... 349
Interaction Equation for the Buckling of Unstiffened Cylinders Under Combined Bending, Torsion, and Internal Pressure, Bertram Klein* ... 583
An Investigation of the Bending of Angle Beams in the Plastic Range, H. Norman Abramson, Harry A. Williams, and Bruce G. Woolpert ... 818
The Load Carrying Capacity of Initially Flat Circular Steel Plates Under Reversed Loading, R. M. Haythornthwaite and E. T. Onat* ... 867
On the Buckling of Stringer Panels, Including Forced Crippling, P. P. Bijlaard ... 491

Stress Analysis & Structures (*Continued*)
On Certain Second-Order Effects in the Limit Design of Frames, E. T. Onat ... 681
On Use of the General Bending Formula, W. P. Rodden* ... 516
Parameters Predicting the Initial and Final Collapse Pressures of Uniformly Loaded Spherical Shells, Bertram Klein* ... 69
Plasticity Coefficients for the Plastic Buckling of Plates and Shells, Alexander Krivetsky* ... 432
A Procedure for the Approximate Analysis of Buckled Plates, Sara R. Boley* ... 337
Rapid Creep in Structures, N. J. Hoff ... 661
Rapid Estimation of the Elastic-Plastic Euler Buckling Loads for Simply Supported Tapered Columns Under Varying Axial Loading, Bertram Klein ... 873
A Short Cut in Computing Product of Inertia, Kenneth G. Merriam* ... 583
Solution of Combined Bending and Torsion Problems by Means of the Electrical Conducting Sheet Analogy, N. E Friedmann and D. Rosenthal* ... 571
Some Corrections and Further Contributions to "Ripple-Type Buckling of Sandwich Columns," A. C. Eringen* ... 142
Strength Under Combined Tension and Bending in the Plastic Range, J. M. Frankland and R. E. Roach* ... 795
Transient Temperature Distributions and Thermal Stresses in a Skin-Shear Web Configuration at High-Speed Flight for a Wide Range of Parameters, H. Schuh ... 829
Transient Temperatures and Stresses in Plates Attained in High-Speed Flight, J. S. Przemieniecki* ... 345
The Ultimate Strength of Multiweb Box Beams in Pure Bending, Robert A. Needham ... 781
Variation of Maximum Thermal Stress in Free Plates, P. J. Schneider* ... 872

SYVERTSON, CLARENCE A., A. J. EGGERS, JR., AND RAYMOND C. SAVIN. The Generalized Shock-Expansion Method and Its Application to Bodies Traveling at High Supersonic Air Speeds ... 231

TAMADA, KŌ, AND YOSHIO SHIBAOKA. On Supersonic Flow Past a Finite Wedge at the Crocco Mach Number ... 261
TAO, L. N. Gas Dynamic Behavior of Real Gases ... 763
THOMSON, T. A. D'EWS. Stagnation Temperature Control for a Blow-Down Supersonic Wind Tunnel* ... 340
THOMSON, T. A. D'EWS, AND R. E. MEYER. Note on the Unsteady Heat Regenerator* ... 337
TICK, LEO J. Gaussian Outputs from Non-Gaussian Inputs* ... 208
TIDSTROM, K. D., P. S. KLEBANOFF, AND G. B. SCHUBAUER. Measurements of the Effect of Two-Dimensional and Three-Dimensional Roughness Elements on Boundary-Layer Transition* ... 803
TRIBUS, MYRON, AND JOHN KLEIN. Forced Convection Through a Laminar Boundary Layer over an Arbitrary Surface with an Arbitrary Temperature Variation* ... 62
TRIBUS, MYRON, AND JAMES E. MAHLMEISTER. Frictional Heating of Nonisothermal Walls* ... 726
TRILLING, L., AND E. E. COVERT. Quasi-Steady Nonlinear Pitching Oscillations in Transonic Flight ... 617
TRUITT, ROBERT WESLEY. Free Streamline Analysis for Slotted Two-Dimensional Supersonic Minimum-Length Nozzles* ... 658
TRUITT, ROBERT WESLEY. Transonic Lift over the Front Surface of a Two-Dimensional Diamond Airfoil* ... 342
TRUMAN, J. C., AND R. T. NEWTON. The Effect of Axial Flow in a Burner on Combustion Oscillation Frequencies* ... 583
TSIEN, S. H. The Supersonic Conical Wing of Minimum Drag ... 805
TSIEN, H. S., AND S. SERDENGECTI. Analysis of Peak-Holding Optimalizing Control ... 561
TYLER, E. F. Aerodynamic Coefficients for Cambering and Aileron Motions* ... 340

VAN DRIEST, E. R., AND J. CHRISTOPHER BOISON. Boundary-Layer Stabilization by Surface Cooling in Supersonic Flow* ... 70
VAN LE, N. Optimum Stage for Axial Flow Turbines* ... 503
VIDAL, R. J., AND G. E. BARTLETT. Experimental Investigation of Influence of Edge Shape on the Aerodynamic Characteristics of Low Aspect Ratio Wings at Low Speeds ... 517
VISICH, MARIAN, JR., AND PAUL A. LIBBY. Laminar Heat Transfer in Two-Dimensional Subsonic Effusors ... 425

WARREN, WALTER R., JR. The Static Pressure Variation in Compressible Free Jets* ... 205
WEISSINGER, JOHANNES. Comment on "Calculation of Span Loading for Arbitrary Plan Forms"* ... 870
WESTMORELAND, JULIUS C., JOSEPH KAYE, GEORGE A. BROWN, AND EDWARD F. KURTZ, JR. Simultaneous Measurements of Velocity and Temperature Profiles for Adiabatic Supersonic Flow of Air in a Tube* ... 575
WICK, ROBERT S. Further Comments on "The Effect of Boundary Layer on Sonic Flow Through an Abrupt Cross-Sectional Area Change"* ... 135
WILLENS, D. Relative Size of Turbojet Engine Components* ... 652
WILLIAMS, HARRY A., H. NORMAN ABRAMSON, AND BRUCE G. WOOLPERT. An Investigation of the Bending of Angle Beams in the Plastic Range ... 818

Wind Tunnels—
An Analytic Method for the Design of Two-Dimensional Asymmetric Nozzles, Hans Peter Liepman ... 701
The Design and Calibration of a Variable Mach Number Nozzle, John Rosén ... 484
Design of Two-Dimensional Continuous-Curvature Supersonic Nozzles, James C. Sivells ... 685
A Dust Method for Locating the Separation Point, A. M. O. Smith and J. S. Murphy* ... 273
The Effect of the Temperature Dependence of King's "Constant" A on the Hot-Wire Sensitivity Coefficient, J. R. Ruetenik* ... 502
An Electrochemical Method of Visualizing the Boundary Layer, Edward W. Geller* ... 869
Fatigue Life of Airplane Structures (Eighteenth Wright Brothers Lecture), Bo Lundberg ... 349
The Flat Plate with an Angle of Attack in a Choked Wind Tunnel, K. Gottfried Guderley ... 844
Note on the Unsteady Heat Regenerator, R. E. Meyer and T. A. d'Ews Thomson* ... 337
On the Boundary Condition for the Flow Along a Perforated Wall, P. F. Maeder and James B. Carroll* ... 203
On the Calibration of Supersonic Wind Tunnels, Jacques A. F. Hill* ... 441
Some Comments on "A Theoretical and Experimental Study of Shock Tube Flows," Darshan S. Dosanjh* ... 797
Stagnation Temperature Control for a Blow-Down Supersonic Wind Tunnel, T. A. d'Ews Thomson* ... 340
Summary of Recent GALCIT Hypersonic Experimental Investigations, Henry T. Nagamatsu ... 165
A Theoretical and Experimental Study of Shock-Tube Flows, I. I. Glass and G. N. Patterson ... 73

WINKLER, EVA M., R. KENNETH LOBB, AND JEROME PERSH. Experimental Investigation of Turbulent Boundary Layers in Hypersonic Flow ... 1

WOOD, R. M., AND C. H. MURPHY. Aerodynamic Derivatives for Both Steady and Nonsteady Motion of Slender Bodies* 870
WOOLPERT, BRUCE G., H. NORMAN ABRAMSON, AND HARRY A. WILLIAMS. An Investigation of the Bending of Angle Beams in the Plastic Range 818
WOOLSTON, DONALD S., AND HARRY L. RUNYAN. Some Considerations on the Air Forces on a Wing Oscillating Between Two Walls for Subsonic Compressible Flow 41

YEH, VICTOR C. M., AND JOSEPH KAYE. Design Charts for Transient Temperature Distribution Resulting from Aerodynamic Heating at Supersonic Speeds 755

YEN, K. T. Approximate Solutions of the Incompressible Laminar Boundary-Layer Equations for a Flat Plate in a Shear Flow* 728
YOSHIHARA, HIDEO, AND OTTO LAPORTE. A Rigorous Method for Finding the Lift of a Certain Class of Airfoils and Remarks on the Meaning of Schrenk's Approximate Rule 787

ZLOTNICK, MARTIN. Some Static Aeroelastic Design Considerations Relating to Flap-Type Control Surfaces* 580

International Conference on Fatigue in Aircraft Structures

Columbia University, New York, January 30–February 1, 1956

Jan. 30 Physical Theories of Fatigue of Metals.
Jan. 31 Prediction of Fatigue Life and Fatigue Strength (Fatigue Testing with Respect to Design).
Feb. 1 Prevention of Fatigue Failure (Fatigue Design).

Papers by invited speakers from Great Britain, Sweden, Germany, and the United States.

Information: Professor A. M. Freudenthal, 716 Engineering, Columbia University, New York 27, N.Y.

ST. LOUIS PUBLIC LIBRARY
OCT 18 1956

28

87

80

SUGGESTIONS *for* CONTRIBUTORS
to the Publications of the
INSTITUTE *of the* AERONAUTICAL SCIENCES

The Institute of the Aeronautical Sciences invites both members and nonmembers from any country to submit papers for publication in the JOURNAL OF THE AERONAUTICAL SCIENCES and the AERONAUTICAL ENGINEERING REVIEW. The Institute, following the practice of other societies, does not pay for contributions.

The following directions for the preparation of papers, if followed by authors, will save correspondence, avoid the return of papers for changes, minimize the work of preparation for the printer, and save the expense due to the charges made for "author's corrections."

MANUSCRIPTS: The original typewritten copy of the paper is desired, double or triple spaced on one side of white paper sheets, consecutively numbered. There should be wide margins to allow for the marking of directions to the printer. Correcting, changing, or adding to papers after they are in type is costly. It is, therefore, imperative that papers submitted be in final form. Typographical errors may be corrected on proofs, but if authors wish to add material, they may do so at their own expense. In mailing, drawings may be rolled but manuscripts should be sent flat. Send by first-class mail (register if you wish for your own protection) to the Editorial Office, Institute of the Aeronautical Sciences, 2 East 64th Street, New York 21, N.Y. All manuscripts will be examined by the Editorial Committee and by the Editor. Authors will be advised as promptly as possible whether the paper is acceptable for publication.

TITLES: The title of the paper should be brief. The name and initials of the author should be written as he prefers. The use of the full name of an author is advocated because of the frequent duplication of initials and surnames which sometimes makes it difficult to establish the identity of the author. This is particularly important for large annual indexing and abstracting services. All titles and degrees or honors are omitted. The name of the organization with which the author is associated should be placed after his name on a separate line. The date on which the paper is received will be inserted by the Editor. The author's title should be indicated in a footnote.

SUMMARIES OR ABSTRACTS: An abstract to be printed at the beginning should accompany each article. It should be adequate as an *index* and as a *summary*. It should contain a statement of major conclusions reached, since summaries in many cases constitute the only source of information used in compiling scientific reference indexes. Abstracts printed in other journals, especially foreign, in most cases, consist of summaries from printed papers. The summary should explain as adequately as possible the major conclusions to a nonspecialist in the subject and should contain from 100 to 300 words, depending on the length of the paper.

SUBHEADINGS: Subheadings should be inserted by the author at frequent intervals. The work of editorial preparation will be simplified by the author's provision of many subheadings.

MATTER USUALLY DELETED: Photographs or illustrations of little technical interest and not showing advances in general practice. Too detailed tabular matter (general results of such tables may be included in the text). Lengthy descriptions of materials or processes or of preliminary experiments or theories that preceded final results; salient features only are of interest.

REFERENCES AND FOOTNOTES: References should appear as footnotes only, numbered consecutively and grouped together at the end of the manuscript. The arrangement should be as follows. For books: [1] Durand, W. F., *Aerodynamic Theory*, 1st Ed., Vol. 1, p. 23; Julius Springer, Berlin, 1934. For magazines: [1] England, C. R., Crawford, A. B., and Mumford, W. W., *Some Results of a Study of Ultra-Short-Wave Transmission Phenomenon*, Proc. I.R.E., Vol. 20, No. 12, pp. 481–482, March, 1933. Please give author, title, edition, volume, page, publisher, and date of publication as indicated. Omission of one required fact causes much extra editorial work and possible inaccuracies.

ILLUSTRATIONS: Illustrations should accompany manuscripts, and each should always be referred to in the text by number. Drawings or graphs should not be larger than 12 × 16 inches, and must be made with jet black India ink on white paper or tracing cloth, the latter being preferred. *Do not use typewriter for lettering.* The smallest lettering on 8 × 10 inch figures should be no less than $^1/_4$ inch high. Cross-section paper (white with black lines) may be used but it should not have more than 4 lines per inch. If finer ruled paper is used, the major division lines should be drawn in with black ink, omitting the finer divisions. In the case of finely ruled paper, only blue-lined paper can be accepted. *Tracing paper and blueprints* are not acceptable. Lettering and all markings must be large enough to be readable after reduction. Mail rolled or flat; never fold. Drawings that cannot be reproduced (including pencil drawings) will be returned to the author for redrawing thus delaying publication of the paper. Photographs should be distinct and show clear black and white contrasts. They must be on glossy white paper. Avoid round and oval photographs.

CAPTIONS AND LEGENDS: Legends or captions must accompany each drawing or photograph submitted. If written on the drawing or photograph, they should be placed below and well outside the part to be reproduced. Each table should have a caption such as Table 1, Table 2, Table 3, etc. Captions should be complete in themselves so as to make the data intelligible to the reader without reference to the text. A duplicate list of captions for figures should be included as the last page of the manuscript. Use "Fig. 1" (not Figure 1), "Figs. 3 and 4," etc., in both the text and the numbering of illustrations. In the text, "Eq. (1)" or "Eqs. (1) and (2)" is used, not "Equation (1)." In captions and legends, except for "Fig." and "Eq.," and in table headings write all words in full; do not abbreviate.

MATHEMATICAL WORK: Only the simplest formulas should be typewritten; all others should be carefully written in pen and ink, the writing to be large enough so that ample room is provided to mark mathematical matter for the printer. A considerable spacing for marking should be allowed above and below all equations. All complicated equations should be repeated on separate sheets with plenty of space left for marking. The solidus should be used for simple fractions appearing within the text. Make all expressions clear to the typesetter. Greek letters used in formulas should be clearly designated by name on the margin of the manuscript.

SYMBOLS AND ABBREVIATIONS: The symbols recommended in the American Standards Association Standard "Letter Symbols for Aeronautical Sciences," ASA Y10-7—1954, should be used wherever practicable. All symbols should be clearly written and carefully checked. The difference between capital and lower-case letters should be clearly distinguished and care taken to avoid confusion between zero (0) and the letter (o), between the numeral (one) and the letter (ell) and the prime (′), between alpha and a, kappa and k, u and mu, v and nu, n and eta. All subscripts and exponents should be clearly marked, and dots and bars over letters or mathematical expressions should be avoided. Avoid complicated exponents and subscripts. When it is necessary to repeat a complicated expression, it should be represented by some convenient symbol. Standard abbreviations should be used, and it should be noted that most abbreviations are lower case such as m.p.h., b.m.e.p., i.h.p., b.hp., hp., . . . etc.

CORPORATE MEMBERS

OF THE

INSTITUTE OF THE AERONAUTICAL SCIENCES

ACADEMY OF AERONAUTICS, INC.
ADAMS RITE MANUFACTURING COMPANY
AEROJET-GENERAL CORPORATION
AEROLAB DEVELOPMENT COMPANY
AERONCA MANUFACTURING CORPORATION
AEROPHYSICS DEVELOPMENT CORPORATION
AEROQUIP CORPORATION
AGAWAM AIRCRAFT PRODUCTS, INC.
AIR ASSOCIATES, INC.
AIRBORNE ACCESSORIES CORPORATION
AIRBORNE INSTRUMENTS LABORATORY, INC.
AIRCRAFT RADIO CORPORATION
ALLIS-CHALMERS MANUFACTURING COMPANY
ALLISON DIVISION, GENERAL MOTORS CORPORATION
ALUMINUM COMPANY OF AMERICA
AMERICAN AIRLINES, INC.
AMERICAN NON-GRAN BRONZE COMPANY
AMERICAN PHENOLIC CORPORATION
AMERICAN STEEL & WIRE DIVISION, UNITED STATES STEEL CORPORATION
ANDERSON, GREENWOOD & CO.
ARDE ASSOCIATES
ARMA DIVISION, AMERICAN BOSCH ARMA CORPORATION
ASSOCIATED AVIATION UNDERWRITERS
AVIEN, INC.
AVRO AIRCRAFT LIMITED
BAKER STEEL & TUBE COMPANY
BEECH AIRCRAFT CORPORATION
BELL AIRCRAFT CORPORATION
BENDIX AVIATION CORPORATION
THE BG CORPORATION
BOEING AIRPLANE COMPANY
BOOZ, ALLEN & HAMILTON
BRISTOL AERO ENGINES LIMITED
CALIFORNIA PANEL & VENEER COMPANY
CANADAIR LIMITED
THE CESSNA AIRCRAFT COMPANY
CHANCE VOUGHT AIRCRAFT, INCORPORATED
THE CHASE MANHATTAN BANK
CIBA COMPANY, INC.
THE CLEVELAND PNEUMATIC TOOL COMPANY
CLIFFORD MANUFACTURING COMPANY, DIVISION OF STANDARD-THOMSON CORPORATION
CONSULTANTS & DESIGNERS, INC.
CONTINENTAL MOTORS CORPORATION
CONVAIR, A DIVISON OF GENERAL DYNAMICS CORPORATION
CORNELL AERONAUTICAL LABORATORY, INC.
CORYDON M. JOHNSON CO., INC.
CURTISS-WRIGHT CORPORATION
DECKER AVIATION CORPORATION
DOAK AIRCRAFT COMPANY, INC.
DOUGLAS AIRCRAFT COMPANY, INC.
THE DOW CHEMICAL COMPANY
DZUS FASTENER COMPANY, INC
EASTERN AIR LINES, INC.
EATON MANUFACTURING COMPANY
EDO CORPORATION
ELASTIC-STOP NUT CORPORATION OF AMERICA
ELECTROL INCORPORATED
ENGINEERING SUPERVISION COMPANY
ESSO STANDARD OIL COMPANY
ETHYL CORPORATION
FAIRCHILD CAMERA AND INSTRUMENT CORPORATION
FAIRCHILD ENGINE AND AIRPLANE CORPORATION
FEDERAL TELECOMMUNICATION LABORATORIES, DIVISION OF INTERNATIONAL TELEPHONE AND TELEGRAPH CORPORATION
THE FIRESTONE TIRE & RUBBER COMPANY
FLETCHER AVIATION CORPORATION
FLIGHT REFUELING, INC.
THE GARRETT CORPORATION
AIRESEARCH MANUFACTURING CO.
GENERAL ELECTRIC COMPANY
GENERAL PRECISION EQUIPMENT CORPORATION
G. M. GIANNINI & CO., INC.
THE B. F. GOODRICH COMPANY
THE GOODYEAR TIRE & RUBBER COMPANY, INC.
GRUMMAN AIRCRAFT ENGINEERING CORPORATION
HARVEY ALUMINUM DIVISION OF HARVEY MACHINE CO., INC.
ROBERT HEWITT ASSOCIATES
INDUSTRIAL SOUND CONTROL, INC.
INSURANCE COMPANY OF NORTH AMERICA COMPANIES
THE INTERNATIONAL NICKEL COMPANY, INC.
JACK & HEINTZ, INC.
JOHNS-MANVILLE SALES CORPORATION
EARLE M. JORGENSEN CO.
WALTER KIDDE & COMPANY, INC.
KOLLSMAN INSTRUMENT CORPORATION
LAVELLE AIRCRAFT CORPORATION
LEAR, INCORPORATED
THE LIQUIDOMETER CORPORATION
LOCKHEED AIRCRAFT CORPORATION
LOEWY CONSTRUCTION COMPANY, INC.
LONGINES-WITTNAUER WATCH COMPANY, INC.
LONGREN AIRCRAFT COMPANY
MANNING, MAXWELL & MOORE
MARQUARDT AIRCRAFT COMPANY
THE GLENN L. MARTIN COMPANY
McDONNELL AIRCRAFT CORPORATION
MELETRON CORPORATION
MINNEAPOLIS-HONEYWELL REGULATOR COMPANY
NATIONAL CREDIT OFFICE, INC.
NORTH AMERICAN AVIATION, INC.
NORTHROP AIRCRAFT, INC.
NUCLEAR DEVELOPMENT CORPORATION OF AMERICA
PAN AMERICAN WORLD AIRWAYS, INC.
THE PARKER APPLIANCE COMPANY
PESCO PRODUCTS DIVISION, BORG-WARNER CORPORATION
PHILLIPS PETROLEUM COMPANY
PIASECKI HELICOPTER CORPORATION
THE PURE OIL COMPANY
RADIOPLANE COMPANY
J. B. REA COMPANY, INC.
REACTION MOTORS, INC.
REPUBLIC AVIATION CORPORATION
E. V. ROBERTS AND ASSOCIATES
ROHR AIRCRAFT CORPORATION
PAUL ROSENBERG ASSOCIATES
RYAN AERONAUTICAL COMPANY
SANDBERG-SERRELL CORPORATION
SCHRILLO AERO TOOL ENGINEERING COMPANY
SHELL OIL COMPANY
SIMMONDS AEROCESSORIES, INC.
SOCONY MOBIL OIL COMPANY, INC.
SOLAR AIRCRAFT COMPANY
R. DIXON SPEAS
SPERRY GYROSCOPE COMPANY DIVISION OF SPERRY RAND CORPORATION
STANDARD OIL COMPANY OF CALIFORNIA
STANDARD OIL COMPANY (INDIANA)
STANLEY AVIATION CORPORATION
THE STEEL PRODUCTS ENGINEERING COMPANY
STROUKOFF AIRCRAFT CORPORATION
STURGESS, INC.
SUMMERS GYROSCOPE COMPANY
THOMPSON PRODUCTS, INC.
TOOLKO ENGINEERING COMPANY
TRANS WORLD AIRLINES, INC.
TURBO PRODUCTS, INC.
UNION CARBIDE AND CARBON CORPORATION
UNITED AIR LINES, INC.
UNITED AIRCRAFT CORPORATION
UNITED STATES AVIATION UNDERWRITERS, INC.
UNITED STATES RUBBER COMPANY
VARD, INC.
VICKERS INCORPORATED
WESTERN GEAR WORKS
WESTINGHOUSE ELECTRIC CORPORATION
WESTON ELECTRICAL INSTRUMENT CORPORATION
WINDER AIRCRAFT CORPORATION
WYMAN-GORDON COMPANY
YOUNG RADIATOR COMPANY